



**HAL**  
open science

# Development of an analytical strategy for the study and preservation of painted metal objects in museum collections

Julie Gordon

► **To cite this version:**

Julie Gordon. Development of an analytical strategy for the study and preservation of painted metal objects in museum collections. Analytical chemistry. Sorbonne Université, 2022. English. NNT : 2022SORUS171 . tel-03828278

**HAL Id: tel-03828278**

**<https://theses.hal.science/tel-03828278v1>**

Submitted on 25 Oct 2022

**HAL** is a multi-disciplinary open access archive for the deposit and dissemination of scientific research documents, whether they are published or not. The documents may come from teaching and research institutions in France or abroad, or from public or private research centers.

L'archive ouverte pluridisciplinaire **HAL**, est destinée au dépôt et à la diffusion de documents scientifiques de niveau recherche, publiés ou non, émanant des établissements d'enseignement et de recherche français ou étrangers, des laboratoires publics ou privés.

# Sorbonne Université

Ecole doctorale 388

Chimie Physique et Chimie Analytique de Paris-Centre

*Laboratoire MONARIS UMR 8233 SU/CNRS et Synchrotron SOLEIL*

---

## **Development of an analytical strategy for the study and preservation of painted metal objects in museum collections**

---

Par Julie GORDON

Thèse de doctorat de Chimie Analytique

Dirigée par Ludovic Bellot-Gurlet et co-encadrée par Solenn Réguer

Présentée et soutenue publiquement le 24 mai 2022

Devant un jury composé de :

Katrien Keune	Professor, University of Amsterdam & Rijksmuseum	Rapportrice
Austin Nevin	Head of conservation, The Courtauld Institute of Art	Rapporteur
Laura Brambilla	Professeure HES associée, HES-SO	Examinatrice
Marine Cotte	Directrice de recherche CNRS, ESRF	Examinatrice
Anne-Laure Carré	Ingénieur de recherche Ministère de la Culture, CNAM	Examinatrice
Ludovic Bellot-Gurlet	Professeur, Sorbonne Université	Directeur de thèse
Solenn Réguer	Scientifique de ligne DiffAbs, SOLEIL	Co-encadrante



*To my parents, K.G.<sup>2</sup>, for instilling in me a  
love of learning, for always supporting me,  
and for teaching me to go forth with  
Determination, Drive, and Discipline!*



# Acknowledgements

This work was funded by the DIM Matériaux Anciens et Patrimoniaux (Région Ile de France) and Synchrotron SOLEIL, and so I wish to thank them for their support of this research.

To the members of the jury: I would like to express my gratitude to you all for agreeing to be examiners of my thesis work. Extra appreciation goes to Katrien Keune and Austin Nevin for their attentive reading of my manuscript and for their thoughtful comments and feedback.

During the course of my involvement in this project, from the early beginnings when I was a Master student intern to now, at the end of this doctoral thesis project, I have had the opportunity to work with and learn from many formidable people. From the Institut National du Patrimoine in the north to the LISA laboratory in the east, from the Musée des Arts et Métiers and the MONARIS laboratory in the centre to Synchrotron SOLEIL in the southern outskirts, I have traced a literal network across Paris and with it, have had the good fortune of adding new acquaintances to my social network as well. The work that was accomplished during the last four years could not have succeeded without the help and participation of a long list of people:

A mes encadrants :

Un grand merci à Solenn Réguer pour ton temps, ta patience, ton mentorat et ta confiance en moi pour reprendre ton projet. Nous avons passés des beaux jours et nuits de manip ensemble à SOLEIL ainsi que tous les autres endroits que ce projet nous a mené, et je veux assurer à tout le monde que tu étais bien là à mes côtés pendant toute cette thèse, même si ça ne se voit pas dans les épisodes de « la Thèse de Julie » :-)

A Ludovic Bellot-Gurlet : mes remerciements remontent au début de mon aventure parisienne, en 2017 quand je pensais encore que je serais ici pour seulement un an, quand je découvrais à peine le monde des sciences du patrimoine. Nous voilà maintenant en 2022 avec une thèse de doctorat complétée ! Tu m'as donné l'opportunité de découvrir la recherche et la croisée de mes deux passions, les sciences et l'histoire. Merci pour toutes les conversations de sujets diverses mais toujours fascinantes, pour ton temps, tes conseils, ton enthousiasme.

Merci à Anne-Laure Carré, Rémi Catillon et Lionel Dufaux pour les tours du Musée des Arts et Métiers et des réserves, pour les histoires fascinantes des différentes œuvres, pour vos conseils pour ce projet, et surtout pour votre collaboration pour l'obtention des prélèvements, ces microfragments d'histoire qui figurent énormément dans cette thèse.

Merci à Sigrid Mirabaud pour la formation et l'aide avec les expériences GC-MS (j'ai bien compris que ce n'est pas une machine simple !) et de m'avoir initié au côté « organique » des peintures.

Merci également à Anne Genachte-Le Bail de m'avoir aidé avec le côté pigments / « inorganique » des peintures, pour l'accueil chaleureux pendant les journées passées à l'Inp, et surtout d'avoir assuré le rôle important de la collecte des prélèvements sur les objets historiques.

Merci à Marie-Anne Loeper-Attia pour l'accueil et les conseils pratiques de la restauration, et à Sandie Le Conte pour sa collaboration avec ce projet et de m'avoir donné l'opportunité d'exercer mes compétences d'enseignement avec les étudiants de l'Inp.

A Aurélie Verney-Carron, merci de m'avoir toujours accueilli avec un grand sourire au LISA, d'avoir assuré les cycles de vieillissement des coupons pendant si longtemps et pour l'assistance avec les mesures de colorimétrie.

A Julie Schröter, merci pour tes conseils et d'avoir partagé tes expériences sur le traitement des métaux peints, c'était un plaisir de collaborer avec toi pour continuer les recherches que tu as commencé.

A mes collègues de MONARIS, les permanents et à tous les autres que j'ai pu croiser ces 5 dernières années depuis mon stage M1, un grand merci pour l'accueil, pour m'avoir intégré et surtout pour avoir pris le temps de m'expliquer tous les petits détails de la culture et l'actualité française pendant nos cafés de midi. Je tiens à remercier Céline Paris pour sa gentillesse et disponibilité et le temps qu'elle a passé avec moi pour me former sur les instruments ou pour discuter des résultats. A big shout-out aux autres doctorants, particulièrement à ceux avec qui j'ai pu partager un bureau, pour le soutien moral et pour tous les échanges qu'on a eu au labo, à la cantine, ou au Baker.

A mes collègues du Synchrotron SOLEIL : l'équipe DiffAbs, Dominique Thiaudière, Cristian Mocuta, Philippe Joly, merci pour l'accueil chaleureux sur la ligne de lumière et pour toute votre aide pendant nos manip ; Sébastien Schoeder et Matthieu Réfrégiers : merci à vous deux de nous avoir accueilli pour nos manip « à l'étranger » sur les lignes PUMA et DISCO ; le nomade Fred Picca que j'ai surtout trouvé sur DiffAbs en train de jouer soit des belles symphonies, soit de la K-pop – merci pour ton aide avec le traitement des données et les drôles d'échanges sur tout ! ; l'équipe d'IPANEMA, merci pour les beaux moments passés en séminaire, en laboratoire ou en pot de fin d'année ! Un grand merci à Maëva L'Héronde pour sa disponibilité et pour son aide avec l'utilisation des instruments et pour la préparation de mes échantillons ; merci à Anthony Beauvois et Rebecca Cervasio pour votre collaboration pour l'organisation des Petits Déjeuners Scientifiques de SOLEIL, et aux autres doctorants et post-docs avec qui j'ai pu échanger pendant ces réunions ; et finalement, merci au groupe de communication de SOLEIL ainsi qu'à l'équipe Ya+K pour l'organisation et la réalisation de la série de vidéos « La Thèse de Julie » - ça va me faire un joli souvenir de mes années en thèse !

To my friends and family, thank you for your support, your love and your encouragement, especially in the last few months of thesis writing. I am very grateful to my mother for all of the time she spent reading and correcting my English in this thesis (along with the rest of my past projects that got me to this point!). Thank you to las chicas, Sibora and Evi, for always being there for me. A special mention to my roommate, Anna, with whom I've formed a special bond due to our shared experience of finishing a thesis amidst a pandemic, lockdowns, curfews, and being far from home. Thank you for your positive attitude, your advice, and for all of the fun pizza and pasta nights! And finally to Leo. First, of course, mee. That translates to: I could not have done this without you. Which is a bit ironic since I did do it "without you". Regardless, you managed to be there for me without fault, day in and day out, from 7000+ km away. Grazie per tutto.

# Table of Contents

<b>PREFACE</b> .....	<b>I</b>
<b>INTRODUCTION</b> .....	<b>1</b>
<b>CHAPTER I LITERATURE REVIEW</b> .....	<b>7</b>
I.I THE PAINTED METAL SYSTEM: STRUCTURE, COMPOSITION, AND REACTIVITY .....	9
<i>I.I.I Historic iron-based artefacts</i> .....	9
<i>I.I.II Paint coatings for metal structures</i> .....	12
<i>I.I.III Paint coating degradation</i> .....	23
<i>I.I.IV Degradation of the painted metal system</i> .....	25
<i>I.I.V Summary and problem statement</i> .....	28
I.II CURRENT METHODS IN THE CONSERVATION OF PAINTED IRON ARTEFACTS.....	29
<i>I.II.I Preventive conservation</i> .....	29
<i>I.II.II Remedial conservation</i> .....	30
<i>I.II.III Methods for testing conservation treatments</i> .....	35
I.III SUMMARY AND PRESENTATION OF RESEARCH OBJECTIVES .....	37
<b>CHAPTER II MATERIALS AND METHODS</b> .....	<b>39</b>
II.I RESEARCH AXE I: STUDY AND CHARACTERISATION OF A CORPUS OF HISTORICAL PAINTED METAL OBJECTS STORED IN INDOOR MUSEUM CONDITIONS .....	41
<i>II.I.I The Musée des Arts et Métiers (CNAM): organization and environmental conditions</i> .....	41
<i>II.I.II Creation of a database of painted metal objects</i> .....	42
<i>II.I.III Criteria and selection of the study corpus</i> .....	43
<i>II.I.IV Corpus description</i> .....	43
<i>II.I.V Collection of micro-samples for analysis</i> .....	46
<i>II.I.VI Cross-section preparation</i> .....	46
II.II RESEARCH AXE II: STUDY OF THE EFFECTIVENESS OF CONSERVATION TREATMENTS ON A MODEL PAINTED METAL SYSTEM .....	48
<i>II.II.I Choice of representative materials for the model coupons</i> .....	48
<i>II.II.II Preparation of model painted metal coupons</i> .....	49
<i>II.II.III Initial state of samples: fresh vs pre-aged, and natural aging</i> .....	50
<i>II.II.IV Choice of conservation treatments</i> .....	52
<i>II.II.V Preparation and application of the conservation treatments</i> .....	53
<i>II.II.VI Choice of artificial aging parameters</i> .....	55
<i>II.II.VII Summary of experimental design for Axe II</i> .....	57
II.III ANALYTICAL STRATEGY .....	60
II.IV CHARACTERISATION TECHNIQUES .....	64
<i>II.IV.I Photographic monitoring</i> .....	64



II.IV.II Colorimetry.....	64
II.IV.III Measurement of paint coating thickness.....	66
II.IV.IV Stereomicroscope.....	67
II.IV.V Optical microscopy.....	67
II.IV.VI Raman microscopy.....	68
II.IV.VII Infrared spectroscopy.....	70
II.IV.VIII Scanning Electron Microscopy coupled to Energy-Dispersive X-ray spectroscopy.....	73
II.IV.IX Gas Chromatography-Mass Spectrometry.....	74
II.IV.X Synchrotron source, SOLEIL.....	76
II.IV.XI X-ray fluorescence spectroscopy.....	76
II.IV.XII X-ray Absorption Near-Edge Structure spectroscopy.....	78
II.IV.XIII Deep-UV Photoluminescent imaging.....	82
<b>CHAPTER III ANALYTICAL STUDY OF PAINTED METAL OBJECTS FROM THE 19<sup>TH</sup>-20<sup>TH</sup> CENTURIES .....</b>	<b>85</b>
III.I OBJECT DESCRIPTIONS AND SAMPLING.....	87
III.II CHARACTERISATION CASE STUDIES.....	96
III.II.I Tandem P03.....	96
III.II.II Tandem P05.....	110
III.II.III Chaudière P02.....	118
III.III DISCUSSION OF THE CHARACTERISATION OF HISTORICAL SAMPLES.....	131
III.III.I Pigments.....	131
III.III.II Binder components.....	134
III.III.III Alteration products.....	135
III.IV CONCLUSIONS AND PERSPECTIVES.....	139
<b>CHAPTER IV A MULTI-SCALE ANALYTICAL STUDY OF THE EFFECTS OF CONSERVATION TREATMENTS ON THE AGING OF MODEL PAINTED METAL SURFACES .....</b>	<b>141</b>
IV.I PHOTOGRAPHIC STUDY OF THE MODEL COUPONS.....	143
IV.I.I Linseed oil-coated metal coupons.....	143
IV.I.II Lead white-painted metal coupons.....	147
IV.I.III Chrome green oxide-painted metal coupons.....	151
IV.II COLORIMETRIC STUDY OF THE PAINTED METAL SURFACES.....	155
IV.II.I Initial materials.....	155
IV.II.II Colour monitoring throughout testing of conservation treatments.....	157
IV.III MICROSCOPIC STUDY OF THE PAINTED METAL SURFACES.....	162
IV.III.I Linseed oil-coated metal coupons.....	162
IV.III.II Lead white-painted metal coupons.....	163
IV.III.III Chrome green oxide-painted metal coupons.....	164
IV.IV FTIR STUDY OF THE PAINT COATINGS.....	166

## Table of Contents

<i>IV.IV.I FTIR absorption bands of interest</i> .....	166
<i>IV.IV.II Reference spectra of linseed oil binder</i> .....	171
<i>IV.IV.III Reference spectra of conservation treatments</i> .....	171
<i>IV.IV.IV Lead white-painted metal coupons</i> .....	178
<i>IV.IV.V Chrome green oxide-painted metal coupons</i> .....	199
<i>IV.IV.VI Discussion of the FTIR analysis of the paint coatings</i> .....	213
<i>IV.IV.VII Conclusions on the FTIR study of the paint coatings</i> .....	217
<b>IV.V XANES STUDY OF THE Pb-L<sub>3</sub> EDGE OF THE LEAD WHITE-BASED PAINT COATING</b> .....	220
<i>IV.V.I Reference compounds</i> .....	220
<i>IV.V.II Initial state of materials</i> .....	223
<i>IV.V.III Fresh and pre-aged lead white paint from coupons treated with corrosion inhibitor and aged by relative humidity cycles (LW-f-CI-RH and LW-pa-CI-RH)</i> .....	224
<i>IV.V.IV Fresh and pre-aged lead white paint from coupons treated with resin-wax mixture and aged by relative humidity cycles (LW-f-RW-RH and LW-pa-RW-RH)</i> .....	225
<i>IV.V.V Fresh and pre-aged lead white paint from coupons treated with corrosion inhibitor and aged by light exposure (LW-f-CI-LT and LW-pa-CI-LT)</i> .....	227
<i>IV.V.VI Fresh and pre-aged lead white paint treated with resin-wax mixture and aged by light exposure (LW-f-RW-LT and LW-pa-RW-LT)</i> .....	228
<i>IV.V.VII Conclusions on the XANES analyses of the lead white-based paint coatings</i> .....	230
<b>IV.VI SUMMARY OF THE EVOLUTION OF UNTREATED AND TREATED PAINTED METAL COUPONS THROUGHOUT ARTIFICIAL AGING</b> .....	231
<i>IV.VI.I Aging by relative humidity</i> .....	231
<i>IV.VI.II Aging by light exposure</i> .....	235
<b>IV.VII DISCUSSION ON THE EFFECTS OF THE CONSERVATION TREATMENTS ON THE AGING OF MODEL PAINTED METAL COUPONS</b> .....	238
<b>GENERAL CONCLUSIONS AND PERSPECTIVES</b> .....	241
<b>REFERENCE LIST</b> .....	249
<b>APPENDIX</b> .....	261
<b>APPENDIX A. ENVIRONMENTAL CONDITIONS IN THE STORAGE FACILITIES OF THE MUSÉE DES ARTS ET MÉTIERS (CNAM), OCTOBER 2016-APRIL 2017</b> .....	263
<b>APPENDIX B. SUMMARY OF FINDINGS FROM CONSULTATION OF RESTORATION REPORTS FROM THE MUSÉE DES ARTS ET MÉTIERS (CNAM)</b> .....	264
<b>APPENDIX C. PROTOCOL: PREPARATION OF SODIUM TETRADECANOATE (NAC<sub>14</sub>) SOLUTION</b> .....	266
<b>APPENDIX D. PROTOCOL: PREPARATION OF RESIN-WAX MIXTURE</b> .....	267
<b>APPENDIX E. ASSESSMENT OF SAMPLING POSSIBILITY ON HISTORIC OBJECTS IN CNAM COLLECTIONS</b> .....	268
<b>APPENDIX F. OBJECT SAMPLING LOCATIONS</b> .....	269
<b>APPENDIX F.I TANDEM (INV. 21811): SAMPLING LOCATIONS</b> .....	269

APPENDIX F.II CHARRUE (INV. 17001): SAMPLING LOCATIONS.....	271
APPENDIX F.III CHAUDIÈRE (INV. 36181): SAMPLING LOCATIONS .....	273
APPENDIX F.IV SÉRIE DE MESURES (INV. 60005): SAMPLING LOCATIONS .....	275
APPENDIX F.V BALANCE (INV. 05005): SAMPLING LOCATIONS .....	277
APPENDIX F.VI LANTERNE (INV. 16726): SAMPLING LOCATIONS.....	278
APPENDIX F.VII LOCOMOTIVE (INV. 16732): SAMPLING LOCATIONS.....	280
APPENDIX F.VIII CHÂSSIS (INV. 18440): SAMPLING LOCATIONS .....	281
APPENDIX F.IX VÉLOMOTEUR (INV. 20564): SAMPLING LOCATIONS.....	282
<b>APPENDIX G. MEASUREMENT OF COATING THICKNESS BEFORE AGING .....</b>	<b>283</b>
<b>APPENDIX H. COLORIMETRY DATA.....</b>	<b>284</b>
APPENDIX H.I COLORIMETRY DATA: LINSEED OIL-COATED COUPONS .....	284
APPENDIX H.II COLORIMETRY DATA: LEAD WHITE-PAINTED COUPONS .....	285
APPENDIX H.III COLORIMETRY DATA: CHROME GREEN OXIDE-PAINTED COUPONS .....	286
<b>APPENDIX I. OBJECT DATA SHEETS .....</b>	<b>287</b>

# Preface

This thesis work is part of the **CoPaiM** project (New Strategies for the **C**onservation of **P**aintings on **M**etal) and is co-financed by the DIM MAP (Domaine d'Intérêt Majeur Matériaux anciens et patrimoniaux, Région Ile de France) and Synchrotron SOLEIL. The thesis work was supervised by Ludovic Bellot-Gurlet (MONARIS - Sorbonne Université/CNRS) and Solenn Réguer (Synchrotron SOLEIL). The different themes addressed in this project required the collaboration of experts from different fields, including physicists, chemists, conservation scientists, conservation-restoration professionals, and museum curators. The institutions partnered with the CoPaiM project include the research laboratory and metals workshop of the restoration department of the INP (Institut National du Patrimoine, Aubervilliers, France), the LISA laboratory (Laboratoire Interuniversitaire des Systèmes Atmosphériques, UMR 6240 Université Paris-Est Créteil/Université de Paris/CNRS), the Musée des Arts et Métiers (CNAM - Conservatoire National des Arts et Métiers, Paris, France), the MONARIS laboratory (UMR8233 Sorbonne Université/CNRS) and the DiffAbs beamline of Synchrotron SOLEIL.

The partners that oversaw the design and implementation of the CoPaiM project include:

- Solenn Réguer, Beamline scientist, SOLEIL.
- Ludovic Bellot-Gurlet, Professeur, MONARIS.
- Céline Paris, Ingénieure d'étude CNRS, MONARIS.
- Rémi Catillon, Restorer, head of the restoration workshop, Musée des Arts et Métiers.
- Anne-Laure Carré, Ingénieure de recherche, head of the Materials collection, Musée des Arts et Métiers.
- Lionel Dufaux, Head of the Transportation collection, Musée des Arts et Métiers.
- Sigrid Mirabaud, Conservatrice en chef du Patrimoine, Institut National d'Histoire de l'Art.
- Anne Genachte-Le Bail, Régisseuse de collection, DRAC Occitanie.
- Marie-Anne Loeper-Attia, Conservator-restorer, Musée de la Musique-Philharmonie de Paris, Institut National du Patrimoine.
- Julie Schröter, Independent restorer, scientist at the Haute Ecole Arc (Neuchâtel, Switzerland).
- Mandana Saheb, Chargée de recherche CNRS, LISA.
- Aurélie Verney-Carron, Maîtresse de conférences, LISA.

The professional titles are given in French when necessary to avoid translation issues.



# Introduction

Painted metals of cultural heritage<sup>1</sup> are found in museum collections as both decorative and functional objects. Those that are present in indoor collections can be classified into two categories (Schroter, 2008):

- i. Objects originally used in exterior conditions and now stored in an indoor (museum) environment. Examples of these include: signs, gates, architectural ornaments, funerary art, industrial and technical objects.
- ii. Objects that were always intended for interior use, such as: scientific instruments, furniture, paintings, etc.

The materials and techniques used to prepare painted metals can be diverse due to different factors, including the intended use of the object (working objects vs artistic pieces), the desired aesthetics, and the intended atmospheric conditions (indoor vs outdoor) but will also be dependent on the materials available according to the periods or places of production. Furthermore, the conditions experienced by an object during its “working life” can have an important effect on its state of alteration at the moment that it enters a museum collection. In general, objects of a decorative nature will have experienced less harsh conditions than objects that had an operational function.

Artistic paintings on metal have been prepared in Europe since the mid-16<sup>th</sup> century (van der Graaf, 1972) using various supports such as silver, iron, tinned iron, copper, or copper with a surface coating of silver, tin, lead, or zinc; however, copper appears to have been most frequently used (Canadian Conservation Institute, 2017). Due to the smooth surface of the metal substrate, it does not require a thick preparation layer that would otherwise be needed on other types of supports (canvas, wood, etc.). The metal is also less sensitive to climatic variations which reduces the risk of mechanical damage to the painting. However, the inconvenience is that the metallic support is prone to corrosion which can cause degradations that hinder the legibility of the work (Schroter, 2009).

Some examples of paintings on metal of a more artistic nature include funerary decorations based on copper, tin, iron, silver, or zinc (Olender & Wantuch-Jarkiewicz, 2019; Schroter, 2009), oil paintings on zinc (Chua, 2019; Olender & Wantuch-Jarkiewicz, 2019), oil paintings on tinfoil (A. R. Veiga, 2010), miniature portraits and other oil paintings on copper (A. Veiga et al., 2015), oil paintings on iron (Sutter, 2017), and painted shields made of tinfoil or lead alloy (Lauridsen et al., 2015). Several studies in the

---

<sup>1</sup> The term cultural heritage describes both tangible and intangible works or objects of importance for a society due to their aesthetic, historic, scientific or social value (Vecco, 2010).

literature cover the characterisation (Albini et al., 2020) and the degradation (Pavlopoulou & Watkinson, 2006) of paintings on copper as it was the most common metallic support.

Technical heritage encompasses objects used for industrial, transportation, scientific, agricultural, and other similar applications. Earlier production of technical objects containing painted metals occurred at a smaller scale due to artisanal fabrication but experienced an increase in uniform preparation methods with the onset of mass-production processes in the 19<sup>th</sup> century, leading to their extensive presence in everyday life. There are more than 250 technical museums in France alone (Ocim, 2021), which highlights the importance of these collections. In the literature, a few studies exist on painted metal artefacts of industrial or technical heritage that include, among others, automobiles (Degrigny et al., 1995), painted iron signs (Sutter, 2013; Pöllnitz et al., 2019), a toy car (Jouet, 2020), industrial machines (Goergen, 2007), locomotives (Goergen, 2007), lanterns (Messerschmidt, 2014), painted hospital doors (Hansen et al., 2018), and powerplant energy generators (Tissot et al., 2020). Documentation is most often in the form of reports from conservation-restoration projects which are not always widely accessible. Moreover, there have been few analytical studies that have explored the manufacturing techniques and materials, the alteration phenomena present on these artefacts, or that have rigorously studied possible conservation strategies. The study and conservation of industrial or technical heritage is a more recent domain than that of artistic works (Mirambet-Paris & Mirambet, 2011), which explains the relatively fewer studies on industrial and technical artefacts.

This thesis aims to improve the knowledge and strategies used for the conservation of historic painted metal objects found in museum collections. As explained above, painted metals can be found on a vast range of artefacts that can present a variety of materials and alteration states depending on their original function and historical usage. For the sake of narrowing the possible cases encountered, and given the lack of literature that exists on painted metal artefacts of technical heritage despite their ubiquitous nature in modern history, this study focuses on **painted metal artefacts of European technical heritage dated to the 19<sup>th</sup>-early 20<sup>th</sup> centuries.**

The field of conservation-restoration consists of specialists who are experts in the practices required for treatment and conservation of heritage objects. However, in order to improve the understanding of certain aspects of the objects, from the identification of original materials and manufacturing techniques, to causes of observed alteration phenomena, or to evaluate the effectiveness of proposed conservation treatments, collaboration with scientists is often sought to investigate these queries. The application of scientific analysis and research towards the understanding and preservation of cultural heritage artefacts is referred to in recent years as “heritage science” or “conservation science”. In this work, a collaboration between conservator-restorers and scientists was established to address the challenges surrounding the proper conservation of historic painted metal objects found specifically in

an indoor environment. While the indoor environment presents less harsh conditions for conservation in comparison to outdoor storage, the challenge lies in the complexity of the objects: they are composite systems of metal and paint that can contain a range of materials and furthermore are in varying states of conservation depending on their history of use before entering the museum collections. Prior to developing a conservation strategy, a good knowledge of the object is necessary, which includes an understanding of its material composition and current state of alteration. The material composition can sometimes be presumed based on historical techniques, but often varies depending on the function and historical use of the artefact; an example of this is technical objects which were used as exhibition models and not for their intended functional use, and often present more decorative designs than their operational counterparts. Once an understanding of the composition and state of conservation of the material system has been established, the objects can be treated by restoration methods such as cleaning, consolidation/stabilisation, repainting (if necessary), and then can be further protected by applying conservation treatments. In the case of the painted metal system, the development of conservation treatments is a challenge because the treatment must be appropriate for use on both materials, the paint and the metal, which have quite different properties and requirements for conservation. Its effectiveness is also dependent on the environmental conditions in which it is used. Some promising treatments are currently being introduced in the conservation-restoration field, but their chemical behaviour and protective nature must be evaluated to improve the confidence surrounding their use.

To address these questions, this thesis is structured in two research axes:

The **first research axe (Axe I)** of this thesis work was designed to improve the knowledge of the material composition of the painted metal system found on historic objects of technical heritage. The aim was to characterise the original products as well as possible alteration products via a survey of formulations and techniques cited in historical sources, macroscopic observations of the objects, and the analysis of micro-samples collected from representative areas on a corpus of historic painted iron objects dating from the 19<sup>th</sup>-early 20<sup>th</sup> centuries. The nature of the products but also their distribution within the system were of interest in this study, and so the samples were prepared as cross-sections in order to fully observe the sample stratigraphy. A series of complementary analytical techniques was used to collect information on the morphological, chemical, and structural aspects of the stratigraphy of the studied samples.

The **second research axe (Axe II)** addresses the question of which conservation treatments are most suitable for conserving historic painted metal objects. The solution is not simple due to the composite nature of the objects studied: the sensitivities of both the paint coating and the metal support must be considered. In this work, two different conservation treatments that have been proposed as promising



treatments for the painted metal system were selected for testing: a sodium carboxylate solution with corrosion inhibiting properties, and a transparent barrier coating composed of a mixture of resin and wax. The aim was to improve the understanding of the long-term protection efficiency of these treatments as well as their chemical behaviour when subjected to different environmental factors present in museum storage collections. Painted metal model coupons were prepared to create a simplified version of the composite system on which the conservation treatments could be tested. The treatments were evaluated by subjecting the model samples to controlled artificial aging processes by either climatic (relative humidity) cycles or light exposure. The evolution of the model painted metal system in the presence or absence of the conservation treatments was studied using complementary analytical techniques ranging from the macro to the microscale.

These two research axes shall be presented in this manuscript, which is structured as four main chapters followed by general conclusions and perspectives for the work.

**Chapter 1** gives a review of the literature and the background information required to understand the questions addressed by this thesis. It begins by providing a physicochemical description of the painted metal (specifically, iron) system and its different alteration processes, which allows to understand the complexity and variability of the state of the historic painted metal artefact. It also presents the requirements for conservation methods used for painted metals and discusses the advantages and limitations of the current strategies. Following the delineation of these different aspects, the research questions and objectives of this study are defined.

In **Chapter 2**, the materials and methods used during this work are presented. The experimental design of both research axes is first explained in detail, followed by the analytical strategy applied in each case. The protocols for the preparation of the different samples and conservation treatments used are also given. Finally, the techniques and experimental parameters employed during the study are described.

**Chapter 3** contains the results of the first research axe of this work, which concerns the study and characterisation of a corpus of historical painted metal objects from a museum collection. The objects in the corpus and the acquired micro-samples are first described. Given the extensive characterisation work conducted during this thesis, not all of the analyses are shown in the body of the text. A selection of three case studies that demonstrate the analytical strategy applied to the samples are detailed in this chapter, while the other analyses can be found in the appendix. The chapter concludes with a presentation of the overall results obtained on the entire corpus and a discussion of the observed trends.

**Chapter 4** presents the results of the second research axe of this work, which aims to investigate the effect of two different conservation treatments on the aging of a model painted metal system. The

evolution of the model samples under artificial aging conditions, with or without treatment, was examined by complementary techniques. The results obtained from these different methods are first presented individually in order to demonstrate in detail the changes which can be revealed by each technique, which include colour and other visual aspects, molecular changes and structural changes. To conclude the chapter, the main observations from each technique are compared and discussed in order to reach a final conclusion on the effects of the conservation treatments on the aging of the model samples with full consideration of the different aspects and scales (visual, molecular, structural) needed to assess their suitability for use on historic artefacts.

Finally, the main results from this thesis work are summarised in the **General conclusions and perspectives**. They are discussed from a more holistic point of view with regards to what new information has been brought to the questions surrounding the understanding and conservation of historic painted metals. New inquiries that have emerged from this study are outlined and future perspectives are discussed.



# Chapter I Literature review

In this chapter, a review of the literature on the original materials used for painted metal objects of industrial or technical origin will be presented, followed by a description of their degradation phenomena. This will pose the basis of what aspects need to be considered for the proper conservation of these artefacts. Following this first part, the second section will cover current conservation methods in use for painted metallic heritage, with an emphasis on solutions that are appropriate for iron-based artefacts presenting an aged paint coating. The aim of this chapter is to review the reasons behind the conservation challenge that is presented by historic painted metals.



## I.I The painted metal system: structure, composition, and reactivity

An object identified as a painted metal is a **composite system** composed of a metallic structure covered with either a monolayer or multilayered paint coating. In the field of conservation and restoration, metals and paintings are often addressed separately due to their different material composition and reactivity. The challenge in conserving composite systems such as painted metals is to develop strategies that take into account the requirements of all the components simultaneously. The characteristics and behaviour of each individual species as well as their effect on one another should be understood.

Paints and metals are individually their own vast fields of research, and an extensive review of both materials is beyond the scope of this research study. Given the extensive use of iron-based supports in technical heritage, the focus from a material point of view is on the painted iron system. This section will begin with an overview of the fundamental aspects needed to understand the composition and degradation of the materials before treating them as two interactive components of a composite system. The function of each component in the context of the system will be explained to fully understand the design of a painted iron system. Finally, we will look into the causes of degradation specific to the composite system.

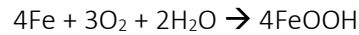
### I.I.I Historic iron-based artefacts

Iron, the most abundant metal on earth, is found naturally in mineral form as oxides, sulfates and carbonates (Dillmann et al., 2015). The metal has been extracted from iron ores with various processes of heat and reduction since around 2000 BC. However, mass-production of steel (an iron-carbon alloy with good workability) was not available until the introduction of the Bessemer process and the open hearth process in the 1850s-60s. From this point onwards, a revolution in industrial production occurred in which steel was used as the material of choice in many domains, including construction, transportation, machinery, tools, instruments, etc. (Spoerl, 2004).

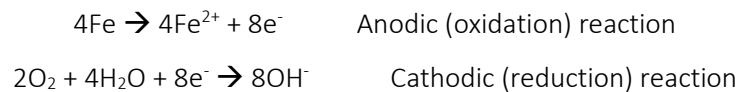
#### I.I.I.i Degradation of the iron structure

Possible degradations of iron-based metallic objects include corrosion and mechanical damage. While the latter can be controlled by proper storage and handling, corrosion is an electrochemical process, the characteristics of which are dependent on the environmental conditions (Mayne, 1973; Walker, 1982). For example, objects found in marine conditions, buried in soil, immersed in water, or stored in indoor conditions will all experience different types of corrosion processes, resulting in the formation of different corrosion products at the surface of the altered objects.

In this study we are only concerned with atmospheric corrosion, characterised by the cyclic condensation and evaporation (wet/dry cycles) of a layer of aqueous electrolyte on the metal surface (Monnier, 2008). The mechanism for the atmospheric corrosion of iron can be described by the following overall reaction:



This process shows that iron metal, in the presence of oxygen and water, will form iron oxyhydroxides (iron corrosion products); it is a redox reaction based on two half equations:



In a first step,  $\text{Fe}^{2+}$  and hydroxide ions are produced and combine to give ferrous hydroxide ( $4\text{Fe}(\text{OH})_2$ ); the ferrous hydroxide is then transformed into rust (expressed in the generic form  $4\text{FeOOH}$ ) in the presence of oxygen.

A spatial separation of the cathodic and anodic reaction sites at the metal surface creates an electrochemical cell in which current will flow from cathode to the anode. In the case of iron corrosion, this cell is created by the spontaneous processes of oxidation of iron metal and reduction of oxygen and water. The flow of current due to the coupling of these redox half-reactions fuels the production of iron corrosion products.

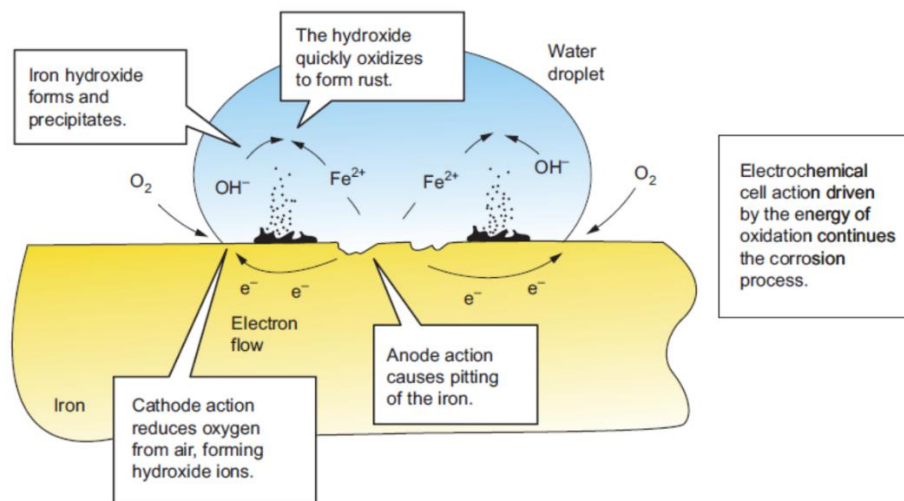


Figure I-1 Corrosion of Iron. From (Tator, 2015).

The process is mainly dependent on the climatic conditions, namely the presence and levels of oxygen, humidity, temperature, and other stimulating species. The conditions can vary depending on the atmospheric setting (industrial, urban, rural) and will influence the rate of the corrosion processes. Corrosion reactions are observed to begin at a relative humidity of 60% and an oxygen content of 3%

(Monnier, 2008; Walker, 1982). The nature of the phases that form depend on several parameters of the system, including the pH, the dissolved oxygen content, the electrolyte composition and the presence of pollutants (Monnier, 2008). The morphology of the corrosion layer and the nature of the products within it will evolve over the different time periods of the corrosion process: from the initiation of corrosion at the metal surface to the long-term establishment of a corrosion layer with a thickness of several hundred micrometers containing a complex mixture of iron oxides and oxyhydroxides (Monnier et al., 2010).

For short to mid-term corrosion (a few minutes to several years), the corrosion system is organized in two distinct layers: an internal layer that is dense and protective (sometimes referred to as a passive layer) and is composed of goethite ( $\alpha$ -FeOOH) and/or maghemite ( $\gamma$ -Fe<sub>2</sub>O<sub>3</sub>), and a less dense external layer composed of goethite, lepidocrocite ( $\gamma$ -FeOOH) and magnetite (Fe<sub>3</sub>O<sub>4</sub>) (Monnier, 2008). In the case of long-term corrosion (hundreds of years), three types of morphologies have been reported: a single layer of mainly goethite; a dual layer system with a goethite-based internal layer and a lepidocrocite-based external layer; and a trilayer system in which a top-layer containing impurities from the environment is present on the bilayer system. Other phases that have been detected within these layers include magnetite, maghemite, akaganeite ( $\beta$ -FeOOH), and some millimetric-sized streaks of feroxyhyte ( $\delta$ -FeOOH) and ferrihydrite (5Fe<sub>2</sub>O<sub>3</sub>.9H<sub>2</sub>O) (Monnier, 2008). Goethite and maghemite are relatively stable phases, while lepidocrocite, ferrihydrite, and feroxyhyte have a high reactivity and their presence will have an influence on the corrosion processes. The corrosion layer may also contain traces of other elements such as Ca, Cl, S, P, or K which originate either from the metal substrate or from the environment; their presence can also affect the reactivity of the system (Monnier, 2008).

The corrosion of iron can also be stimulated by other species found in its environment. It is particularly sensitive to hygroscopic species and acidic vapours (Walker, 1982). For example, sulfur dioxide (SO<sub>2</sub>) is present in the atmosphere both naturally and due to combustion processes. It dissolves in the presence of water to become the strong acid H<sub>2</sub>SO<sub>4</sub>. The acid reacts with the iron surface to produce iron sulfates: in the presence of oxygen, these are converted to iron oxides, but sulfuric acid is regenerated, thus continuing the corrosion process. Another example is chlorides species, which can be present due to industrial pollution or even sweat residues left by handling. These can stimulate corrosion due to their hygroscopic nature but also by increasing the conductivity of the electrolyte solution, thereby improving the conditions required for corrosion.



### **I.I.I.ii Corrosion control: the role of the paint coating**

The corrosion process is the result of a redox reaction that depends on a transfer of electrons. To inhibit the corrosion process, the flow of current must be interrupted. Some ways of achieving this are by the limiting one or both of the two redox half-reactions.

To limit the cathodic reaction, oxygen and water must be separated from the source of electrons; this can be achieved with a barrier layer that will block the passage of electrons from the metal to the surrounding atmosphere but that is also impermeable to oxygen and water. The application of a paint coating to the metal surface is an established solution for preventing corrosion. However, studies have shown that paint and varnish films are not completely impermeable to water and oxygen (Mayne, 1973) and therefore do not totally limit the cathodic reaction.

The anodic reaction can be limited in two ways: cathodic protection or anodic passivation. In the first method, a supply of electrons to the anodic site decreases the rate of iron oxidation. The electrons may be supplied by metallic pigments that are less noble (i.e. more reactive, prone to oxidation) than iron and thus act as sacrificial anodes. In the case of anodic passivation, the iron corrosion rate is slowed by the use of inhibiting pigments that function by passivating the iron surface (Mayne, 1973; Hollner, 2009).

Paints and varnishes that do not contain inhibitive pigments can still function as a barrier method due to their high ionic resistance; that is, they impede the migration of ions towards the metal surface (ex. diffusion of NaCl found to be slower than diffusion of water and oxygen). It appears that the ability of ionic species to permeate the coating depends on the crosslinking density of the coating (Mayne, 1973). However, pigments are generally included due to their delivery of desired properties for the metal coating. A more detailed presentation of the function and composition of the paint coating is given in the following section.

### **I.I.II Paint coatings for metal structures**

A coating is a material used to cover a substrate that delivers both protective and aesthetic properties. Coatings may be clear or pigmented and are classified as a varnish or a paint, respectively. In the case of metallic objects, protective (pigmented) coatings have been applied to metal surfaces to prevent corrosion since ancient times. In Pliny the Elder's *Natural History* (circa 79 A.D.), he describes the protection of iron from rust "by an application of ceruse, gypsum, and tar" (Pliny the Elder, 1855).

Up until the 20<sup>th</sup> century, metals were painted with a coating containing pigments and natural binders such as vegetable oils and/or resins (Schroter, 2009; Stoye et al., 2010). An increase in the scientific understanding of the corrosion process and the physicochemical properties of paints over time led to

an optimization of corrosion control technology in the 19<sup>th</sup> and 20<sup>th</sup> centuries, as seen by the escalation of research and patents for metal coatings since the mid-1800s (C. A. Smith, 1981).

The desired properties of a paint coating for a metal support are the following (Kendig & Mills, 2017; Stewart, 2019; Stoye et al., 2010):

- Good adhesion to the support.
- High resistance (insulating, non-conducting) and impermeability.
- Mechanical properties: elasticity, hardness/scratch resistance.
- Aesthetics: colour, gloss, conveyance of information.

The properties of the coating are determined by its material composition and structure.

The composition of a paint coating can be separated into two primary components: the pigment and the vehicle. Pigments have primarily an aesthetic purpose (colour, opacity, etc.) but often have other important functions (ex. corrosion inhibition, catalyst for film drying, extenders, etc.) as well. The vehicle is a fluid medium within which the pigments are insoluble and dispersed. It includes the binder (the structural component of the coating), in some cases a solvent to improve the rheological properties of the paint during application, and some additives (e.g. UV stabilisers, wetting agents, thickeners, etc.) which provide various other properties to the coating. During drying, the solvent evaporates and the binder dries by physical or chemical processes to form a durable coating with good mechanical and barrier properties. It also provides adhesion onto the substrate (Lyon et al., 2017).

In order to protect the metal substrate against corrosion, the paint coating should act as an insulator and impermeable barrier against the migration of charged species, oxygen, and water. This is dependent in part on the thickness of the coating but also on its composition. The crosslinked network formed by the cured binder has hydrophobic properties, while the presence of pigments can increase the pathway of diffusion for water and oxygen (Leidheiser, 1982). Homogeneity in the paint coating is important, as areas of variable composition may show increased rates of corrosion (Kendig & Mills, 2017; Leidheiser, 1982).

Coatings were applied by hand until the improvement of industrial production processes in the 1900s; turpentine was the main solvent of choice during application (C. A. Smith, 1981; Stoye et al., 2010). Prior to application, the surface of the metal substrate was cleaned to improve the adhesion of the coating. Corrosion products, dust, and grime are removed by mechanical action, followed by a surface treatment. In the 19<sup>th</sup> century, a mixture of nitric acid, sulphuric acid, and water was often used as a treatment. Some sources describe the application of hot linseed oil to the metal surface prior to applying a paint coating as a treatment that improves adherence (C. A. Smith, 1981). These are just a few

examples but since historical manufacturing recipes are not always available and there are few characterisation studies, it is hard to say how representative they are of the practices of the time.

Coatings for metal structures generally contain 2-3 layers (Bierwagen, 1996), including a base coat/primer in contact with the metal substrate and an external top-coat. A multilayer system which includes additional intermediate layers will have a greater protective function as each layer acts as an extra barrier against corrosion agents in the surrounding environment. The layers may have different compositions depending on their desired protective or aesthetic properties:

- i. The **base coat** (primer, ground, etc.) needs to present good barrier properties (high impermeability and ionic resistance) and good adhesion to the metal substrate. The binder provides high cross-linking density and adhesion while corrosion inhibiting pigments are typically included since it is the layer closest to the metal (Prochaska & Tordonato, 2017).
- ii. **Intermediate** layers need to present good barrier properties (obtained through high cross-link density) as well as good adhesion to the surrounding layers.
- iii. Finally, the **topcoat** is the most exterior layer. It should be highly resistant to environmental factors such as humidity and light and should also deliver the desired aesthetic qualities.

At the end of the 19<sup>th</sup> century, scientific testing of protective paint coatings for iron resulted in the following recommendations: 1-2 coats of freshly ground red lead pigment in raw linseed oil, followed by at least two coats of paint composed of either iron oxide pigments or zinc oxide pigment in linseed oil (C. A. Smith, 1981). However, the field of corrosion control was evolving, and other formulations were tested and introduced. Despite the obvious aesthetic role of some types of objects, especially those used as demonstration models or to convey information (signage, etc.), the techniques used are not often discussed in the industrial literature. It is possible that paint coatings whose function was purely aesthetic were derived from formulations already in use in the artistic domain, as is often the case even today. An overview of the typical composition of pigments and binders used in historical paint coatings for iron metal structures is presented in the following sections.

### I.I.II.i Pigments

Pigments are inorganic or organic compounds of natural or synthetic origin that are insoluble in a binder and impart colour or other physicochemical or mechanical functions. Some examples of the role of pigments in a paint coating include (Lyon et al., 2017; B. K. Sharma, 2006):

- Optical (aesthetic) properties: colour, high tinting strength, opacity, gloss control, texture.
- Coating properties: siccative properties, ease of application, flexibility, cost.
- Protective properties: corrosion inhibition, reflection of UV light.

These functions depend on the nature of the pigments and are included in the paint formulation depending on the desired properties of the coating. A comprehensive overview of traditional pigments used in the 19<sup>th</sup>-early 20<sup>th</sup> centuries is given in works such as *The Artist's Assistant* (Carlyle, 2001) and the *Artists' Pigments* series (Feller et al., 1986; Roy, 1993; FitzHugh et al., 1997; Berrie et al., 2007). The choice of pigments used in paint coatings for metal structures mainly depends on the desired aesthetic and technical properties as well as cost.

In terms of aesthetics, pigments will often be chosen for their colour, but also for other characteristics such as tinting strength and resistance to fading. To lower the cost of the paint coating, pigments known as **extenders** will be included in the formulation. These are compounds with a high refractive index that scatter light and provide opacity without altering the colour of the paint coating. Extender species are usually mineral compounds such as carbonates, silicates, sulphates and oxides. Some examples include calcium carbonate, calcium sulfate, silica and China clay (Kaolin, hydrated aluminum silicate) (Lin, 1998).

Pigments may also be included to provide a technical or protective function within the paint coating. The main types include driers (siccatives) and inhibitive (anticorrosive) pigments. **Driers** are so-called because they accelerate the drying of oil paint. Originally, compounds based on lead, zinc, cobalt and manganese were used as driers. Some pigments such as lead acetate, lead white, red lead, and litharge are known for their drying properties (Carlyle, 1999). Due to their toxicity, they were eventually replaced by organometallic driers like cobalt, calcium and zirconium naphthenate and are used in oil and alkyd-based coatings (IARC, 1989). **Inhibiting** pigments have an anticorrosive effect in paint coatings due their ability to suppress the anodic half-reaction of the corrosion process (that is, the oxidation of iron); this can occur by different mechanisms depending on the nature of the compound. Pigments may inhibit corrosion by modes known as cathodic protection or anodic passivation (see I.I.I.ii Corrosion control: the role of the paint coating).

Pigments that provide cathodic protection to the iron substrate should be metallic and less noble than iron; a common example is metallic zinc (in the form of zinc dust/powder) (Kendig & Mills, 2017; Mayne, 1973). These pigments will generally be present in the base coat/primer of the metal coating because direct contact between the pigments and the iron substrate is required to ensure a conductive pathway for the flow of electrons. Pigments which function by anodic passivation are activated by the corrosive environment; their inhibitive action begins when they react with water which has permeated the coating. The main inhibitor pigments used in the time period of interest were chromates (often zinc or strontium chromates) and basic pigments which form soaps when mixed with linseed oil (Mayne, 1973). In the presence of water and oxygen, zinc chromate dissociates to give zinc cations and chromate anions which simultaneously inhibit both the cathodic and anodic reactions, respectively (Walker, 1982). Basic pigments such as red lead, lead white, and calcium carbonate can react with fatty acids in the binder to

produce metal soaps. Lead, zinc, barium, strontium, and calcium soaps formed from the oleic, linoleic and linolenic fatty acids found in linseed oil paint were observed to have corrosion-inhibiting properties in the presence of water and oxygen. Specifically, the oxidation of the soaps were found to yield corrosion-inhibiting compounds that can form a passive layer at the iron surface, inhibiting further oxidation (Mayne, 1973). The toxicity of the Pb and Cr(VI)-containing pigments motivated research into alternative inhibitive pigments. Nontoxic ZnO was found to have similar inhibitive properties to Pb-based compounds, and chromates were replaced mainly by phosphates and molybdates (IARC, 1989; Kendig & Mills, 2017).

The aesthetic and functional characteristics of the pigments are not mutually exclusive: a pigment may provide colour but also have anticorrosive properties, as is the case of the pigment red lead. Examples of common pigments used in industrial paint coatings (i.e. for metal substrates) are presented in Table I-1.

Table I-1 Common pigments used in the preparation of paint coatings in the 19<sup>th</sup>-early 20<sup>th</sup> centuries (details from (Buxbaum & Pfaff, 2005; Gettens et al., 1967; IARC, 1989; Izzo, 2011; La Nasa et al., 2018; Lauridsen et al., 2015; "Leaded Zinc Oxide," 2016; Radepont, 2013; Roy, 1993; B. K. Sharma, 2006))

Colour	Pigment	Chemical composition	Historical use
White	Lead white	$2\text{PbCO}_3 \cdot \text{Pb}(\text{OH})_2$	Antiquity – late 20th cent.
	Leaded zinc oxide	ZnO with 10-55% Pb content	ca. 1896 - 1920
	Zinc oxide	ZnO	1840 - present
	Titanium dioxide	$\text{TiO}_2$	1920s - present
	Lithopone	Coprecipitate: ZnS (30%) and $\text{BaSO}_4$ (70%)	1850-decrease in use after 1960s
Red	Red lead	$\text{Pb}_3\text{O}_4$	2nd cent. BC / 2nd cent. AD - late 20th cent.
	Iron oxide: hematite	Hematite: $\alpha\text{-Fe}_2\text{O}_3$	Prehistory - present
	Cadmium red	CdS-CdSe	Early 19th cent. - mid-19th cent.
	Vermilion/Cinnabar (synthetic/natural)	HgS	Natural: antiquity - 1880 Synthetic: 8th cent. - late 20th cent.
Blue	Ultramarine blue/Lazurite (synthetic/natural)	$\text{Na}_8[\text{Al}_6\text{Si}_6\text{O}_{24}]\text{S}_n$	Natural (mineral lazurite): antiquity (rarely used due to high cost) Synthetic: 1828 - present
	Cobalt blue	$\text{CoAl}_2\text{O}_4$ $\text{CoO} \cdot \text{Al}_2\text{O}_3$	Early 19th cent. - present
	Prussian blue	$\text{Fe}_4[\text{Fe}(\text{CN})_6]_3$	1704 - present
	Phthalocyanine blue	$\text{C}_{32}\text{H}_{16}\text{CuN}_8$	1930s - present
Green	Chromium oxide	$\text{Cr}_2\text{O}_3$	Mid-19th century - present
	Chrome green	Mixture of Prussian blue and Chrome Yellow	19th cent. - present
	Phthalocyanine green	Chlorinated/brominated derivative of Phthalocyanine blue	1930s - present

Colour	Pigment	Chemical composition	Historical use
Yellow	Litharge/Massicot	PbO	Antiquity - later 20th cent.
	Chrome Yellow, other yellow chromate pigments Lead or zinc chromates	PbCrO <sub>4</sub> and PbCrO <sub>4</sub> ·PbSO <sub>4</sub> K <sub>2</sub> O·4ZnCrO <sub>4</sub> ·3H <sub>2</sub> O	Pb chromate: Early 1800s - present Zn chromate: produced 1850 (mainly in use as corrosion inhibitor after 1914) - present Sr, Ba chromate: Mid-19th century - present
	Ochre	α-FeOOH (goethite)	Prehistory - present
Black	Carbon black, lamp black, etc.	Carbon (varying purity)	First produced ca. 1500 BC
Orange	Chrome orange	PbCrO <sub>4</sub> ·PbO, Basic lead chromate	Early 1800s - present
Brown	Burnt umber (dark brown with red undertone), burnt Sienna (red-brown), etc.	Umber: Fe <sub>2</sub> O <sub>3</sub> (45-70%) with MnO <sub>2</sub> (5-20%) Sienna: Fe <sub>2</sub> O <sub>3</sub> (ca. 50%) with MnO <sub>2</sub> (<1%)	Prehistory - present
Metallics	Powders of copper, copper/zinc alloys, zinc, aluminum, etc.	Cu, Zn, Al, etc.	19th century - present

An increase in the development of synthetic pigments was seen over the course of the 20<sup>th</sup> century and pigments containing toxic heavy metals such as Pb or Cr were replaced with less harmful alternatives. Some pigments which were frequently used in paint coatings for metal substrates during the 19<sup>th</sup>-early 20<sup>th</sup> centuries are presented below.

Up until the 19<sup>th</sup> century the main white pigment was **lead white**, a mixture of basic lead carbonate  $2\text{PbCO}_3 \cdot \text{Pb}(\text{OH})_2$  (hydrocerussite) and neutral lead carbonate  $\text{PbCO}_3$  (cerussite) (Gettens et al., 1967; Gonzalez, 2016). Hydrocerussite occurs naturally as a mineral but has been prepared synthetically since antiquity. In linseed oil it is observed to accelerate the drying of the paint film, and therefore also functions as a drier pigment. From the 19<sup>th</sup> century to around 1920, the available white pigments included basic lead carbonate, basic lead sulfate, zinc oxide, leaded zinc oxide, and lithopone (IARC, 1989). Due to the toxicity of lead white, less harmful alternatives for the white pigment began to be researched. Commercialisation of **zinc white** ( $\text{ZnO}$ ) began around 1820 and was a primary choice for white pigments up until the mid-19<sup>th</sup> century, at which point **titanium white** ( $\text{TiO}_2$ ) became the white pigment of choice. Another common white pigment, although not the primary option, was **barium sulfate** ( $\text{BaSO}_4$ ). In its natural form it is the mineral barite, and it was introduced as a pigment in 1782 as an alternative to lead white. Natural iron oxide impurities give the pigment a pinkish hue and an early industrial practice was to mix the pigment with ultramarine or other blue pigments to improve the white colour. The synthetic form of the pigment was introduced in around 1820 and was used as an extender in lead white paints. It also appears in the white pigment **lithopone** as a co-precipitate with  $\text{ZnS}$  (Feller et al., 1986). The use of lithopone began just before World War I but generally declined by 1950 (IARC, 1989). The main industrial uses of barium sulfate (alone or in lithopone form) were as an extender for lead white paints or as primers for metal surfaces. It has a lower refractive index than lead white and therefore a lower opacity in paint, which meant that it could not totally replace lead white as a white pigment on its own.

As for coloured pigments, **red lead** was often used as a primer for iron and steel substrates (Feller et al., 1986). The red pigment is composed of lead tetroxide  $\text{Pb}_3\text{O}_4$  and is one of the earliest artificially made pigments. The naturally occurring form of the pigment is the mineral minium, although it is rarely used as a pigment; however, the names red lead and minium are sometimes used equivalently. Industrial production began in the 17<sup>th</sup> century, and in the 18<sup>th</sup> century, it was prepared from lead and litharge ( $\text{PbO}$ ). In oil paint, it has a high refractive index which provides good opacity in oil paints. It accelerates the curing of drying oils, especially in the presence of litharge, a property which is related to its ability to form lead soaps (Feller et al., 1986). A coating containing this pigment has good adhesion to the substrate and low permeability to moisture and oxygen. The first patent for its use as a protective coating for metal occurred in 1852. Despite the high-performance properties of this pigment, important



disadvantages of its use are that it is toxic and is prone to discoloration under certain conditions (Feller et al., 1986).

The pigment **chrome yellow** ( $\text{PbCrO}_4$  and  $\text{PbCrO}_4 \cdot \text{PbSO}_4$ ) was widely used during the 19<sup>th</sup>-20<sup>th</sup> centuries (Feller et al., 1986). It was an expensive pigment and was mixed with extenders such as barite, gypsum, alumina, and lead sulfate. Chrome yellow is also found in a green pigment known as **chrome green** as a mixture with Prussian blue. Other yellow chromate pigments such as **zinc or strontium chromates** were used in paint coatings for metal substrates starting around 1914 due to their corrosion-inhibiting properties.

The pigment **chromium green oxide** is composed of chromium oxide  $\text{Cr}_2\text{O}_3$  and gives an opaque olive-green colour (FitzHugh et al., 1997). It has a high refractive index which distinguishes it from its hydrated form which is transparent and blue-green in colour. It is a very permanent (resistant to fading) pigment that was introduced in the first half of the 19<sup>th</sup> century, although its high cost prevented it from being widely used. It was used in automotive paint finishes as a mixture with aluminum flakes.

### **I.I.II.ii Binders**

The binder is an organic medium within which the pigment is dispersed. It hardens upon drying into a crosslinked polymer network to form a durable coating with good mechanical properties. It also provides adhesion onto the substrate and protects the substrate by forming a hydrophobic barrier. Historically, drying oils, and in particular linseed oil, were used in coatings for metals. Furthermore, natural resins have long been added to drying oils to improve the durability of the resulting paint film. A manual published in 1922 from the French publisher Roret on the techniques of painting and varnishing on metal and wood describes the recommended use of pigmented paint coatings containing a mixture of oil and copal for metal surface coatings (Fink, 1922). Developments in polymer chemistry starting in the 1920s brought about the replacement of the oil binder with synthetic formulations based first on cellulose nitrate, then on polyurethanes, epoxies, or alkyd resins (IARC, 1989; Schroter, 2009). However, in the context of this thesis the production period of the studied objects is limited to the early 20<sup>th</sup> century, thus allowing to focus on oil-based coatings.

#### ***Linseed oil***

Linseed oil is commonly used as a binder in oil paints. In fact, linseed oil is classified as a drying oil, that is, an oil with certain chemical characteristics that allow it to change from an oily substance to a hard film in the presence of oxygen. Naturally occurring drying oils are mainly composed of triacylglycerols: mixtures of three fatty acids connected through an ester linkage to glycerol. The principal drying acids have an 18-carbon fatty acid chain containing two or more double bonds, although fatty acids with

saturated and shorter or longer chains can also be present (J. D. J. van den Berg, 2002). See Figure I-2 for an example of the structure of a triacylglycerol as well as some common fatty acid molecules.

Van den Berg (J. D. J. van den Berg, 2002) reported the typical fatty acid composition and proportions (as a % of total fatty acid composition) of linseed oil as the following:

- Triply unsaturated linolenic (C18) acid (48-60%).
- Doubly unsaturated linoleic (C18) acid (12-19%).
- Monounsaturated oleic (C18) acid (10-24%).
- Saturated palmitic (C16) acid (4-10%), stearic (C18) acid (2-8%).

The mechanisms behind the curing and aging of drying oils are complex and not fully understood. One of the basic principles is that the speed of the drying is highly linked to the number of double bonds present in the fatty acid chains of the oil binder. These functional groups serve as the site for various reactions that lead to cross-linking (polymerisation) and hardening of the film. An advanced description of the curing mechanisms of drying oils can be found in the thesis work of J.D.J van den Berg (J. D. J. van den Berg, 2002).

In practice, coatings made with linseed oil alone are soft due to slow drying rates; to accelerate the drying (and hardening) of the binder, different techniques are used. Driers (siccatives) may have been added to the oil to catalyze the curing process. The oil may also have been pre-polymerised by heat treatment, in the presence or not of oxygen and or metallic driers, to improve the drying rate and physical properties of the cured film (Izzo, 2011; J. D. J. van den Berg, 2002); examples of these are boiled linseed oil, blown oil, and stand oil.

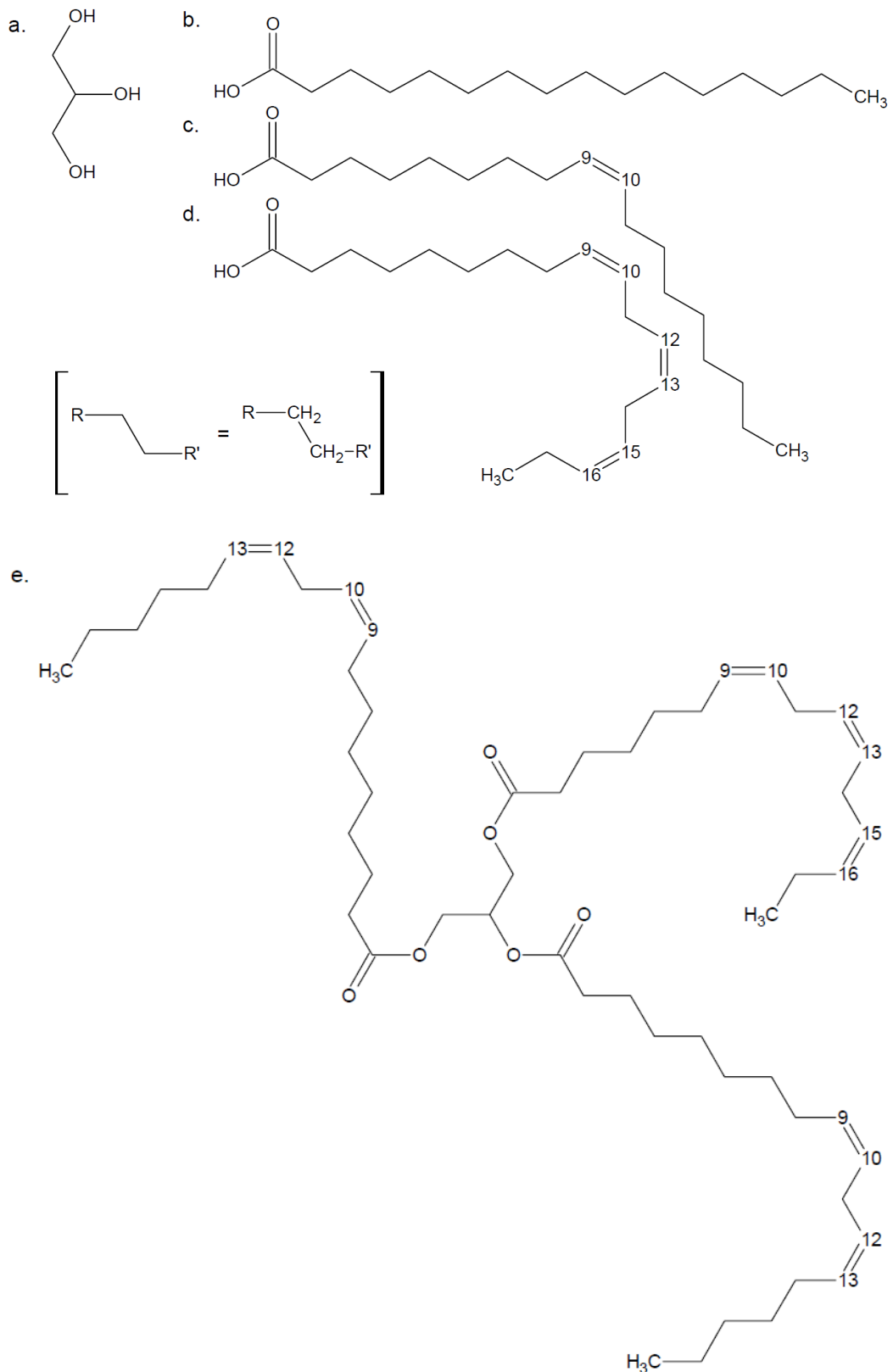


Figure I-2 Composition of a generic drying oil: a) glycerol; b) palmitic acid; c) oleic acid; d) linolenic acid; e) a triglyceride structure with linoleic (two double bonds) and linolenic (three double bonds) fatty acids. From (J. D. J. van den Berg, 2002).

## **Resins**

The identification of resins on painted metal artefacts can be attributed to either their inclusion as a component of the binder or as a varnish. In the literature, both pine colophony and copal are mentioned as having been added to oil for use in paint coatings (Fink, 1922; K. J. van den Berg, 2003). Pine colophony (a resin from the *Pinaceae* family) is mainly composed of abietic acid and is prone to oxidation processes, producing compounds such as dehydroabietic acid and 7-oxo-dehydroabietic acid (Daher, 2012). Various types of copals exist, including Manila and Kauri copal (*Araucariaceae* family) and African copals (*Fabaceae* family). The main identifying compounds for these resins are polycommunic acid (Manila copal), a copolymer of communic acid and communal (Kauri copal), and polyzoic acid (African copals) (K. J. van den Berg, 2003).

### **I.I.III Paint coating degradation**

Oil paint is known to be sensitive to different environmental factors including temperature, water (as condensation or relative humidity), light, and pollutants. Other situations, such as an improper preparation or ill-suited conservation-restoration treatments, can also be causes for paint degradation. These changes manifest themselves visually as blistering, swelling, cracking, flaking, or discoloration of the paint layer (J. D. J. van den Berg, 2002). Many of the alterations are linked to changes in chemical composition and structure; therefore, the state of alteration of the paint coating can be studied by identification of the degradation products. In some cases, the components of the paint (pigments, binder) are individually responsible for perceived alteration (ex. discoloration of certain pigments, yellowing of oil binder), while in other cases, the interaction between the paint components can lead to degradation (ex. metal soap aggregation).

#### **I.I.III.i Pigment degradation**

In the case of pigments, the main visual alteration is discoloration (i.e. fading, darkening, colour change). Origins of these changes include exposure to light, heat, relative humidity (Saunders & Kirby, 2004), reaction with atmospheric pollutants such as sulfur and nitrogen-containing gases (Saunders, 2000; G. D. Smith & Clark, 2002), or restoration intervention. Many studies have been conducted on the alteration of traditional pigments used for both industrial and artistic means and an extensive review of the literature was published by Coccato et al. (Coccato et al., 2017). A selection of studies related to the degradation of pigments often present in the composition of paint coatings for metallic objects are listed in Table I-2.

Table I-2 Commonly observed alteration phenomena of some pigments used in historic painted metal coatings.

Pigment	Degradation product(s), general process	Source
Lead white $2\text{PbCO}_3 \cdot \text{Pb(OH)}_2$	<u>Darkening</u> : reaction of lead carbonate with trace $\text{H}_2\text{S}$ in air to produce $\text{PbS}$ (galena); transformation of lead carbonate into $\text{PbO}_2$ (plattnerite).	(Vagnini et al., 2018) (Lussier & Smith, 2007)
Chrome yellow $\text{PbCrO}_4$	<u>Darkening</u> : subject to alteration in presence of oil, lead oxide, or Prussian Blue pigment; Reduction of $\text{Cr(VI)}$ to $\text{Cr(III)}$ .	(Monico et al., 2011)
	In presence of $\text{SO}_2$ , $\text{PbCrO}_4$ becomes a mixture of $\text{PbSO}_4$ and $\text{Cr(III)}$ compounds.	(Monico et al., 2011)
Red lead $\text{Pb}_3\text{O}_4$	<u>Lightening</u> : conversion to $\text{PbCO}_3$ (cerussite). <u>Darkening</u> : conversion to $\text{PbO}_2$ (plattnerite) or $\text{PbS}$ (galena).	(Aze et al., 2008)
Vermillion $\text{HgS}$	<u>Lightening</u> : reaction with $\text{Cl}^-$ ions to produce $\text{Hg}_2\text{Cl}_2$ (calomel) and other chlorinated phases. <u>Darkening</u> : phase transformation from red cinnabar to black metacinnabar.	(Spring & Grout, 2002) (Radepont, 2013)

### I.I.III.ii Binder aging and degradation

Many studies have been conducted in the last decades to elucidate the aging processes of linseed oil binders (Wheeler, 1950; Lazzari & Chiantore, 1999; Colombini et al., 2002; J. D. J. van den Berg, 2002; Erhardt et al., 2005; Bonaduce et al., 2012; Modugno et al., 2019). It is a highly complex process with various competing mechanisms. The drying of a linseed oil coating begins with a process known as autoxidation, in which atmospheric oxygen reacts with the unsaturated fatty acids in the oil and initiates the polymerisation process that results in a hardened, cross-linked film. In addition to the polymerised network, degradation products resulting from autoxidation processes are formed. These may be volatile low molecular weight products such as aldehydes or other hydrocarbons. Many of these products may evaporate from the film, but some will be trapped within the coating and undergo further conversion to carboxylic acids known as diacids: these are short-chain fatty acids (7-11 carbons) which are fairly stable products and act as chemical markers of aged (oxidised) oil paints (J. D. J. van den Berg, 2002). In particular, the diacids present in highest proportion are those derived from the oxidative degradation (and subsequent isomeration) of the unsaturated C18 fatty acids, such as azelaic (C9), suberic (C8), sebacic (C10), and pimelic (C7) acids.

The speed of the drying process is dependent on different factors such as exposure to heat, pre-treatment of the oil, and presence of drier compounds. Once the paint coating has hardened, its composition continues to evolve through different processes that progress at a slower rate over many years. In addition to oxidative degradation, exposure to water causes hydrolysis of the triglyceride ester bonds of the linseed oil, releasing fatty acids that remain free or that are bound to the polymer network.

These degradation processes cause the paint film to become more polar over time, which can make it more sensitive to the use of certain solvents. Furthermore, the release of volatile degradation products can cause a densification and shrinking of the paint film (J. D. J. van den Berg, 2002).

### **I.I.III.iii Pigment-binder interaction**

In the presence of metallic ions from either pigments or driers, free fatty acids from the binder can combine with the cations to form metal soaps which reinforce the structure of the paint film. Lead and zinc-based compounds, including lead white, red lead, and zinc white, are particularly efficient at forming metal soaps in paint. The beneficial role of metal soaps is sometimes negated by their association to other phenomena which can lead to degradation of the paint. The metal soaps tend to aggregate and form protrusions, or else migrate through paint layers, leading to deterioration. GC-MS analyses of metal soap aggregates in aged oil paints have found that the main fatty acids present are palmitic, stearic and azelaic acids (Higgitt et al., 2003). Lead soap formation in oil paints has been linked to certain environmental factors such as variations in relative humidity, high temperature or light exposure (Keune, 2005; Keune et al., 2016). Due to their degrading effect on heritage paintings, metal soaps have been the subject of many studies in recent years (Plater et al., 2003; Keune & Boon, 2007; Robinet & Corbeil, 2003; J. Hermans et al., 2016; Casadio et al., 2019; Garrappa et al., 2020; Izzo et al., 2021).

Metal soaps may also have been included in the original formulation of the paint as stabilisers, thickeners, plasticisers, wetting agents, etc. Aluminum and zinc stearates have been added to paints as dispersing agents since the 1920s; other possible metal cations include sodium, potassium, calcium, magnesium, and zinc (La Nasa et al., 2018). It can be difficult to distinguish between the origin of metal soaps identified in paint samples as original additives in the formulation of the paint or as degradation products (Cotte et al., 2017).

### **I.I.IV Degradation of the painted metal system**

The degradation of the painted metal system should be regarded as a bilateral process. Both the metal substrate and the paint coating have been shown to be unstable under certain conditions and over the long term. The environmental setting (industrial, urban, rural, marine, etc.) experienced by the painted metal system plays an important role in the progression of alteration phenomena, as explained in the previous sections. The combination of these factors for both the paint and metal, as well as their effect on each other, leads to a large range of possible states of alteration. Some of the most common degradation phenomena of the painted metal system have been investigated by several studies over

the last decades (Leidheiser, 1982; Tator, 2015; Kendig & Mills, 2017; Lyon et al., 2017) and are presented here.

### Effect of the deterioration of the paint coating on the metal support:

Despite the intended role of the paint coating as a protective barrier for the metal substrate, no coating can completely prevent the occurrence of corrosion (Lyon et al., 2017). The painted metal system is susceptible to different aggravators, including mechanical damage accumulated during use, intrinsic defects in the formulation/preparation of the materials, surface contamination under the coating due to improper surface preparation, and physicochemical alteration of the coating composition due to exposure to environmental reagents.

These stressors can lead to the accumulation of mechanical alterations such as scratches, microscopic cracks and fissures, chemical changes such as decreases in cross-linking density due to the degradation of the binder, or loss of adhesion at the interfacial region, all of which ultimately lead to a failure of the barrier properties of the coating. Corrosive agents such as water, oxygen, or ionic species can reach the metal substrate by permeation through zones with decreased cross-linking density (Figure I-3), which result from voids left by solvent evaporation, pigment aggregation, degradation of the binder polymeric system, or through direct access through scratches or fissures due to mechanical damage (Tator, 2015).

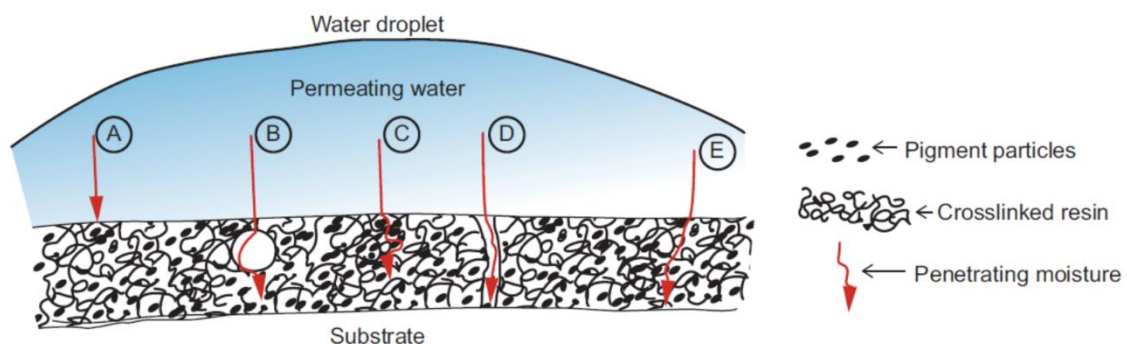


Figure I-3 Modes of permeation of water due to variations in cross-linking density within the coating: a) High cross-link density (no permeation); b) Void spaces left by solvent evaporation; c) Pigment agglomeration; d) Void from scratch, crack, or fissure; e) Low cross-linking density due to binder degradation. From (Tator, 2015).

**Effect of the deterioration of the metal support on the paint coating:**

The main degradation of the metal support is linked to the oxidation of iron due to the presence of a corrosive environment. The corrosion of the metallic substrate in a painted metal system is mainly due to the degradation of the protective paint coating, as seen above, but can also be initiated from a lack of a surface treatment prior to application of the paint layer which can lead to a favourable conditions for the development of corrosion reactions (Iezzi, 2011). The corrosion products formed take up more volume than the pure metal, leading to a loss of adhesion and visual alterations ranging from blistering to rupturing to a full loss of a part of the paint coating, which further exposes the underlying metal (see Figure I-4). Aesthetically, surface modifications of the paint coating may occur, such as the development of an uneven surface due to the underlying formation of corrosion products, or staining of the paint coating due to migration of the  $Fe^{2+}$  ions into the paint coating and subsequent oxidation (Lyon et al., 2017).

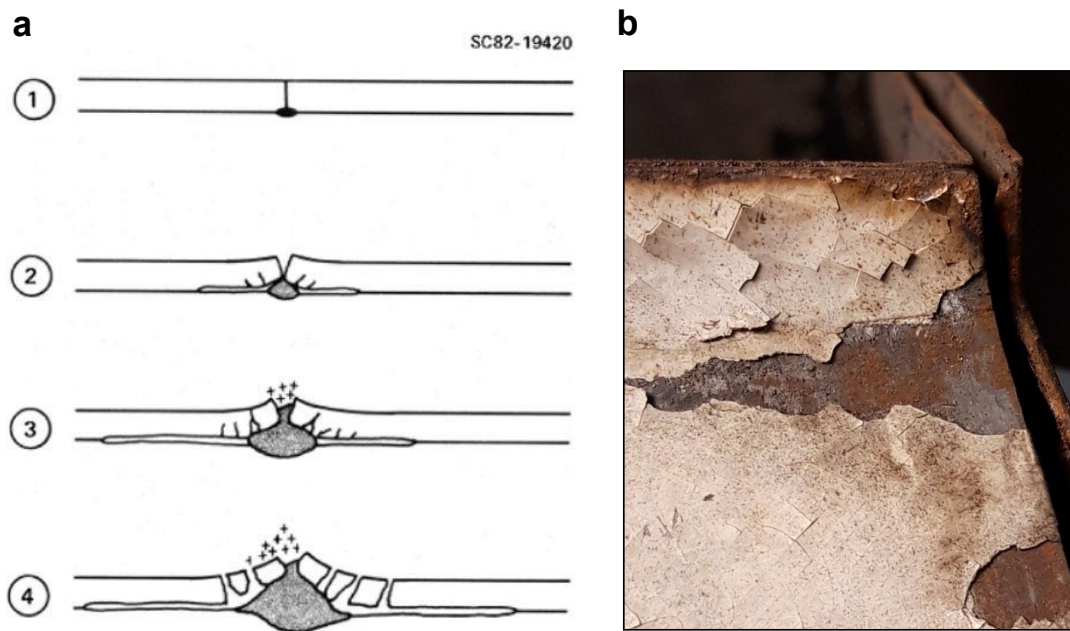


Figure I-4 Failure of a paint film due to corrosion of metal support: a) Schematic of coating rupturing from (Kendig & Mills, 2017); b) Photograph of the *Chaudière* (an object studied in this thesis), showing staining of the paint, paint loss, and corrosion of exposed metal substrate.



## I.I.V Summary and problem statement

This section presented the function of a paint coating on a metal structure as both a protective barrier for preventing corrosion of the iron metallic object as well as delivering a desired aesthetic appearance. The composition of a protective and aesthetic paint coating is described with emphasis on the historic methods and materials used during the 19<sup>th</sup>-early 20<sup>th</sup> century. It was shown that the paint coating is a complex mixture of pigments, an organic binder, and other additives. It is prone to alterations of different origin, including (photo)oxidation, hydrolysis, and pigment-binder reactions. Changes in the chemical composition of the paint can reduce its barrier properties, allowing corrosion to occur at the paint-metal interface. Concurrently, formation of corrosion products can weaken the adhesion of the paint coating and place mechanical stress on the film structure, causing blistering and eventually paint loss. Exposure of the underlying metal substrate will further weaken the structure of the object due to increased corrosion, and furthermore leads to a dramatic loss of the aesthetic design of the surface. Oftentimes it is in this fragile, altered, possibly active state that painted metal objects exist when they enter the collections of a museum, and to which challenge conservators are faced. Indeed, strategies for conserving an altered painted metal artefact are not straightforward as all of the components present need to be considered. The materiality of the objects must first be determined, followed by the development and testing of suitable conservation treatments.

## I.II Current methods in the conservation of painted iron artefacts

This section mainly addresses the state of the art on strategies for the conservation of painted iron objects of industrial and technical heritage stored in indoor atmospheric conditions.

As seen in the previous section, the main degradation phenomena of painted metals are the loss of the protective and/or aesthetic properties of the paint coating as well as the corrosion of the underlying metallic structure. Visual signs of alteration appear as cracking, blistering, or flaking of the paint film, formation of corrosion products in areas where the metal has been left exposed, and possible staining of the paint film where corrosion has formed underneath.

The main conservation objectives for painted metals artefacts are therefore to consolidate the paint coating, to stabilize the metal, and finally to protect the whole composite painted metal system. The types of conservation methods are divided into three categories in order of increasing invasiveness of the method, as defined below (Corr, 2018):

- i. **Preventive conservation:** Control of environment and other factors that can cause damage and degradation of the object.
- ii. **Remedial conservation:** “Stabilise or retard the deterioration of the heritage and to diminish future risk without compromising its material and historical integrity.”
- iii. **Restoration:** “A complex ensemble of actions which can include the integration and replacement of non-original elements, reconstruction, retouching and infilling. It is aimed at facilitating the appreciation, understanding and utilisation of the cultural heritage.”

Common considerations and approaches for preventive and remedial conservation of painted metals will be presented here.

### I.II.I Preventive conservation

Methods of preventive conservation seek to remove or control deterioration factors in the environment to reduce or delay the degradation of heritage artefacts. In the case of composite systems, the choice of conservation conditions must consider the weaknesses of all the materials present. For paints in general, it is recommended to maintain climatic conditions at constant values of 40-60% relative humidity (RH) and 16-25°C. Variations in RH conditions can cause stress to the paint film. At low temperatures and low RH, the paint may become brittle, while at high temperatures degradation reactions are accelerated (Canadian Conservation Institute, 2017). Light exposure can lead to fading or

other alterations of the paint and must be controlled. For metals, the exposure to corrosive agents such as oxygen, moisture, and other aggressive species (hygroscopic compounds, sweat residues, dust, acidic vapors, etc.) should be limited. Possible solutions include keeping the RH levels as low as possible, maintaining uniform temperature, using dessicants, air filters, etc. Acidic vapours may be present in the museum collections environment due to their release by the materials present on other objects, such as wood, plastics, varnishes, glues, etc. It has been recommended to cover the acid-sensitive objects with impenetrable covers (Walker, 1982).

The recommended climatic conditions for the composite painted metal system are a constant RH level maintained between 40-50 % RH (Canadian Conservation Institute, 2017). This provides a compromise between the needs of the paint layer and the metal: the metal requires low RH levels to reduce the risk of corrosion, but at low RH the paint will become brittle and weak. The temperature should be maintained at a constant level between 16-25°C; fluctuations should be avoided as this can cause variations in the RH levels. Photochemical aging can be limited by reducing both the intensity and length of periods of light exposure.

## I.II.II Remedial conservation

To introduce the practice of remedial conservation, a quote on an important aspect of conservation treatments, reversibility, is given here:

*“Reversibility is still a major criterion of good conservation treatment, one that sets conservators apart from skilled restorers or repairers. The “Principle of Reversibility” is one of the factors which establish our unique intent to project our work into the distant future. Conservators have an obligation to assure to the best of their ability that the condition of an object remain unchanged long after treatment is completed. Knowledge of how conservation materials age, how they interact with the object, and how the object responds to its environment is therefore necessary to fulfill this obligation”* (Appelbaum, 1987).

This quote emphasizes the importance of having a thorough understanding of the immediate and long-term effects of conservation treatments on the artefact to which they are applied. This requires foremost a comprehensive knowledge of the material composition of the object, followed by testing of the treatments on real or model systems. The challenge for composite objects is that treatments must be appropriate for all the components of the system. The selection criteria for a protective treatment for altered painted metal objects are the following (Schroter, 2008; Shashoua & Matthiesen, 2010).

**General requirements for conservation treatments:** long-term stability (minimum 3 years); reversibility, conservation of original surface appearance (= transparency), simple and homogeneous application; non-toxic; adequate hardness/durability, anti-static.

**Requirements specific for conservation of corroded metal:** hydrophobic/impermeability (against moisture and oxygen); natural look (no shine); does not acidify over time; good adhesion; non-aqueous application.

**Requirements specific for conservation of aged paints:** cold application; soluble in non-polar solvents; level/smooth surface once applied; lack of colour change over time; consolidating effect if applicable.

The remedial action practiced on altered painted metals is usually the removal of corrosion products and application of a corrosion inhibitor to stabilize the metal, followed by treatment with a transparent protective coating to impermeabilize the system against further alteration. Common surface treatments used in the conservation field for stabilization of iron-based artefacts include corrosion inhibitor solutions of tannins (tannic acid) or benzotriazole (BTA) (Cano & Lafuente, 2013). However, BTA presents health hazards and tannins can significantly darken the corrosion products, and so research in recent years has sought alternative solutions. Among these include *Opuntia ficus indica* extract (OTH) and 3-phenyl-1,2,4-triazole-5-thione (PTS), which showed promising results but are better suited for short term protection. Long-chain fatty acids derived from plant oils in either carboxylic acid ( $\text{HC}_n$ ) or sodium carboxylate ( $\text{NaC}_n^-$ ) form, where  $n$  = the number of carbons in the fatty acid chain, have been shown to have better protection properties than the traditional treatments (Rocca & Mirambet, 2007; Hollner, 2009; Mirambet et al., 2010; Degriigny, 2011). Characterisation studies (Hollner, 2009) have shown that the protective effect is related to the precipitation of iron carboxylates at the surface of the metal which acts as a passivation layer against further corrosion (Figure I-5).

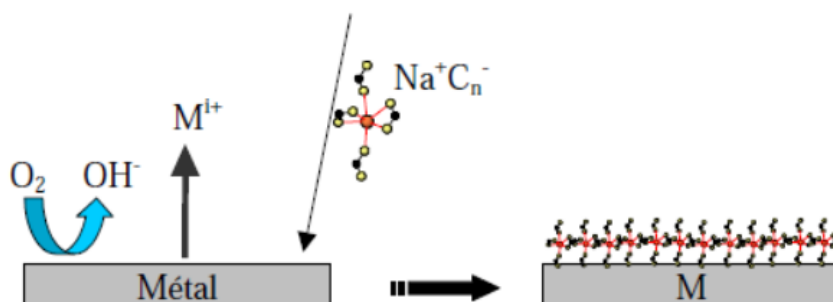


Figure I-5 Mechanism of interaction of sodium carboxylate with metal substrate. Adapted from (Hollner, 2009).

The efficiency of protection should increase with chain length of the film, yet this parameter cannot be fully exploited due to the amphiphilic nature of long-chain carboxylates (a polar carboxylate head group and a non-polar hydrocarbon chain). Due to their structure, they tend to form micelles at a certain

concentration which complicates the ability to prepare a solution for treatment. Studies have found that NaC<sub>10</sub> presents a good compromise between protective effect and solubility in water (Mirambet et al., 2010). The effect of the solution concentration on efficacy has also been studied: it was found that the minimum concentration for inhibition at any chain length is 0.05 M, and that no significant increase in protection efficiency is observed above this level (Hollner, 2009).

Studies on the protection efficiency of sodium decanoate (NaC<sub>10</sub>) for iron substrates showed a significant reduction of the corrosion rate on model samples (Hollner, 2009). Sodium decanoate has also been implemented on several metallic heritage objects with satisfactory aesthetic and protective results (Mirambet et al., 2004; Hollner, 2009; Degriigny, 2011). The passivation layer that forms can easily be removed using an organic solvent like ethanol (Hollner, 2009). The non-toxicity, invisibility, and ease of reversibility of these treatments makes them very promising for use as conservation treatments for iron metallic heritage. The main issue is that the inertness of these corrosion-inhibiting treatments towards paint coatings on metal artefacts has not yet been experimentally shown and must therefore be demonstrated before their use is validated as a treatment for painted metal systems.

After stabilization of the metal, the entire system can be treated with a transparent coating that acts as a protective barrier against external environmental factors. The choice of coating is dependent on different factors, in particular the environment in which the treated object will be stored. Objects destined to be kept outdoors will experience harsher environmental conditions and the choice of treatment must be more durable; some studies on outdoor protective coatings for (painted) iron and steel are mentioned here for interest's sake (Bruggerhoff, 2007; Shashoua & Matthiesen, 2010; Lawson, 2016).

For artefacts stored in indoor controlled conditions, the setting is more favorable for their conservation, but degradation factors can still be present as described earlier. Products used for surface protection by conservation professionals and that have been deemed appropriate for indoor painted metal artefacts are the following: synthetic resins Paraloid B72<sup>®</sup>, Laropal K80<sup>®</sup>, Laropal A81<sup>®</sup> and microcrystalline wax Cosmoloid H80<sup>®</sup> (Schroter, 2008). Waxes and varnishes are often used as conservation treatments as they present good protection efficiency and do not significantly modify the surface appearance of the artefact; however, the efficiency of protection is short term and requires replacement, necessitating the use of solvents to remove the aged coatings. In the case of altered painted surfaces which become more polar over time, non-polar solvents should be prioritised (Schroter, 2008).

A series of tests of different transparent coatings on model painted iron coupons (Schroter, 2008) showed that the best results were obtained when using Paraloid B72<sup>®</sup>, a reference standard treatment

in the domain, or a 30:10 wt% resin-wax mixture of Regalrez 1126® and Cosmoloid H80® in white spirit. Details on these materials and their use in conservation are detailed in the following insert.

**Transparent coatings best suited for use on historic painted metals (following tests by J. Schroter (Schroter, 2008)):**

**Paraloid B72®** (Lawson, 2016) is an acrylic resin (copolymer of ethyl methacrylate:methyl acrylate) that is favoured for its transparency, solubility, hardness (glass transition temperature: 40°C) and reversibility. It is usually dissolved in acetone in a 10-15% w/v dilution.

**Regalrez®** is a low-molecular weight hydrocarbon resin of different grades based on molecular weight (varieties include 1018, 1085, 1094, and 1126). It is a copolymer of styrene and styrene derivatives. The grade Regalrez 1126® has a glass transition temperature of 65°C, making it durable at room temperature. It is normally dissolved in aliphatic solvents. Its stability (resistance to UV degradation) and aesthetic properties (saturation, gloss) make it a well-adapted product for conservation practices (Piena, 2001).

**Cosmoloid H80®** is the commercial name for a synthetic microcrystalline wax that is widely used as a protective coating for industrial heritage artefacts (Shashoua & Matthiesen, 2010; Lawson, 2016). It is derived from petroleum and is composed of long-chain alkane hydrocarbons (Svečnjak et al., 2015). The preferred solvent for this product is white spirit (petroleum distillate with low aromatic content) (Lawson, 2016).

The mixture of resin and wax presented a good alternative to the widely used Paraloid B72® and is especially adapted to altered painted metals, since their ability to be used with non-polar solvents (in contrast to Paraloid B72® which uses slightly polar solvents) is preferred. The advantages and disadvantages of using a mixture of the resin and wax components as opposed to their individual use are summarised in Table I-3.

**Table I-3 Comparison of the use of synthetic resins and waxes for conservation of painted metals individually and as a mixture (Schroter, 2008).**

	Resin	Wax	Resin-wax mixture
<b>Advantages</b>	Good colour saturation Cold application possible Forms hard film when dry	Hydrophobic Chemical stability Soluble in non-polar solvents Low shine/gloss	Increased hydrophobicity thanks to wax Improved colour saturation Desired aesthetic (low shine) Can be used with non-polar solvents
<b>Disadvantages</b>	Less hydrophobic than wax Shiny aspect Sensitive to UV/RH Possible yellowing	Poor colour saturation Attracts dust Requires heat for application	Proportion is important: otherwise, possible separation of components

The resin-wax mixture of Regalrez 1126®-Cosmoloid H80® shows an accumulation of the advantages of each individual component. In particular, the addition of wax increases the hydrophobicity of the mixture in contrast to the resin alone, thereby improving the impermeability of the coating and furthermore allowing greater solubility in non-polar solvents. The use of wax also allows to control the

shine or gloss of the surface appearance, while the resin provides good colour saturation. The ratio of resin:wax was tested and was found to be an important parameter, as in many cases the mixture did meet required standards of viscosity and homogeneity. The ratio of 30:10 wt% of resin to wax fulfilled the desired criteria for a transparent coating for painted metals. This formulation has been used in the conservation of real painted metal artefacts and was reported to fulfill the mechanical and aesthetic requirements of a treatment for painted metals (Schroter, 2009; Sutter, 2013). In practice these treatments have been shown to be effective in terms of their inertness towards the materials and in their ability to stabilize the objects, but few studies have looked into their use on painted metal surfaces and moreover their effectiveness in the presence of different environmental stressors. It is these questions in particular that this current research addresses.

### I.II.III Methods for testing conservation treatments

In recent years, two major studies among many others have been conducted on the conservation of metallic heritage: the **POINT** project (*Protection temporaire d'Objets métalliques base fer et cuivre à l'aide d'Inhibiteurs de corrosion Non Toxiques*) and the **PROMET** project (Developing new analytical techniques and materials for monitoring and protecting metal artefacts and monuments from the Mediterranean region). The broad aims of these projects were to develop new protective materials for metals and new ways of testing these materials. A standardized methodology for the testing of treatments for metal artefacts was developed from these studies and is detailed in Figure I-6.

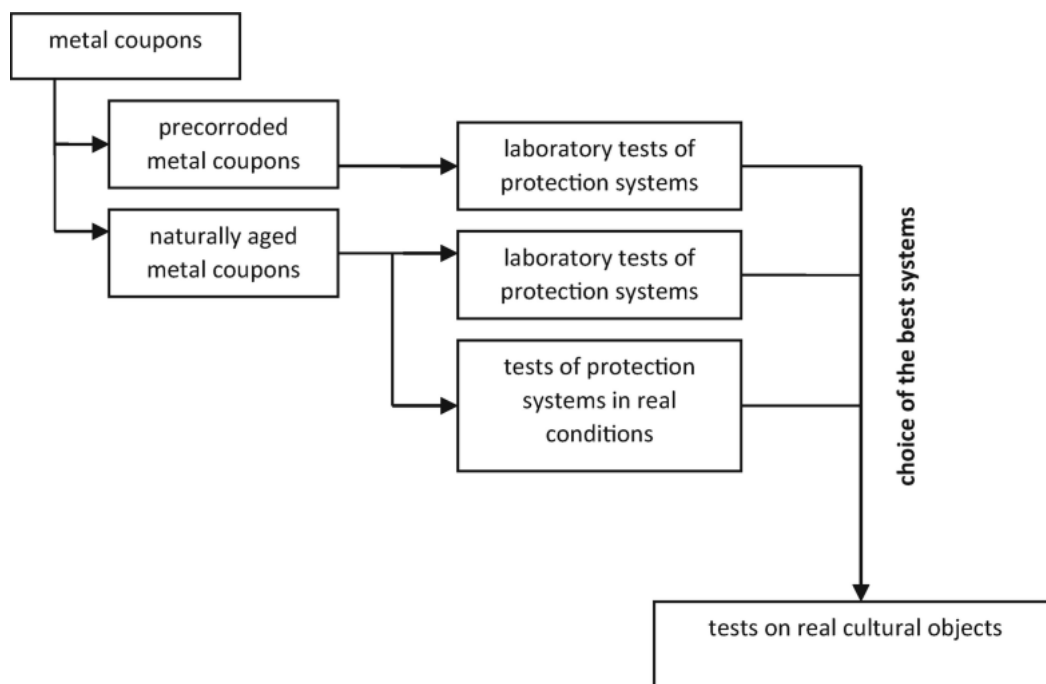


Figure I-6 Methodology from the PROMET project. From (Argyropoulos et al., 2021).

In particular, they introduced the use of model metal coupon replicates and natural/artificial aging experiments to test the efficiency of the protection treatments. The artificially aged coupons were pre-aged before treatment to more closely resemble the surface of an aged artefact. The conditions used in the POINT project, which represent extreme environmental conditions for museum objects, are listed in Table I-4. Pre-aging conditions were maintained for 131 hours (5 days and 11 hours), followed by application of the protection treatment. The coupons were then further aged under the aging conditions for 432 hours (18 days).



**Table I-4 Aging conditions used in the POINT project (Degrigny, 2011).**

Phase (time in hours)	Pre-aging Conditions	Aging conditions
16h	40°C, 100% relative humidity (RH)	40°C, 90% RH
8h	20°C, 60% RH	20°C, 60% RH

The PROMET project used slightly different pre-aging and aging conditions for the preparation and corrosion testing of steel coupons (Degrigny et al., 2007):

- PROMET pre-aging conditions: 24 hours at 30°C and 100% relative humidity (RH), 24 hours at 25°C and 50-60% RH, 24 hours at 30°C and 100% RH.
- PROMET aging conditions: 16 hours at 90% RH and 35 °C, 8 hours at room conditions (20 - 25 °C and RH 50 - 60%). Cycles continued for a minimum of 30 cycles.

These studies provide a basis from which to develop a testing protocol for conservation treatments on painted metals, but the applied aging conditions only address the aging of the metal. To adapt the artificial aging conditions to ensure degradation of the paint coating, relative humidity levels should cycle to less than 40% RH (under which level, oil paint is known to weaken). Furthermore, the presence of the paint coating introduces a new sensitivity to light exposure for the painted metal system that is not applicable to uncoated metal surfaces. Artificial photochemical aging is often used in the conservation field to study degradation processes of light-sensitive materials or to create degraded materials to serve as models of naturally aged objects. Samples are exposed to light in a climatically controlled chamber for a chosen duration of time. It is difficult to relate artificial exposure time to natural light aging; it is necessary to study the materials of interest following the aging experiments to determine their degree of alteration (Saunders & Kirby, 2001).

Using model samples has the benefit of being able to test conservation treatments under controlled conditions and provides a better visibility of the reproducibility of the results. However, it should be acknowledged that historic objects will present much more variability in their composition and aging processes, making tests on model systems not totally representative of the real-life situation. As seen in the standard methodology presented in Figure I-6, treatments also need to be tested on model coupons in natural aging conditions, and finally on real, naturally aged artefacts before their use is validated.

### I.III Summary and presentation of research objectives

This chapter has presented, from a physicochemical and conservation point of view, historic painted metal objects of industrial or technical heritage of the 19<sup>th</sup>-early 20<sup>th</sup> centuries. The presentation of the material constituents of the painted iron system and its common degradation processes demonstrate that historic painted metal artefacts are complex, composite systems with variable states of alteration when they arrive in museum collections. There is currently a lack of studies in the literature on not only the original materials used for these objects but also on their current state after 100-200 years of alteration. This presents a challenge to the conservator-restorer as the choice of an acceptable conservation procedure highly depends on an in-depth understanding of the physicochemical state of the system.

The first research axe of this current work aims to contribute to this gap in knowledge by conducting an analytical characterisation of the material composition and structure of microsamples obtained from historic painted iron objects currently stored in the indoor collections of the Musée des Arts et Métiers (CNAM) in Paris, France. This characterisation work is important because it will allow us to present a survey of the materials and techniques used for the preparation and maintenance of these objects. It will also allow for the documentation of the current states of conservation of the objects, as well as the underlying alteration processes, thanks to a multi-scale analysis of the object starting from a global assessment of its condition down to a micro-scale description of the stratigraphy of the painted metal system.

The second part of this chapter addressed current conservation-restoration methods used for painted metal artefacts. It was shown that methods currently in use are borrowed from common treatments for the individual components of the painted metal system: these include corrosion inhibitors which are often used for metal artefacts and transparent barrier coatings which are used for the conservation of various materials, including painted surfaces. In practice, their use on each of the individual components has proved acceptable (no surface alteration, reversible, non-toxic), but the treatments are not always totally adapted to the requirements of the painted metal system, and there is a lack of certainty on their long-term efficiency. This review allows to highlight the current issues in the conservation of painted metals, notably the lack of adequate or validated treatments and the need for scientific testing on new treatments to prove their inertness towards the painted metal system and their efficacy of protection in the long term.

The second research axe of this work will explore the protective behaviour of two promising treatments, a sodium carboxylate corrosion inhibitor and a resin-wax mixture, that are currently in use on altered

painted metal systems by some conservation-restoration specialists. Specific aspects of the effect of the conservation treatments shall be addressed:

- Do the corrosion inhibitors interact with the paint coating?
- How do the treatments age when exposed to controlled environmental conditions?
- Do they show significant protective behaviour (characterised as preservation of the original structure of the paint) when exposed to environmental conditions that lead to aging?

The processes are undoubtedly complex owing to the multiple components present not only in paint but in the entire composite system of a treated painted metal. The addition of environmental aging factors further complicates the possible pathways for degradation. In order to dissect the various steps and processes involved, the system must first be studied in a simplified form. A methodology involving the artificial aging of painted metal model samples that represent the most basic components of the painted metal system will allow us to put forth a preliminary interpretation of the protective effect of the studied treatments. The evolution of the treated painted metal system shall be monitored by several complementary analytical techniques. The information gained from this research will provide greater insight into the chemical behaviour of the proposed treatments and will aid in validating the current conservation practices.

## Chapter II Materials and methods

The aim of this chapter is to present the materials and methods used during this work. The experimental design of both research axes is first explained in detail, followed by the analytical strategy applied in each case. The protocols for the preparation of the different samples and conservation treatments used are also given. Finally, the techniques and experimental parameters employed during the study are described.



## **II.I Research Axe I: Study and characterisation of a corpus of historical painted metal objects stored in indoor museum conditions**

As stated in the introduction, the impetus for this research stemmed from a problematic often encountered by conservation and restoration professionals: how to best conserve the composite system of painted metal present in industrial and technical museum collections? In order to understand the alteration processes at play and develop a method to prevent or delay them, a complete understanding of the material system itself must first be acquired. A representative corpus of painted metal objects showing signs of degradation needed to be assembled with the aim of characterising the original materials used and the alteration products that had formed during the life of the object.

### **II.I.I The Musée des Arts et Métiers (CNAM): organization and environmental conditions**

The large scientific and technical collections of the Musée des Arts et Métiers (“Museum of Arts and Trades”) in Paris, France contain many examples of painted metal objects of industrial heritage and were an ideal starting point for selecting a research corpus. The collections are home to a diverse selection of items that vary in size (from a few centimeters to several meters), utility (industrial, agricultural, scientific, transportation, etc), conservation state, time period and material composition (metal, wood, leather, plastic, rubber, etc). The storage facilities of the Musée des Arts et Métiers are located in a vast building designed by the architect François Deslaugiers; it was built between 1993 and 1994 and is located in Saint-Denis (north of Paris). The objects arrived in the storage facilities in 1996 after having previously been exposed in the Museum or in storerooms without a thoroughly controlled environment. They are arranged on shelving units made of a metallic structure and wooden shelves. The environmental conditions for the storage facility are set to a temperature of 18°C and a relative humidity of 45%. However, these conditions have a tendency to fluctuate with changes in the outdoor conditions. For example, the relative humidity values varied between 30-70% over a period of monitoring from October 2016 to April 2017, despite a recently renovated ventilation system (see Appendix A). The building itself is concrete with a painted floor. The lighting is primarily by fluorescent tubes which are only turned on when people are present in the premises. For air pollution and pest control, air recycling systems and green light insect traps have been installed (Insectron® Museum, Abiotec). The facilities are cleaned twice a year but only at floor level.

## II.1.II Creation of a database of painted metal objects

The first step of the study was to produce a condition survey on the state of conservation of painted metal objects located in the museum's storage facility, of which 23 have thus far been documented. This was completed with the assistance of curators and conservator-restorers from the Musée des Arts et Métiers (Rémi Catillon, Anne-Laure Carré) and from the Institut National du Patrimoine (Marie-Anne Loeper-Attia, Anne-Marie Geffroy, Marie Fays, Marie Grima, Julia Jouet). The objective was to list the materials identified on the object, to describe the observed alterations (mechanical and physicochemical), to document the observations with photographs, and to determine their state of conservation. An initial classification of alteration origin was put forward, linking the observed degradation phenomena to either instability of the paint coating or of the metal support.

Following this assessment, a database for managing the condition survey of the objects was designed with input from the curators and conservation professionals. The database is divided into four parts: identification of the object, nature of the different components (including metal and coating type), description of the mechanical and physicochemical alterations of the main components, and diagnosis of the state of degradation. A standard format of an object datasheet in the database can be seen in Table II-1.

**Table II-1 List of information collected during the condition survey and stored in the database.**

<b>Identification</b>	<ul style="list-style-type: none"> <li>• Denomination</li> <li>• Localization</li> <li>• Function</li> <li>• Type of storage</li> <li>• Size</li> <li>• Photograph</li> </ul>
<b>Materials</b>	<ul style="list-style-type: none"> <li>• Metal: <ul style="list-style-type: none"> <li>Nature of the principal metal</li> <li>Other metals: iron, copper, white metals or aluminum</li> </ul> </li> <li>• Coating: <ul style="list-style-type: none"> <li>Morphology of coating, mono or multi-layer, over or juxtaposed layer...</li> <li>Type of coating: transparent or non-transparent, paint, varnish, ...</li> </ul> </li> <li>• Other materials: organic, petroleum-based components</li> </ul>
<b>Alterations</b>	<ul style="list-style-type: none"> <li>• Mechanical and chemical degradations of the metal; uniform or localized corrosion</li> <li>• Alteration of other materials</li> <li>• Mechanical and chemical alteration of the coating: optical and physical changes of the coating such as fissures, deformation, ...</li> <li>• Presence of dust</li> </ul>
<b>Diagnosis</b>	<ul style="list-style-type: none"> <li>• Evolution of alterations: static or ongoing</li> <li>• Causes of the degradation: <ul style="list-style-type: none"> <li>Alteration due to the metal part or the coating</li> <li>Alteration due to the combination of the coating and metal</li> <li>Alteration due to the use of the object</li> </ul> </li> </ul>

### II.I.III Criteria and selection of the study corpus

The preparation of the database gathering the condition surveys of several painted metal objects present in the museum collections revealed a large range of characteristic materials and historical periods. It was decided that the selection of a study corpus for this thesis work had to be limited to certain criteria so that the scope of the study did not become too vast. The criteria were narrowed to iron-based alloys for the metal structure and oil-based paints for the coatings. The criterion for the historical date of manufacture of the objects was restrained to a period encompassing the 19<sup>th</sup> to early 20<sup>th</sup> century, due to the development of new synthetic binders for paint coatings starting in the 1920s (Stoye et al., 2010). Finally, the objects in the corpus were required to present evidence of alteration so that the degradation phenomena of the painted metal system could be analytically investigated.

By applying these criteria to the database of painted metal objects found in the museum collections, an initial list of objects was submitted to constitute the study corpus for this thesis work. Due to our intention to obtain microsamples for analytical characterisation, the objects in the list were classified by the curators of the museum by their potential for sampling (see Appendix E). This classification was based on several factors, notably the historical value of the object and its degree of alteration. Nine objects were approved to constitute the corpus of this work.

### II.I.IV Corpus description

The nine objects in the corpus are seen in Figure II-1 and are subsequently described. They are listed by their French name and their “nickname”, as they’ve been referred to during this doctoral work, is underlined in the title. The objects will be referred to by this short name for the remainder of this thesis.





Figure II-1 Photographs of the nine objects that comprise the corpus of the study: a) *Tandem*; b) *Charrue*; c) *Balance*; d) *Lanterne*; e) *Chaudière*; f) *Série*; g) *Locomotive*; h) *Châssis*; i) *Véломoteur*. More details about each object can be found in the text by their corresponding figure reference. See text for object dimensions.

*Figure I-1a. Tandem quatre places à moteur auxiliaire*

The “Quadruplette” (inv. 21811) is a unique object crafted by its inventor, Boyan Siméonoff, to accommodate the whole family on road trips; it is a four-seat bicycle supplemented by a small auxiliary motor. Designed just after World War II (1945-1950), it was given to the museum in 1965. It is a well-used object with an undocumented history of interventions. Its dimensions are 3 m (length), 80 cm (height) and 60 cm (width).

*Figure I-1b. Charrue Brabant double*

The reversible Brabant plow (inv. 17001), dated to between 1872 and 1936, is an agricultural device that was inventoried by the museum in the 1930’s, making it difficult to trace its history in the museum exhibition display. It was an exhibition model of the company Magnier-Bédu and was never used for its actual agricultural function. Its dimensions are 210 cm (length), 78 cm (width), and 106 cm (height).

*Figure I-1c. Balance de vérificateur pour 50 kilogrammes*

The weighing scale (inv. 5005) is a scientific instrument used as a 50 kg checkweight. Its historical significance is linked to the important metrological work performed by the Conservatoire National des Arts et Métiers (CNAM, Paris). It stood among the collection of weights and measures sent by the CNAM to The Great Exhibition of 1851 in London. Its dimensions are 182 cm (height), 162 cm (length) and 57 cm (width).

*Figure I-1d. Lanterne à trois feux avec volets*

The three-light acetylene gas lantern with glass panes (inv. 16726) is dated to around 1906 and entered the museum's railway collection in 1930. It is a display piece, never used for its intended industrial purpose. Its dimensions are 37.5 cm (height), 15 cm (length) and 12 cm (width).

*Figure I-1e. Maquette de chaudière de moteur*

The model of an engine boiler (inv. 36181) is of unknown provenance. It is a scale model of a large marine steam engine of British origin as shown by the name plaque and is dated to the 1880s. Its dimensions are 90 cm (length), 60 cm (height) and 60 cm (width).

*Figure I-1f. Série de 6 mesures à grains auxiliaire*

The set of six measuring containers (inv. 60005) is also of unknown provenance. It is dated to around 1850 by comparison with similar pieces in the collection. The series contains six replicates, each in the form of a cylinder with a handle on the side and were used to measure grains. The dimensions of a single measure in the set are 52 cm (height) with a diameter of 62 cm.

*Figure I-1g. Locomotive à vapeur de type 110 Planet Engine "Mathieu Murray"*

The *Mathieu Murray* locomotive (inv. 16732) is a scale model of a steam locomotive that was involved in the first major train accident in France on the 8<sup>th</sup> of May 1842 (*8 Mai 1842*, n.d.). The model, made circa 1842-1843, was used in court proceedings during the legal aftermath. It entered the museum's collection in 1930. The object measures 65 cm (height), 42 cm (length) and 36 cm (width).

*Figure I-1h. Châssis automobile système Angeli*

The automobile chassis from an Angeli system (inv. 18440) dates from 1920 and entered the museum collections in 1942. A document was found in the museum archives that discusses an intended restoration of the object; it is unknown whether this restoration took place. Its dimensions are 2 m (length), 1.50 m (width) and 1 m (height).

Figure I-1i. *Vélocycle électrique*

The Fulmen electric motorbike (inv. 20564) is a used object that had a mileage of 55000 km when it was donated to the museum in 1955. Its manufacture dates from 1932-1933. The object was restored in 2005 but the details of the intervention are unknown. Its dimensions are 1.70 m (length), 0.5 m (width) and 0.7 m (height).

The objects have different functions: they serve either an agricultural, transportation or utilities purpose (see Table II-2). Some were built to be demonstration models while others were actual working objects during their life before entering the museum collections.

Table II-2 Object functions within the study corpus.

Function	Number of objects, object name
Agricultural	1: Charrue (model)
Transportation	4: Châssis, Vélocycle, Tandem, Locomotive (model)
Utilities	4: Série, Lanterne, Balance, Chaudière (model)

## II.I.V Collection of micro-samples for analysis

Millimetre-sized samples were collected with a scalpel in inconspicuous altered areas of the previously detailed objects and contained, when possible, the corrosion products, the totality of the paint layers, and any organic top layers. Obtaining the entire painted metal system, ie. including the metal support, was more difficult due to the invasive nature and difficult sampling technique of cutting into the metal. It was possible to sample the full system on just one object, the *Vélocycle*, due to the geometry of the sampling site/location.

In total, 41 samples were collected on the 9 objects: 7 on the *Tandem*, 5 on the *Charrue*, 2 on the *Balance*, 4 on the *Lanterne*, 12 on the *Chaudière*, 5 on the *Série*, 1 on the *Locomotive*, 2 on the *Châssis*, and 3 on the *Vélocycle*. See Appendix F for sampling reports for each object that include the sampling locations.

## II.I.VI Cross-section preparation

After an initial observation of the samples using a stereomicroscope, a selection of samples representative of the coatings present on each object was chosen to be embedded in resin and prepared as cross-sections for further analysis of the stratigraphy. Table II-3 describes the samples and the number of samples that were embedded.

Table II-3 List of objects, number and types of samples obtained and number of embedded samples.

Object	Number of samples obtained	Sample Description(s)	Number of samples prepared as cross-section
<i>Tandem</i>	7	Blue paint; Green paint; Corrosion products	4
<i>Charrue</i>	5	Yellow paint on red paint; Blue paint; Corrosion products	2
<i>Balance</i>	2	Black paint on blue paint	2
<i>Lanterne</i>	4	Black paint; Corrosion products	2
<i>Chaudière</i>	12	White paint; Red paint; Black paint; Corrosion products	4
<i>Série</i>	5	Mixed black paint, orange paint, corrosion products	4
<i>Locomotive</i>	1	Black paint on grey paint	1
<i>Châssis</i>	2	Black and red-orange paint	2
<i>Vélocoteur</i>	3	Black on red paint; Black paint on metal substrate	3*

\* The sample containing the metal substrate was not embedded due to its rarity and because it already presents a view of the stratigraphy by the way it was cut while sampling.

An epoxy resin (Resineco), composed of two parts resin to one part catalyst, was prepared in order to embed the samples obtained from the historic objects. A first layer of resin was poured into silicon molds with tablet shapes and allowed to harden to create the base. The sample was then placed on the base and the remaining resin was poured slowly over top. The embedded sample was left to dry for three days. The cross-section of the embedded sample was exposed by either cutting through the middle of the sample with a diamond wire saw (Escil model W3032) to produce two faces or polished down from the end of the resin tablet to obtain just one face. The diamond wire saw had a wire diameter of 130  $\mu\text{m}$  and the granulometry of the diamond particles was 20  $\mu\text{m}$ . In cases where two cross-section faces of a sample were prepared, they are referred to as faces A and B of the sample in question (for example: Tandem P03A and Tandem P03B). A mirror finish of the cross-sections was obtained by polishing using the Struers TegraPol-35 polisher with several subsequent SiC abrasive papers starting from a grit size of 1200 to 4000 (particle size 14  $\mu\text{m}$ -5  $\mu\text{m}$ , respectively). Final polishing was completed by hand using diamond pastes with granulometries of a 3  $\mu\text{m}$ , 1  $\mu\text{m}$ , and finally ¼  $\mu\text{m}$ . Ethanol was used as a lubricant to avoid using water. After polishing, the samples were rinsed with ethanol and dried using compressed air. In a few cases (fragments of samples from the *Locomotive* and the *Vélocoteur*), the black paint present in the sample partly dissolved when it was embedded in resin, inhibiting the ability to study the cross-section of these samples.

## II.II Research Axe II: Study of the effectiveness of conservation treatments on a model painted metal system

The aim of this research axe was to study the protective effect of conservation treatments used on the aged painted metal system. Two conservation treatments currently in use by professionals for the stabilization of either the paint or the metal alone were selected for testing. This study addresses several key questions:

- Does the treatment for the stabilization of the metal interact with the paint coating?
- How do the treatments age when exposed to specific environmental conditions?
- Do the treatments show significant protective behaviour (defined as preservation of the original structure of the paint) of the painted metal system when exposed to environmental conditions that normally lead to aging of the untreated system?

The answers to these questions depend on the composition of the painted metal system, the type of conservation treatment, and the environmental conditions, and the three may often have a combined effect. To differentiate and understand the influence of the different factors, the system must first be studied in a simplified form. An experimental protocol was designed in which the conservation treatments were applied to model coupons representing a basic treated painted metal system and were then submitted to artificial aging conditions in order to test the protective effect of the treatments in a controlled manner. Different experimental conditions were tested to study the impact of varying certain parameters. The details of the experimental design are explained in the following sections.

### II.II.I Choice of representative materials for the model coupons

To parallel the selection criteria for the material composition of the historical objects selected for our study corpus (see II.I Research Axe I: Study and characterisation of a corpus of historical painted metal objects), a model painted metal system composed of an iron-based metallic coupon coated with a layer of paint was prepared, where the paint is composed of a single pigment dispersed in a binder. Boiled linseed oil (from Sennelier) was chosen for the binder because of its historical use in the preparation of coatings for metals (Schroter, 2009). The pigments were chosen so that aesthetic colour changes such as yellowing or lightening/darkening of the paint could be observed. For this, a light and a dark-coloured pigment were chosen. Basic lead (II) carbonate, commonly known as **lead white** (from Alfa Aesar) was selected for the light-coloured pigment because lead-based pigments are often used in coatings for metal (Schroter, 2008). Chromium (III) oxide, also known as chrome oxide green or **chromium green**

**oxide** (from Kremer), was chosen as the dark-coloured pigment due to the presence of dark green coatings on many of the historical painted metal objects in the museum collections. Three types of model coupons were prepared: one series using lead white pigment and linseed oil (LW coupons); a second using chromium green oxide pigment and linseed oil (CrGO coupons); and a third where the linseed oil binder was applied without pigment to one half of the metal coupon, leaving the other half exposed as bare metal (LO coupons). The last-mentioned type serves as a reference series of coupons for comparison with the painted coupons.

### II.II.II Preparation of model painted metal coupons

63 soft iron coupons (45x100mm) were polished using silicon carbide grinding paper (grit 220) to remove corrosion and grease, as well as to ensure a good adhesion for the paint coating. They were pierced near the top (intended to allow for possible suspension during artificial aging) and their corresponding number was engraved on the backside. Each coupon was cleaned for two minutes in an ultrasonic bath (Fisher Scientific FB 15051) with ethanol to remove any adhering particles and dried using compressed air.

The white pigment lead (II) carbonate  $(\text{PbCO}_3)_2 \cdot \text{Pb}(\text{OH})_2$  was obtained from Alfa Aesar and the green pigment chrome (III) oxide  $\text{Cr}_2\text{O}_3$  was obtained from Kremer Pigmente. Boiled linseed oil was obtained from Sennelier. The pigments were ground in a mortar and mixed with the oil binder until a homogeneous mixture was obtained. The amounts of pigment and binder used are listed in Table II-4.

**Table II-4 Quantities used for the preparation of the paint coatings.**

Pigment	Mass of pigment	Mass of binder	Oil absorption
Lead (II) Carbonate - $(\text{PbCO}_3)_2 \cdot \text{Pb}(\text{OH})_2$ (Alfa Aesar®)	50.525 g	10.512 g	20.8 %
Chrome (III) Oxide - $\text{Cr}_2\text{O}_3$ (Kremer Pigmente®)	20.210 g	6.492 g	32 %

Adhesive tape was applied around the border of the coupons with a width of about 5 mm from the edge. The paint was then applied using a paintbrush (model Leonard n°6, Gerstaecker) in a manner as to be as uniform and homogeneous as possible: starting from the top corner, brushstrokes were made first widthwise from left to right, then lengthwise from top to bottom. Only one layer was applied. The control coupons were painted with the oil binder only, following the same method. The tape was then removed and remaining adhesive residue was cleaned using ethanol. The coupons were stored in a lightproof oven at room temperature with silica gel and left to air-dry for 8 days.

In total, 63 painted metal coupons were prepared, where 24 were painted with a lead white oil paint, 12 were painted with a chrome green oxide oil paint, and 24 were coated with the linseed oil-binder

alone. Three extra coupons remained and were painted with a swatch of each type of coating. See Figure II-2 for examples of the coupons.

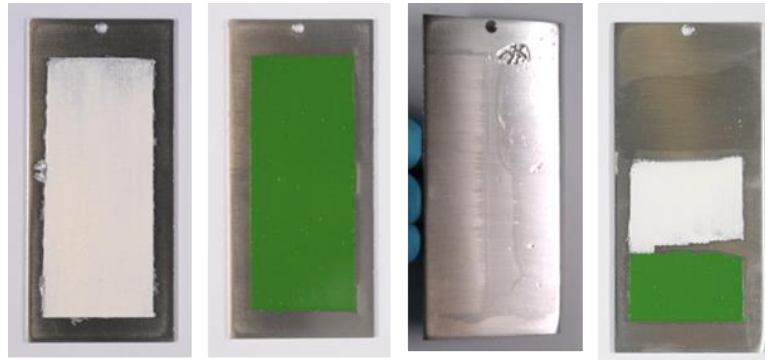


Figure II-2 Examples of metal coupons painted with (from left to right): lead white oil paint, chrome green oxide oil paint, linseed oil, and a coupon with swatches of the three coatings. Coupons measure 45 mm x 100 mm.

### II.II.III Initial state of samples: fresh vs pre-aged, and natural aging

In order to simulate an application of the conservation treatments on historic painted metal objects with various states of alteration, a “fresh” (representing a relatively young object) and “pre-aged” (representing an older, naturally aged object) set of each type of model coupon was prepared before application of the conservation treatments.

The pre-aged model coupons were exposed to four cycles (24 hours/cycle) of alternating climatic conditions, where one cycle consisted of 16 hours of a wet phase and 8 hours of a dry phase. Saturated salt solutions were used to achieve a constant relative humidity at set temperatures (Greenspan, 1977). The wet phase was carried out in an oven set at 50°C in which a container holding a saturated solution of  $K_2SO_4$  created a relative humidity of 97%. The dry phase was carried out at ambient temperature (20°C) in a benchtop desiccator cabinet in which a saturated solution of  $K_2CO_3$  was placed to produce a relative humidity of 44%. The samples were transferred between the two environments for four days, and the treatment ended with 88 hours of constant wet phase conditions. The variation in relative humidity over the entire pre-aging experiment is shown in Figure II-3.

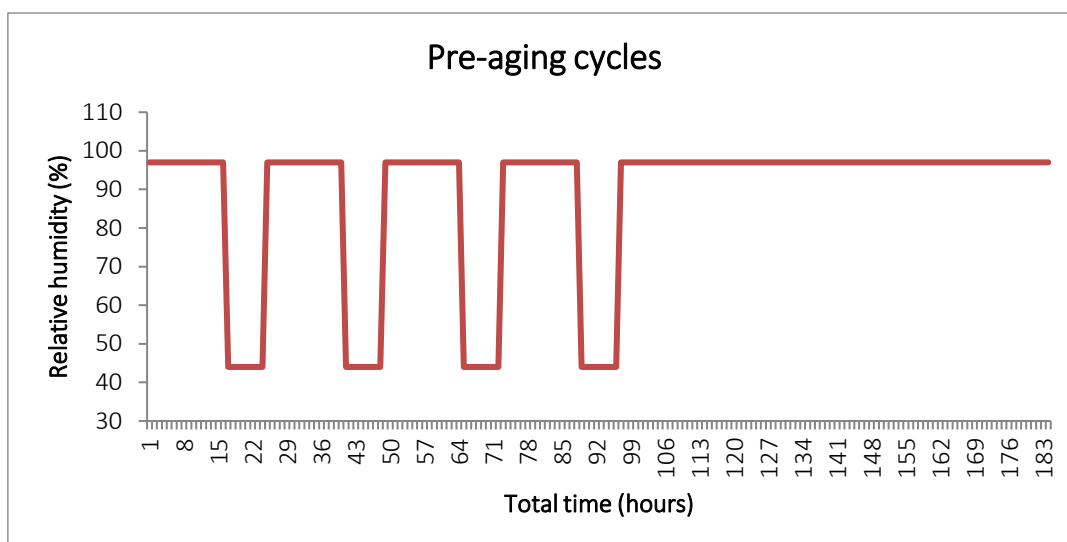


Figure II-3 Graphical representation of the variations in relative humidity (%) over time during the artificial pre-aging treatment.

**Comment on the chronology of this work:** The preparation of the model coupons and the pre-aging treatment was conducted in a first stage of the project, before this thesis. Therefore, in addition to the pre-aging treatments, all of the coupons experienced 1.5 years of natural aging. During this transition period, all coupons were stored in a closed laboratory cupboard in ambient conditions and were not exposed to light.

After the 1.5 years of natural aging, corrosion products were observed to have formed on the exposed metal border of the painted coupons that had experience the pre-aging treatment; Raman analysis confirmed the products to be those expected from atmospheric corrosion. Following the recommendations of a metal restoration specialist (Marie-Anne Loeper-Attia), a fibre-glass brush was used to mechanically remove the corrosion that formed on the bare metal surrounding the painted area prior to applying the conservation treatments. An airgun was used to remove the corrosion dust residue from the coupons after cleaning to prevent contamination of the paint layer.

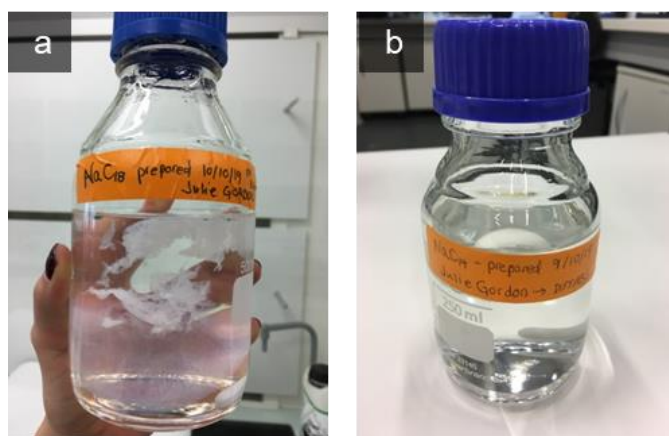
Before applying the conservation treatments, a “scratch” was made in the paint layer using a scalpel to trace a cut lengthwise down the middle of the paint layer. It is meant to simulate a mechanical scratch that could happen during handling and opens a direct pathway for possible corrosive agents to access the underlying metal (Li & Leroux, 2016).



## II.II.IV Choice of conservation treatments

Two conservation treatments were chosen for this study: a protective coating composed of a resin-wax mixture, generally used for painted surfaces, and a long-chain carboxylate solution that functions as a corrosion inhibitor by stabilizing the metal support. The idea was to choose treatments that use different mechanisms of protection. The coating dries after application to form an impermeable barrier to external environmental factors while the corrosion inhibitor protects the metal surface by forming a thin passive layer.

The initial options for the choice of a corrosion inhibitor to test included sodium carboxylates  $\text{NaC}_{10}$  (most frequently studied in the literature),  $\text{NaC}_{12}$  or Vegerust (a commercial product containing  $\text{NaC}_{18}$  and other unknown components).  $\text{NaC}_{18}$  was initially selected for this project because the efficacy of protection of sodium carboxylates should increase with the alkyl chain length (Mirambet et al., 2004). However, the solubility of these compounds decreases with the increasing chain length, and preparation of a homogeneous solution of  $\text{NaC}_{18}$  was not achieved (Figure II-4a). A compromise between solubility and chain length was achieved with  $\text{NaC}_{14}$  instead (Figure II-4b); this was the carboxylate used as the tested corrosion inhibitor treatment on the metal coupons. The solution was prepared with a concentration of 0.05 M, as per the literature which has shown that there is no significant increase in efficacy of protection above this concentration (Hollner, 2009).



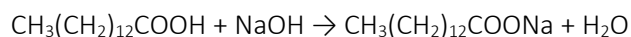
**Figure II-4 Sodium carboxylate solutions prepared during this thesis: a) The 0.05 M  $\text{NaC}_{18}$  solution shows problems with solubility and the formation of soaps; b) A homogeneous fully dissolved solution of 0.05 M  $\text{NaC}_{14}$ .**

The choice for the composition of the resin-wax mixture was based on the results of a previous study (Schroter, 2008) which showed good results on metal coupons painted with a lead white paint. In the study, a 30:10 wt% mixture of Regalrez 1126® resin and Cosmoloid H80® microcrystalline wax dissolved in toluene was used. However, due to the toxicity of toluene, petroleum benzine (a type of white spirit with low aromatic content) was selected for the solvent in this study.

## II.II.V Preparation and application of the conservation treatments

Presented here is a basic overview of the preparation of the conservation treatments. See Appendix C and Appendix D for the detailed preparation protocols.

A 0.05 M solution of the **corrosion inhibitor** sodium tetradecanoate ( $\text{NaC}_{14}$ ) was prepared from tetradecanoic acid ( $\text{HC}_{14}$ ) and sodium hydroxide ( $\text{NaOH}$ ) according to the following balanced equation:



2.8546 g of  $\text{HC}_{14}$  was added to 250 mL of a 2:1 solution of ethanol:water to improve the solubility of the long-chain fatty acid. The solution was stirred and heated to 40°C during addition of the acid. 0.5 M  $\text{NaOH}$  was added in a dropwise manner until all of the  $\text{HC}_{14}$  had dissolved and a pH of 8.5-9.5 was reached. The solution was stored in an airtight glass bottle in a dark laboratory cupboard.

The **resin-wax mixture** Regalrez 1126®-Cosmoloid H80® (30:10 wt%) was chosen for the coating. Petroleum benzene was used as the solvent. 10 g of the Cosmoloid H80® wax pellets (from Kremer Pigmente) were weighed and added to 60 g of the solvent and left to sit for a few hours. The mixture was then heated to 70°C to dissolve the wax. 30 g of the Regalrez 1126® resin pellets (from CTS Europe) were wrapped in a gauze sheet and suspended in the mixture for two days to allow the resin to swell before being added to the mixture. The resin-wax mixture was stored in an airtight glass bottle.

The coupons were treated with either the corrosion inhibitor or the resin-wax mixture (see Table II-5 for assignments). Prior to application, an airgun was used to remove any dust or debris from the surface of the coupon. The resin-wax mixture was stirring continuously during the application to ensure that the components were fully mixed (Figure II-5a). The conservation treatments were applied by paintbrush as per standard practice in the restoration field (Schroter, 2008). The brush was dipped once in treatment, wiped on the rim of the beaker to remove excess product and then applied to the bottom half of the painted surface (Figure II-5b).

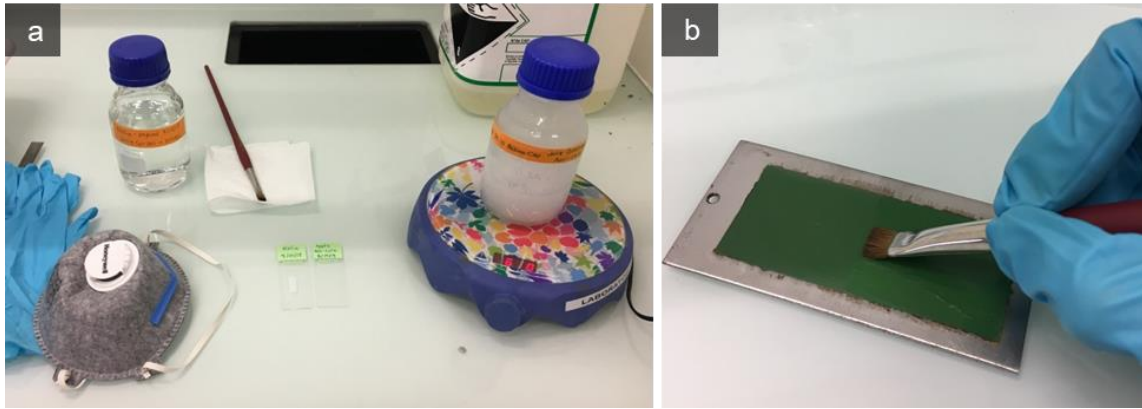


Figure II-5 Application of conservation treatments: a) Equipment and solutions of corrosion inhibitor (left) and resin-wax mixture (right); b) Application of the treatment by paint brush to the lower half of the painted surface of the model coupon.

Only one half of the painted surface was treated to allow us to study and compare the aging of the painted metal surfaces with and without the conservation treatment (Figure II-6). In the case of the coupons with a small swatch of each coating type (Figure II-2), the product was applied to the right side of the paint swatch (with respect to the pierced hole at the top of the coupon). The application procedure for each type of coupon were kept as constant as possible to create reproducible and comparable results. The coupons were laid flat in a plastic tub and covered with a paper sheet. They were dry in 1-2 days.

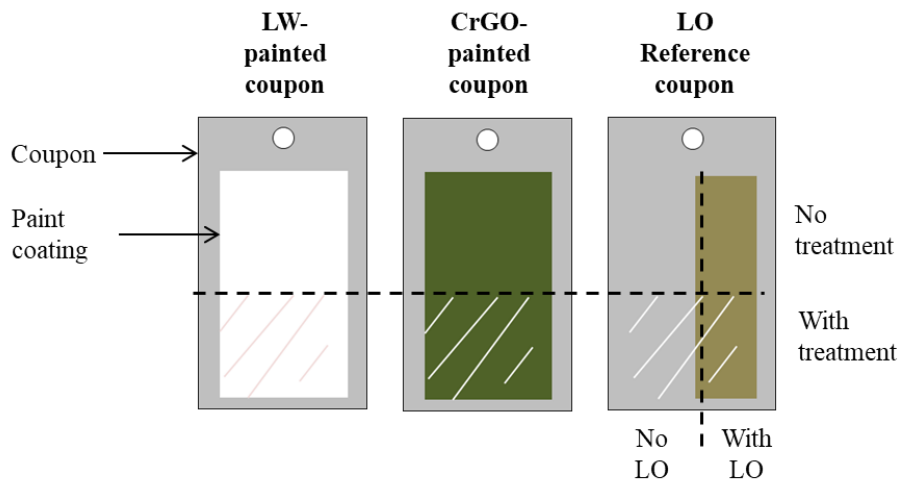


Figure II-6 Schematic representation of the painted metal coupons, showing the areas covered by the paint coating (lead white (LW)-based paint, chrome green oxide (CrGO)-based paint, the oil binder (linseed oil (LO) on the reference model) and the zones where the conservation treatments were applied.

## II.II.VI Choice of artificial aging parameters

Artificial aging was used to accelerate the degradation of the materials to study the effectiveness of the conservation treatments on the painted metal system in the time available for this project. While it is not equivalent to natural aging, it permits to simulate the behaviour of the system in response to known aging factors present in storage facilities. Two types of environmental stressors were chosen for the study: climatic cycles and light exposure. Paint is sensitive to variations in relative humidity (RH), low or high temperatures, and exposure to light, while metal is mainly sensitive to variations in relative humidity. In order to force the aging of the model coupons, harsh conditions of relative humidity and light exposure were applied. These aging factors have different effects on the degradation of the materials and were tested separately to simplify the interpretation of the findings.

### Relative humidity cycles

One set of model coupons was artificially aged by undergoing climatic cycles based on variations in relative humidity (RH). The conditions for the relative humidity cycles were derived from those used in the POINT project (see I.II.III Methods for testing conservation treatments) and were adapted to painted metals in our study by decreasing the lower limit of the RH cycles to 33%, i.e. below the recommended lower limit of 40% RH for painted metals (Canadian Conservation Institute, 2017).

One cycle consisted of 16 hours of a wet phase (97% RH) followed by 8 hours a dry phase (33.1% RH), for a total of 24 hours/cycle. The wet phase was carried out in an oven set at 50°C in which a container holding a saturated solution of  $K_2SO_4$  created a relative humidity of 97%. The dry phase was carried out at ambient temperature (20°C) in a benchtop desiccator cabinet in which a saturated solution of  $MgCl_2$  was placed to produce a relative humidity of 33.1%. The samples were transferred between the two environments during the work week and were left in the wet phase conditions outside of the laboratory's working hours.

The samples were exposed to the RH cycles for an initial phase of 3 weeks (Phase I). FTIR analysis of the coupons after Phase I indicated minimal changes in the composition of the paint film so the samples were submitted to a second aging period of 6 weeks (Phase II) to increase their degradation. These alteration phases took place over the following periods:

- Phase 1: October 21 to November 12, 2019 (3 weeks).
- Phase 2: Feb 2020 (3 weeks), June-July 2020 (3 weeks).

### **Light exposure aging**

A second set of samples were artificially aged by light exposure. The purpose is to accelerate the photoaging of the samples by using intense light exposure conditions in order to investigate the effect of the presence of the conservation treatments on any aesthetic and chemical changes. According to Feller (Feller, 1994), the shortest wavelength in sunlight is 290 nm; this increases to 315 nm if it passes through a window (in the case of indirect sunlight exposure). These are the lower limits of wavelength to be considered in accelerated light aging. No UV filters were used for this reason. The samples were laid flat in a benchtop xenon arc weathering-testing instrument (ATLAS Sunset XLS+) and left for 21 days (504 hours) with the following parameters:

- Energy range: 300-800 nm continuous spectrum.
- Intensity: 400 W/m<sup>2</sup>.
- Filters: none.
- Temperature: 35°C.

The samples received a total radiant exposure of 725,760 kJ/m<sup>2</sup>. The total exposure delivered to the painted metal samples was severe to ensure a degradation of the materials.

## II.II.VII Summary of experimental design for Axe II

The aged and treated painted metal model coupons were prepared by the following steps:

1. Cut and polish metal coupons.
2. Preparation of paint: lead white (LW) or chrome green oxide (CrGO) pigments in linseed oil.
3. Application of paints or linseed oil binder to coupons.
4. Pre-aging cycles (half the coupons).
5. Cleaning of corrosion on the non-painted edges on the front side of coupons.
6. Longitudinal “scratch” along centre of painted surface.
7. Application of conservation treatment: corrosion inhibitor (CI) or resin-wax mixture (RW).
8. Artificial aging cycles: relative humidity cycles or light exposure.

The full methodology is represented graphically in Figure II-7.

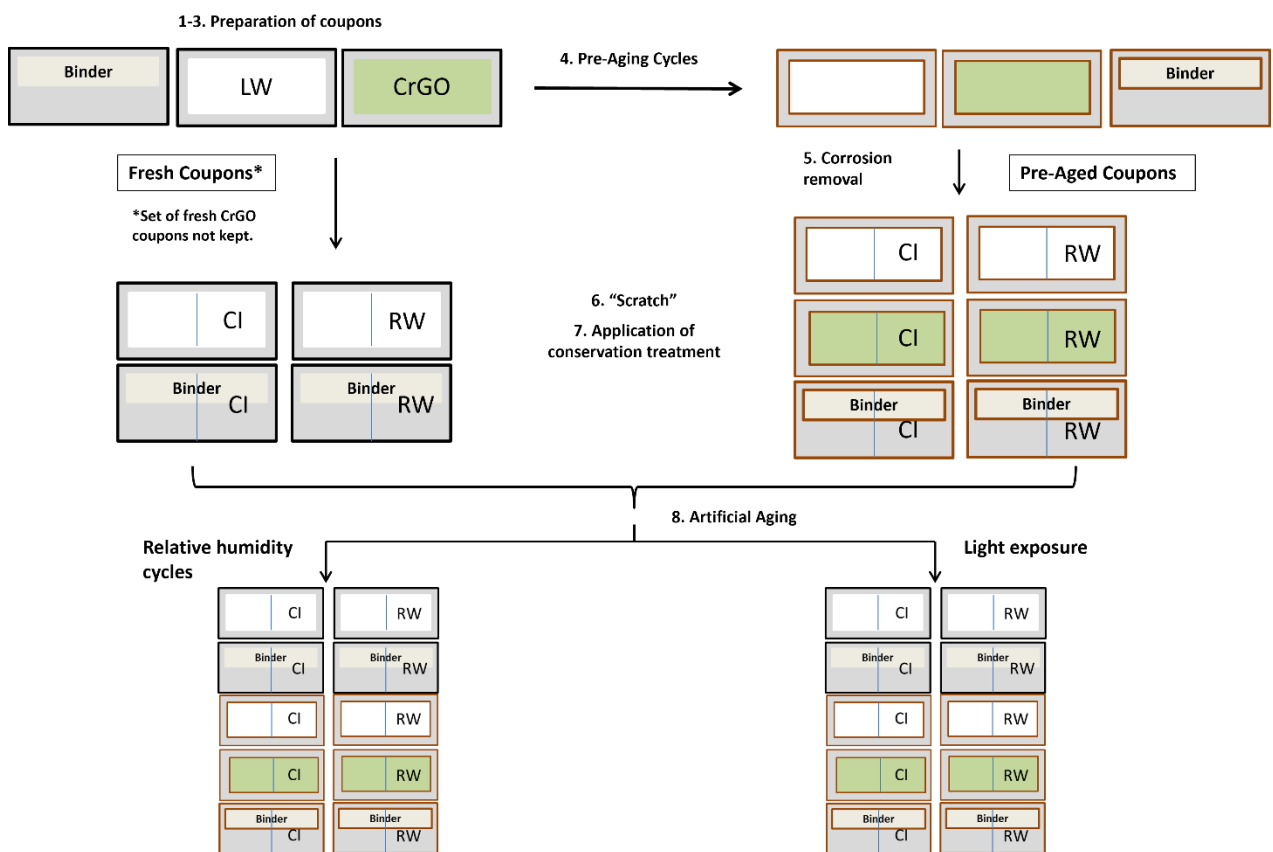


Figure II-7 Schematic diagram of the preparation and aging steps of the painted metal model coupons. Numbers 1-8 correspond to the protocol steps listed in the text. Coupons were painted with lead white (LW) or chrome green oxide (CrGO)-based paint, or the linseed oil binder. Coupons were treated with either the corrosion inhibitor (CI) or the resin-wax mixture (RW).

In total, 63 painted metal coupons were prepared with either a lead white or chrome green oxide-based paint or a linseed oil binder coating. Three coupons were painted with a swatch of each type of coating. For each type of coupon, experimental combinations were designed by varying the initial state of alteration (“fresh” or “pre-aged”), the type of conservation treatment (corrosion inhibitor or resin-wax mixture), and the type of artificial aging conditions (relative humidity cycles or light exposure). Three replicates per experimental combination were prepared. The coupons are numbered 1 to 63 and their corresponding experimental treatment can be found in Table II-5.

**Table II-5 Numerical assignment of the model samples and their corresponding experimental conditions. LW: lead white-based paint; CrGO: chrome green oxide-based paint; LO: linseed oil binder coating.**

Aging	Relative humidity (RH) cycles											
Treatment	Corrosion inhibitor						Resin-wax mixture					
Initial state	Fresh			Pre-aged			Fresh			Pre-aged		
Coating type	LW	CrGO	LO	LW	CrGO	LO	LW	CrGO	LO	LW	CrGO	LO
Coupons numbers	1		25	4	49	28	7		31	10	52	34
	2	62	26	5	50	29	8	63	32	11	53	35
	3		27	6	51	30	9		33	12	54	36
Aging	Light (LT) exposure											
Treatment	Corrosion inhibitor						Resin-wax mixture					
Initial state	Fresh			Pre-aged			Fresh			Pre-aged		
Coating type	LW	CrGO	LO	LW	CrGO	LO	LW	CrGO	LO	LW	CrGO	LO
Coupons numbers	13		37	16	55	40	19		43	22	58	46
	14	-	38	17	56	41	20	-	44	23	59	47
	15		39	18	57	42	21		45	24	60	48

Only pre-aged versions of the full-sized chrome green oxide-painted coupons were prepared. The swatches of green paint on coupons 62 and 63 served as sources of fresh chrome green oxide paint coating; they were treated with either of the two conservation treatments along the right half of the paint swatch and were aged by relative humidity cycles. Observations and measurements of coupons 62 and 63 allowed to obtain data for fresh chrome green oxide paint that could be compared with the pre-aged coupons that otherwise experienced the same experimental conditions.

The coupons and representative datasets will be referred to in the text using a short form notation comprised of abbreviations that represent their corresponding experimental treatment. The abbreviations are defined in Table II-6.

Table II-6 List of experimental variables applied to model coupons and corresponding abbreviations.

Experimental parameter	Variables	Abbreviation
Pigment/Type of coating	Lead white/Lead white-based paint	LW
	Chrome green oxide/ Chrome green oxide-based paint	CrGO
	Linseed oil	LO
Initial state of alteration	Fresh	f
	Pre-aged	pa
Conservation treatment	Corrosion inhibitor	CI
	Resin-wax mixture	RW
Artificial aging type	Relative humidity cycles	RH
	Light exposure aging	LT

For example, using the correlation table (Table II-5) we see that coupon 4 is a lead white (LW)-painted coupon that has been pre-aged (pa), treated with the corrosion inhibitor (CI), and artificially aged by relative humidity cycles (RH). In the text, data acquired from the treated zone of coupon 4 will be referred to as LW.pa.CI.RH. The untreated zone on the same coupon will be referred to as LW.pa.RH. As there are several replicate coupons (at least 3) that may be described with the same code, the exact coupon number may also be used in the text when it is necessary to specify which sample was observed/measured.



## II.III Analytical strategy

Several complementary multi-scale analytical techniques were employed in this work to characterise the studied samples. The choice of technique was dependent on the type and form of sample, and the information sought. The samples from both research axes contain aged forms of the painted metal system (the model coupons being a much simpler form of the historical samples), meaning the presence of a variety of inorganic and organic compounds including pigments, corrosion products, and binders, and so the applied analytical strategy must be able to characterise all of these different components. Additionally, despite the choice of appropriate and specific techniques, analysis by just one technique might not be sufficient to fully identify a component. Different aspects of the components, such as physical characteristics, morphology, elemental composition, and chemical structure need to be studied and compared to fully understand and characterise the studied system. Another point to be highlighted is the need for multi-scale techniques and imaging techniques. The samples, especially the historical artefacts, are heterogeneous at multiple scales, and the analytical techniques must be able to probe the full extent of these heterogeneities. Of particular interest are the analyses conducted in imaging mode which allow to visualize the distribution of these differences at different scales. Therefore, multi-scale complementary techniques were employed depending on the analytical objectives, which were principally the characterisation of original materials or of alteration products.

The two research axes address different cases and aspects of the painted metal system, necessitating unique analytical methodologies. The strategies will be explained separately in the following paragraphs.

### **Axe I strategy: Characterisation of historic painted metal samples**

While visual observation of the historical objects can provide a good starting point for understanding the different characteristics of the painted metal system, including the physical aspects of the metal and the paint, the layer structure and the state of alteration, these observations need to be supplemented with micro-scale analytical measurements in order to properly characterise the different structural, physical and chemical aspects of the system. This requires obtaining micro-samples from the historical objects which can be analysed directly or as embedded cross-sections in order to observe and analyze the stratigraphy of the system. It is of particular interest to study the stratigraphy which allows to properly describe the layer structure of the system, to identify the distribution of the material components with respect to one another, and to visualize degradation phenomena at the micro-scale within the painted-metal system. Studying the interfaces of the paint layers and of the paint coating

with the corrosion layer (if present) permits to describe how the layers of different composition interact with each other.

To fully characterise both the original materials as well as the degradation products present in the historic samples, an analytical strategy was implemented to identify the following aspects:

- Morphology.
- Elemental composition.
- Chemical structure.

Due to the composite nature of the painted metal samples, which contain multiple components of both organic and inorganic nature, several instrumental techniques were employed. Table II-7 presents a list of the primary and secondary (applied when complementary information was required) techniques employed in Axe I.

**Table II-7 Analytical techniques used to study different characteristic aspects of the historic samples.**

	<b>Morphology</b>	<b>Elemental composition</b>	<b>Chemical structure</b>
<b>Primary techniques (base analytical strategy)</b>	Stereomicroscope  Optical Microscopy (OM) – light and fluorescence	Micro- X-Ray Fluorescence ( $\mu$ XRF)	Micro- Raman spectroscopy (Raman)  Micro- X-Ray Absorption Near-Edge Structure Spectroscopy ( $\mu$ XANES)  Gas Chromatography coupled to Mass Spectrometry (GC-MS)
<b>Secondary techniques (applied when complementary information is required)</b>	Scanning Electron Microscopy (SEM)	Energy Dispersive X-ray Spectroscopy coupled to SEM (SEM-EDS)	Fourier Transform Infrared Spectroscopy (FTIR)  Micro- X-Ray Diffraction ( $\mu$ XRD)  Deep-UV Photoluminescence (DUV-PL) imaging

The general analytical strategy was to first observe and photograph the samples using a stereomicroscope or at a smaller scale using an optical microscope under visible and UV light to describe the morphology of the stratigraphy and to distinguish the different layers present. The sample cross-sections were mapped using synchrotron micro-X-Ray Fluorescence ( $\mu$ XRF) which allowed to determine the elemental distribution of the stratigraphy and therefore the composition in each previously defined layer. A few samples were also imaged using scanning electron microscopy (SEM) for a high-resolution visualization of contrast in morphology or composition, depending on the detection mode used. The

samples that were imaged by scanning electron microscopy were also mapped using energy-dispersive x-ray spectroscopy (SEM-EDS). The combination of XRF and EDS used under different environmental conditions (atmosphere or vacuum), at different excitation energies and at different scales allows to determine the exact elemental composition of the samples, including major and trace elements, light and heavy elements, etc.

The chemical structure of the phases present was investigated using both spectroscopic and separative techniques. Raman spectroscopy was used to determine the characteristic vibrational signature of the analysed material, which was matched with reference spectra from the literature to identify the phases present; it was mainly used to characterise the pigments and corrosion products present in the different layers. For certain elements of interest, such as Pb or Zn which were often identified in pigments in the paint layers, or Fe which is found in the corrosion products, micro-X-ray absorption spectroscopy ( $\mu$ XANES) was used to probe the chemical environment of these specific elements. It is a powerful tool for selective analysis within a complex mixture of phases such as the paint layers. The information gained from this technique is complementary to the Raman analyses as it can detect the same principal phases, but it is more sensitive to changes in bonding or structure around the probed element which can be suggestive of the occurrence of degradative processes.

To further investigate possible degradation products in the paint layers, in particular metal soaps which may result from the interaction of lead and zinc-based pigments with fatty acids from the oil binder, the distribution of the molecular species within the paint layers of some sample cross-sections was observed using high-resolution synchrotron deep-UV photoluminescence (DUV-PL) imaging. Finally, to characterise the organic content of the samples, gas chromatography coupled to mass spectroscopy (GC-MS) was used to obtain a separation and identification of the components. The presence of individual or groups of chemical species which are characteristic of the composition of a certain family or type of material were used to identify the binder, varnish and/or organic pigments present in the analysed sample. Separation of the distinct layers within the samples was attempted but not achieved, therefore the chromatographic results are representative of all the paint layers present in the samples and do not contain information on the distribution of the components within the respective stratigraphies. Fourier Transform Infrared Spectroscopy (FTIR) was used to characterise the binder of some paint samples obtained from the museum objects; this was not applied to all the samples however due to the better discrimination of materials obtained via GC-MS analysis.

Depending on the techniques and the information of interest, measurements were acquired as point analyses, imaging or mapping mode. The latter two combine chemical/structural information with spatial distribution, allowing us to interpret the results in the context of the sample layer structure. Point

analyses were acquired in zones of interest (e.g. within specific layers, at interfaces, in areas presenting different characteristics to the bulk) to identify the materials present specifically at these positions.

**Axe II strategy: Evaluation of the protective effect of conservation treatments on the aging of the model painted metal system**

The main analytical objective was to understand the effect of the presence of the tested conservation treatments on the evolution of the painted metal coupons throughout artificial aging. Various aspects may indicate an evolution, including changes in visual aspect, colour and/or chemical structure. A multi-scale combination of appropriate techniques, listed in Table II-8, was used to observe these aspects at each step of the experimental procedure. The collected observations/measurements acquired on the untreated and treated paint coatings at each step were compared to determine the effectiveness of protection of the conservation treatments on the painted metal system in different experimental conditions.

**Table II-8 Aspects of interest in the evolution of the model painted metal coupons and the analytical techniques used to monitor the evolution.**

Aspect investigated	Technique used
Visual appearance	Photography
	Optical microscopy
Colour of paint coating	Colorimetry
Chemical structure	Fourier-Transform Infrared Spectroscopy (FTIR)
	X-Ray Absorption Near-Edge Structure Spectroscopy (XANES)

## II.IV Characterisation techniques

### II.IV.I Photographic monitoring

Photographs of the model samples were taken after every step of the aging protocol. The same camera and lighting conditions were applied each time by using a copy stand. The lamps were set at a distance of 35 cm and an angle of 45° with respect to the samples. Due to the difference in reflectivity of the painted surface and the metal border, the samples were sometimes tilted by hand to improve the visibility of the surface.

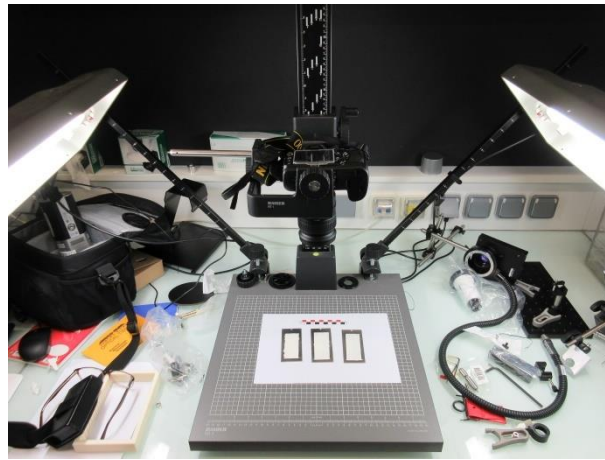


Figure II-8 Copy stand used to photograph the evolution of the model samples.

### II.IV.II Colorimetry

The measurement of colour is a complex idea because colour is a perceived phenomenon. Its perception is based on three elements: a light source, an object and an observer. To compare colours, it is necessary to have a standardized system for the characterisation of colour. Such a system was developed that is based upon the trichromatic specification of colour. Colour specification can be achieved by defining a colour stimulus (a perceived colour) as the additive mixture of the amounts (intensities) of three primaries. Often, the three primaries are red, green and blue as their addition gives the largest possible number of colour combinations (Westland, 2016). The specific set of relative intensities of each primary required to “match” a given colour are referred to as tristimulus values. Hence, tristimulus values constitute a colorimetric specification.

If the tristimulus values are considered as vector components, a three-dimensional representation of colour can be constructed and is called a colour space. In 1976, the *Commission Internationale de l'Eclairage* (CIE) developed a colorimetric system based on these principles known as CIELAB.

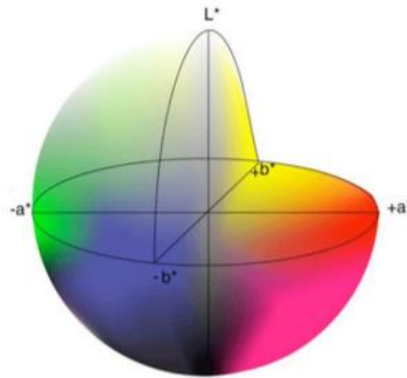


Figure II-9 3D representation of the CIELAB colour space, from (Moghaddam et al., 2013).

The colour space (Figure II-9) is uniform (the distance between two points is proportional to the colour difference between two colours represented by those points) and is defined by the coordinates  $L^*$ ,  $a^*$  and  $b^*$ :

- $L^*$  axis: luminance (roughly correlated to “lightness”) ( $L^* = 0 =$  black stimuli,  $+L^* =$  white stimuli).
- $a^*$  axis: red-green axis ( $+a^* =$  red colour stimuli,  $-a^* =$  green colour stimuli).
- $b^*$  axis: yellow-blue axis ( $+b^* =$  yellow colour stimuli,  $-b^* =$  blue colour stimuli).

Perceived colour difference can roughly be measured by the equation:

$$\Delta E_{ab}^* = [(\Delta L^*)^2 + (\Delta a^*)^2 + (\Delta b^*)^2]^{1/2}$$

Where coordinate differences in colour space are calculated as follows:

$$\Delta L^* = L_1^* - L_0^*$$

$$\Delta a^* = a_1^* - a_0^*$$

$$\Delta b^* = b_1^* - b_0^*$$

$\Delta E_{ab}^*$  represents the Euclidean difference between two sets of coordinates (representing two colour stimuli) in the colour space. The  $\Delta E^*$  values do not contain information about what aspects of the colour stimuli are different; to determine this, the differences in the  $L^*$ ,  $a^*$  and  $b^*$  should be considered.

The formulae of the CIE 1976 LAB system have been corrected over the years as the original colour space was found to be non-uniform for saturated colours; however, the formulae became much more complex. The 1976  $\Delta E_{ab}^*$  formula shown here has the convenience of being a simple calculation that can still be used for colour comparisons that do not require a high degree of accuracy.

Colour can be measured using a spectrophotometer that makes use of a colorimetric system. The characterisation of colour requires defining a standard observer, a standard illuminant, a measuring geometry and a reference standard (Schanda, 2007). The standard observer is defined by its colorimetric functions; in this case the CIELAB system is used. The standard illuminant/source has a specific spectral distribution. To simulate daylight, the standard illuminant CIE D65 is often used. A measuring geometry of 2° is close to the perpendicular observation of colour but permits to measure the reflected signal with the scattering component included (SCI) or excluded (SCE). The reference standard is a perfect reflecting diffuser, such as a pressed powder of magnesium oxide or barium sulfate.

#### **Instrumentation and measurement parameters**

A Konica Minolta CM-700D spectrophotometer was used to collect colour measurements of the untreated and treated zones of the painted surface of the model metal coupons. The standard illuminant used was D65 and the standard observer was 2°. The light source is a pulsed xenon lamp with a UV cut filter. It contains a diffraction grating and a silicon photodiode array detector for measurement of the reflectance spectrum. A white calibration was completed before beginning measurements. The measured point was 8 mm in diameter. Measurements were acquired in three points per zone, where each measurement is an average of 5 acquisitions. Each acquisition includes the CIE L\*, a\* and b\* colour space values as well as the reflectance spectrum over the range of 360 to 740 nm.

#### **Just Noticeable Difference (JND)**

Conventions exist for defining whether a colour difference is significant, or “perceptible”. In this work, the threshold of a  $\Delta E^*_{ab} > 2.3$  (G. Sharma & Bala, 2017) is used to define the lower limit of a “Just Noticeable Difference” (JND) in colour. This value is very approximate and is less accurate for more saturated colours. Other sources define a “perceptible at a glance” colour difference with a larger range of values, where  $\Delta E^*_{ab}$  is between 2 and 10 (Graphic Communications Open Textbook Collective, 2015).

### **II.IV.III Measurement of paint coating thickness**

A Sylvac Calibration Standard Dial Gauge (Figure II-10) was used to measure the coating thickness on the model samples. The thickness of the paint or oil binder coating on the metal coupon was measured once dry. Pairs of measurements of the coating and adjacent bare metal substrate were acquired and the difference was calculated as a rough estimate of the thickness of the coating. Three measurements per sample were acquired and averaged and this was repeated for three replicates per type of painted metal coupon (LW painted, CrGO painted, LO coated).

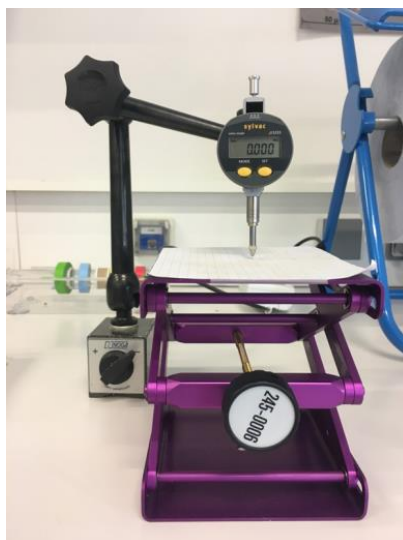


Figure II-10 Experimental setup of the dial gauge used to measure the coating thickness.

#### II.IV.IV Stereomicroscope

Several models of stereomicroscopes with a zoom functionality (SMZ models) were used in different laboratories for quick observations of the samples. In some cases, a digital camera was coupled to the microscope to photograph the samples.

#### II.IV.V Optical microscopy

Samples were observed with reflected polarized, natural and ultraviolet (UV) light using objectives from 5× to 100× magnification with an Eclipse LV100 D-Nikon Microscope. A halogen light source was used for the visible light images and a mercury light source was used for the fluorescence observations. Images were acquired in bright-field, dark-field and fluorescence modes using the NIS-Elements imaging software. Fluorescence images were obtained using filter cube combinations UV-2A ( $\lambda_{ex}$ : 330-380 nm,  $\lambda_{em} > 420$  nm) and B2A ( $\lambda_{ex}$ : 450-490 nm,  $\lambda_{em} > 515$  nm). In cases where the focus was not uniform everywhere in the image, which was often the case at high magnification, the Extended Focal Imaging (EFI) process was used to combine images over several increments of focal point in order to achieve a clear image.

During observation and imaging of the historic sample cross sections, the samples were oriented so that the paint-metal interface was at the bottom of the image. The identified layers in the stratigraphy were numbered from top to bottom.



## II.IV.VI Raman microscopy

Raman microscopy combines the functionalities of an optical microscope with a Raman spectrometer, thus giving an instrument that can produce data that are linked chemically and spatially. It is useful for characterising heterogeneous samples as the confocal microscope can be used to obtain measurements with a high spatial resolution (in the micrometer range). Raman spectra are a unique structural “fingerprint” of the analysed phase and can be used to identify materials by comparison with reference spectra. It is considered a selective and non-destructive tool (provided that the laser power is controlled) and is a complementary technique to infrared spectroscopy.

Raman spectroscopy is based on the exploitation of the Raman effect, which is the inelastic scattering of incident photons. For Raman scattering to occur, a vibrational transition must induce a change in polarizability of the analyte bond. The difference in energy between the incident light and the scattered photon is called the Raman shift and corresponds to a change in vibrational state of the analyte; the shift is therefore independent of the incident wavelength. The scattered light may be higher in energy (anti-Stokes scattering) or lower in energy (Stokes scattering) than the incident light. As vibrational transitions are quantized, the anti-Stokes and Stokes scattering lines are observed symmetrically around the elastic (no change in energy) Rayleigh scattering signal. The Stokes lines are more intense and are therefore used to measure the Raman signal. A typical Raman spectrum plots intensity as a function of the Raman shift in wavenumbers ( $\text{cm}^{-1}$ ).

Raman scattering is a weak phenomenon resulting in a signal with an intensity proportional to  $1/\lambda^4$ , where  $\lambda$  is the incident wavelength. It is not always possible to take advantage of this relationship to improve the intensity of the Raman signal due to other simultaneously occurring phenomena such as fluorescence, the intensity of which can mask the weak Raman scattering. Fluorescence is more likely to be present in the signal when higher energy (lower wavelength) light sources are used. A monochromatic light source such as a laser is normally used with wavelengths in the UV, visible or near-IR regions. The appropriate wavelength should be selected to have the best compromise between Raman scattering intensity, a possible (intense) fluorescence signal, laser excitation intensity and sample integrity. A filtering system must be used to block the intense Rayleigh scattering signal from reaching the detector.

### Instrumentation and measurement parameters

Different Raman spectrometers were used depending on the desired excitation wavelength:

*LabRam HR 800 (Horiba Jobin Yvon)*: With this spectrometer the 458 nm line of an  $\text{Ar}^+$  laser was used and focused on the sample with a 100× Olympus objective to give a spot size of about 1  $\mu\text{m}$ . The laser

power was adjusted to around 100  $\mu\text{W}$  at the surface of the sample to avoid material degradation during analysis. Spectra were collected for 3 to 30 seconds with 3 to 20 accumulations. The spectral resolution was about 3  $\text{cm}^{-1}$  using a 600 lines/mm grating. The instrument uses a grating to disperse the signal, an Edge filter to remove the Rayleigh scattering signal and a CCD detector cooled by the Peltier effect to collect the Raman signal.

*Senterra (Bruker Optics)*: Two Raman excitation wavelengths were used with this instrument: 785 nm from a diode laser and 532 nm from a frequency doubled Nd-YAG laser. Using the 785 nm wavelength laser, a 50x IR or a 100x IR Olympus objectives are used, giving spot sizes of about 13  $\mu\text{m}$  and 7  $\mu\text{m}$ , respectively. Using the 532 nm wavelength laser, 50x or 100x Olympus visible range objectives are used, giving spot sizes of about 4  $\mu\text{m}$  and 1  $\mu\text{m}$ , respectively. The laser power was 3 mW at the sample surface for both lasers and acquisition times between 2 and 10s. The spectral resolution was about 5  $\text{cm}^{-1}$ .

*RFS 100/S FT-Raman (Bruker Optics)*: The instrument uses an excitation wavelength of 1064 nm from a Nd-YAG laser. The signal is analysed using a Michelson interferometer and detection is accomplished by a germanium detector cooled with liquid nitrogen. Raman measurements were acquired with a 40x long working distance (LWD) IR Leica objective, giving a beam spot of about 28  $\mu\text{m}$ . The laser power was 100 mW (50 mW at the sample surface). A minimum of 6000 accumulated scans (500 scans = 15 min) was required to obtain a sufficient signal-to-noise ratio.

### **Selection of optimal conditions**

Tests were conducted to find the optimal Raman analysis conditions for each material. For corrosion products, the best spectra were acquired using the 458 nm laser with a laser power of 100  $\mu\text{W}$  at the sample surface. The historic samples were analysed initially with the 785 nm laser and conditions were then adjusted (ex. change of laser wavelength, microscope objective, number of acquisitions) depending on the quality of the resulting spectra.

### **Sample preparation**

An advantage of using Raman spectroscopy is that no specific sample preparation is required. Samples were analysed as powders, paint flakes or as embedded cross-sections.

### **Data treatment**

Opus 7.0 and LabSpec 5 were used for data analysis of the Raman spectra. On some spectra the fluorescence contribution has been removed with baseline subtraction to improve the observation of the Raman bands. Identification of the spectra was accomplished by comparing the characteristic bands with reference spectra found in the literature or in databases.

## II.IV.VII Infrared spectroscopy

Infrared (IR) spectroscopy can be used to identify constituents of a sample by probing the molecular structure of a material. It is based upon the absorption of an incident IR beam by vibrational modes of chemical groups in the analysed sample. The versatility of this technique and the availability of instruments in many institutions makes it a preferred choice in the field of conservation science. In this thesis work, it was used in two measurement modes: attenuated total reflection (ATR) mode and specular reflectance (RS for *réflexion spéculaire*) mode.

For a molecule to absorb infrared radiation, a change in dipole moment (charge distribution) must occur during vibration or rotation. (Skoog et al., 2017) The frequencies of the vibrational modes of most molecules occur in the mid-IR region (4000 to 200  $\text{cm}^{-1}$ ); it is this region that is analysed to identify the molecular structure of the samples. The resulting spectrum obtained from an IR spectroscopic analysis of a sample contains absorption bands where the frequency (or wavenumber) positions are related to specific vibrational modes of the molecular structure of the sample.

Analysis by IR spectroscopy can be exploited by transmission or reflection. Due to the nature of the studied samples in this work, only reflection modes were utilised. Different types of reflection may occur: specular, diffuse, or Attenuated Total Reflectance (ATR). Specular reflection occurs when the angle of the incident beam is equal to the angle of the reflected beam and is the case for smooth surfaces. Diffuse reflection occurs when a rough surface causes the incident beam to be reflected in randomly oriented directions.

In an infrared spectroscopy experiment in specular reflectance mode, if the surface at the point of analysis contains an IR active material, absorption will occur, and the reflected light will be attenuated at the absorbed frequencies. If the surface is sufficiently reflective it is possible to neglect the diffuse reflection and from the reflectance spectrum calculate a "pseudo-absorbance" spectrum whose characteristics are similar to those of an absorption spectrum. The possibility of obtaining readily interpretable spectra by this method of measurement is therefore limited by the surface characteristics of the sample being analysed.

The IR spectrum of a sample can also be analysed in attenuated total reflectance (ATR) mode (Figure II-11). This mode is based upon the principle that when two materials with different refractive indices are put into contact and a beam is passed from the higher refractive index material to the lower refractive index material, a total reflection will occur. As the incident angle increases, more light will be reflected until a critical angle is reached at which total reflection is reached (Skoog et al., 2017). In the

ATR apparatus, a crystal of high refractive index (diamond, Ge, ZnSe, etc.) is placed in contact with the sample (Daher, 2012).

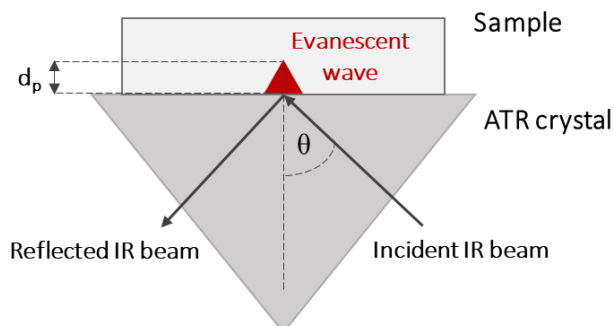


Figure II-11 Illustration of the principle of the FTIR-ATR measurement mode.

Incident radiation may enter the sample (an “evanescent wave”) but is rapidly attenuated to within a few microns. The effective penetration depth  $d_p$  depends on the wavelength of the incident beam, on the incident angle and on the index of refraction of the two materials at the interface where reflection is occurring, and is described by the following equation:

$$d_p = \frac{\lambda_c}{2\pi[\sin^2 \theta - (n_s/n_c)^2]^{\frac{1}{2}}}$$

Where:  $\lambda_c$  = wavelength in crystal ( $= \lambda/n_c$ ),  $\theta$  = angle of incidence,  
 $n_s$  and  $n_c$  are refractive indices of sample and ATR crystal, respectively.

Some of the energy of the evanescent wave is absorbed by the material it penetrates as well, as the reflected beam. The signal that emerges from the sample has therefore undergone a total reflection that has been attenuated by the absorption of the few cubic microns of material it passes through. The collected signal is plotted as absorption as a function of the frequency (in wavenumbers  $\text{cm}^{-1}$ ). Fourier transformation (FT) of the signal by an interferometer allows to obtain a spectrum with a high signal-to-noise ratio and is achieved in low amount of time.

ATR measurements can be acquired with or without sampling, making it an interesting option for the analysis of cultural heritage. However, it requires a good contact between the crystal and the sample and in some cases the applied pressure can damage the sample.

#### Instrumentation and measurement parameters

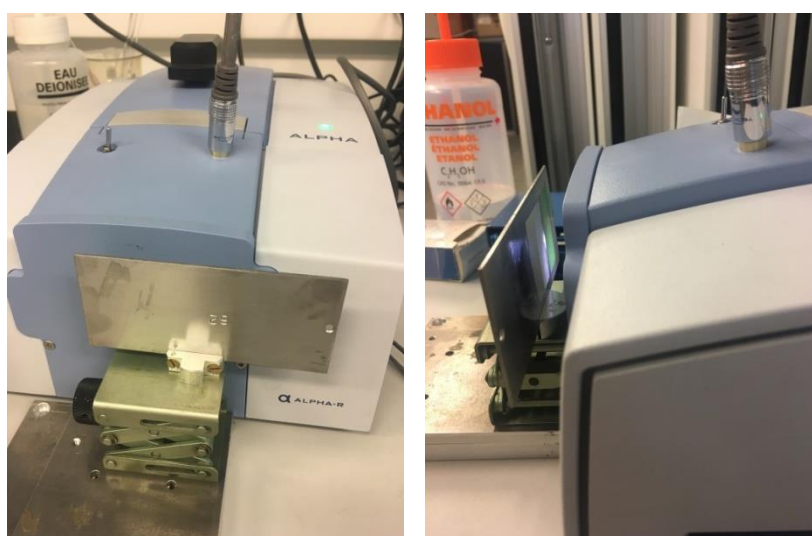
Infrared spectra were acquired using a Bruker Alpha FTIR spectrometer using either its ATR or specular reflectance measurement module.

### *FTIR ATR*

The Alpha ATR module is based on a diamond crystal and an anvil is used to press the sample onto it. Millimetre-sized samples were acquired from the model coupons using a scalpel on the painted surface in the zone of interest. Care was taken to take note of which face (interior/exterior) was being placed in contact with the ATR crystal. This was not always possible due to the state of the sample after sampling (rolled up, many fragments, powder). Reference spectra for the conservation treatments were obtained from samples collected from dried films previously applied on glass slides. Spectra were acquired with a spectral resolution of  $4\text{ cm}^{-1}$  as an average of 64 scans over the range of  $4000\text{-}400\text{ cm}^{-1}$ . A background reference without any sample in contact with the ATR crystal was acquired before beginning analysis of the samples and was reacquired every three to four hours.

### *FTIR RS*

The Alpha specular reflectance module combines mirrors that focus and collect the IR beam at a  $45^\circ$  angle to the surface of the sample which is placed at a working distance of 15 mm (Figure II-12), giving a beam spot size of about 5 mm. Three spectra per zone of interest were collected at evenly spaced points. Reference spectra of the conservation treatments were measured from zones surrounding the paint film where the treatment had been applied on bare metal. Spectra were acquired with a spectral resolution of  $4\text{ cm}^{-1}$  as an average of 64 scans over the spectral range of  $4000\text{-}400\text{ cm}^{-1}$ . A background reference measurement was acquired on a gold mirror before starting analysis of the samples and was reacquired every three to four hours.



**Figure II-12** Bruker Alpha FTIR spectrometer with its specular reflectance module and with the model coupon in place for analysis, viewed from behind (left) and from the side (right).

### **Data treatment**

OPUS 7.0 software was used for the treatment of the FTIR data. Spectra were pre-processed by applying an atmospheric correction to subtract any residual signal attributed to water and carbon dioxide. The baseline was subtracted manually. For data analysis, spectra were normalized at certain wavenumbers (specified in figure captions in the results chapters) for comparison. In the case of the data acquired in specular reflectance mode where three spectra per zone were collected, a representative spectrum was selected when all three were identical. Otherwise, each type of spectra is presented for discussion.

## **II.IV.VIII Scanning Electron Microscopy coupled to Energy-Dispersive X-ray spectroscopy**

Scanning Electron Microscopy (SEM) is an imaging technique for examining the morphology of the observed samples with a high spatial resolution (~100 nm). The technique is based upon the interactions of a beam of electrons with matter. Different phenomena result from this interaction which provide information on different material aspects of the analysed sample. Two signals of interest in SEM imaging are the production of Secondary Electrons (SE), which give information on the topography of the surface of the sample, and Backscattered Electrons (BSE), which are sensitive to the atomic number of the encountered atoms and therefore carry information on sample composition. The SEM-BSE image shows differences in the backscattering intensity amongst the analysed layers as a greyscale, where lighter grey is representative of higher backscattering. Backscattering intensity increases with atomic number, so differences in elemental composition can also be inferred from the greyscale values. Interaction of the electron beam with matter can also induce the production of characteristic X-rays due to X-ray fluorescence (see II.IV.XI X-ray fluorescence spectroscopy), which is the basis of Energy-Dispersive X-ray Spectrometry (EDS). Coupling of SEM imaging with EDS allows to map the distribution of the elemental composition.

### **Instrumentation and measurement parameters**

A Zeiss Supra 55 VP scanning electron microscope with a field emission gun (SEM-FEG) was used with an acceleration voltage of 5 to 20 kV to observe the topography and chemical contrast of the sample layers thanks to secondary and backscattered electron modes (SE and BSE). EDS analyses were conducted at 20 kV at a working distance of 6.5 mm, using a Quantax EDS nano and microanalysis system (Bruker) based on a silicon drift detector (SDD). The samples were carbon coated before analysis to reduce accumulation of electrical charge at the surface of the sample.

## II.IV.IX Gas Chromatography-Mass Spectrometry

Gas chromatography coupled to Mass Spectrometry (GC-MS) is a separative technique that can be used to identify the organic components present in the analysed samples. The presence of one or a group of components can serve as markers for the characterisation of materials and is used in this work to determine the binder used in the paint formulation of our historic samples. A secondary aim of using this technique was to identify degradation products of the paint, such as free fatty acids and metal soaps, which would complement our FTIR study on the aging of treated painted metal coupons throughout the process of artificial aging. GC-MS gives more specific molecular characterisations of the composition of the samples but is a more complex technique to implement than FTIR. Furthermore, it necessitates that the analytes of interest be volatile, and this often requires sample preparation steps. It is also a destructive technique as a fragment of the sample is consumed during analysis.

### **Instrumentation and measurement parameters**

A Trace GC Ultra gas chromatograph (Thermo Scientific) and an ISQ single quadrupole mass spectrometer (Thermo Scientific) was the instrument used for the GC-MS analyses. Samples were injected automatically; the split injector was set at a temperature of 290°C with a total flow of 50 mL/min and split ratios of 33 or 15 (depending on amount of analyte in sample). The components of the samples were separated using a Rxi 5Sil MS non-polar fused silica capillary column from Restek (length 20 m, internal diameter 0.18 mm, film thickness 0.18 µm) with H<sub>2</sub> as the carrier gas (flow rate 1.5 mL/min). To optimize the analysis time, a temperature program was used (50°C for 1 min, ramp of 20°C/min until 320°C and 320°C for 5 minutes). The column-MS interface temperature is set at 320°C. Fragmentation of the analytes was achieved using electron impact ionization mode at 70 eV and the ion source temperature was 250°C.

### **Sample preparation**

Fragments of the samples were cut using a scalpel until a total mass of ~1 mg was acquired for analysis. Separation of the paint layers was not successfully achieved and so the analyses were conducted on all the paint layers of the sample. The collected fragments were added to a glass vial along with other components such as solvents, derivatization reagents and an internal standard as detailed below.

The samples required a derivatization step prior to injection because the components must be volatile in order to separate them with gas chromatography. Two different sample preparation methods were used depending on the analytes of interest and are listed in Table II-9.

Table II-9 Sample preparation procedures for GC-MS analysis.

Sample preparation method	Procedure (for ~1 mg sample)	Objective
1	0.1 mL MethPrep-II, 0.025 mL of 1 mg/mL IS solution, 30 min @ 60°C.	Identification of the main components (fatty acids and terpenoids).
2	0.1 mL BSTFA, 0.025 mL IS, 30 min @ 80°C, evaporation under N <sub>2</sub> @ 40°C, 0.125 mL cyclohexane.	Degradation products of the paint (free fatty acids and metal soaps).

Sample preparation method 1 used the derivatization reagent MethPrep-II (MPII), a 0.2 N methanolic solution of m-trifluoromethylphenyl trimethylammonium hydroxide (TMTFTH). It is one-step transesterification reagent that converts the oil-based and terpenoid components of the binder into methyl esters which are more easily analysed by GC-MS. 0.1 mL of MethPrep-II was added to a ~1 mg fragment of sample along with 0.025 mL of the 1 mg/mL solution of the internal standard, giving a final internal standard concentration of 0.2 mg/mL. The mixture was heated at 60°C for 30 minutes and then injected. This preparation method was mainly applied to characterise the binder present in the paint layers of the historic samples.

Sample preparation method 2 used BSTFA (N,O-Bis(trimethylsilyl)trifluoroacetamide + 1% TMCS (catalyst)), a silylating agent that creates trimethylsilyl (TMS) derivatives of hydroxyl groups. 0.1 mL of BSTFA and 0.025 mL of internal standard (IS, see hereafter) solution were added to 1 mg of sample and the mixture was heated at 80°C for 30 min. The solvent was then evaporated with nitrogen gas at 40°C and redissolved in 0.125 mL of cyclohexane before injection. This method was mainly used for studying the presence of degradation products such as free fatty acids and fatty acid carboxylates (metal soaps) in both the historic and model paint coating samples.

Hexacosanoic acid methyl ester (C<sub>20</sub>:0) was selected as an internal standard (IS) for the quantification of the samples (although in the end the quantitative analysis was not completed as part of this work). It is a long chain fatty acid that will produce a similar analytical signal to the other fatty acids yet is not present in the molecular composition of oil-based paint. The addition of an internal standard was used to improve the accuracy of the data by accounting for any variability that may occur during the sample preparation steps or during injection of the sample. A 1 mg/mL solution was prepared by dissolving 3.05 mg of the standard in 3.05 mL of cyclohexane.



## Data treatment

Xcalibur software was used for data acquisition and analysis. The mass spectra of peaks in the obtained chromatograms were compared to references in the NIST Mass Spectral library in order to identify their chemical structure.

## II.IV.X Synchrotron source, SOLEIL

Synchrotron-based techniques are an important addition to the repertoire of available instrumental analysis techniques. The high flux of the synchrotron beam combined with high performance detectors allows to conduct analyses with a higher sensitivity compared to lab sources. A broad range of energies are available, from UV to hard X-rays, and the beam can be shaped to different spatial resolutions (bulk, micro, nano). Limitations of using a synchrotron source include the availability of beamtime (accessible through a project selection process). In addition, precautions should be taken due to possible damage to the sample due to the energy and high flux of the beam. All of the synchrotron experiments conducted in this thesis took place at SOLEIL (*Source Optimisée de Lumière d'Energie Intermédiaire du LURE, Laboratoire pour l'Utilisation du Rayonnement Electromagnétique*) synchrotron in Saint-Aubin, France on three different beamlines:

- **DiffAbs** is a hard X-ray beamline which combines X-Ray **D**iffraction and **A**bsorption to study a large variety of materials (energy domain 3-23 keV); used here for XRF, XRD and XAS experiments at macro and micrometric scales.
- **PUMA** (French for "*Photons Utilisés pour les Matériaux Anciens*") is a hard X-ray imaging beamline optimized for the scientific communities of the heritage sciences (energy domain 4-60 keV); used here for XRF and XAS experiments at the micrometric scale.
- **DISCO** (**D**ichroism, **I**maging, and **m**ass **S**pectrometry for **C**hemistry and **biO**logy) is a low-energy VUV to visible beamline (energy domain 1-20 eV = 60-700 nm) with three endstations that cover microscopy, atmospheric pressure, and circular dichroism experiments; used here for DUV-PL imaging and hyperspectral mapping at the micrometric scale (Giuliani et al., 2009).

## II.IV.XI X-ray fluorescence spectroscopy

X-Ray Fluorescence (XRF) spectroscopy is an element-sensitive technique that allows to detect the elemental composition of a sample. The use of a synchrotron source allows to increase the spatial resolution by using a micro-beam while maintaining a high analytical sensitivity due to the available X-ray flux and highly sensitive and efficient detectors. It is non-destructive (if we take care that the high flux of the synchrotron beam does not damage the sample) and can be used in large and fast mapping

mode to acquire the elemental distribution. In this thesis it was mainly used to characterise the elemental composition and distribution within the stratigraphy of the samples obtained from the historic painted metal objects.

XRF spectroscopy is based upon the principle that irradiation of an atom with an X-ray beam will excite a core electron, leaving behind a core hole and an excited atom. An electron of higher energy will relax in order to fill the core hole and in doing so, will give off energy in the form of a photon: this phenomenon is known as X-ray fluorescence (see Figure II-13). The energy of the ejected photon is characteristic of the element because it depends on the differences in energy between the levels of its unique electronic structure and can therefore be used to characterise the elemental composition of the sample. An X-ray fluorescence experiment functions by exciting a sample with an incident energy above the binding energy of the core electron (values are available in tables) and collecting the emitted signal which is a combination of all of the characteristic fluorescent X-rays of each element in the sample (Figure II-13).

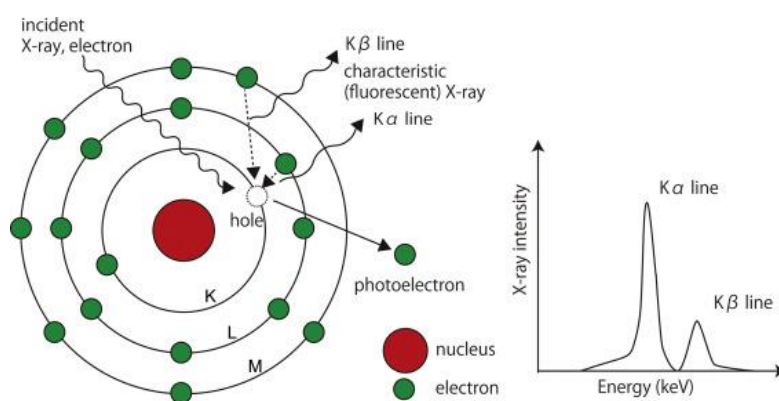


Figure II-13 Schematic representation of the principle of X-ray fluorescence spectroscopy. Figure from: (Uo et al., 2015).

### Instrumentation and measurement parameters

Micro-XRF analyses were performed at the DiffAbs beamline and at the PUMA beamline (Synchrotron SOLEIL, France).

Different excitation energies were used depending on the element of interest. For the initial investigation of the full elemental composition of the sample cross-sections, an incident energy of 18 keV was used. XRF maps were collected using the flyscan mode (Leclercq et al., 2016), where a full XRF spectrum is collected at each pixel which allows elementary maps with a micrometric resolution to be obtained on the whole sample in a short amount of time (~1 hour). All XRF experiments were performed at room temperature and atmospheric pressure (Ar K lines from ambient air are visible in XRF spectra),

implying difficulties in detecting the fluorescence signal from light chemical elements (such as Si, P), especially when present in small quantities.

- **On DiffAbs**

The microbeam was focused using a Kirkpatrick–Baez (KB) mirror optics setup to achieve a beam size of 8  $\mu\text{m}$  x 6  $\mu\text{m}$ . The surface to be analysed was oriented at an angle of 45° with respect to the beam axis. The X-ray fluorescence signal was obtained by a four-element SDD (Vortex-ME4®, Hitachi) and a 50 ms/pixel dwell time.

- **On PUMA**

A KB mirror focused the X-ray beam to a beam size of 4  $\mu\text{m}$  x 5  $\mu\text{m}$ . The surface to be analysed was oriented at an angle of 45° with respect to the beam axis. The XRF signal was acquired by a SGX Sirius SD silicon drift detector installed at 90° from the incident beam.

### **Sample preparation**

The samples are usually prepared as polished cross-sections in order to analyse more favourably the stratigraphy, but samples without any preparation were also analysed.

### **Data treatment**

Data processing was performed using the PyMCA software (Solé et al. 2007). The total XRF spectrum was calibrated using three known characteristic rays and fit with the applied experimental parameters (incident energy, measurement geometry) and with adjustment of the appropriate background. A batchfitting process was applied to each map using the chosen fit parameters.

## **II.IV.XII X-ray Absorption Near-Edge Structure spectroscopy**

X-ray Absorption Near-Edge Structure (XANES) spectroscopy is an element-specific technique that can be used to determine the chemical speciation of an element of interest. In this work, XANES was employed to determine the speciation of several elements of interest. In the historic samples, elements of interest for XANES analysis (such as Pb, Zn, Fe, etc.) were selected after determining the elemental composition and distribution from XRF elemental maps of the analysed cross-sections. On the model painted metal coupons, XANES was employed to monitor changes in the local environment of Pb in the lead white-painted metal coupons throughout artificial aging.

X-ray Absorption Spectroscopy (XAS) depends upon the interaction of incident X-ray radiation with matter, thus giving information about the local environment of an element of interest by studying its absorption behaviour around a specific absorption edge. An incident X-ray photon may excite an inner

shell (core) electron of an atom if its energy corresponds to the binding energy of the core shell. As the incident energy is increased over a known binding energy threshold, a sharp increase in absorption will be detected, corresponding to the excitation of the core-electron. This is referred to as an absorption edge. An atom can have several absorption edges that correspond to the excitation of electrons from different core shells. These edges are called K, L, M, etc. and refer to electronic transitions from shells with the principal quantum number  $n = 1, 2, 3$ , etc. respectively. The X-ray absorption spectra can be measured either directly by transmission or indirectly by measuring the corresponding characteristic X-ray fluorescence signal of the probed element. Transmission measurements require the preparation of thin slices

Figure II-14 shows an example of an X-ray absorption spectrum. The spectrum presents structural characteristics that are indicative of the electronic behaviour of the atom as a function of incident energy. The region within 50 eV of the absorption edge is referred to as X-ray absorption near-edge structure (XANES). The XANES region can provide information about the oxidation state and geometry around the atom. Past the XANES region to about 1,000 eV is the region known as Extended X-ray Absorption Fine Structure (EXAFS). The EXAFS region is used to study bond length and coordination number of the atom (Penner-Hahn, 2003).

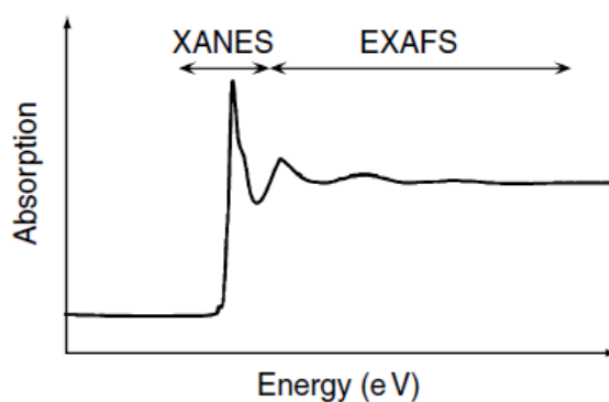


Figure II-14 Example of a XAS spectrum (Penner-Hahn, 2003).

The steepest increase in absorption is referred to as the absorption edge and may be measured as the energy at half-height or as the maximum of the first derivative of the spectrum at that point. This measurement is not so straightforward as the spectrum can present unresolved structures in the edge region which can complicate defining an exact edge energy position. The intensity maximum of the largest peak is referred to as the “white line” and can be measured as the post-edge zero crossing in the first derivative of the spectrum. The XANES region (including the positions of the absorption edge and the white line) can be used as a characteristic fingerprint of chemical environments that, with comparison with known reference standards, can lead to an accurate identification of unknown phases.

In the case of the materials studied in this work, the edge position is known to increase with oxidation state; monitoring of changes in the edge position can therefore provide insight into modifications of the chemical speciation.

XAS is typically a synchrotron-based technique because it requires a tunable source of intense radiation. The beam can be focused to micrometric dimensions in order to obtain measurements with a high spatial resolution. All types of samples may be measured, making it a versatile technique. The technique is limited by the fact that since X-rays are highly penetrating, material up to a certain depth of penetration shall be excited; the resulting signal may be affected by matrix effects such as scattering or self-absorption by other atoms before exiting the sample.

### Instrumentation and measurement parameters

XANES experiments were conducted at the DiffAbs and PUMA beamlines at Synchrotron SOLEIL. Spectra were collected in fluorescence mode from zones of interest on the cross-sections of the historic samples, the painted metal coupons and reference compounds. The following absorption edges were investigated: Pb L<sub>3</sub> edge, Zn K edge, Fe K edge, Sr K edge, Ba L edge and Br K edge. Measurements were acquired with 1-5 scans/point depending on the quality of the signal.

#### *XANES on painted metal coupons*

The untreated and treated zones of the lead white-painted model coupons were analysed in fluorescence mode at the Pb L<sub>3</sub> edge (Figure II-15). A summary of the coupons analysed at each aging step is summarised in Table II-10.

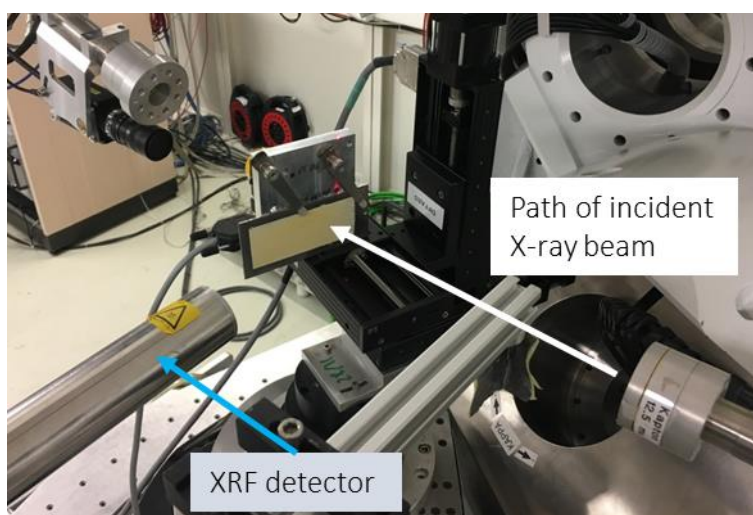

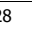


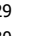


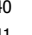
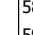

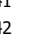
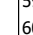





Figure II-15 XANES set-up in fluorescence mode (DiffAbs beamline).

Table II-10 Summary table of XANES measurements performed on model coupons.

Aging	Relative Humidity cycles (RH)															
Treatment	Corrosion Inhibitor						Resin-Wax Mixture									
Pre-aging	Fresh			Pre-aged			Fresh			Pre-aged						
Pigment	LW	CrGO	LO	LW	CrGO	LO	LW	CrGO	LO	LW	CrGO	LO				
Coupons (#)	1			25	4		49	28	7			31	10		52	34
	2		62	26	5		50	29	8		63	32	11		53	35
	3			27	6		51	30	9			33	12		54	36
Aging	Light exposure (LT)															
Treatment	Corrosion Inhibitor						Resin-Wax Mixture									
Pre-aging	Fresh			Pre-aged			Fresh			Pre-aged						
Pigment	LW	CrGO	LO	LW	CrGO	LO	LW	CrGO	LO	LW	CrGO	LO				
Coupons (#)	13			37	16		55	40	19			43	22		58	46
	14			38	17		56	41	20			44	23		59	47
	15			39	18		57	42	21			45	24		60	48

**Legend:**

Code	Aging step
	Fresh and pre-aged samples
	Treated samples, after Phase I aging (RH, light)
	Treated samples, after Phase II aging (RH)

**Sample preparation**

The historical samples are usually prepared as polished cross-sections in order to analyse more favourably the stratigraphy, but samples without any preparation were also analysed. The model coupons were analysed directly without any preparation.

**Data treatment**

Post-processing and analysis of the XANES data was completed using the Athena software (Ravel & Newville, 2005). For comparison between different experiments (as in the case with the model painted metal coupons), the XANES spectra were calibrated using an energy shift correction which was calculated from the difference between the experimental absorption edge measured from a metal reference sheet of the element of interest and the tabulated absorption edge. Spectra were then normalised prior to comparison with references and other spectra.

In the case of data acquired in the same zone (for example untreated or treated zones of a model coupon), spectra were merged when appropriate to create one representative spectrum. The energy positions of the Pb L<sub>3</sub>-edge and the white line were calculated from the maximum and post-edge zero crossing of the first derivative of the spectra, as seen in Figure II-16. The XANES spectra acquired on the coupons were compared with reference XANES spectra of different Pb compounds that could potentially be present in the paint in order to characterise the different species identified.

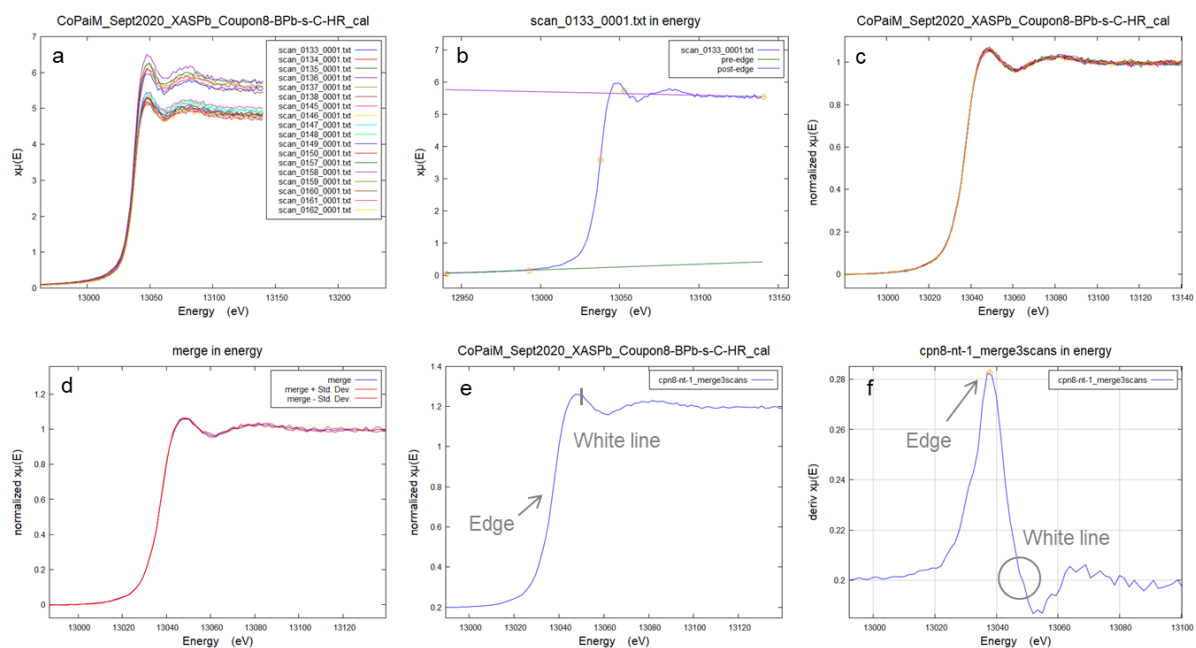


Figure II-16 Examples of normalization, merging and measurement of edge and white line positions: a) all scans before normalization; b) assignment of pre-edge, edge and post-edge; c) normalized spectra; d) merge of three replicate scans with standard deviation in red; e) merged scan with positions of edge and white line indicated; f) first derivative of scan with positions of edge and white line indicated.

## II.IV.XIII Deep-UV Photoluminescent imaging

Deep-UV photoluminescent imaging (DUV-PL) is a technique with high spatial resolution that was used in this work to discriminate between the various molecular phases present in the historic sample cross-sections based on their photoluminescent properties. Analysis was focused particularly on the interfaces and in areas that presented signs of alteration. The tunable excitation wavelength and selection of different emission filters allows to discriminate different components present in a complex matrix, such as the paint layer cross-sections. Coupling of these analyses with the previous characterisation results was expected to improve the understanding of the alteration processes occurring within and at the interfaces of these painted-metal systems. In the context of this work, the measurements carried out were of an exploratory nature. They were mainly an opportunity to evaluate the information that can be provided by this additional characterisation of the paint cross-sections.

### Instrumentation and measurement parameters

Full-field (hundreds of square micrometers) photoluminescence images obtained by a set of filters of different wavelength ranges with high spatial resolution (several hundred nanometers) were collected using the TELEMOS end-station at the DISCO beamline. The excitation wavelength was scanned between 250 and 350 nm to target the different pigments present and the emission was recorded from 350 to 800 nm using a series of narrow bandpass filters. Hyperspectral maps were acquired by recording

the entire fluorescence spectrum using the POLYPHEME end-station in order to discriminate between the various components present.

### **Sample preparation**

Measurements are carried out on prepared polished sections of historic sample cross-sections in order to be able to observe the whole stratigraphy.





## Chapter III Analytical study of painted metal objects from the 19<sup>th</sup>-20<sup>th</sup> centuries

This chapter is dedicated to the study and characterisation of historic painted metal objects dating from the 19<sup>th</sup>-early 20<sup>th</sup> centuries that are currently stored in an indoor, controlled environment. Painted metals present a technical challenge for the conservation field due to their composite nature. Both the paint coating and the metal support have unique recommendations for their conservation which cannot always be simultaneously fulfilled, and even more so within storage facilities where a variety of other materials are present. In addition, objects found in museum collections have all experienced a previous life of (often undocumented) usage and environmental conditions before entering the controlled storage environment (see section II.I.I for description of museum storage conditions), resulting in a range of states of alteration that must be considered. The aim of this study is therefore twofold: firstly, to deepen the current knowledge of the material composition of the painted metal system found on historical objects presenting signs of alteration, and secondly, to investigate observed degradation phenomena in order to understand the alteration processes at play.

The results of an initial condition report of 23 painted metal objects found in the scientific and technical collections of the Musée des Arts et Métiers, prepared with conservation-restoration professionals and detailing the material aspects and state of conservation of each object, will first be presented. From this database of condition reports, nine painted iron objects presenting signs of degradation were selected to form the corpus on which this study is based. 41 samples were acquired from altered areas found on each object; these sampling locations and first observed trends shall be presented. Subsequently, the most representative samples from each object were prepared as cross-sections in order to conduct a detailed characterisation of their stratigraphy. The cross-sections have been analysed via multiple complementary techniques to characterise the morphological, elemental, and structural characteristics of the components found within the respective systems. A series of examples has been chosen to illustrate the detailed results of the characterisations. Finally, the overall results of the characterisation study will be presented and general trends as well as special cases will be discussed.



### III.1 Object descriptions and sampling

The following descriptions of the nine objects constituting the studied corpus are adapted from a database of condition reports of painted metal artifacts found within the collections of the Musée des Arts et Métiers which was prepared by conservation and restoration specialists (see section II.1.II). The material composition and observed state of conservation of each object is presented.

The *Tandem* (Figure III-1) is mainly iron based, with some parts composed of either copper or other unidentified white metals. Other materials are present such as leather and plastic. Several single or multilayered paint coatings are present on the metallic structure: a blue paint on a copper alloy; a green paint on a blue paint on a white metal; a varnish on a blue paint on an iron alloy; a black paint on an iron alloy; and a blue paint on an iron alloy. The blue paint is mainly found on the frame while the green paint is located on the front lamp, the front and back fenders and the chain guard. Several types of alteration are observed. The paint coatings present mechanical alterations, including scratches, microfissures, deformation, flaking and paint loss. For the parts where the iron support is exposed by paint loss, the corrosion of the metal is generalized and compact or else localised and loose. Furthermore, a poor adhesion is observed between the paint coating and the metal and between the paint layers themselves (Figure III-1c,d).

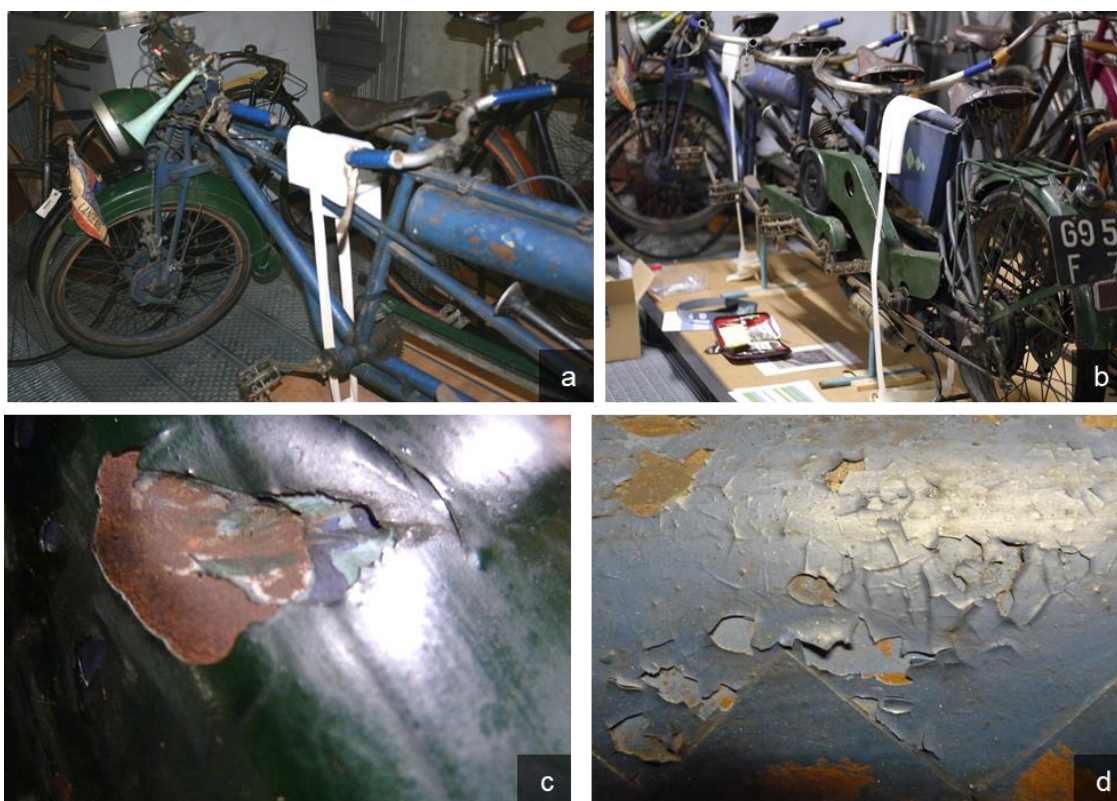


Figure III-1 Photographs of the *Tandem* (Quadruplette): front (a), back (b), details of surface alterations (c,d).  
Dimensions (l x w x h): 3 m x 80 cm x 60 cm.

The *Charrue* (Figure III-2) is made primarily of an iron alloy but contains some parts composed of a copper alloy. A blue paint coating is present on most of the surface of the object, although the wheels are painted red. Painted designs of various colours (yellow, gold, orange, pink, red, white, green and black) are present over much of the object (Figure III-2c,d), which confirms the esthetic quality of the object (used as a model rather than a working object). A light layer of dust covers the entirety of the object. The observed coating alterations are scratches, microfissures, flaking and paint loss. The metal presents some scratches and corrosion is present in areas that were not painted or that were left exposed by paint loss.

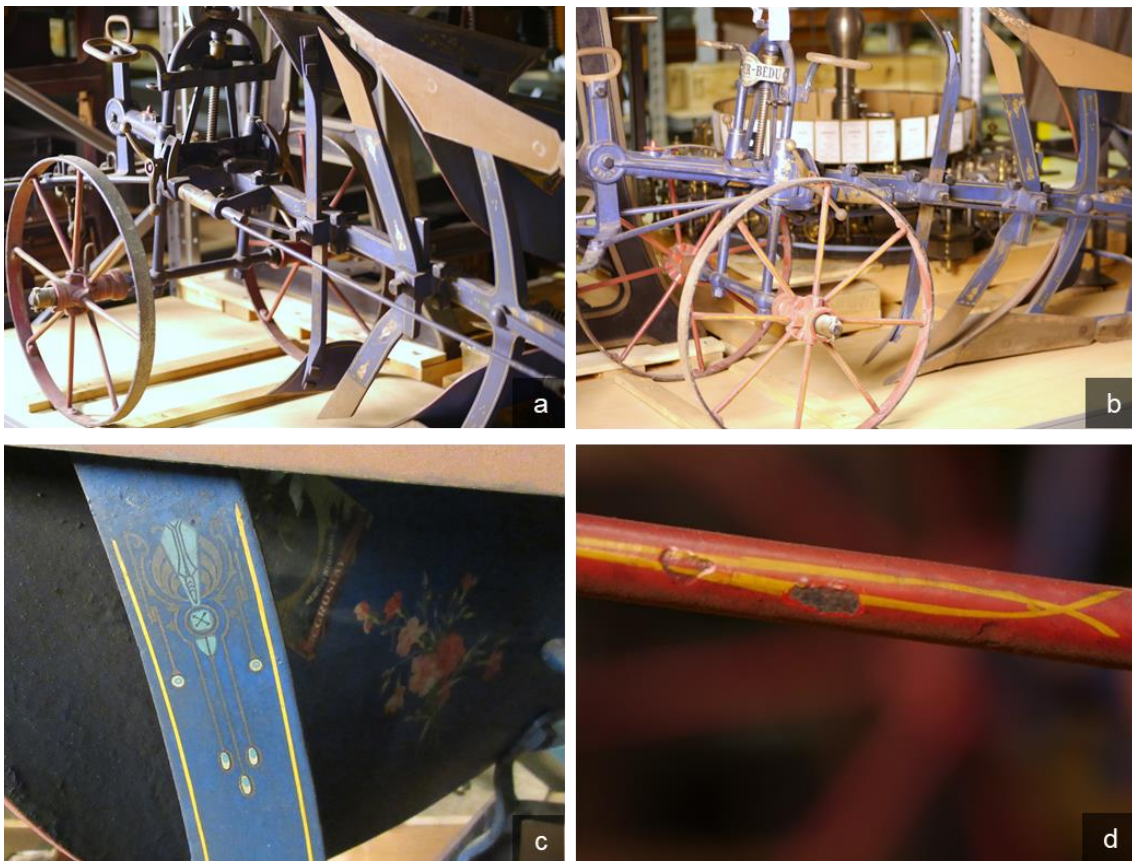


Figure III-2 Photographs of the *Charrue* (double Brabant plow): front right (a); back right (b); closer view of painted details (c,d). Dimensions (l x w x h): 210 cm x 78 cm x 106 cm.

The *Chaudière* (Figure III-3) is composed of two connected symmetrical cylinders: the cylinder on the right is made of wood while the left cylinder is iron based. White metals are also present. Three zones of painted metal are present on the object: a first consisting of two coats of red paint applied to the iron-based cylinder; a second as a white paint coating on iron-based metal located on the central pieces connecting the two cylinders; and finally, a third consisting of a black paint found on the interior face of the iron-based cylinder and on the areas made of white metal. The object is mounted on a varnished wood base. Physicochemical alterations are present on the metal (scratches, deformation, localised corrosion in gaps left by paint loss) as well as on the paint coating (cracking, flaking, paint loss,

discolouration, loss sheen/gloss). A large proportion of the red paint coating applied to the left metal cylinder shows grey/black discoloration (Figure III-3b), while the white paint coating shows brown staining mainly at corners where the metal support has corroded (Figure III-3c).



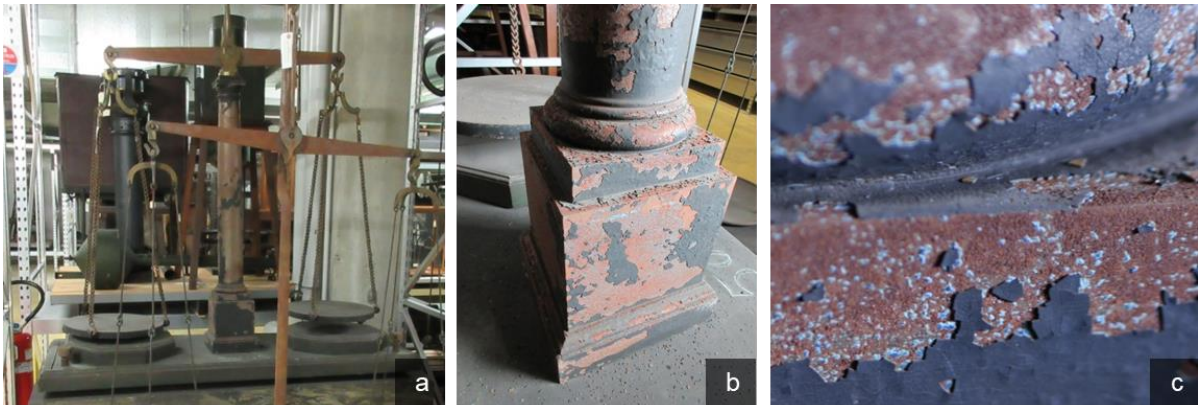
Figure III-3 Photograph of the *Chaudière* (Model of engine boiler). Dimensions (l x w x h): 90 cm x 60 cm x 60 cm. Surface alteration is shown in images b and c.

The *Série de 6 mesures* (Figure III-4) are covered in a brown-grey coating and a bright orange paint layer is observed underneath through gaps left by paint loss. Scratches, microfissuring and flaking of the paint are frequently observed over the totality of the surface of the object, and some painted areas appear to have lightened in colour. A general superficial layer of dust is present. The object presents uniform corrosion in all areas where the metal support has been exposed.



Figure III-4 Photograph of three measures (a) of the *Série de 6 mesures* (Set of six measuring containers). Dimensions (h x d): 52 cm x 62 cm. Surface alteration with paint loss and corrosion (b).

The *Balance* (Figure III-5) is composed of two weight pans attached to a beam that is supported by a central column and a base. The central column is iron based while the base is made of wood. The object is covered in dust, particularly in areas with horizontal surfaces. The metallic parts were originally coated with multiple layers of paint consisting of a black layer on a light blue layer. The paint coatings present fissures, flaking and major paint loss, particularly on the central column. A lightening of the painted surfaces is noticed in some areas. The object presents generalized corrosion in areas and is especially visible where the metal has been exposed by paint loss but is most likely also corroded under the remaining pieces of paint.



**Figure III-5 Photographs of the *Balance* (Weighing scales): full object (behind object in foreground (a)); detail of the base of the stand (b) and close view of altered surface on base of stand (c). Dimensions (l x w x h): 162 cm x 57 cm x 182 cm.**

The *Lanterne* is a three-light acetylene gas lantern with glass panes (Figure III-6). The casing is iron based but the base and stand of the lantern are copper based. Both metals are painted with the same coating: a black paint on a grey paint. The painted surfaces present scratches, microfissures, flaking and paint loss, along with some localised spots of colour brightening and reduced shine. The black paint presents problems of adherence to the metal support, as evidenced by many fallen paint flakes around the base of the lantern. A small quantity of dust is present on top of the casing. Two forms of iron corrosion are observed: one is localised on the handle rivet and has a heterogeneous, shiny appearance, while the less exposed areas of the object present corrosion with a loose, powdery texture.

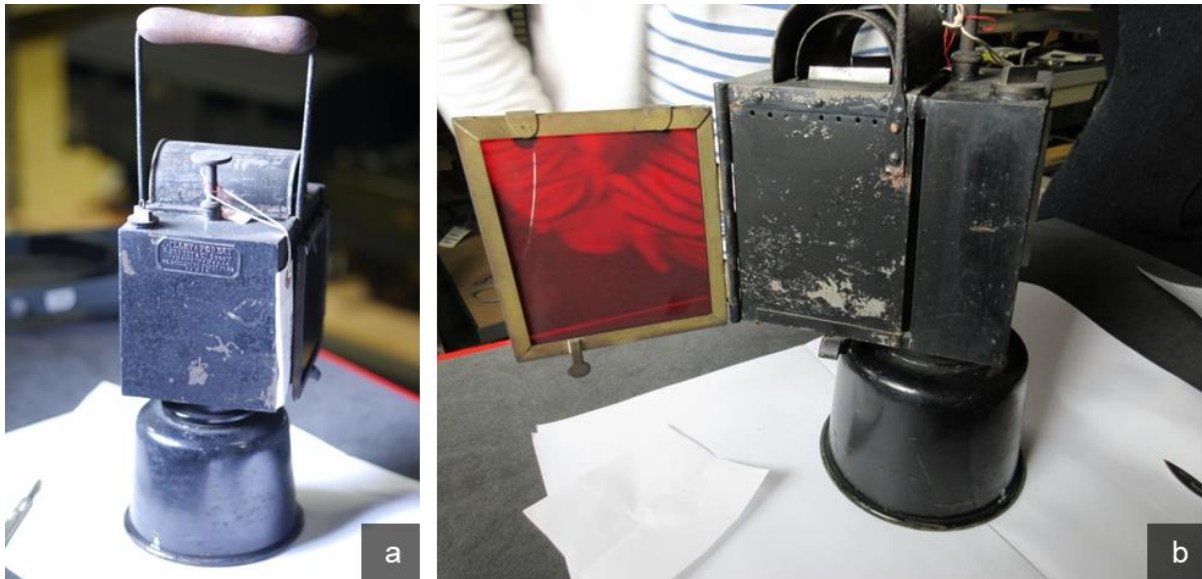


Figure III-6 Photographs of the *Lanterne* (Lantern): closed (a) and open (b). Dimensions (l x w x h): 15 cm x 12 cm x 37.5 cm.

The *Locomotive* (Figure III-7) is principally iron based, with some parts composed of either copper or a white metal. The iron and copper parts are painted with a black paint over a grey paint. The coating shows paint loss and changes in colour and shine. Orange spots of corrosion are visible on the iron-based sections while the copper sections only present localized corrosion.



Figure III-7 Photographs of the *Locomotive* (model of Matthieu Murray locomotive): full object (a); detail of the surface (b). Dimensions (l x w x h): 42 cm x 36 cm x 65 cm.

The *Châssis* (Figure III-8) is mainly iron based with some parts in white metal. It has opaque, multilayer paint coatings of different colours, including black/grey, green and red-orange paint. The paint coating presents alterations such as the formation of a whitish haze (primarily on the wheels), disintegration of the film, and paint loss. The exposed iron parts show localised compact corrosion.





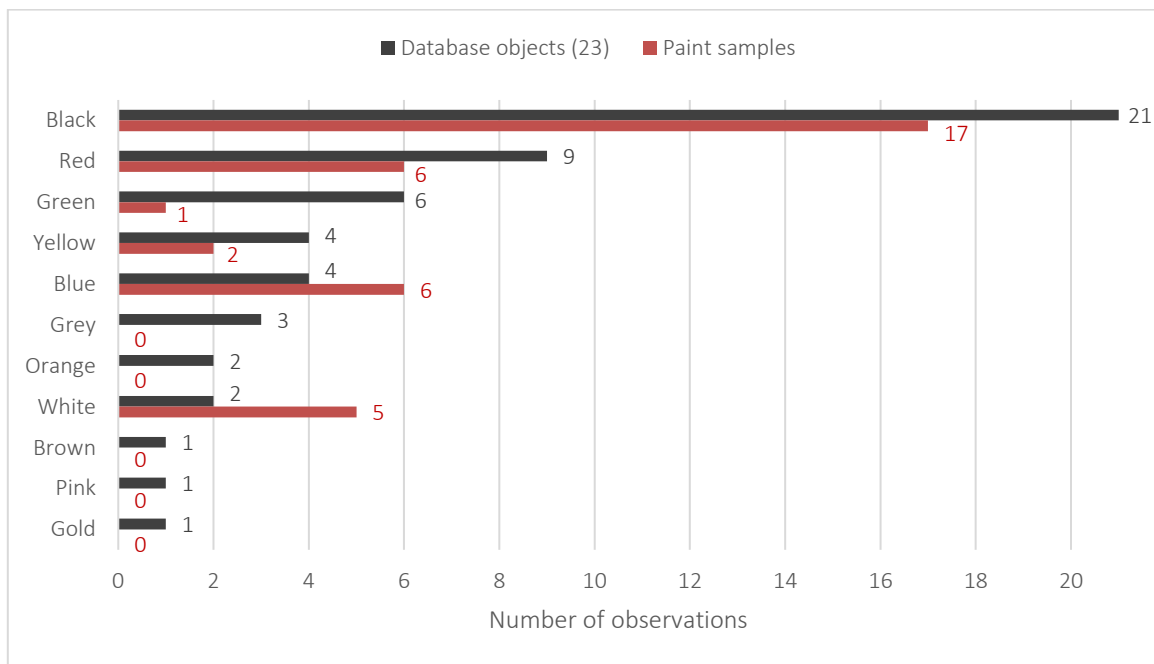
Figure III-8 Photograph of the *Châssis* (Automobile chassis): full object (a); detail of the paint alteration on the front right axle (b). Dimensions (l x w x h): 2 m x 1.5 m x 1 m.

The *Vélocoteur* (Figure III-9) is mainly iron and copper based, with some white metals present as well. The painted areas show an opaque black coating on metal. A uniform layer of dust covers most of the surface. The paint presents different alteration phenomena: scratches, microfissures, flaking, paint loss, and some modification of reflectivity (shine/mattness). The exposed metal presents mechanical alterations (scratches, deformations) as well as homogeneous generalised corrosion on the iron-based parts of the wheels. Some small white points of white corrosion products are present on aluminum-based parts.



Figure III-9 Photographs of the *Vélocoteur* (Electric motorbike): full object (a); detail of the paint alteration at the bottom right of the front fender (b). Dimensions (l x w x h): 170 cm x 50 cm x 70 cm.

The condition reports conducted on each object in the painted metals database demonstrate the various types of paint coatings, metal supports, and alteration phenomena that can be encountered on historical painted metal objects. The most common topcoat observed is a black paint layer, although various other colours of paint are equally observed (see Figure III-10). The frequency of occurrence of the colours gives an indication of the desired esthetic of these objects. Some objects only contain one type of coating while others have several; the *Chaudière* has the greatest variety (3 types). The most common alterations of the paint coatings are microfissuring, flaking and paint loss. Delamination of the paint layers and changes in the surface aspect are noticed in a few cases. Corrosion is present on all the objects and most often in areas left exposed by paint loss.



**Figure III-10 Observed topcoat colours on the 23 painted metal objects in the museum database (black) and obtained as paint samples on nine painted metal objects (red). Note that multiple samples were obtained from the same coating type of the same object.**

The 41 samples collected from the objects are representative of either the types of paint coatings present or of the corrosion products seen to have formed on the exposed metal sections. Of the 41 samples, four are only corrosion products and do not contain any paint. The topcoat colours of the collected paint samples are shown in Figure III-10. The samples obtained were dependent on the state of alteration of the coated surface, meaning that not all coating colours were sampled. Photographs and descriptions of sampling locations for each object are presented in Appendix F. The summary of the number of samples collected per object along with their main characteristics is presented in Chapter II. A selection of samples (free and as cross-sections) is displayed in Figure III-11. Microscope observations were used to describe the organization of the layers in each sample. In general, the paint coating

contains a minimum of two layers but many more can be present. It is not always possible to ascertain whether the layers observed are original or were applied as a repainting of the surface as either a maintenance or restoration intervention. Corrosion products are not always present in the samples, which may be explained either by the lack of formation of a significant corrosion layer under the paint coating, or by a weak adherence between the paint and corrosion products at their interface. Furthermore, the corrosion-metal interface is rarely present due to sampling limitations: obtaining the full paint coating, corrosion products and metal support is both invasive for the historical object but also technically challenging. Only one sample containing the full painted metal system was obtained during this study, the sample *Vélocycle* P03, seen in Figure III-11.I. In any case, it should be specified that these samples represent an incomplete stratigraphy of the painted metal system and that this analytical work is focused on the identification of the composition of the paint layers, the corrosion products, and the observation of the behaviour of the components at the paint-corrosion interface.

In the following section, three case studies have been selected to demonstrate the full extent of analyses completed on the microsamples in view of characterising the painted metal stratigraphy. The case studies demonstrate different examples of layer structure, paint layer composition, and alteration phenomena that can be found in a painted metal system. They include samples collected from the *Tandem* (samples P03, P05) and the *Chaudière* (sample P02). The characterisation of the other samples will not be shown in this chapter but will be included in the Appendix (see Appendix I). The results obtained from all the samples are discussed in a general manner in the discussion section of this chapter.

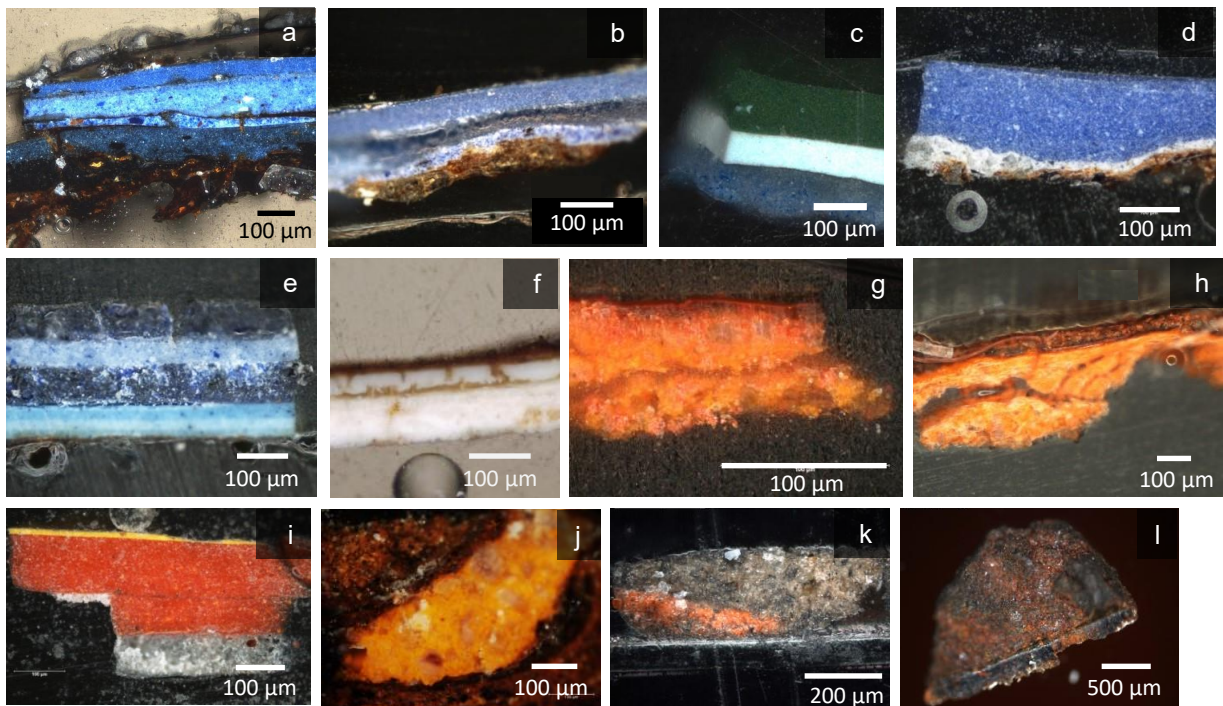


Figure III-11 Selection of samples (free and cross-sections) from studied objects: Tandem P03A (a), Tandem P07A (b), Tandem P05 (c), Charrue P03B (d), Balance P01A (e), Chaudière P02B (f), Chaudière P05B (g), Série P02B (h), Charrue P02B (i), Série P01A (j); Châssis P02 (k); Vélocoteur P03 (l, free sample containing complete painted metal stratigraphy). Samples are oriented so that the exterior layer is at the top and the layer closest to the paint-metal interface is at the bottom.

## III.II Characterisation case studies

### III.II.I Tandem P03

The sample P03 of the *Tandem* was acquired close to the screw of the back wheel (see Appendix F.i), from an area with a thick blue paint coating. The underlying iron-based support is corroded. The exterior face of sample Tandem P03 presents a dark blue paint layer with a large amount of surface dirt and dust (Figure III-12.a). On the interior face (Figure III-12.b), orange-brown, black, and grey products of various sizes are distributed across the surface and resemble iron corrosion products.

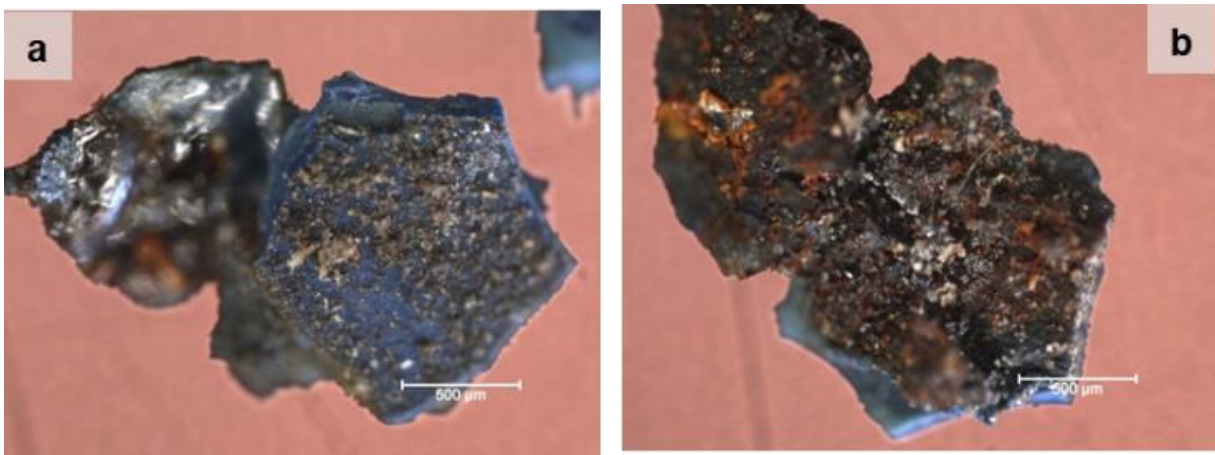


Figure III-12 Microscope images of Tandem P03 sample (scale bar 500 µm): (a) exterior face; (b) interior face.

#### III.II.I.i Morphology of the sample stratigraphy

Light and fluorescence microscopy were used to study the stratigraphy of the cross-section: 6 layers were identified in the microscope images of Tandem P03A (Figure III-13.b).

The first layer (layer 1) is a dark reddish-brown colour and corresponds to corrosion products of the metal support. The thickest section of the layer is about 215 µm. The corrosion products in layer 1 do not fluoresce under either excitation mode (Figure III-13.c,d).

Layer 2 is the first paint layer: it varies between 16-70 µm in thickness and is dark blue in colour. The granulometry appears homogeneous throughout the paint layer, although some larger dark blue/black grains (20-30 µm) are present that do not fluoresce. Individual orange grains can also be seen in layer 2, and a fissure towards the left-side of the layer appears to be filled with orange corrosion products.

A very thin layer (3) of about 12 µm seems to be present on top of layer 2: it presents the same general aspect as layer 2, but the presence of a dark line at certain points along the supposed interface suggests that they are separate layers.

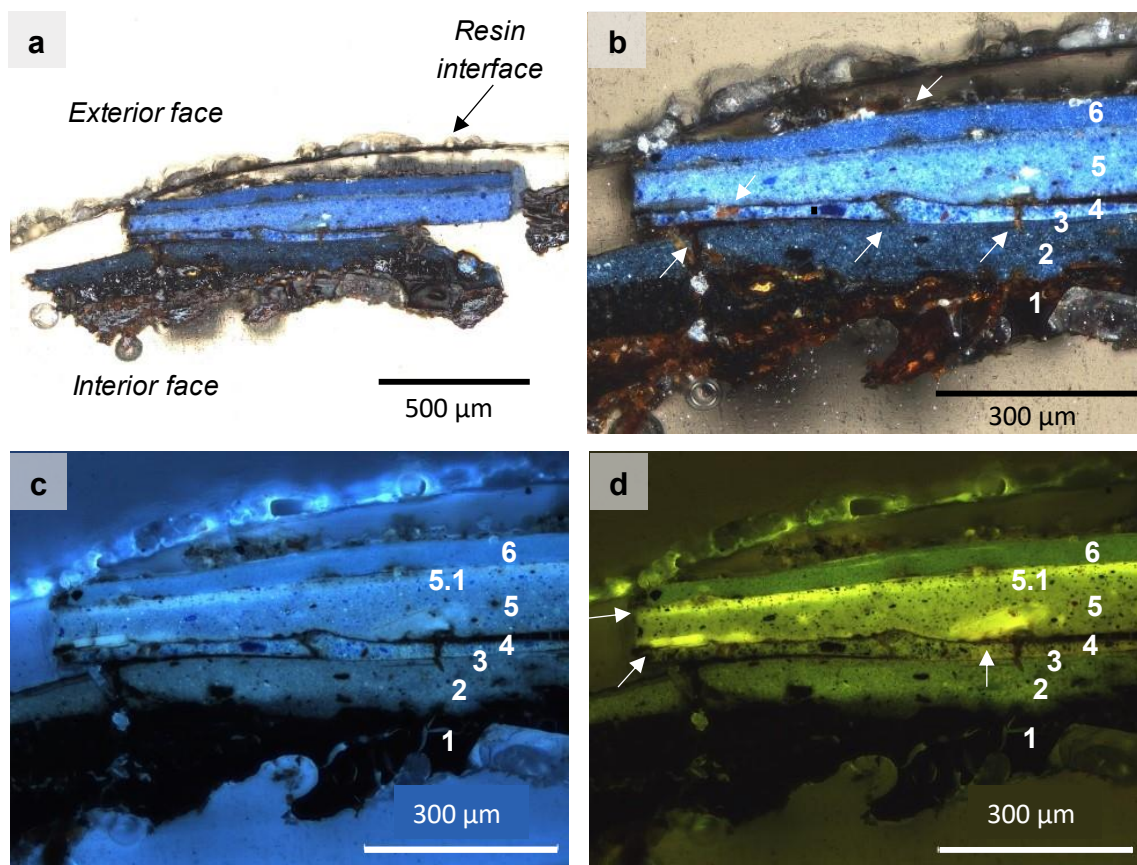


Figure III-13 Microscope images of the cross-section Tandem P03A: (a) full stratigraphy, natural light; (b) magnified view of layers, natural light; (c) UV2A filter combination  $\lambda_{\text{ex}}$ : 330-380 nm,  $\lambda_{\text{em}} > 420$  nm; (d) B2A filter combination  $\lambda_{\text{ex}}$ : 450-490 nm,  $\lambda_{\text{em}} > 515$  nm. Areas of interest are indicated by arrows.

Layer 4 (11-20  $\mu\text{m}$ ) is 11-17  $\mu\text{m}$  thick and is a much lighter blue than the preceding blue paint layers. It has a more heterogeneous aspect with dark blue grains dispersed throughout the layer that vary in size from about 5-20  $\mu\text{m}$ . Orange grains and fissures are observed at various points along layer 4.

Layer 5 is the thickest of the paint layers (around 100  $\mu\text{m}$ ) and has similar characteristics to layer 4. The dark blue grains observed under natural light in layers 4 and 5 appear dark blue with the UV2A filter but black with the B2A filter. Furthermore, small points of intense fluorescence are present in layers 4 and 5 in UV2A mode, suggestive of a highly luminescent pigment.

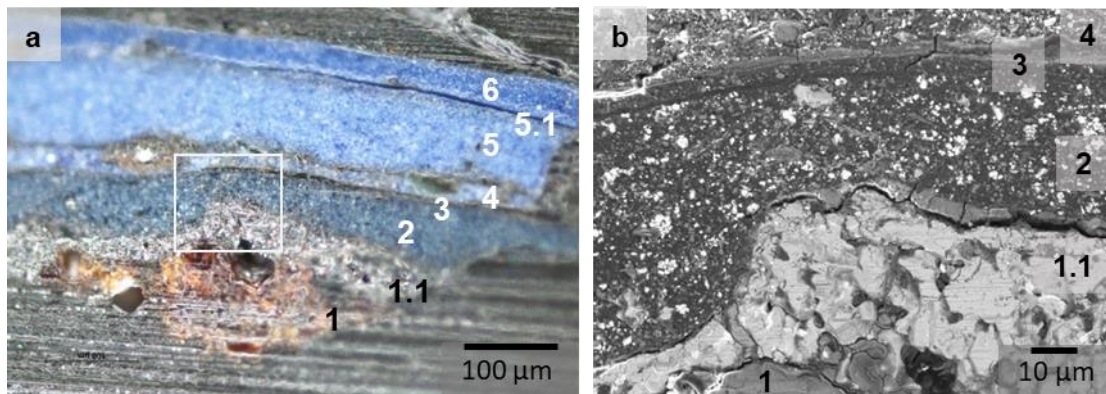
Some areas of intense fluorescence are visible in layer 5 (indicated by arrows in Figure III-13.d); notably, a layer of constant thickness (about 28  $\mu\text{m}$ ) spans the top edge of layer 5. It is assigned the number 5.1 as an area of interest within layer 5.

The most external layer, layer 6, presents a different aspect compared to the previous layers. It is also a blue paint, but darker than layers 4 and 5 and lighter than layer 2. Its grain size distribution is homogeneous, and it has a constant thickness of  $\sim 30$   $\mu\text{m}$ . The layer has a homogeneous fluorescence behaviour and the emission is not as intense as in layers 4 and 5. The external face of layer 6 presents

some grey-brown products and most likely corresponds to the dust and dirt observed on the external face of the sample before embedding (Figure III-12.a).

Poor adhesion is observed between paint layers 3 and 4 and layers 4 and 5 along the entire span of the interface and some orange corrosion products are present in the void left by the separation. Some dark spots are present along the interface of layers 5 and 6. The altered zones, especially the fissures and separation between the paint layers, appear black in UV2A mode.

Tandem P03B (Figure III-14.a) shows a similar stratigraphy with a few slight differences (possibly due to the amount of polishing applied to the cross-section at the time the photograph was acquired). A grey layer (thickness  $\sim 30\text{-}60\ \mu\text{m}$ ) is present between the red-orange corrosion products and the most interior paint layer (layers 1 and 2 in Tandem P03A, Figure III-13.b). It could possibly be a preparation base coat) layer. The corresponding area will be assigned the number 1.1 indicating that it is an area within layer 1 that presents a slightly different aspect.



**Figure III-14 Cross-section Tandem P03B. (a) Light microscope image with white square around zone of interest imaged by SEM. (b) SEM-BSE image (10 kV) of the zone of interest. Layers 1-4 are labeled.**

SEM in backscattered electron (BSE) mode (Figure III-14.b) was used for the observation of differences in chemical composition and morphology of the layers in the zone of interest on Tandem P03B (marked by white square in Figure III-14.a). Layer 1.1 appears lighter grey than layer 1, confirming the difference in composition suggested by the OM image. Layer 2 shows a mixture of grains of different sizes (1-10  $\mu\text{m}$ ) with different scattering intensities dispersed within a low scattering (dark grey) matrix, suggesting a mixture of pigments: grains that appear as white suggest the presence of heavier elements. Layer 3 shows less contrast with smaller light grey grains ( $\sim 1\ \mu\text{m}$ ) within the same dark matrix as layer 2. Layer 4 shows a completely different aspect to layers 2 and 3: it presents an overall lighter shade of grey, indicative of an elemental composition containing heavier elements. The granulometry is diverse, ranging from less than 1  $\mu\text{m}$  to 5  $\mu\text{m}$ .

The observations acquired on the cross-sections by light, fluorescence and electron microscopy led to a detailed description of the morphological characteristics of the stratigraphy of Tandem P03 and is

presented in Table III-1. 7 distinct layers are recognized: the corrosion layer at the paint-metal interface (layer 1); a grey layer, potentially a preparation layer, mixed with corrosion products (layer 1.1); dark blue paint layers with mixed granulometry (layers 2 and 3); light blue paint layers with dark blue grains (layers 4 and 5); and a final coat of medium blue paint with a homogeneous texture (layer 6). An area along the surface of layer 5 presents different fluorescence properties to the bulk of the layer and is distinguished as layer 5.1.

**Table III-1 Description of stratigraphy of sample Tandem P03: summary of morphology and luminescence analyses and first assignments.**

Layer number	Description (morphology and luminescence properties)	Thickness	Assignment
1	Dark reddish-brown; no emission	215 $\mu\text{m}$	Corrosion products
1.1	Grey, granular; no emission	~30-60 $\mu\text{m}$	Preparation layer? Corrosion products?
2	Dark blue, homogeneous fine granulometry, some large dark grains present (20-30 $\mu\text{m}$ diameter); blue and green emission	16-70 $\mu\text{m}$	Paint layer
3	Dark blue, homogeneous fine granulometry; blue and green emission	12 $\mu\text{m}$	Paint layer
4	Light blue with dark blue grains (5-20 $\mu\text{m}$ diameter); blue and green emission	11-17 $\mu\text{m}$	Paint layer
5	Light blue with dark blue grains (5-20 $\mu\text{m}$ diameter); blue and green emission	100 $\mu\text{m}$	Paint layer
5.1	Surface layer along layer 5, indistinguishable under light microscopy; intense green emission under UV	28 $\mu\text{m}$	Surface alteration? Interaction between layer 5 and 6?
6	Blue, fine homogeneous granulometry; blue and green emission	30 $\mu\text{m}$	Paint layer



### III.II.I.ii Chemical composition of the sample stratigraphy

The surface of Tandem P03A was mapped using synchrotron micro-XRF spectroscopy. The sum of the spectra acquired over the whole sample surface is shown in Figure III-15. The most intense fluorescence lines correspond to Fe, Zn, Pb and Sr. Lower amounts of Ca, Ba, Mn, Cu and Br are also present in the sample.

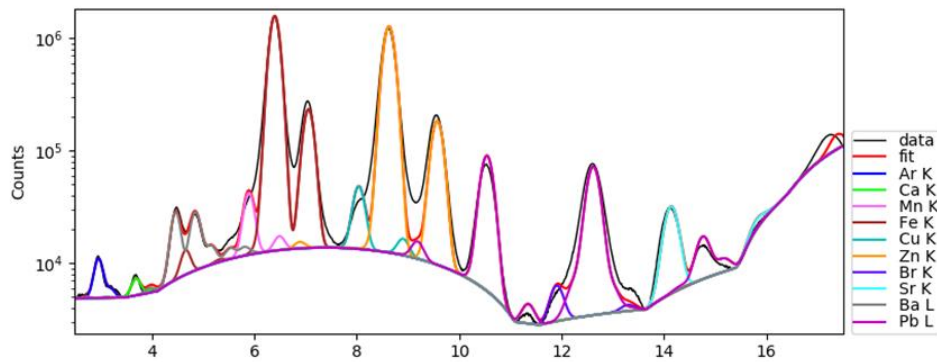


Figure III-15 Sum of XRF spectra (Incident energy = 18 keV) obtained on cross-section Tandem P03A.

The XRF distribution maps of the elements detected in Tandem P03A are displayed in Figure III-16. Layer 1 contains mainly Fe with lower amounts of Mn, corresponding to the corrosion products. Layer 1.1 contains Fe, with low amounts of Ba and Mn, suggesting a mix of iron corrosion products and Ba-based compounds. The dark blue layer 2 contains Ba, Sr, Pb and Zn. The composition of layer 3 cannot be distinguished from the other layers in these maps. Light blue layer 4 contains Zn, Pb, Ba, Sr and Cu. Similarly, light blue layer 5 contains mainly Zn with some Pb, Ba, Cu, Mn and Br, although the Br K $\alpha$  line (11.92 keV) is at the base of the Pb L $\beta$  line (12.6 keV), making its distribution uncertain. It should be noted that in contrast to other layers containing Ba, almost no Sr is detected. The layer 5.1 contains Zn, Pb, Ba and possibly Sr (the interface between 5 and 6 is unclear). The top blue layer 6 contains Zn, Ba and Sr. Low amounts of Ca are present in all layers but is particularly intense along the exterior face of the sample and may correspond to the components of the dust and dirt observed on the loose sample before embedding. Fe is seen not only at the paint-metal interface but also between layers 4 and 5 in areas where corrosion products were observed under optical microscopy. It is also observed along the exterior face of the sample.

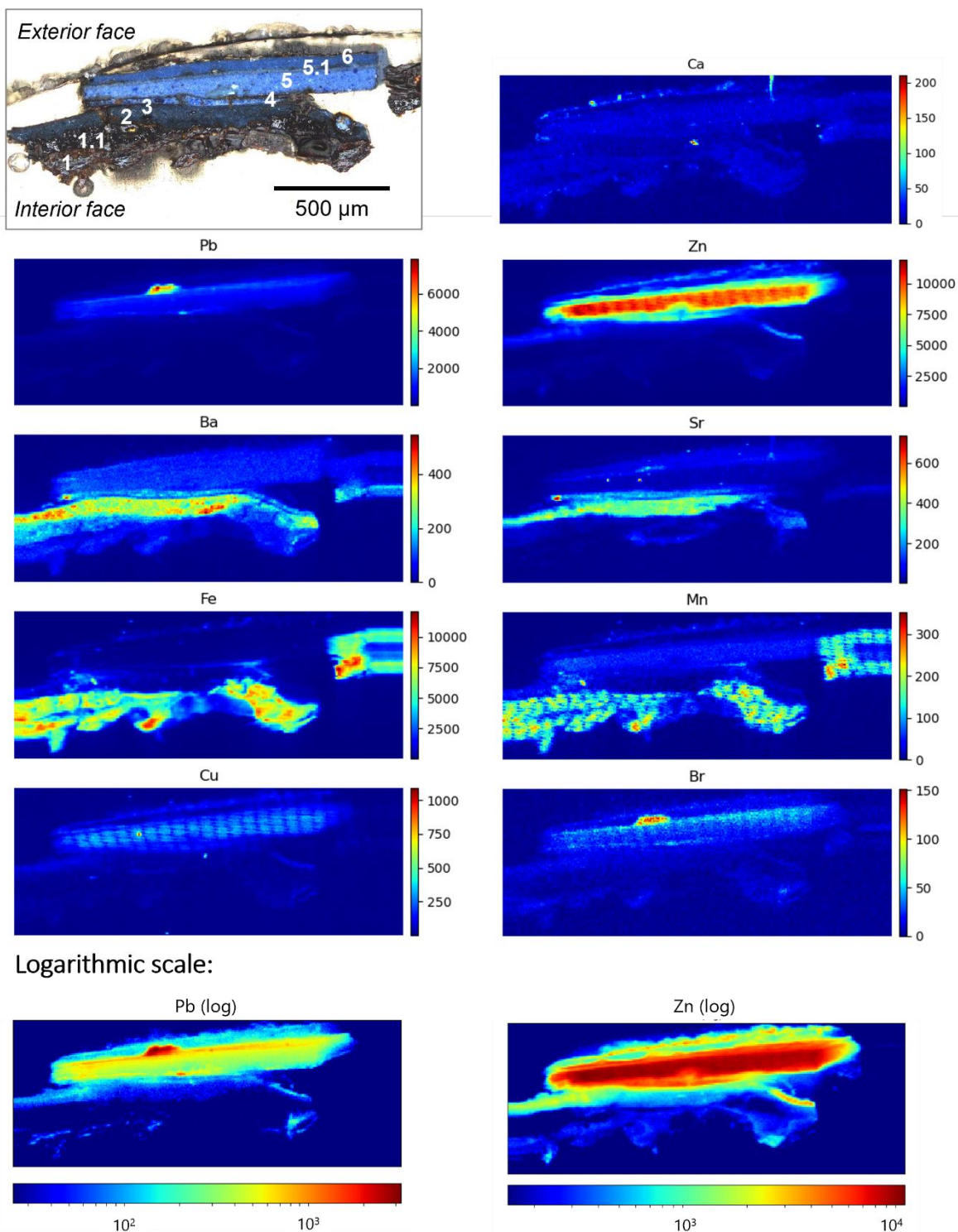


Figure III-16 Synchrotron micro-XRF elemental distribution maps of the sample Tandem P03A. Intensity scales are arbitrary.

Tandem P03B was analysed using SEM-EDS to identify the lighter elements in the various layers. Figure III-17.a shows the cross-section Tandem P03B and the zone of interest (marked by a white square). A map of the zone of interest was obtained and the individual elemental distributions are shown in Figure III-17.c-g. Layer 1.1 contains O and Fe with a small amount of Si and traces of Na and Al. Layer 2 contains

mainly Na, Al, Si and O, although small grains containing Fe are also seen scattered throughout the layer. Layer 3 cannot be distinguished from layer 2, inferring an identical composition. The top left corner of the Na map shows an intense signal, suggesting that layer 4 contains a greater amount of Na than in the preceding layers.

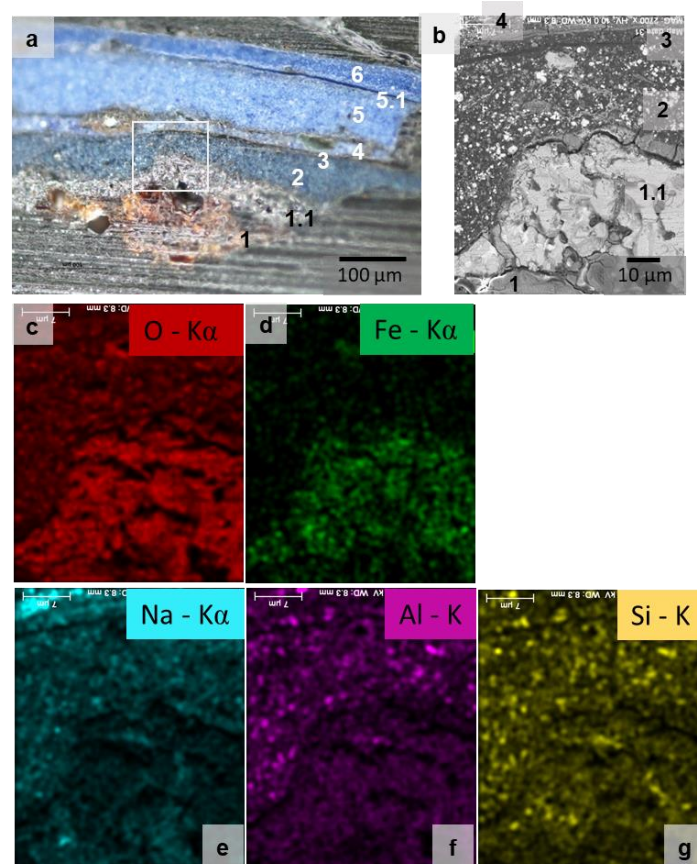


Figure III-17 SEM-EDS mapping of the zone of interest on sample Tandem P03B (represented as white square in light microscope image (a)): SEM-BSE image of zone of interest (b); Elemental maps of oxygen, iron, sodium, aluminum and silicon (c-g, respectively).

### III.II.I.iii Structural study of the sample stratigraphy

The Tandem P03A cross-section was analysed by Raman spectroscopy to investigate the compounds constituting the various layers. Several points in each layer were analysed in two sessions, in 2017 (Figure III-18.a) and 2018 (Figure III-18.b), hence the repetition of point number assignment.

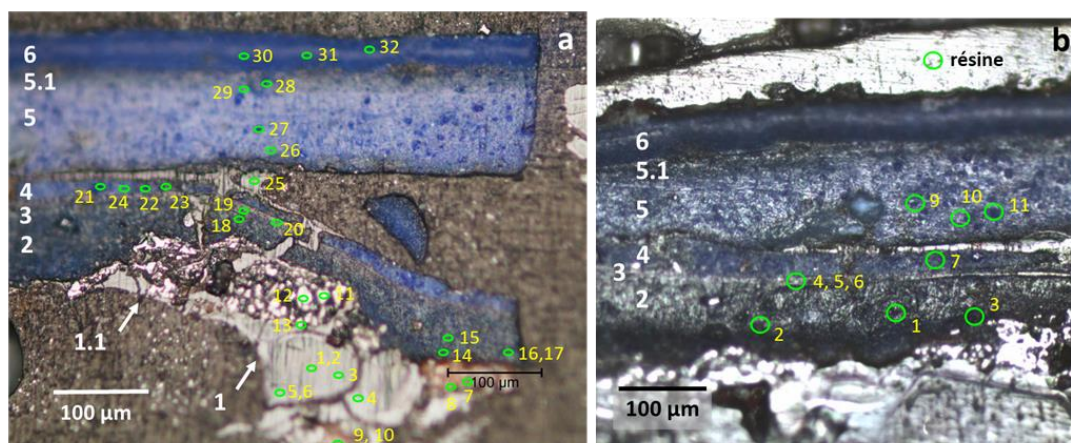


Figure III-18 Raman analysis (785 nm; laser power 3 mW; 100x IR objective) measurement locations marked by green circles and yellow numbers on Tandem P03A: a) Initial measurements (2017); b) Follow-up measurements (2018). The stratigraphic layers are marked by white numbers along the left-hand side.

The most representative Raman spectra per layer are listed below. In layer 1 (Figure III-19.a), corresponding to the layer of corrosion, spectra were obtained that contain characteristic Raman bands of the iron corrosion products hematite  $\alpha\text{-Fe}_2\text{O}_3$  (221, 286, and  $397\text{ cm}^{-1}$ ) and some form of iron oxyhydroxide  $\text{FeOOH}$  ( $306$ ,  $425$ , and  $545\text{ cm}^{-1}$ ) (Bellot-Gurlet et al., 2009). In layer 1.1 (Figure III-19.b), the spectrum contains unassigned bands at  $210$ ,  $274$ ,  $384$ ,  $1266$  and  $1877\text{ cm}^{-1}$ . The closest correspondence for these bands is goethite  $\alpha\text{-FeOOH}$  (Monnier et al., 2011). In the blue paint layer 2 (Figure III-20), the blue pigments ultramarine blue ( $\text{S}_3^-$  and  $\text{S}_2^-$  in  $\text{Na}_8[\text{Al}_6\text{Si}_6\text{O}_{24}]\text{S}_n$ ) and Prussian blue ( $\text{Fe}_4[\text{Fe}(\text{CN})_6]_3$ ) were detected by characteristic bands at  $549$  and  $2151\text{ cm}^{-1}$ , respectively. The white pigments titanium white ( $\text{TiO}_2$ ), lithopone ( $\text{ZnS}$  and  $\text{BaSO}_4$ ) and lead white ( $2\text{PbCO}_3\cdot\text{Pb}(\text{OH})_2$ ) were identified by their characteristic bands at  $143$ ,  $988$  and  $1058\text{ cm}^{-1}$ , respectively (Caggiani et al., 2016). The points analysed in blue paint layer 3 (Figure III-21) give spectra with bands characteristic of titanium white and ultramarine blue. In layer 4 (Figure III-22), the acquired spectra contain Raman bands characteristic of previously identified pigments ultramarine blue, lithopone, lead white, and titanium white, and a first identification of the synthetic pigment phthalocyanine blue (copper phthalocyanine,  $\text{C}_{32}\text{H}_{16}\text{CuN}_8$ ) thanks to the bands at  $750$ ,  $1082$ ,  $1343$ , and  $1528\text{ cm}^{-1}$  (Caggiani et al., 2016). Ultramarine blue was the only pigment identified in layer 5 (Figure III-23), although weak bands at  $1180$  and  $1377\text{ cm}^{-1}$  are also present in the spectra, suggesting the presence of another unidentified organic component, possibly belonging to a component in the binder. The spectra acquired along the top edge of layer 5 (layer 5.1, spectra not shown) and in layer 6 (Figure III-24) only show ultramarine blue bands as well. Most of the acquired spectra present a high intensity of background fluorescence which may have impeded identification of other pigments with weaker Raman signals.

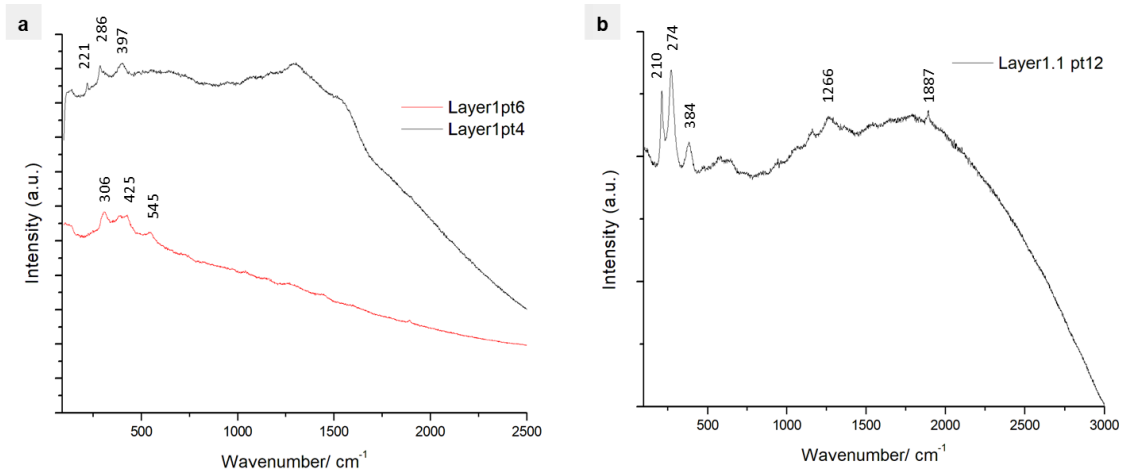


Figure III-19 Raman spectra (785 nm laser) acquired on the Tandem P03A: points 4 and 6 acquired in layer 1 in 2017 (a), point 12 acquired in layer 1.1 in 2017 (b). Refer to Figure III-18 for measurement locations.

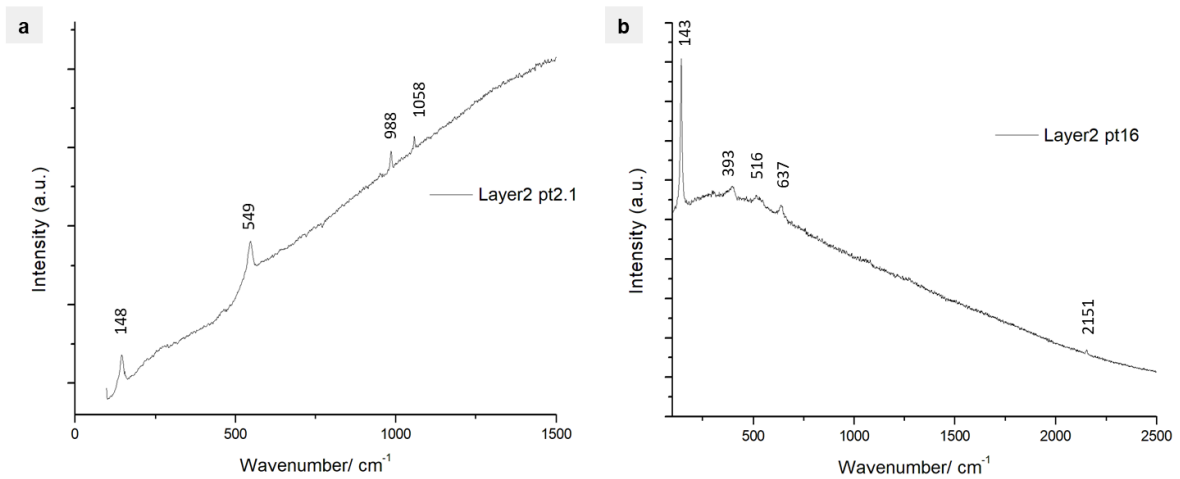


Figure III-20 Raman spectra (785 nm laser) acquired in layer 2 of the Tandem P03A: point 2.1 acquired in 2018 (a), point 16 acquired in 2017 (b). Refer to Figure III-18 for measurement locations.

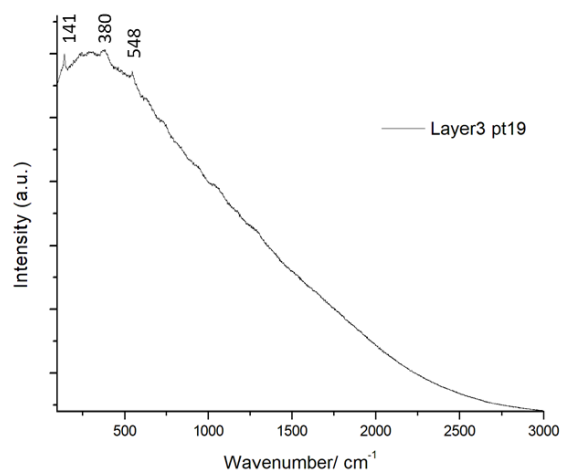


Figure III-21 Raman spectrum (785 nm laser) acquired in layer 3 of the Tandem P03A: point 19 acquired in 2017. Refer to Figure III-18 for measurement locations.

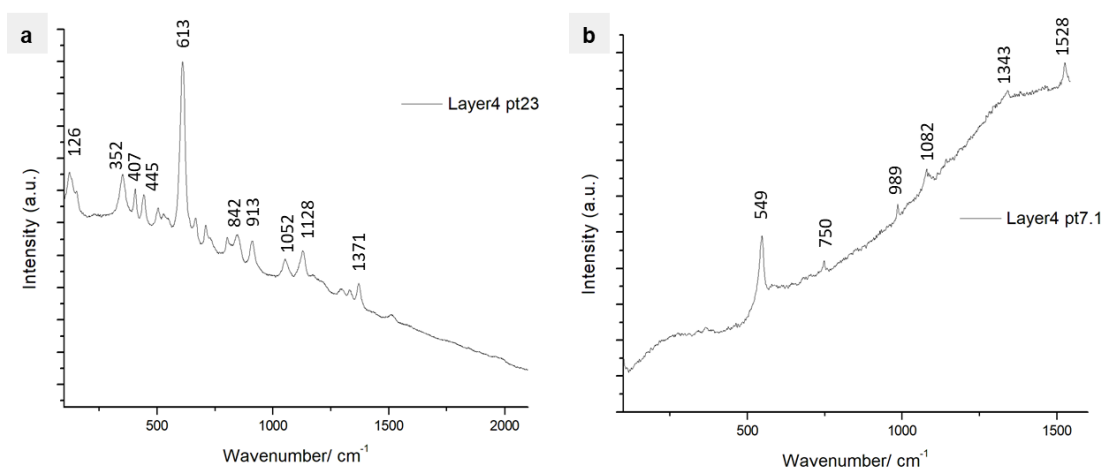


Figure III-22 Raman spectrum (785 nm laser) acquired in layer 4 of the Tandem P03A: point 23 acquired in 2017 (a), point 7.1 acquired in 2018 (b). Refer to Figure III-18 for measurement locations.

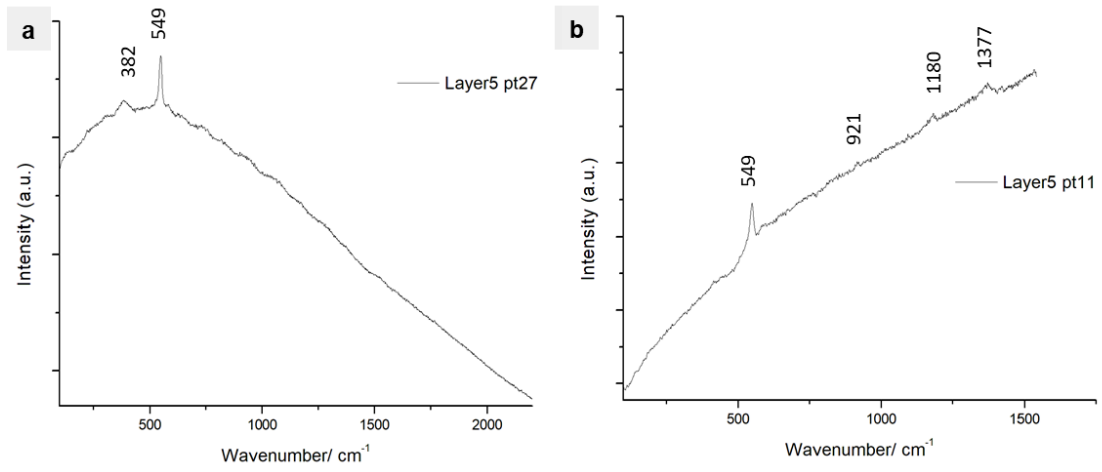


Figure III-23 Raman spectrum (785 nm laser) acquired in layer 5 of the Tandem P03A: point 27 acquired in 2017 (a), point 11 acquired in 2018 (b). Refer to Figure III-18 for measurement locations.

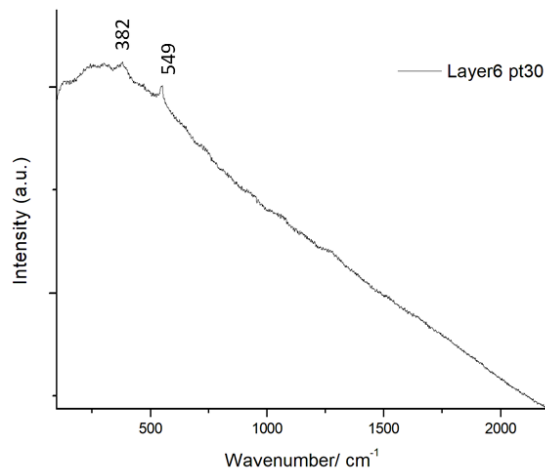


Figure III-24 Raman spectrum (785 nm laser) acquired in layer 6 of the Tandem P03A: point 30 acquired in 2017. Refer to Figure III-18 for measurement locations.

XANES spectra at the Pb L<sub>3</sub> edge were acquired as profiles across the interfaces of layers 2 to 5 and 5 to 6 (Figure III-25) with the aim of investigating the local environment of Pb in these areas presenting signs of alteration (separation of layers, fluorescence along the top edge of layer 5). The acquired spectra are grouped by profile location and shown in Figure III-25b. A difference of 2.3 eV is measured between the white line positions of the two groups. Both groups were found to have similar forms to reference spectra of basic lead(II) carbonate (lead white) and lead soaps of palmitic and azelaic fatty acids, although these three species have similar spectra and are difficult to distinguish, especially due to the noise present in the acquired spectra. The shift towards lower energies of the white line of the layer 5-6 group is suggestive of the characteristic form of the PbSO<sub>4</sub> XANES reference spectrum, inferring a similar lead coordination structure.

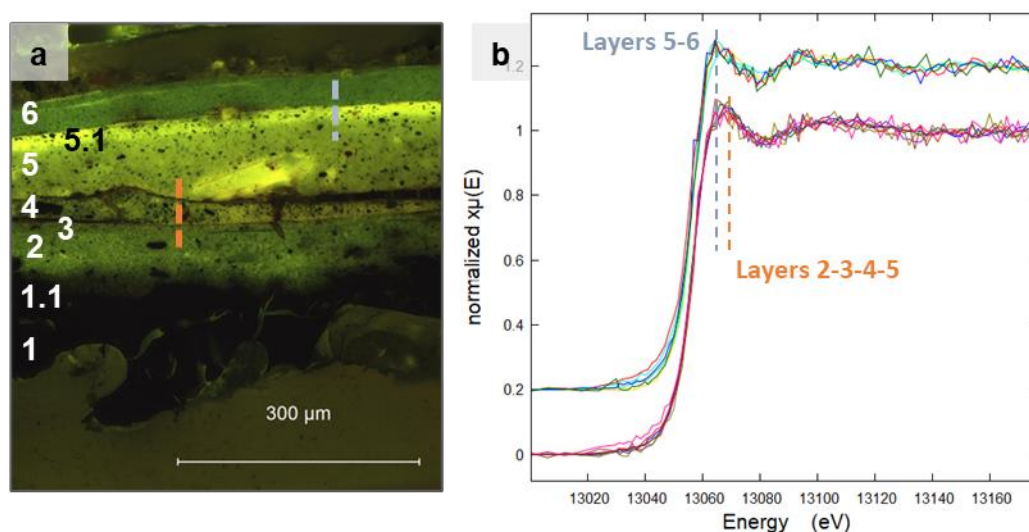


Figure III-25 XANES profiles at the Pb L<sub>3</sub> edge acquired across layers 2-5 and 5-6 (orange and grey profiles shown in fluorescence (B2A mode) microscope image of Tandem P03A (a)); (b) XANES spectra grouped by profile. Positions of white lines are indicated by dashed lines.

#### III.II.I.iv Summary of characterisations of Tandem P03

The morphological, elemental, and structural characteristics of the sample Tandem P03 were studied using various techniques and the results are listed in Table III-2.

The dark red-brown **layer 1** at the paint-metal interface was found to contain Fe which is related to the presence of iron corrosion products such as goethite and hematite.

The grey **layer 1.1** containing mainly Fe and Ba with low amounts of other elements may be a mixture of iron corrosion products and the first paint layer.



The first blue paint **layer 2** shows a varied elemental composition: Na, Al and Si correspond to the identified pigment ultramarine blue; Fe is due to the presence of the pigment Prussian blue; Ba and Sr correspond to the presence of lithopone; Pb corresponds to the identified lead white pigment. Titanium white was also identified, although Ti was not identified in the elemental analysis due to the overlap of its X-ray fluorescence signal by that of Ba. The presence of Prussian blue was only detected in layer 2 and may explain the layer's darker shade of blue in comparison to the subsequent layers.

The very thin blue paint **layer 3** was indistinguishable from its surrounding layers in XRF and SEM-EDS maps, but the Raman analysis revealed a similar composition to layer 2 with the identification of titanium white and ultramarine blue.

The blue **layer 4** shows a similar elemental composition to the previous layers, with additional presence of Zn and Pb. These correspond to the identified pigments lithopone and lead white. Ultramarine blue, titanium white and the synthetic pigment phthalocyanine blue were also identified. The presence of phthalocyanine blue allows to date the application of layer 4 to at least 1935 (the year the pigment became commercially available (Defeyt et al., 2013)).

Ultramarine blue was the only pigment identified in layers **5, 5.1 and 6**, although the elemental composition (mainly Zn, lower amounts of Pb, Ba, Cu, Mn, Br) suggests the presence of other pigments, such as lead white, lithopone, zinc white, phthalocyanine blue/green. The XANES Pb L<sub>3</sub> edge measurements acquired on **layer 5** gave spectra with a similar form to lead white. The XANES measurements also suggest the presence of a compound with the same coordination as PbSO<sub>4</sub> in the alteration **layer 5.1**, as well as lead soaps in all the paint layers (layers 2-6). A low amount of Ca was detected with homogeneous distribution in the majority of the stratigraphy, underlining that it is not a constituent of the paint formulation. It is present in concentrated points along the external face of the sample but most likely corresponds to dust products. A XANES profile measured at the Pb L<sub>3</sub> edge across layers 5-6 gave spectra that suggest the presence of a lead compound with a chemical environment resembling that of PbSO<sub>4</sub>.

The binder of this specific sample was not determined, although GC-MS analysis of another blue paint sample from the same object (sample Tandem P06) revealed the presence of components characteristic of an aged drying oil and of a *Pinaceae* resin. The analysis was conducted on the whole sample and is not layer specific.

Table III-2 Characterisations (organized by technique) of each layer in the sample Tandem P03.

Layer number	Morphological description	Elemental composition		Structural characterisation	Binder characterisation
	<i>Microscopy (OM, UV, SEM)</i>	<i>SEM-EDS</i>	<i>Synchrotron micro-XRF</i>	<i>Raman 785 nm; XANES Pb L<sub>3</sub> edge</i>	<i>GC-MS</i>
<b>1</b>	Dark reddish-brown corrosion layer (~215 µm); no emission	O, Na, Fe	Fe, Mn, Ca	Iron oxyhydroxides (Goethite?), Hematite	Aged drying oil, <i>Pinaceae</i> resin (from sample Tandem P06)
<b>1.1</b>	Grey, granular corrosion/preparation layer (~30-60 µm); no emission	Fe, O; low amounts of Na, Al, Si	Fe, Mn, Ba, Ca	Goethite?	
<b>2</b>	Dark blue paint layer, homogeneous fine granulometry, some large dark grains present (16-70 µm); blue and green emission	Na, Al, Si, O; low amounts of Fe	Ba, Sr, Pb, Zn, Ca	Ultramarine blue, Prussian blue, Titanium white, Lead white, Lithopone; Lead soaps	
<b>3</b>	Dark blue paint layer, homogeneous fine granulometry (12 µm); blue and green emission	Na, Al, Si, O; low amounts of Fe	Not distinguishable from other layers 2 and 4	Titanium white, Ultramarine blue; Lead soaps	
<b>4</b>	Light blue paint layer with dark blue grains (11-17 µm); blue and green emission	Na, Al, Si, O	Zn, Pb, Ba, Sr, Cu, Ca	Ultramarine blue, Lithopone, Lead white, Titanium white, Phthalocyanine blue; Lead soaps	
<b>5</b>	Light blue paint layer with dark blue grains (100 µm); blue and green emission	Not analysed	Zn; some Pb, Ba, Cu, Mn, Br, Ca	Ultramarine blue, unidentified organic compound (binder?); Lead soaps	
<b>5.1</b>	Continuous alteration layer along top face of layer 5 (28 µm), indistinguishable by light microscopy; intense green emission under UV	Not analysed	Zn, Pb, Ba, possibly Sr, Ca	Ultramarine blue; Lead soaps	
<b>6</b>	Blue paint layer, fine homogeneous granulometry (30 µm); blue and green emission	Not analysed	Zn, Ba and Sr, Ca	Ultramarine blue; Lead soaps	

### III.II.II Tandem P05

Contrary to most of the samples, Tandem P05 was obtained from a light-colored metallic substrate, suggesting a possible surface treatment such as tinning or galvanization (zincing) of the iron support. The underlying metal did not appear to be highly corroded. The observations of the sample by light microscopy reveal a multi-layered and multi-coloured paint system. The exterior face (Figure III-26.a) presents a discontinuous dark green paint layer over about half of the sample, revealing a light blue paint layer underneath. The paint loss of the green layer suggests poor adhesion with the light blue paint layer. The interior face (Figure III-26.b) shows the same light blue paint as a continuous layer followed by a fragment of underlying dark blue paint. The dark blue paint layer is the most interior paint layer and, given its discontinuity across the interior surface, it may have been an original paint layer that was later repainted with the subsequent light blue and green paint layers. Brown and grey powder are scattered over the interior face.

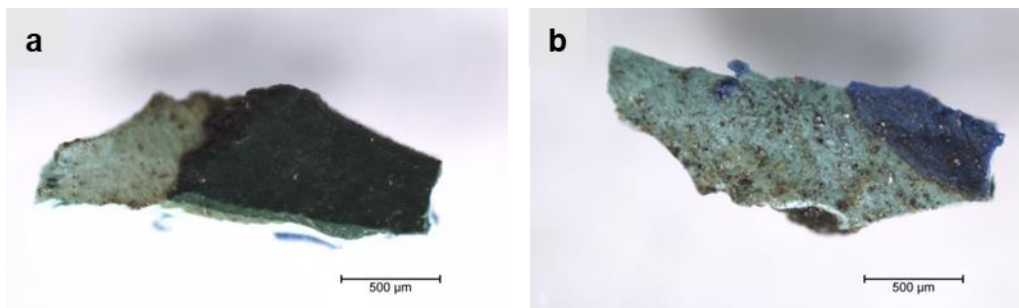


Figure III-26 Microscope images of sample Tandem P05. (a) Exterior face; (b) Interior face.

#### III.II.II.i Morphology of the sample stratigraphy

Tandem P05 was embedded in resin and polished down to obtain just one cross-section face. It was then observed by light and fluorescence microscopy (Figure III-27).

In the dark blue paint layer 1 (78 µm thick), corresponding to the layer applied directly to the metal, some white, light blue and dark blue grains are visible (see Figure III-27.c). It shows a medium level of emission with the UV2A filter (Figure III-27.d).

Depending on the imaging mode used, layer 2 (65-95 µm thick) appears light blue (Figure III-27.a) or white (Figure III-27.b). The paint layer contains a low amount of blue pigment in an otherwise reflective white matrix and emits intensely in B2A mode (Figure III-27.e).

The dark green paint layer 4 (100 µm thick), corresponding to the outer layer, appears to have a homogeneous aspect with a fine distribution of dark green and light green/yellow particles (see Figure III-27.c) and does not fluoresce under either of the excitation modes used.

A dark brown product of uneven thickness (around 30-45  $\mu\text{m}$ ) is observed between layers 2 and 4, but only along one part of the interface, and emits weakly in the UV2A mode. It will be referred to as layer 3 (see Figure III-27.b). During the condition report of the object, the green layer was seen to be separating from the lower paint layers. The brown product in layer 3 may possibly be a restoration treatment used to hold the top layer in place.

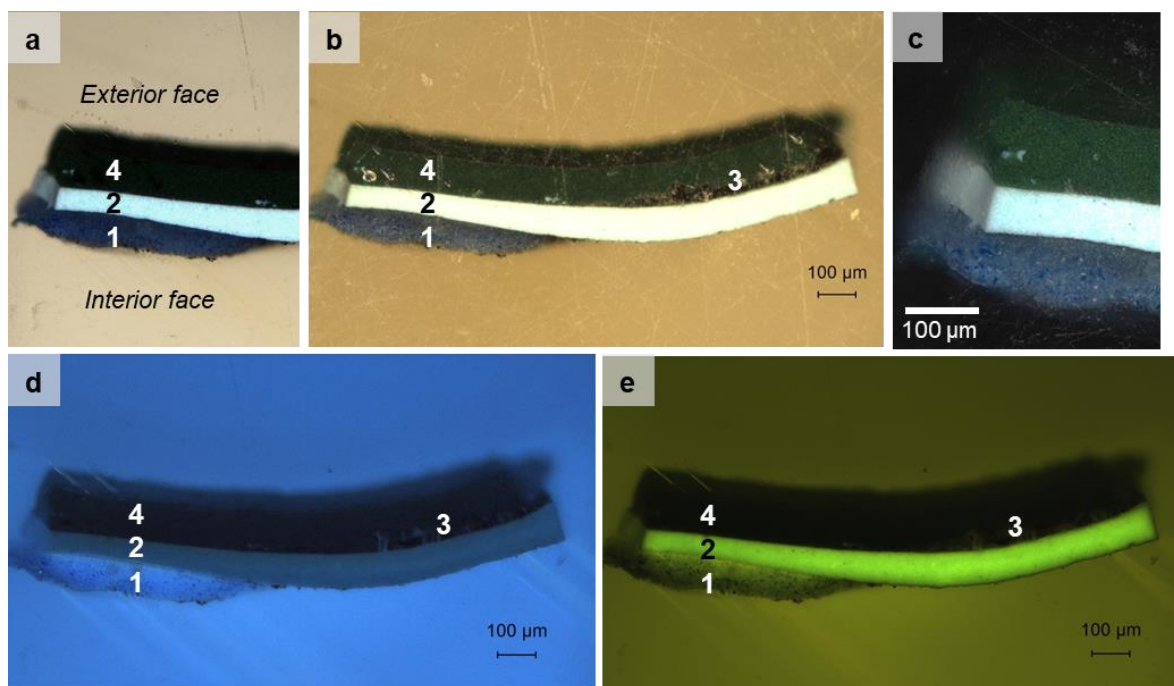


Figure III-27 Light and fluorescence microscopy images of the cross-section Tandem P05: bright field (a); dark field (b); magnified view of b, dark field (c); UV2A filter combination  $\lambda_{\text{ex}}$ : 330-380 nm,  $\lambda_{\text{em}} > 420$  nm (d); B2A filter combination  $\lambda_{\text{ex}}$ : 450-490 nm,  $\lambda_{\text{em}} > 515$  nm (e).

The observations of the cross-sections with light and fluorescence microscopy led to a detailed description of the morphological characteristics of the stratigraphy of Tandem P05 and is presented in Table III-3.

Table III-3 Description of stratigraphy of sample Tandem P05: summary of morphology and luminescence analyses and first assignments.

Layer number	Description (Morphology and Luminescence properties)	Thickness	Assignment
1	Dark blue, heterogeneous distribution of pigment particles; medium level of blue emission	78 $\mu\text{m}$	Paint layer
2	Light blue; intense green emission	65-95 $\mu\text{m}$	Paint layer
3	Dark brown, uneven; weak blue emission	~45 $\mu\text{m}$	Restoration treatment?
4	Dark green, homogeneous appearance; no fluorescence	100 $\mu\text{m}$	Paint layer

### III.II.II.ii Chemical composition of the sample stratigraphy

The elemental composition of layers 1, 2 and 4 of Tandem P05 was determined by mapping the cross-section with synchrotron micro-XRF spectroscopy. The sum of the spectra acquired over part of the sample surface is shown in Figure III-28. The most intense fluorescence lines are characteristic of emission of Ba, Cr, Mn, Fe, Ti, Cu, Zn, Pb, Br, and Sr.

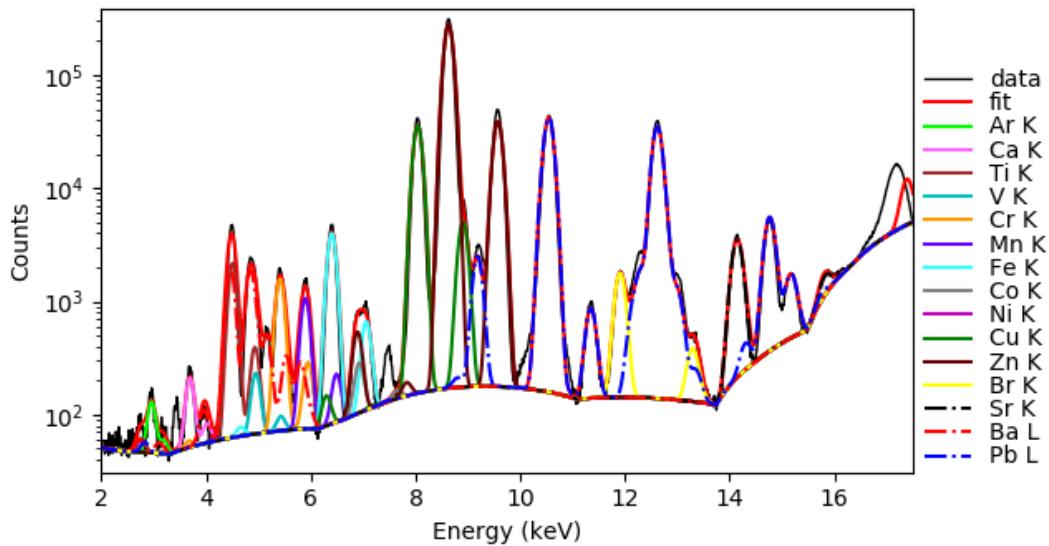


Figure III-28 Sum of synchrotron micro-XRF spectra (Incident energy = 18 keV) obtained on Tandem P05.

The most representative elemental maps of the stratigraphy of Tandem P05 are displayed in Figure III-29. These maps reveal the very different elemental compositions of each layer, in accordance with the visual colour differences observed. The blue layer 1 contains a large amount of Zn and smaller quantities of Ba. The light blue layer 2 contains mainly Zn and in lesser proportion Ti and Ba, as well as an intense spot of Br. The area of the sample that was mapped did not contain layer 3. The green layer 4 contains mainly Pb with lower amounts of Fe and Cr. Local intense points of Fe and of Sr are also present in the stratigraphy. The Cu signal was only detected in areas surrounding the sample, and most likely originated from the sample support. Other elements, such as Ca, V, Co and Ni, had weak signals or had overlapping bands with more intense elements, making their distribution in the maps uncertain.

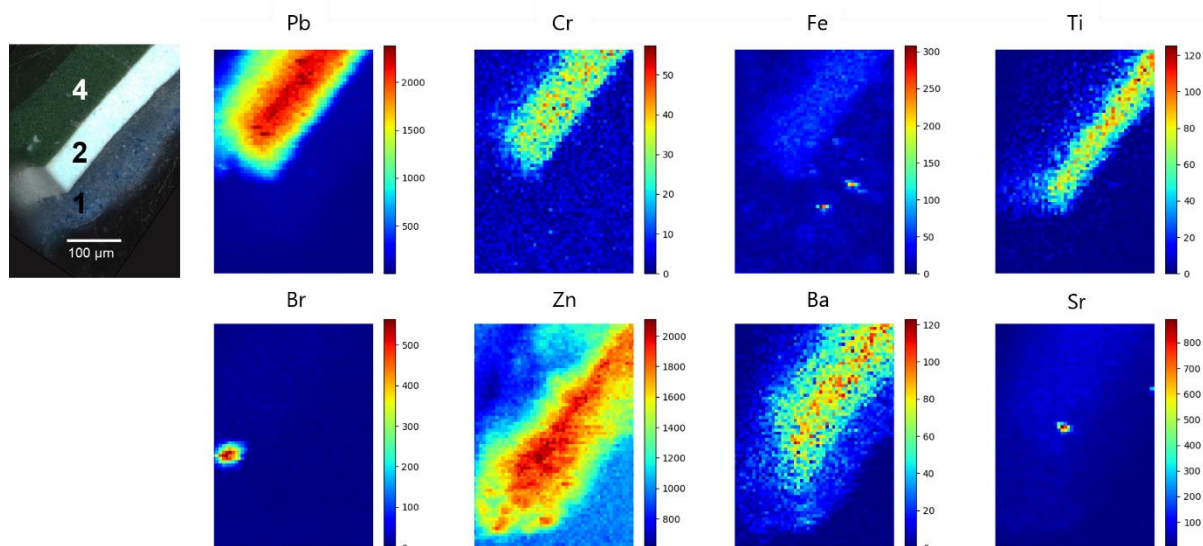


Figure III-29 Synchrotron micro-XRF elemental distribution maps of the cross-section Tandem P05. Intensity scales are arbitrary.

### III.II.II.III Structural study of the sample stratigraphy

Using Raman spectroscopy, certain pigments were identified in layers 1, 2 and 4 of the Tandem P05 sample. Layer 3 was not analysed. The measurement positions are shown in Figure III-30.

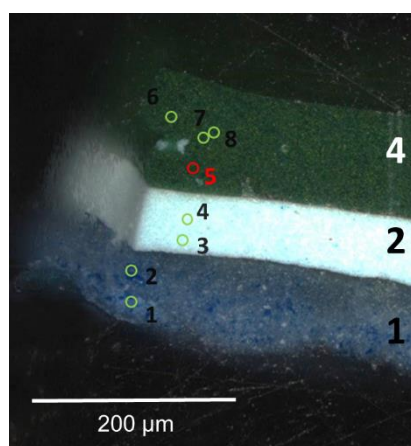


Figure III-30 Measurement positions (green circles) of Raman spectroscopy analysis (785 nm; laser power 3 mW; 100x IR objective) on layers 1, 2 and 4 of Tandem P05. Point 5 (in red) suffered thermal degradation during Raman analysis.

In layer 1 (see Figure III-31), the spectrum acquired at point contains characteristic bands of ultramarine blue ( $548, 583 \text{ cm}^{-1}$ ), lithopone ( $987 \text{ cm}^{-1}$ ) and a weak band at  $2154 \text{ cm}^{-1}$  assigned to Prussian blue (Caggiani et al., 2016). Other bands at  $385, 748$  and  $1527 \text{ cm}^{-1}$  are unassigned. The second spectrum acquired (point 2) also contains the  $547 \text{ cm}^{-1}$  band of ultramarine blue, but has other unassigned bands at  $152, 221$  and  $472 \text{ cm}^{-1}$ .

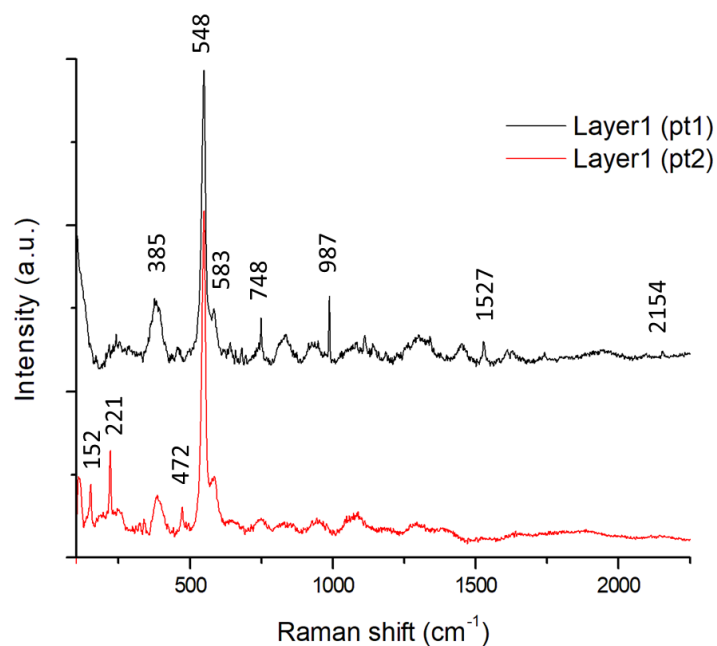


Figure III-31 Raman spectra (785 nm) of points 1 (black) and 2 (red) acquired in layer 1 of Tandem P05, baseline subtracted. Bands of interest are labeled with corresponding wavenumber. The ripples present on the spectra background are related to the Edge filter transmission artifacts, not to vibrational features.

The spectra acquired in layer 2 (see spectrum of point 4 in Figure III-32) contain many well-defined bands as a result of the overlap of the characteristic signals of several different phases. The bands at 144, 236, 446 and 609  $\text{cm}^{-1}$  are assigned to the white pigment titanium white (Caggiani et al., 2016). Lithopone was identified by the bands at 346, 987 and 1142  $\text{cm}^{-1}$ . Other bands are assigned to the blue pigment phthalocyanine blue, a metal-organic complex identified by its characteristic bands at 685, 748, 953, 1008, 1142, 1339, 1452, and 1528  $\text{cm}^{-1}$ . The remaining bands at 777, 817, 1082, 1186, 1213, 1283 and 1538  $\text{cm}^{-1}$  correspond to the phthalocyanine green pigment, the halogenated (Cl, Br) version of the phthalocyanine blue pigment (Caggiani et al., 2016; Scherrer et al., 2009).

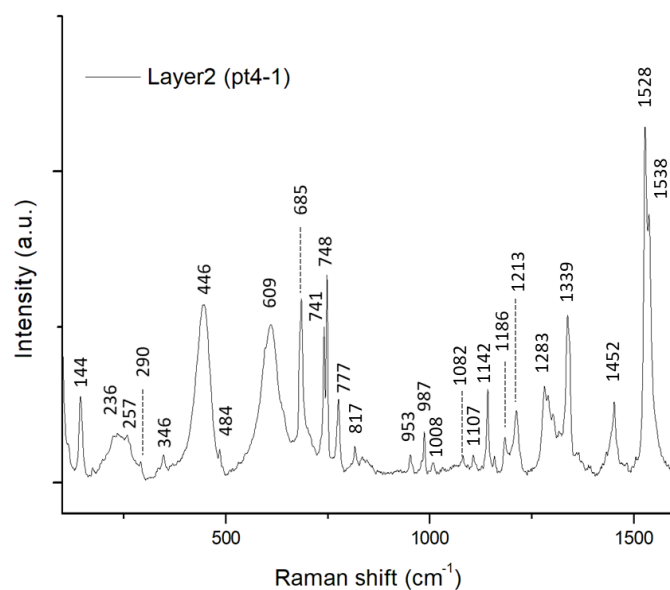


Figure III-32 Raman spectra (785 nm) of point 4 acquired in layer 2 of Tandem P05, baseline subtracted. Bands of interest are labeled with corresponding wavenumber.

The spectra acquired in the green paint layer 4 (points 6, 7, 8) contained similar bands with varying intensities, and a representative spectrum is shown in Figure III-33. Two pigments were identified: Prussian blue, based on bands at 276, 530, 944, 2090 and 2151  $\text{cm}^{-1}$  (Caggiani et al., 2016), and chrome yellow, due to the presence of the bands at 358 and 838  $\text{cm}^{-1}$  (Hansen et al., 2018). This demonstrates that the green colour is in fact a result of the mixture of a blue (Prussian blue) and a yellow (chrome yellow) pigment.

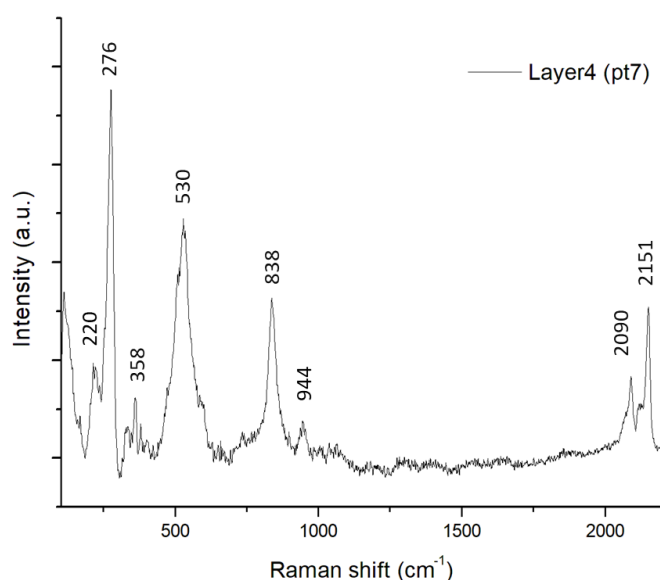


Figure III-33 Raman spectrum (785 nm) of point 7 acquired in layer 4 of Tandem P05, baseline subtracted. Bands of interest are labeled with corresponding wavenumber. The ripples present on the spectra background are related to the Edge filter transmission artifacts, not to vibrational features.



XANES measurements at the Fe K edge were acquired at various positions in the stratigraphy of Tandem P05 based on the detected distribution of Fe by micro-XRF (Figure III-34.a). The spectra acquired at each point are displayed in Figure III-34.b. The scans acquired at layers 3 and 4 resemble metallic Fe, thus confirming the metal constituting the object. The location of points 1 and 2 correlated most likely to the paint coating-metal interface of the sample, as iron corrosion products goethite, or an oxyhydroxide with close coordination (point 1), and hematite (point 2) were identified. Their presence suggests the alteration of the iron support. The spectra acquired in layer 4 (points 5, 6, 7, and 8) correspond to Prussian blue (Gervais et al., 2013).

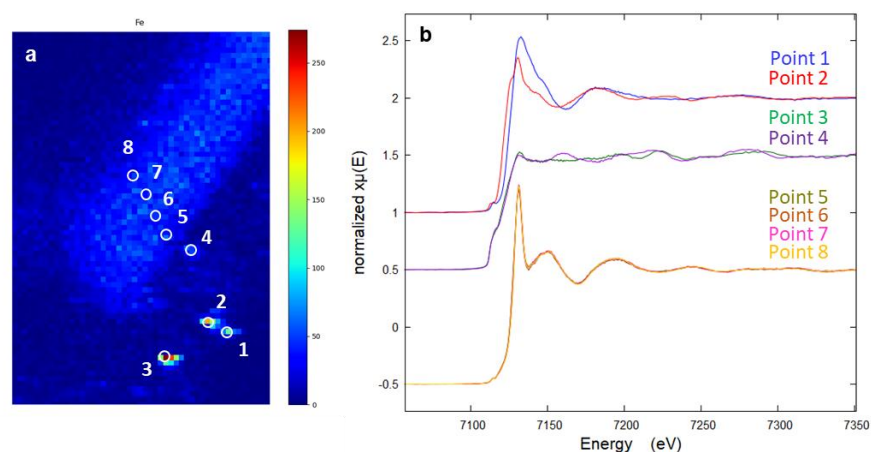


Figure III-34 (a) XRF map of the Fe distribution in the Tandem P05 cross-section, with XANES measurement locations indicated by white circles. (b) Corresponding XANES Fe K edge spectra.

### III.II.II.iv Summary of characterisations of Tandem P05

The combined results from the complementary analyses acquired on Tandem P05 allow to form an in-depth description of the stratigraphy of the sample (Table III-4). Observations with light and fluorescence microscopy defined four distinct layers with different morphological and luminescent properties. In **layer 1**, a dark blue paint layer, the presence of Zn, Ba and Sr correspond to the white pigment lithopone ( $\text{ZnS}$  and  $\text{BaSO}_4$ , with possible Sr substitution), while the presence of Fe corresponds to the pigment Prussian blue ( $\text{Fe}_4[\text{Fe}(\text{CN})_6]_3$ ), identified by both Raman and XANES spectroscopies. The combination of micro-XRF mapping and XANES at the Fe K edge allowed to locate and identify iron corrosion products at the inner face of layer 1 that had not been observed in the microscope images of the cross-section. The pigment ultramarine blue ( $\text{S}_3^-$  and  $\text{S}_2^-$  in  $\text{Na}_8[\text{Al}_6\text{Si}_6\text{O}_{24}]\text{S}_n$ ) was also identified. Furthermore, this layer has the same composition as the blue paint layer 2 in sample Tandem P03 (see Table III-2).

**Layer 2**, a light blue paint layer with intense green emission under UV light, was found to contain Zn and Ba, corresponding to lithopone; Ti, corresponding to titanium white ( $\text{TiO}_2$ ); and a low amount of Br, probably corresponding to the identified synthetic pigment phthalocyanine green (copper phthalocyanine complex (CuPc), halogenated with Cl or Br). Phthalocyanine blue was also identified independently of the green CuPc. The manufacture of blue and green CuPc pigments dates to 1928 (although available commercially 1935) and 1938, respectively (Defeyt et al., 2013; Germinario et al., 2015). Their presence therefore acts as a marker for the earliest possible date of application of this paint layer.

The brown product observed locally between layers 2 and 4 (**layer 3**) did not show a differentiable elemental composition from the surrounding layers and was not further analysed.

The green paint **layer 4** contains Pb and Cr, corresponding to the pigment chrome yellow ( $\text{PbCrO}_4$ ), and Fe, corresponding to the pigment Prussian blue. The combination of these two pigments, a mixture known as chrome green, was used in oil paints starting from the mid-nineteenth century (Feller et al., 1986).

The binder(s) of this sample have not yet been identified.

**Table III-4** Characterisations (organized by technique) of each layer in the sample Tandem P05.

Layer number	Morphological description	Elemental composition	Structural characterisation		Binder characterisation
	<i>Microscopy (OM, UV)</i>	<i>Synchrotron micro-XRF</i>	<i>Raman 785 nm</i>	<i>XANES Fe K edge</i>	<i>GC-MS</i>
1	Dark blue paint layer (78 $\mu\text{m}$ ), heterogeneous distribution of pigment particles; medium level of blue emission	Zn, Ba, Sr, Fe	Ultramarine blue, Lithopone, Prussian blue	Goethite, Hematite	Not analysed
2	Light blue paint layer (65-95 $\mu\text{m}$ ); intense green emission	Zn, Ti, Ba, Br	Titanium white, Lithopone, Phthalocyanine blue, Phthalocyanine green	Not applicable	
3	Dark brown, uneven products (45 $\mu\text{m}$ ); weak blue emission	Layer not differentiable from layers 2 and 4.	Not analysed	Not analysed	
4	Dark green paint layer (100 $\mu\text{m}$ ), homogeneous appearance; no fluorescence	Pb, Cr, Fe	Prussian blue, Chrome Yellow	Prussian blue	

### III.II.III Chaudière P02

The sample P02 acquired on the *Chaudière* was obtained from the right section of the white-painted middle piece (see Appendix F.iii). The exact sampling area contains a white paint on a white metal (possibly tinplate, a thin tin layer on iron support). The coating shows paint loss in some areas and orange-brown corrosion products are present on the underlying iron metal support. The exterior face of Chaudière P02 (Figure III-35.a) shows a brown translucent surface that is more orange in some areas and has large black products along one edge. The corresponding edge on the interior face (Figure III-35.b) also shows a dark brown/black product infiltrating into an otherwise bright white paint surface. Some beige stains and dark spots are also observed on the interior face.

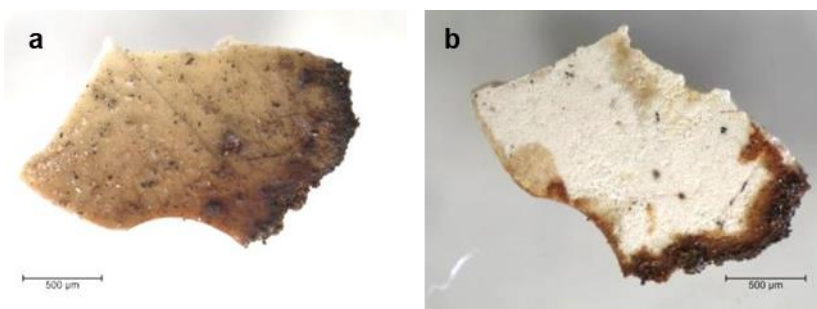


Figure III-35 Microscope images of sample Chaudière P02. (a) exterior face; (b) interior face (scale bars: 500 µm).

#### III.II.III.i Morphology of the sample stratigraphy

The sample Chaudière P02 was embedded in resin and cut with a wire saw to produce two cross-sections which were assigned the labels A and B. The two faces are seen in Figure III-36. Both faces present the same stratigraphy: an inner layer of white paint about 90 µm in thickness (layer 1), followed by a second white paint layer of about 40 µm in thickness (layer 2), and finally a thin orange-brown layer about 10 µm thick as the most exterior layer (layer 3), possibly corresponding to a varnish. Some orange products resembling corrosion products (5-10 µm thick) are present along the interior face and are referred to as zone 4. The two white paint layers are not the same: layer 1 is opaque and particles can be distinguished, while layer two is translucent and has a homogeneous aspect throughout. Figure III-36 shows Chaudière P02B before (c,d) and after (e,f) re-polishing; as the form of the cross-section has changed slightly, both states are presented in order to facilitate comparison with results of various imaging techniques that will be shown later.

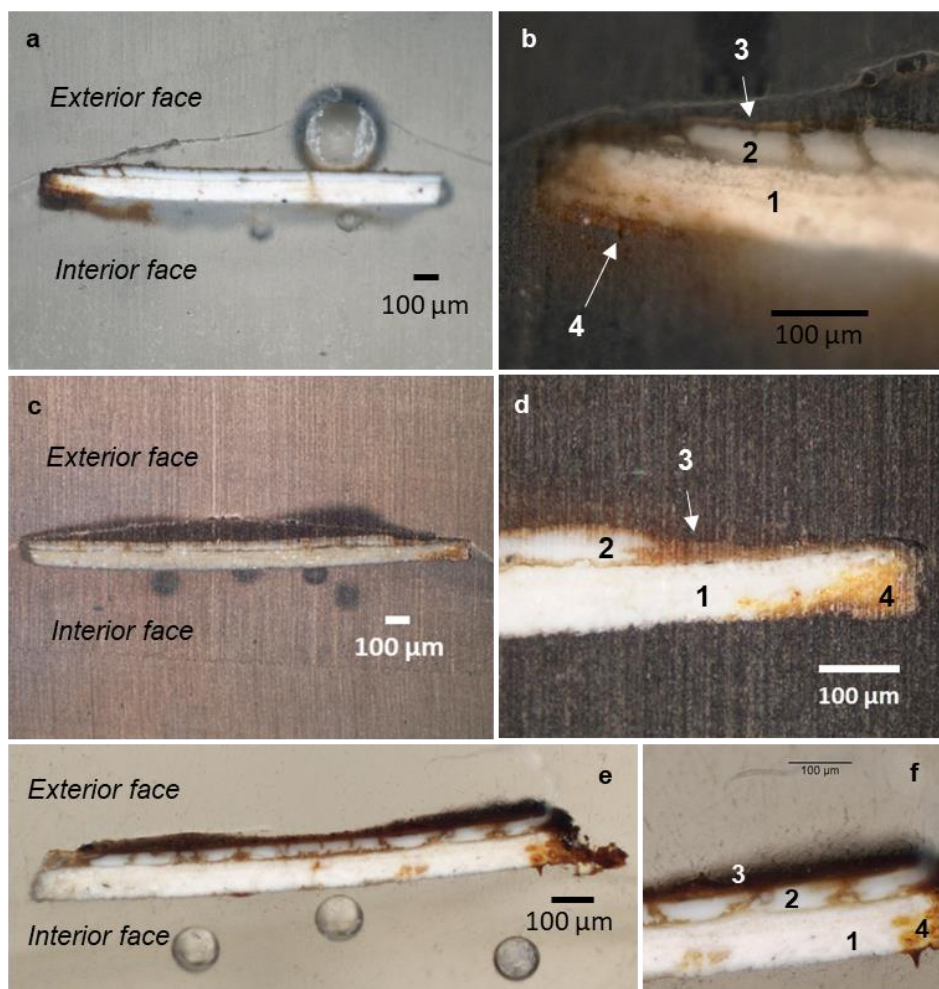


Figure III-36 Microscope images of the cross-section faces of sample Chaudière P02: (a,b) face A (acquired in 2018); (c,d), face B (acquired in 2017); (e,f) face B (acquired in 2020 after re-polishing). Layers are assigned with corresponding number.

The fluorescence microscopy images of Chaudière P02B (Figure III-37) reveal additional information about the composition of the layers in the stratigraphy. The fluorescence emission in layer 1 is not uniform: a 20-40 µm thick layer along the superior edge of layer 1 has a higher intensity of emission than in the inferior level of the layer. This area of interest shall be referred to as layer 1.1. Furthermore, the inferior part of layer 1 shows fluorescence when excited at 330-380 nm while under 450-490 nm excitation it fluoresces to a lesser extent or not at all, as seen along the interior face of layer 1 (Figure III-37.b). In layer 2, some small points of intense fluorescence are scattered throughout the layer; however, these points are only observed using the UV2A filter and not with the B2A filter. The external layer 3 does not fluoresce.

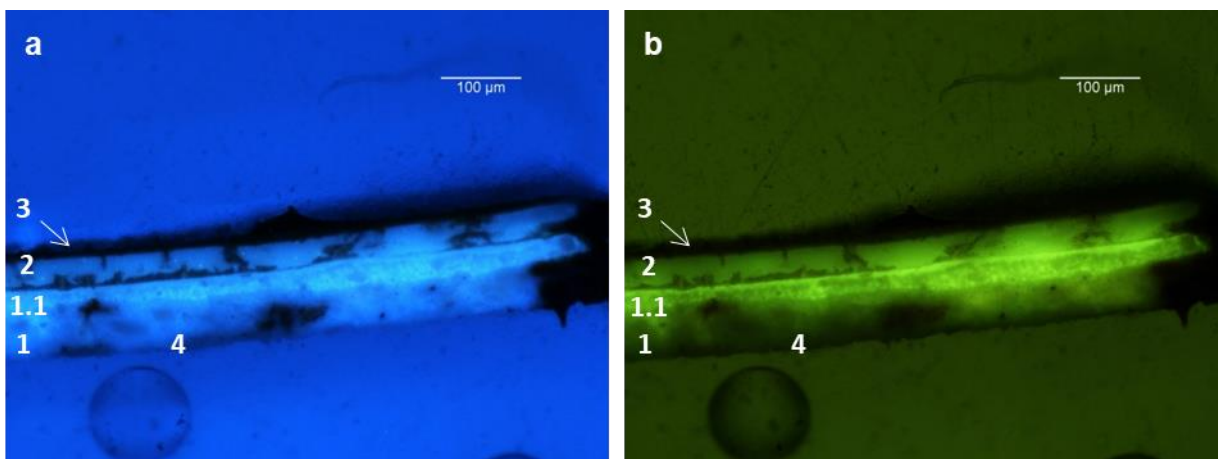


Figure III-37 Microscope images of the cross-section Chaudière P02B sample at 10x magnification under UV illumination. (a) UV2A filter ( $\lambda_{\text{ex}}$ : 330-380 nm,  $\lambda_{\text{em}}$  > 420 nm); (b) B2A filter ( $\lambda_{\text{ex}}$ : 450-490 nm,  $\lambda_{\text{em}}$  > 515 nm).

The synchrotron high-resolution deep-UV photoluminescent (DUV-PL) imaging of Chaudière P02B (Figure III-38) demonstrates the diversity of components present in each layer as evidenced by changes in the luminescence intensity and distribution at different emission ranges. Three emission images presenting the most distinct luminescence distributions were selected to form a false-colour representation of the photoluminescence of Chaudière P02B. The spectral ranges of 535-607 nm, 370-410 nm, and 327-353 nm are represented by the colours red, green and blue, respectively. The inferior section of layer 1 shows fluorescence mainly in the green and blue range, with some aggregates (20-50  $\mu\text{m}$ ) showing a low level of fluorescence in the red region. The superior level on layer 1, referred to as 1.1, has a distinct fluorescence signature as it mainly fluoresces in the red spectral region. Some aggregates of about 20  $\mu\text{m}$  diameter are present all along the layer and exhibit less fluorescence. Layer 2 contains a high density of small points with intense emission between 370-410 nm. These could correspond to the pigment Zinc white (ZnO) which has a strong characteristic emission at 380 nm (Artesani et al., 2017). No luminescence is observed from layer 3, corresponding to the external face of the sample.

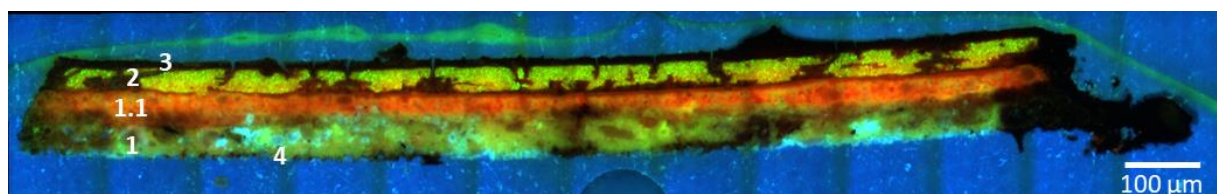


Figure III-38 Cross-section Chaudière P02B: TELEAMOS high-resolution false-colour image ( $\lambda_{\text{ex}}$ : 280 nm). Colour assignments: Red: 535-607 nm; Green: 370-410 nm; Blue: 327-353 nm.

The results of the imaging techniques used to study the morphology of the stratigraphy of Chaudière P02 demonstrate the necessity of the complimentary techniques. Observed by light microscopy alone, the sample appears to be composed of two white paint layers of different thicknesses topped with an

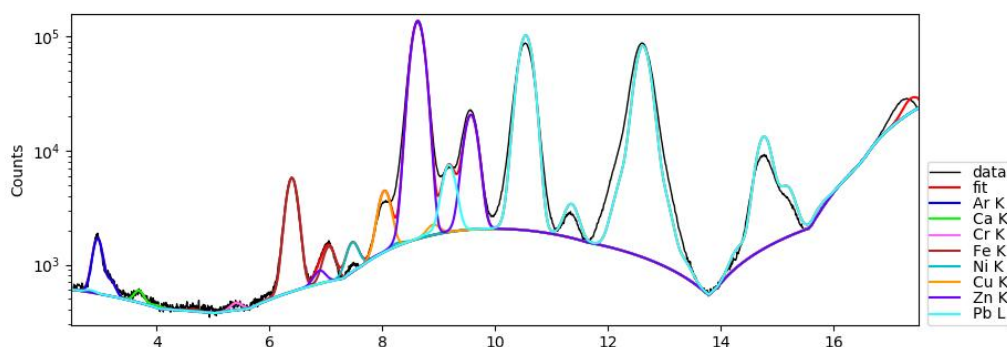
orange-brown varnish. The same sample viewed by fluorescence microscopy and DUV-PL imaging reveals that a layer of uniform thickness presenting a different composition (as inferred by its more intense fluorescence emission) is present along the superior edge of layer 1. The UV and DUV-PL images also reveal small particles in layer 2 that fluoresce at 370-410 nm excitation wavelength that were not observed by light microscopy. The superior spectral and spatial resolution of the DUV-PL imaging technique reveals an even greater complexity of the composition of the layers. The layer assignments and descriptions are summarised in Table III-5.

**Table III-5 Description of stratigraphy of sample Chaudière P02: summary of morphology and luminescence analyses and first assignments.**

Layer/Zone number	Description (Morphology and Luminescence properties)	Thickness	Assignment
1	White, opaque, distinguishable particles	90 $\mu\text{m}$	Paint layer
1.1	Indistinguishable from layer 1 in light microscopy; intense fluorescence emission in UV-Vis microscopy	20-40 $\mu\text{m}$	Paint layer
2	White, translucent, homogeneous; small particles with high fluorescence emission visible by UV microscopy	40 $\mu\text{m}$	Paint layer
3	Orange-brown ; no fluorescence signal	10 $\mu\text{m}$	Varnish?
4	Orange products; no fluorescence signal	5-10 $\mu\text{m}$	Corrosion products?

### III.II.III.ii Chemical composition of the sample stratigraphy

Chaudière P02B was analysed using synchrotron micro-XRF spectroscopy with an incident beam of 18 keV. The sum of the spectra acquired over the whole sample surface is shown in Figure III-39. The most intense fluorescence lines correspond to Fe, Zn and Pb. Lower amounts of Cu and trace amounts of Ca and Cr are detected.



**Figure III-39 Sum of synchrotron micro-XRF spectra (Incident energy = 18 keV) obtained on Chaudière P02B.**

The distribution of the elements of interest in the stratigraphy of Chaudière P02B are displayed in Figure III-40. Layer 1 contains mainly Pb with lower amounts of Ca. Layer 2 contains mainly Zn, with lower

amounts of Cu. The elemental composition of layer 3 is unclear from these maps, although Pb and Fe are observed in areas along the top right edge of the sample. The lower right corner of the sample, designated as zone 4, contains Pb, Fe and a small amount of Ca.

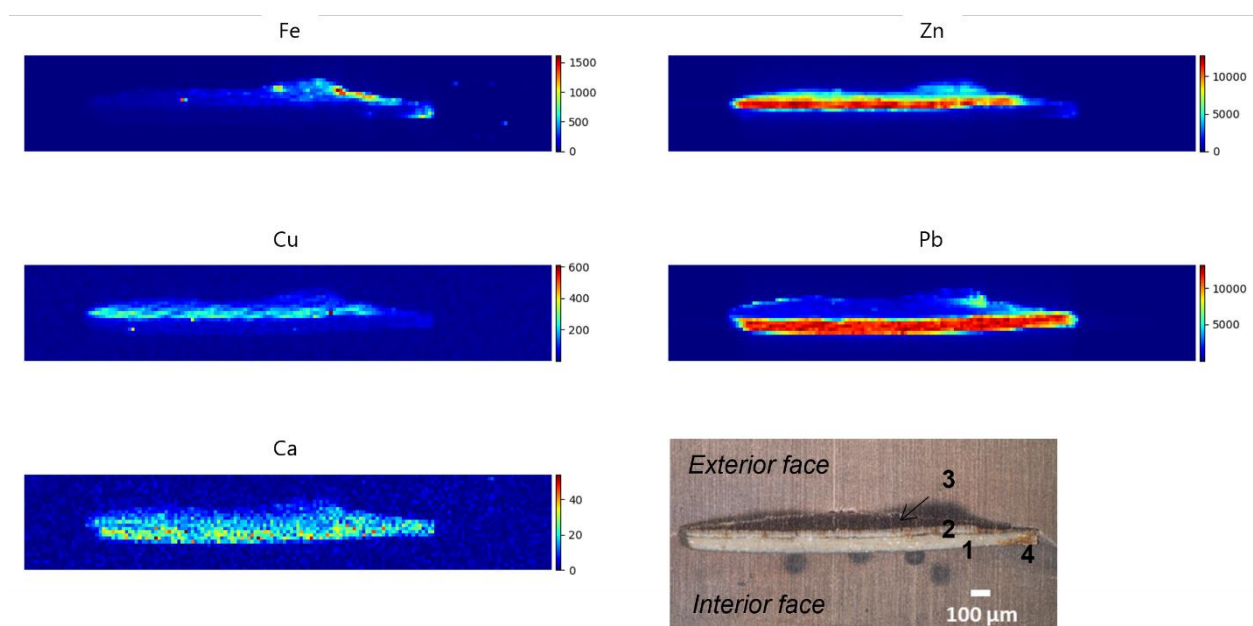


Figure III-40 Synchrotron micro-XRF maps of identified elements in cross-section Chaudière P02B (2017), OM image shown in bottom right corner.

### III.II.III.iii Structural study of the sample stratigraphy

The stratigraphy of Chaudière P02B was studied using Raman spectroscopy to probe the molecular structure of the components in each layer; the measured points are shown in Figure III-41. The most representative spectra of each layer were selected and are shown in Figure III-42. The spectra acquired in layer 1 contain characteristic peaks of lead white at 1049 and 1053  $\text{cm}^{-1}$  (Bell et al., 1997). The spectra obtained in layers 2 and 3 show an intense fluorescence signal, thereby masking any potential Raman bands. The spectra acquired in zone 4 contain Raman bands at 161, 450, 977 and 1055  $\text{cm}^{-1}$ . The band at 161  $\text{cm}^{-1}$  is unassigned, but a shoulder around 147  $\text{cm}^{-1}$  suggests the presence of PbO. PbO, in either tetragonal (litharge) or orthorhombic (massicot) form, is a yellow pigment but has also been found to be a laser degradation product of the dark-brown/black complex plattnerite  $\text{PbO}_2$ , a degradation product of lead-based pigments reacting with air (Burgio et al., 2001). The bands at 450 and 977  $\text{cm}^{-1}$  are characteristic of  $\text{PbSO}_4$  (Burgio & Clark, 2001), while the band at 1055  $\text{cm}^{-1}$  belongs to lead white and is most likely present due to the proximity of the point analysed (point 11) to the bulk material of layer 1.

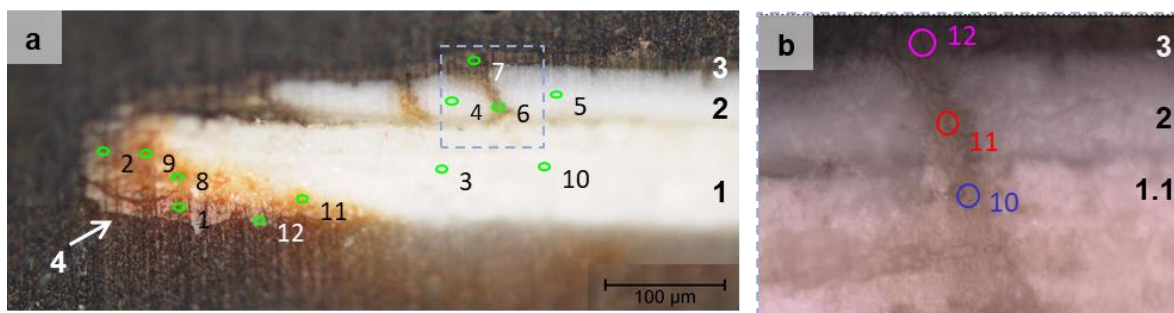


Figure III-41 (a) OM image of cross-section Chaudière P02A: Raman analysis points (785 nm; laser power 3 mW; 100x IR objective) are marked by green ovals and the numbers correspond to the spectrum number. Blue dashed square corresponds to the zone seen in b. (b) OM image of zone analysed by FT-Raman (1064 nm; laser power 50 mW; 40x LWD objective): measurement points are labeled with coloured circles.

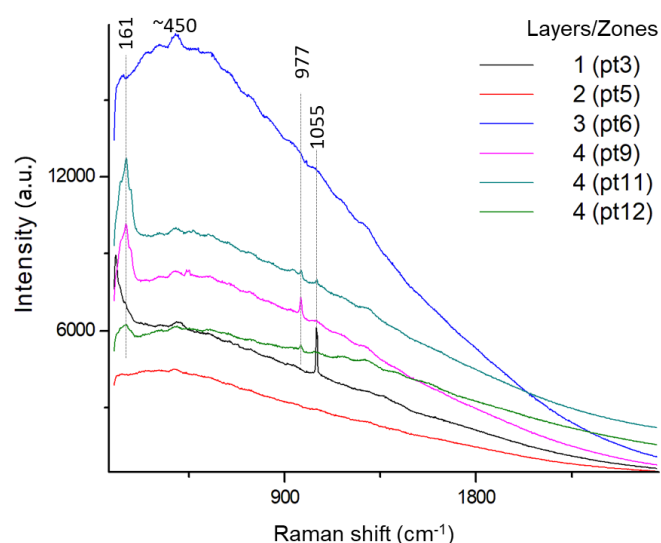


Figure III-42 Raman spectra (785 nm) representative of each layer in the stratigraphy of Chaudière P02A. The ripples present on the spectra background are related to the Edge filter transmission artifacts, not to vibrational features.

Given the lack of Raman bands in the spectra of the points analysed in layers 2 and 3 under the 785 nm laser, further measurements were acquired using FT-Raman with a 1064 nm laser. Points were acquired just below and above the interface of layers 1 and 2 and in the dark brown layer 3 (Figure III-41.b).

Organic bands that did not appear under the 785 nm laser are present in all the acquired spectra (Figure III-43) and are associated to either the paint binder or to infiltration by the embedding resin (identified by the band at 3062  $\text{cm}^{-1}$ ). Pigment bands were also identified: the band for lead white (1050  $\text{cm}^{-1}$ ), has a greater intensity in layer 1.1 than layer 2; bands for lead sulfate (977, 449, 437  $\text{cm}^{-1}$ ) appear in both layer 1.1 and 2; and finally, a weak band at 438  $\text{cm}^{-1}$  in layer 2 might be related to zinc white but might also be part of the trio of characteristic bands of lead sulfate, although the band at 449  $\text{cm}^{-1}$  appears weaker in intensity than it appeared in layer 1.1.



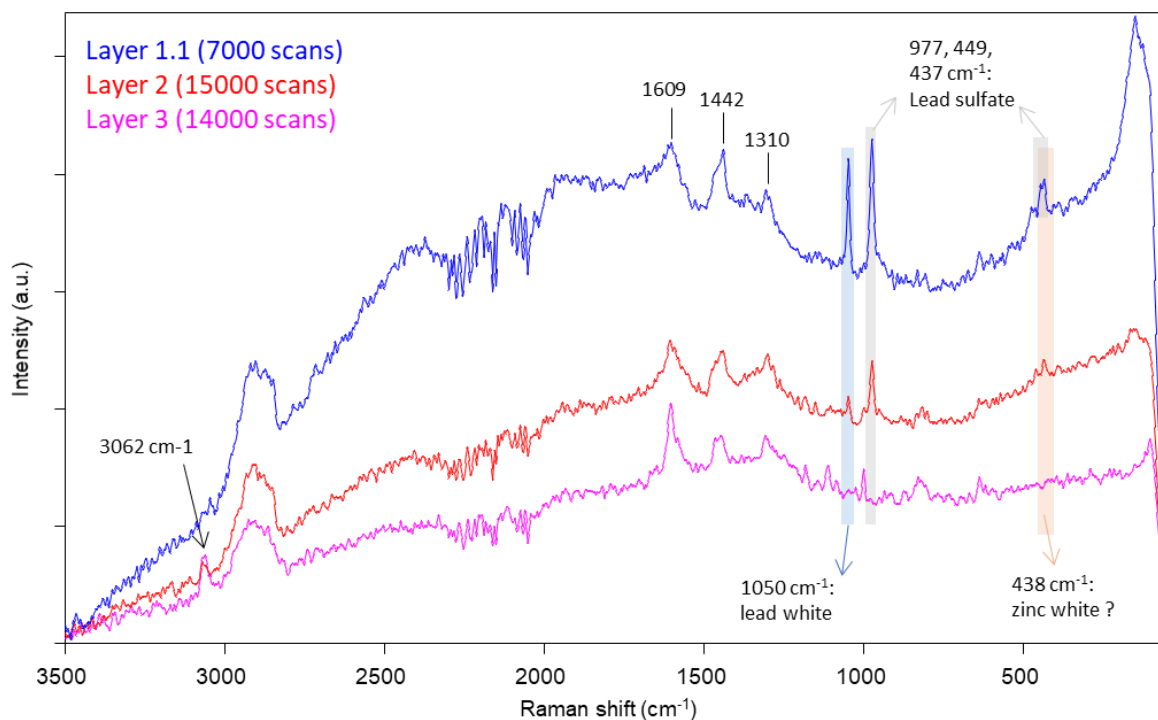


Figure III-43 FT-Raman spectra (1064 nm) of layers 1-3 of Chaudière P02A. The stronger baseline modulation seen between 2000-2350  $\text{cm}^{-1}$  is related to the atmospheric  $\text{CO}_2/\text{H}_2\text{O}$  absorption of the Raman signal in the spectrometer and are noticeable due to the weak Raman signal recorded.

Chaudière P02B was further analysed by XANES to characterise the local environment of Pb and Zn previously identified by micro-XRF mapping. A zone of interest containing the entire stratigraphy was selected for these specific measurements (Figure III-44.a). The same area is shown as a synchrotron DUV-PL false-colour image (Figure III-44.b) and as micro-XRF maps of Pb and Zn (Figure III-44.c and d). Profiles of XANES spectra at both the Pb  $L_3$  and Zn K edges were collected from the exterior face to the interior face: each profile consisted of 25 points collected at 5  $\mu\text{m}$  intervals, thereby encompassing the entire stratigraphy of the sample. The approximate position of the profiles (separation between Pb profile and Zn profile =  $\sim 10 \mu\text{m}$ ) is indicated by the grey dotted arrow in Figure III-44.

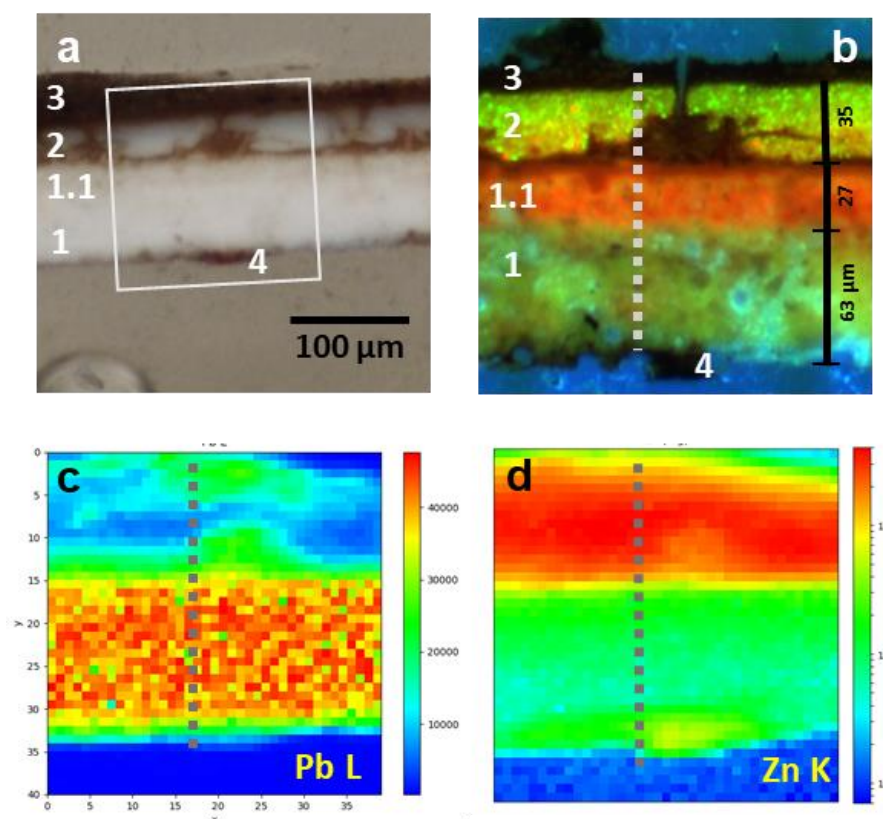


Figure III-44 Cross-section of Chaudière P02B: (a) OM image with zone of interest marked by white square. (b) DUV-PL false-colour image of the zone of interest (excitation wavelength: 280 nm). Colour assignments of emission images: Red: 535-607 nm; Green: 370-410 nm; Blue: 327-353 nm. (c) micro-XRF map of the Pb distribution (linear scale). (d) micro-XRF map of the Zn distribution (logscale). Grey dotted line represents the location of the profile of acquired XANES measurements.

The profile of XANES spectra collected at the Pb L<sub>3</sub> edge are displayed in Figure III-45. The spectra are arranged in order of collection, where the top spectrum corresponds to the exterior face of the stratigraphy and the bottom spectrum corresponds to the interior face. Analysis of the spectra showed no change in the edge position, but the white line position is observed to change and is associated to the presence of three different groups with similar spectral form. The first group of spectra were acquired in the first 35 μm of the stratigraphy, corresponding roughly to the thickness of layer 2. The environment of lead in this first group is similar mainly to that of lead sulfate but may possibly contain a small amount of lead white too. The second group, corresponding to two points over the following 5 μm of the profile which were acquired at the interface of layers 2 and 1.1, appears to have a similar Pb environment to lead white. The third group of spectra, acquired along the final 70 μm of the profile which corresponds to layers 1.1 and 1, presents a spectral form suggesting a Pb environment similar to either lead white or lead soaps (the reference spectra of the latter species are very similar). No difference is detected between the spectra acquired in layers 1.1 and 1, suggesting that a change in Pb environment is not responsible for the observed difference in luminescence behaviour (seen as red emission in Figure III-44.b).

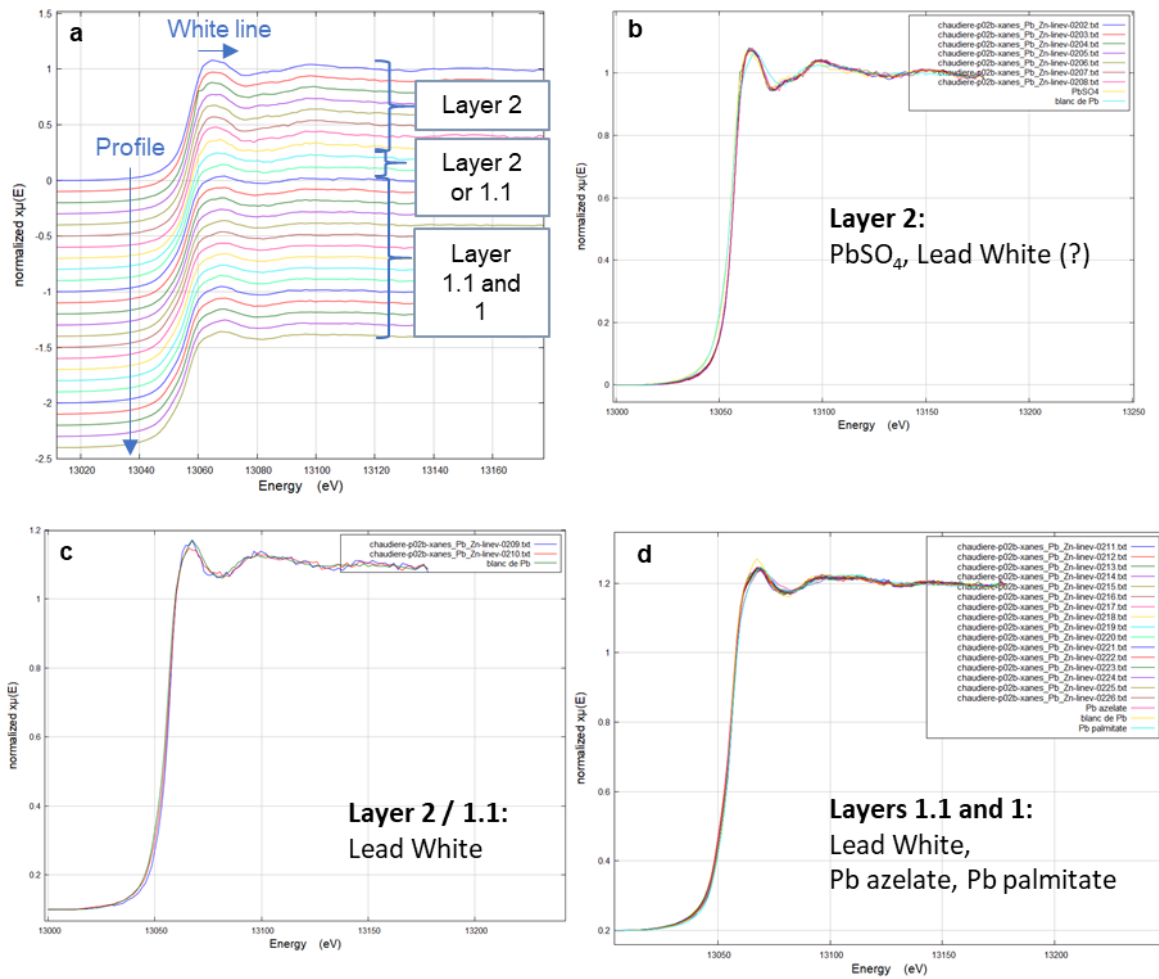


Figure III-45 XANES spectra acquired at the Pb  $L_3$  edge as a profile of points passing from the exterior face to the interior face (top to bottom) of cross-section Chaudière P02B (a). Three groups of distinct spectra (corresponding approximately to the different layers) have been identified (b, c, d).

A profile of XANES spectra were also acquired at the Zn K edge (Figure III-46). The same spectral form is seen throughout the profile with varying degrees of sharpness of the structural features. XANES spectra collected in layer 1.1 have the closest form to the reference spectrum of ZnO. Other Zn references were not acquired but comparison with Zn K edge XANES spectra from the literature suggests a mixture of phases which may include Zn carboxylates (Castorina et al., 2019; Joen. J. Hermans et al., 2019). Another measurement was acquired in layer 2 and the resulting XANES spectrum matches the form of the ZnO reference spectrum (Figure III-47).

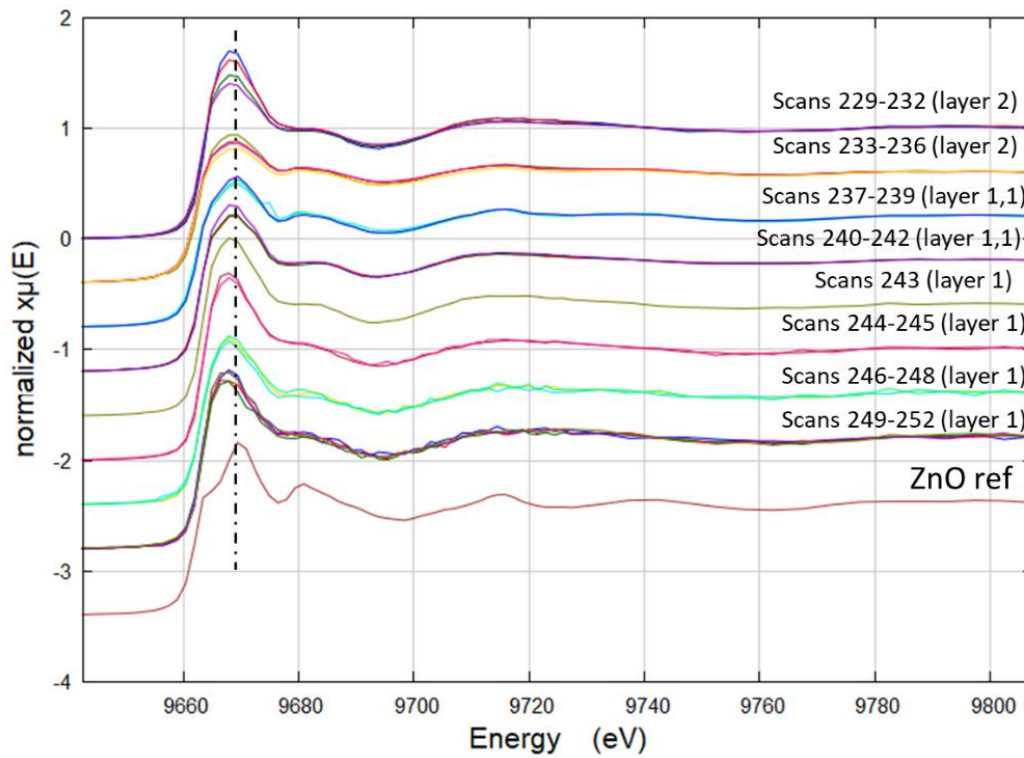


Figure III-46 XANES spectra acquired at the Zn K edge as a profile of points passing from the superior face (layer 3) towards the interior face (layer 1) of cross-section Chaudière P02B. Spectra are grouped by shape similarity.

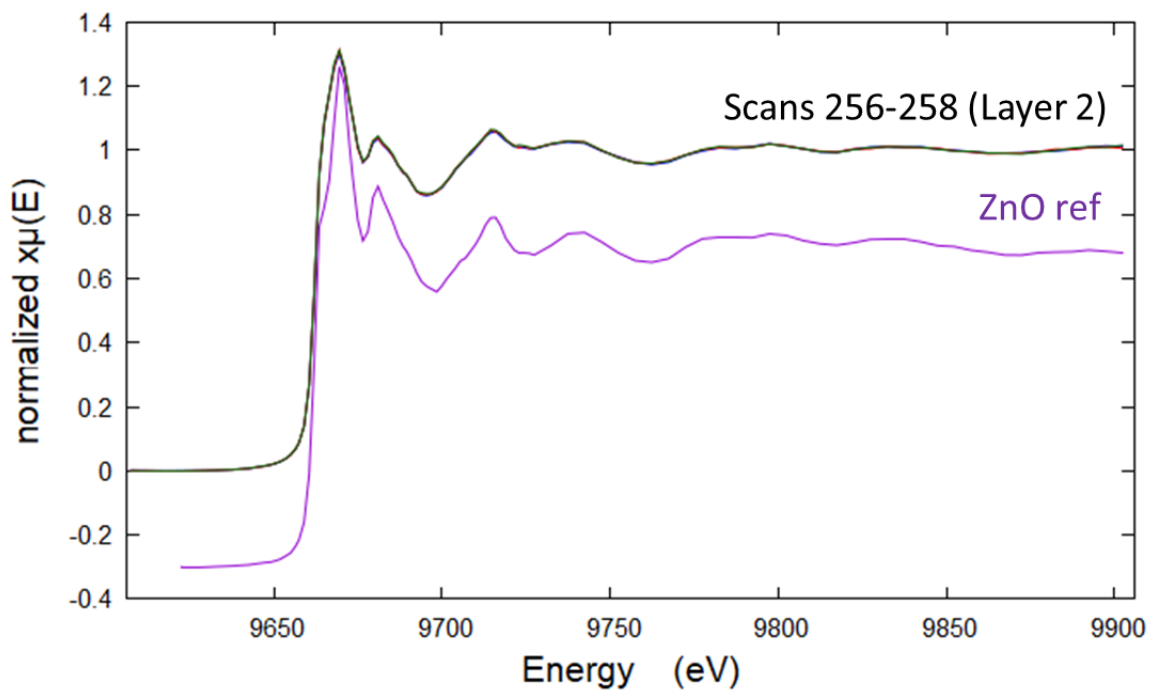


Figure III-47 XANES spectra (scans 256 to 258) acquired at the Zn K edge on a point of interest in layer 2 of Chaudière P02B.

The organic content of Chaudière P02 was investigated by GC-MS analysis. A fragment of the P02 sample was prepared for analysis without layer separation, so the results are representative of the total organic composition. The chromatogram is displayed in Figure III-48.

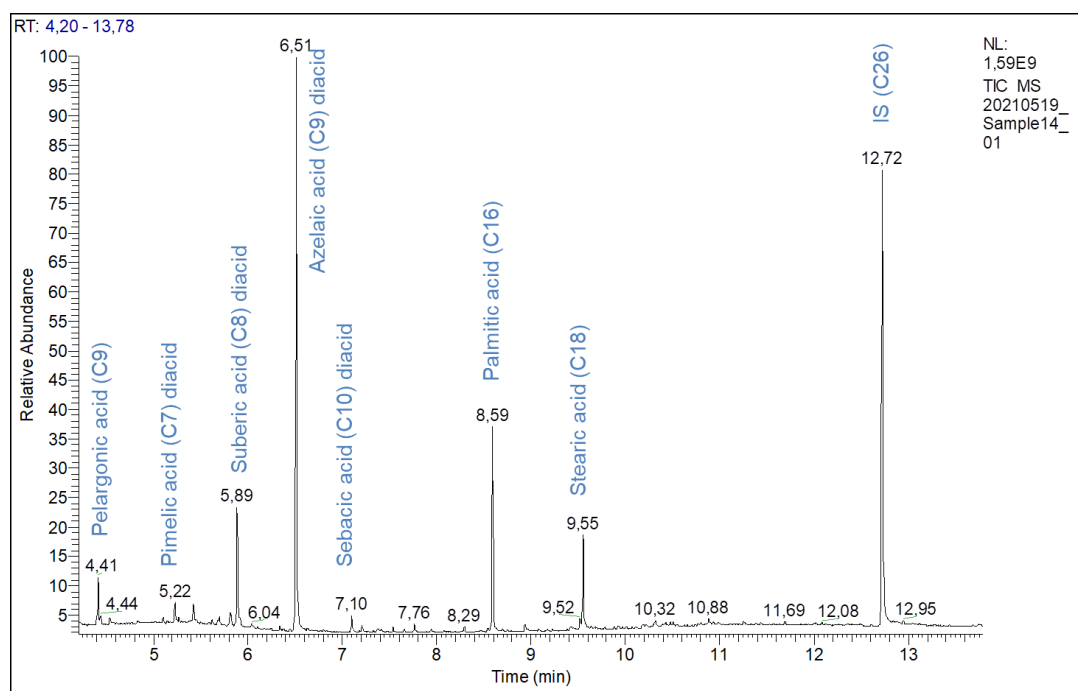


Figure III-48 GC-MS chromatogram of a whole fragment (no layer separation) of sample Chaudière P02. The identified peaks are annotated with their assigned component in the paint (all in methyl ester form); the number of carbons in the fatty acid chain are given in brackets. Hexacosanoic acid (C26) was included as an internal standard (IS) for an eventual quantification study.

Seven major compounds were identified, and their peaks (corresponding to the methyl esters of the mono and dicarboxylic fatty acid components) are annotated on the chromatogram. The high relative intensities of the saturated palmitic and stearic acids suggest a drying oil and most likely a linseed oil given the historical preparation of paint coatings for metals. The dicarboxylic acids, in particular azelaic acid, are markers of an aged oil (J. D. J. van den Berg, 2002). The predominant proportion of azelaic acid and lack of unsaturated fatty acids indicates that the paint is in a highly oxidated state.

### III.II.III.iv Summary of characterisations of Chaudière P02

The results of the complementary techniques used to analyse Chaudière P02 allowed for an in-depth description of the material composition of each layer in the sample (Table III-6). **Layer 1**, the closest to the metal support, is a white paint layer containing lead white pigment and possibly lead soaps as suggested by the Pb L<sub>3</sub> edge XANES spectra acquired in this layer. It contains a lower amount of Zn and the XANES Zn K edge analysis of this layer suggests the presence of a phase with a similar structure to

zinc carboxylates. The detection of lower amounts of Ca suggests other white pigments such as calcite or gypsum, although these were not detected during Raman analysis. Examination under UV light revealed the presence of a layer with different luminescence behaviour along the top edge of layer 1, designated as **layer 1.1**. Raman analysis revealed the presence of a mixture of lead white and lead sulfate in this layer. XANES measurements at the Pb L<sub>3</sub> edge and Zn K edge suggested the presence of, respectively, a Pb-containing phase with a similar environment to lead white or lead soaps and of a Zn-containing phase with a spectral form close to that of ZnO. An explanation for the different luminescence emission characteristics of layer 1.1 in comparison to the other layers has not yet been deduced.

A second white paint layer, **layer 2**, thinner and more translucent than layer 1, was found to contain a phase with the same structure of ZnO by Zn K edge XANES. This identification agrees with the photoluminescence image where small particles with a strong emission between 370-410 nm under 280 nm excitation (characteristic of ZnO) were observed by DUV-PL imaging. Lead white and lead sulfate were detected by Raman and this assignment was confirmed by XANES measurements at the Pb L<sub>3</sub> edge.

The brown external **layer 3** showed the presence of Pb and Fe in some areas but not consistently throughout the layer. No pigment bands were identified by Raman analysis and it showed no luminescence when observed with fluorescence and DUV-PL imaging. The lack of detected emission could be explained by the fact that iron has been shown to quench luminescence (Šima, 2015).

The orange-brown coloured zones within layer 1, assigned the name **zone 4** (often occurring at the paint-metal interface) were found to contain Pb, Fe and low amounts of Ca. The presence of Pb corresponds to the following identified Pb-containing products: lead oxide (possibly a laser degradation product of plattnerite PbO<sub>2</sub>), lead sulfate, and lead white (the main pigment present in layer 1).

GC-MS analysis of the whole sample (no layer separation) revealed the presence of molecules such as palmitic, stearic and azelaic acid, which allowed for the assignment of the binder as an aged drying oil.

No iron corrosion products were detected anywhere in the sample, despite the orange-brown colouring in certain areas and the detection of Fe. It is possible that the quantity of corrosion products was too low to be detected with Raman spectroscopy. Another possible explanation is that the observed discoloration in zone 4 is due to the presence of lead white degradation products, such as brown-black plattnerite PbO<sub>2</sub> (Lussier & Smith, 2007). PbO<sub>2</sub> is a weak Raman scatterer and therefore difficult to detect, and furthermore it may transform by thermal degradation to PbO when exposed to laser powers above 2.5 mW with an excitation wavelength of 781.8 nm (Burgio et al., 2001). The identification of PbO in the discolored regions may indeed be the laser degradation products of PbO<sub>2</sub> formed by the conditions used for the Raman analysis of the samples in this study.

Table III-6 Characterisations (organized by technique) of each layer in the sample Chaudière P02.

Layer number	Morphological description	Elemental composition	Structural characterisation	Binder characterisation
	<i>Microscopy (OM, UV, DUV-PL)</i>	<i>Synchrotron micro-XRF</i>	<i>Raman, XANES (Pb L<sub>3</sub> and Zn K edges)</i>	<i>GC-MS</i>
1	White paint layer (90 µm): opaque, distinguishable particles,	Pb, low amounts of Zn, Ca	Lead white (Raman) Lead white/Lead soaps (XANES)	Oxidised drying oil: palmitic, stearic and azelaic acid
1.1	White paint layer (~27 µm), indistinguishable from layer 1 in light microscopy; intense emission under UV light.	Indistinguishable from layer 1	Lead white, PbSO <sub>4</sub> (Raman) Lead white/Lead soaps, PbSO <sub>4</sub> , ZnO ? (XANES)	
2	White paint layer (40 µm), translucent, homogeneous; small particles with intense emission under UV light.	Zn, Pb, low amounts of Cu	Lead white, PbSO <sub>4</sub> (Raman) PbSO <sub>4</sub> , some Lead white, ZnO (XANES)	
3	Orange-brown (10 µm); no emission under UV light.	Pb and Fe but not consistently throughout layer.	Mainly organic bands (Raman).	
(zone) 4	Orange products (5-10 µm); no emission under UV light.	Pb, Fe, low amount of Ca	PbO, PbSO <sub>4</sub> , lead white	

### III.III Discussion of the characterisation of historical samples

In this section, the results of the analytical characterisation of all the historic samples, including those presented in this chapter as well as the samples presented in Appendix I, are compiled and discussed. It is emphasized that the choice of objects and sampling locations was oriented towards degraded areas on the objects, and so the presented results are particularly representative of the composition of altered paint coatings. As samples were not obtained on well-preserved artefacts it is possible that some of the characteristic materials used on these objects were not recorded in our research. However, a diverse corpus of objects and a significant number of samples were studied, thus providing a considerable overview of the possible constituents that may be found on these types of historic painted metals in technical heritage.

#### III.III.I Pigments

A variety of pigments were identified; they are listed in Table III-7. Most of the identified pigments are traditional compounds that were in use during the 19<sup>th</sup>-early 20<sup>th</sup> century. An exception is phthalocyanine blue and phthalocyanine green, which were synthesized in the mid-1930s. These pigments were identified on the *Tandem* (Quadruplette) which is dated to 1945-1950, slightly later than our main period of study. Many of the coloured pigments were identified arbitrarily throughout the stratigraphy (base coat, mid coat or topcoat), inferring that their role was mainly aesthetic rather than protective. The pigment chrome yellow was only identified in topcoats: once as a decorative paint detailing on the *Charrue*, an exhibition model of a double Brabant plow, and once as a mixture with Prussian blue (giving the pigment chrome green) in a green paint coating on the *Tandem*. Chrome yellow was a relatively expensive pigment (Feller et al., 1986), and its limited occurrence supports this. Other pigments that were identified in the topcoats of the analysed samples were: ultramarine blue, vermilion, zinc white, and carbon black. Some pigments were identified in low amounts throughout the entire paint system, such as gypsum and silica. These were most likely included in the paint formulation as extenders.



Table III-7 Pigments identified in the study of samples from the corpus of 9 historic painted metal objects.

Pigment identified (common name, chemical formula)	Location in stratigraphy (base coat; mid-layers; topcoat)	Identified in samples
Ultramarine blue $S_3^-$ and $S_2^-$ in $Na_8[Al_6Si_6O_{24}]S_n$	Base coat, mid-layers, topcoat	Balance P01, P02 Charrue P03 Tandem P03 Tandem P05
Prussian blue: $Fe_4[Fe(CN)_6]_3$	Base coat, mid-layers	Balance P01, P02 Tandem P03 Tandem P05
Phthalocyanine blue $C_{32}H_{16}CuN_8$ (Copper phthalocyanine (CuPc))	Base coat/mid-layers	Tandem P03 Tandem P05
Vermillion: $HgS$	Topcoat	Chaudière P05
Red lead: $Pb_3O_4$	Base coat, mid-layers, topcoat	Charrue P02 Série P01, P02 Chaudière P05 Vélocycle P01
Chrome yellow: $PbCrO_4$	Topcoat	Charrue P02
Chrome green (mixture of Prussian Blue and Chrome Yellow)	Topcoat	Tandem P05
Phthalocyanine green (halogenated (Cl/Br) CuPc)	Mid-layers	Tandem P05
Lead white: $2PbCO_3.Pb(OH)_2$	Base coat, mid-layers	Chaudière P02 Tandem P03 Balance P01, P02
Zinc white: $ZnO$	Topcoat	Chaudière P02
Lithopone: $ZnS$ (30%); $BaSO_4$ (70%)	Base coat	Charrue P02 Charrue P03
Carbon black	Topcoat	Vélocycle P01
Titanium white: $TiO_2$	Base coat, mid-layers, topcoat	Tandem P05
Gypsum: $CaSO_4. 2H_2O$	Base coat, mid-layers, topcoat	Chaudière P02 (?) Série P02
Silica: $SiO_2$	Base coat, mid-layers, topcoat	Série P01

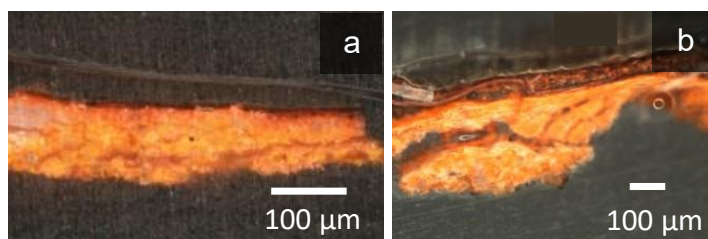


Figure III-49 Cross-sections of samples where red lead was identified in the base coat: Chaudière P05B (a); Série P02B (b).

As expected, many of the paint samples contain anticorrosive pigments such as red lead and other pigments based on lead, zinc, or barium, like lead white, zinc oxide and lithopone. These pigments were identified in the base coat layer of a number of samples, confirming their intended use as the inhibiting component of an anticorrosive primer for the iron substrate. When red lead was identified in a base coat layer, it was often the only layer present in the stratigraphy, or else was covered by a thin topcoat (Figure III-49). Lead white or lithopone were mainly identified in the basecoat of multi-layer paint coatings (Figure III-50). This suggests that additional layers were required to provide adequate protection of the metal.

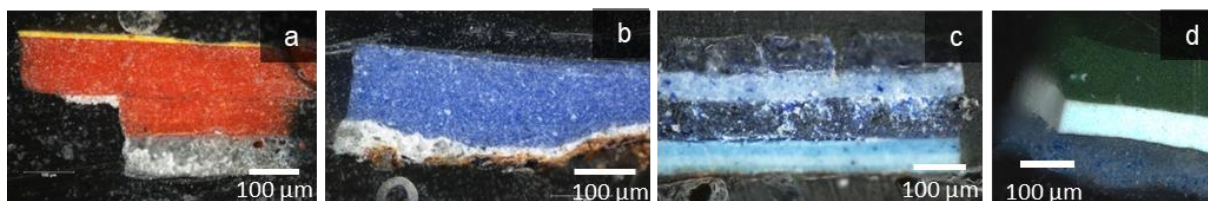


Figure III-50 Cross-sections of samples where lithopone or lead white were identified in the base coat: Charrue P02B (a); Charrue P03B (b); Balance P01A (c); Tandem P05 (d).

It is sometimes difficult to ascertain whether the subsequent layers were all applied during the original preparation of the coating or if the system was repainted at a later date due to a degradation of the original paint layer(s), especially in cases where the composition of the paint layer does not change. However, several of the studied objects were only used as demonstration models and most likely did not endure harsh environmental conditions which would have necessitated retouching of the paint coating. In the case of the *Tandem*, the chronology of the paint layers is clearer: this four-seated tandem bicycle is known to have been regularly used in outdoor conditions and presents several layers of blue paint of differing composition which are most likely layers that were added over time for maintenance or repainting. This demonstrates the importance of comparing the analytical data with the historical documentation, if available.

### III.III.II Binder components

The main role of the chromatographic analyses conducted during this work was for the characterisation of the organic components in the paint binders of the historical samples. As it is particularly difficult to separate the different layers of paint, the results obtained represent the entirety of the organic components in the analysed paint samples and are not layer specific.

The main results are shown in Table III-8. The components detected most often in the paint samples are fatty acids that are attributed to an oxidized drying oil. This confirms the oil-based composition of the paints, as expected for painted metal surfaces up until the introduction of synthetic polymer binders in the 1920s. Based on historical formulations, the binder is most likely a linseed oil. In some samples, components attributed to resins were identified in significant quantities. These were mainly oxidation products of abietic acid, which suggests the presence of an oxidised resin from the *Pinaceae* family. Based on historical recipes for metal coatings, the *Pinaceae* resin could be colophony or Venice turpentine (K. J. van den Berg, 2003; Daher, 2012). Sandaracopimaric acid was only identified in one sample, Locomotive P01, which showed a high content of resin components (including DHA) and a relatively low amount of the fatty acids palmitic and azelaic acid. Sandaracopimaric acid is a component of various resins such as sandarac, Kauri and Manila copal (Daher, 2012) and it is not possible, with the identified biomarkers, to specify which one was used.

**Table III-8 Organic species identified in the historic paint coating samples by GC-MS analysis and attributed material.**

Organic species identified	Attribution	Identified in samples
Fatty acids: palmitic acid, stearic acid, pimelic acid, suberic acid, azelaic acid	Oxidized drying oil	Tandem P06 Chaudière P02 Chaudière P08 Série P02 Charrue P01 Balance P01 Chaudière P09 Locomotive P01
Dehydroabietic (DHA) acid and other oxidised derivatives	Resin (origin: <i>Pinaceae</i> family)	Tandem P06 Chaudière P08 Charrue P01 Locomotive P01
Sandaracopimaric acid	Resin (origin: <i>Cupressaceae</i> or <i>Araucariaceae</i> family)	Locomotive P01

The presence of resin components could be due to the application of a varnish, although no varnish layers of significant thickness were observed on the objects or in the prepared cross-sections. The archives associated to the studied objects contain minimal information on any subsequent restoration interventions. Given the altered state of the sampling locations, we have reason to believe that the objects did not undergo extensive restoration (including varnishing) in the past. However, the relatively high proportion of resin components with respect to the fatty acid components detected in the chromatographic analyses suggests that they have a significant presence in the formulation of several of the analysed paint samples. Mixtures of linseed oil and pine resin were used historically both as paint binders and as varnishes, and the observations presented here seem to suggest that the resin is present within the paint layers rather than as a surface varnish.

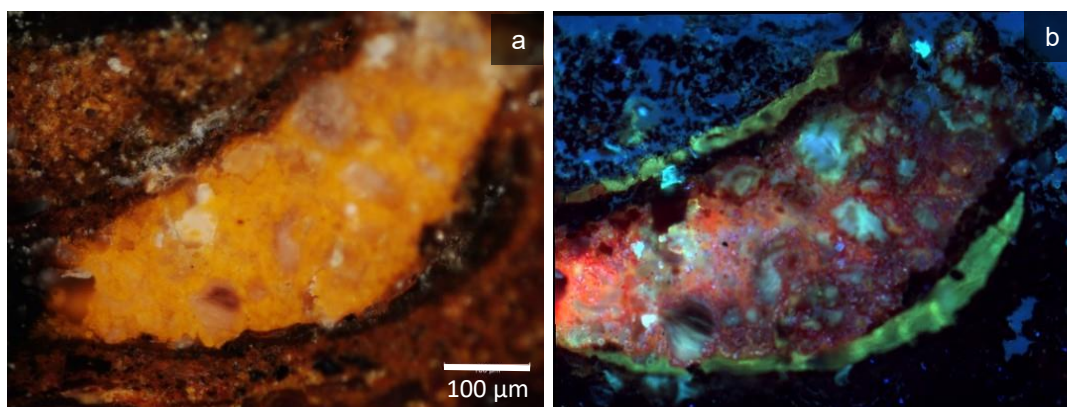
To complete the characterisation of the organic binder formulation used in paint coatings for metal substrates, the cross-sections of the samples could be analysed by FTIR imaging to obtain a spatially linked identification of the organic composition of each layer. In order to obtain high quality spectra, FTIR imaging measurements are often acquired in transmission mode which requires the preparation of thin-sliced samples. This preparation approach was tested during this thesis work but was found to be difficult to acquire stable thin-slices on the weakly-adhering multilayered cross-sections. Furthermore, given that IR spectroscopy does not have a high degree of specificity with respect to a complex system like a paint coating where the presence of pigments may interfere with the identification of the binder, the most conclusive strategy would be to separate the layers of the paint samples and analyse them individually by mass spectrometric techniques such as GC-MS. However, layer separation can also be difficult to achieve. Furthermore, GC-MS analysis consumes the sample, preventing the ability to perform any follow-up analyses by other techniques. An alternative mass spectrometric technique that can also be conducted on the cross-section of the samples in mapping mode is Secondary Ion Mass Spectrometry (SIMS); this technique has been used to characterise the nature and spatial distribution of binding medium components in paint sample cross-sections in previous studies (Keune et al., 2005). Fully characterising the binder components in each layer of the coating stratigraphies will allow to better comprehend the historical techniques used for the manufacture of these objects.

### **III.III.III Alteration products**

A secondary objective of this characterisation work was to investigate the state of alteration of the samples by identifying chemical species related to the degradation of the system. The aspects concerning the paint layers will first be presented, followed by those concerning the metal substrate.

For paints, some cases of alteration, such as the oxidation products of the oil binder composition identified by GC-MS analyses, were expected for aged oil paint samples. The high relative proportion of azelaic acid compared to palmitic and stearic acid indicates that the paint is in an advanced state of aging (Erhardt et al., 2005).

To investigate other cases of alteration that are not as evident, hypotheses on possible aging processes were developed based on the nature of the identified original materials. For example, the identification of lead and zinc-based pigments in an oil-based binder led to the hypothesis that lead and zinc carboxylates (soaps) may have formed in the paint layers, as has often been observed in artist paintings of the same composition (Noble, 2019). The formation of metal soaps can provoke serious degradation of paints and are associated to alterations such as aggregation, protrusions, efflorescence or an increase in transparency of the paint film (Noble, 2019). In the case of coatings for metal substrates, the degradation of the paint film associated to the formation of these aggregates could potentially have an effect on the protective properties of the paint layers.



**Figure III-51 Cross-section Série P01A: light microscope image (a); DUV-PL false-colour image (excitation 280 nm): red emission: 641-708 nm; green emission: 452-486 nm; blue emission: 370-410 nm.**

Cross-sections in which red lead had been identified were re-examined and, in some cases, such as in the cross-section Série P01A (Figure III-51.a), the orange layer containing red lead does not present a homogeneous aspect under optical microscopy: some aggregates are observed that appear white and opaque or else colourless and translucent. An initial inspection with fluorescence microscopy revealed that these aggregates do not present the same luminescence behaviour as the bulk of the orange layer, suggesting a difference in composition. The heterogeneity was further investigated at higher spectral and spatial resolution with deep-UV photoluminescence micro-imaging (DUV-PL) using synchrotron radiation. The luminescence properties of the white aggregates (Figure III-51.b) show that the composition is not uniform in these areas. This could suggest the presence of different molecular species from the interior of the aggregate towards the bulk material which may be linked to various degrees of alteration (Thoury et al., 2019). Further investigation via other methods allowing chemical

imaging of these complex stratigraphies, such as FTIR, SIMS, or SEM-EDS (Keune & Boon, 2007) is required to determine the chemical nature of these species.

Other alterations were investigated based on unusual results obtained during characterisation. For example, in some base or mid-layers a difference in luminescent behaviour was observed along the superior edge compared to the rest of the layer. This was seen notably in layer 5.1 of Tandem P03A and layer 1.1 of Chaudière P02B (presented in the case study section of this chapter). XANES measurements acquired at the Pb L<sub>3</sub> edge on the area of interest in Tandem P03A suggested a lead-containing species with a coordination environment similar to that of PbSO<sub>4</sub>, while the XANES measurements acquired in the bulk of the same layer suggested a lead white environment. PbSO<sub>4</sub> could be an oxidation product of PbS, a black mineral phase that has been associated to the darkening of lead white paint (Goltz et al., 2003; Lussier & Smith, 2007). The formation of PbS has mainly been attributed to a reaction of the lead white pigment with H<sub>2</sub>S in the atmosphere (the main source of H<sub>2</sub>S historically is from air pollution and gas lamps), making the conversion a predominantly surface alteration (Lussier & Smith, 2007). This suggests that the altered layer may have been the topcoat at one point in the object's life and was later repainted, possibly due to surface discoloration.

Evidence of alteration of the metal was present in the form of heterogeneous layers of corrosion products along the metal-basecoat layer interface in some cross-sections. They were not consistently present for reasons mentioned previously: in part due to the limited extent of alteration of the system but also due to limitations of the sampling methodology. Some cross-sections that contain a corrosion layer are shown in Figure III-52. It is observed that the corrosion products have different effects on the paint. Mechanical stress is seen as an upward exertion on the paint system due to an underlying formation of corrosion products (Figure III-52.a). In other cases it is seen to infiltrate the paint layer, seen as staining (Figure III-52.b), or through fissures due to the development of a less-resistant pathway between the metal and the atmosphere (Figure III-52.c). In the case of the Série P01A (Figure III-52.d), it is unclear if the observed "corrosion layers" are present due to actual corrosion of the iron substrate or if the iron oxides are present as pigments in the paint film. Determination of the nature and distribution of the phases throughout the layer could clarify this question.

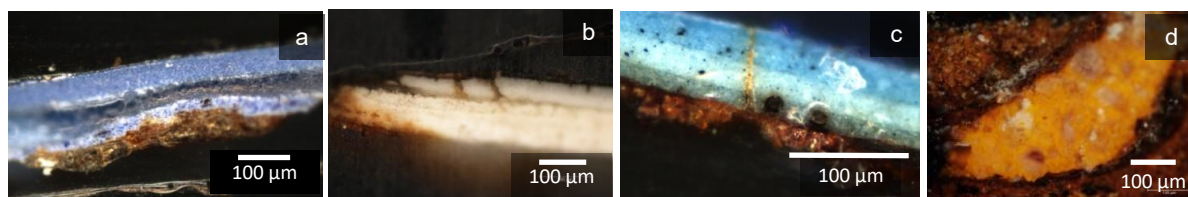


Figure III-52 Cross-sections presenting corrosion products at the paint-metal interface: Tandem P07A (a), Série P01A (b), Chaudière P02A (c), Balance P01A (d).

Corrosion products were identified by point analysis in the corrosion layers using Raman micro-spectroscopy. The main identified phases were lepidocrocite ( $\gamma$ -FeOOH) and goethite ( $\alpha$ -FeOOH), followed by lesser identifications of hematite ( $\alpha$ -Fe<sub>2</sub>O<sub>3</sub>), magnetite (Fe<sub>3</sub>O<sub>4</sub>), maghemite ( $\gamma$ -Fe<sub>2</sub>O<sub>3</sub>) and akaganeite ( $\beta$ -FeOOH). The phases are representative of corrosion products mainly attributed to indoor atmospheric corrosion processes (Monnier et al., 2011). In order to properly understand the reactivity of the corrosion products that have formed under the paint layer, further studies should be conducted that determine the distribution of the phases within the corrosion layer. However, it should be noted that in our current samples the corrosion layer is most likely incomplete given that they do not contain the corrosion-metal interface and therefore the distribution of compounds is not truly representative. Imaging the distribution of components, such as by Raman spectroscopy, would therefore be relevant to implement on samples for which a representative stratigraphy is available. This highlights the need for more invasive sampling that would provide a full stratigraphy of the painted metal system. As this type of sampling is not always desired in the conservation field, alternatives could include sacrificial model samples aged naturally or artificially that can be used to study the behaviour and degradation of the painted metal system, particularly at the interfaces. The use of model samples is explored in the second research axe of this thesis.

## III.IV Conclusions and perspectives

The analytical examination of historical samples provided an in-depth characterisation of the material composition and structure of the altered painted metal system as it might be encountered on museum artefacts. The applied methodology allowed us to identify a large variety of pigments, additives, binder components, alteration products and corrosion products. Upon first observation, the paint coatings for industrial and technical metallic objects appears to be quite uniform in composition and in structure (thickness, homogeneity of constituents), especially compared to cross-sections from artistic paintings. This underlines the purpose of the paint coating as being primarily a protective coating for the underlying metal. However, the stratigraphy is not necessarily “simple”; the analytical observations and characterisations show that the paint coatings are most often composed of multiple layers of varying composition. This design is notably underlined by the presence and the composition of the base coat, in which components with anticorrosive properties, such as red lead, lead white, and lithopone, were observed. The subsequent layers and topcoat have a more variable composition depending on the desired aesthetic look of the object. Furthermore, the presence of multiple layers of differing composition is sometimes attributed to repainting for maintenance purposes, especially in the case of objects that are known to have been “used” (i.e. experienced harsher conditions) as opposed to objects whose purpose was primarily demonstration (model objects). The discussion of alteration processes gives a first suggestion of additional sensitivities that the painted metal surfaces may present in their degraded state. One such concern is the likely presence of metal soap aggregation given the identified lead and zinc-based compounds in the oil binder. The formation of aggregates has been shown in previous studies to be concerning for the conservation of paint coatings. The presence of corrosion products along the paint-metal interface was observed to affect the overlying paint layers by either mechanical or aesthetic alteration; however, full interpretation of the processes occurring at the paint-corrosion-metal interface is limited due to restrictions in collecting samples that include the metal substrate. Given the minimal historical documentation and characterisation studies of painted metal artefacts of industrial heritage from the 19<sup>th</sup>-early 20<sup>th</sup> century, this study provides an important survey of possible historic paint coating formulations that may be encountered by conservation and restoration professionals on these types of objects.

The obtained results are representative of altered painted metal surfaces. To address the other possible materials present in less-altered areas, *in situ* measurements may need to be put in place to respect the sampling limitations (i.e. do not detract from the legibility of the object). Other perspectives for this work include continued analytical studies that concentrate on the alteration processes that have been suggested in this chapter. The identification and comprehension of their behaviour will be essential for fully describing the state of alteration of the painted metal system on these objects, an understanding



of which is necessary to develop suitable conservation strategies. Along these lines is the characterisation of the paint coating-metal interface, which would provide important insight into the physicochemical interactions occurring in this area and could help to explain the often-observed adhesion issues. Due to the invasiveness of acquiring micro-samples of the full painted metal system from historic objects, the use of model samples is a good alternative, as discussed in the second research axe of this thesis (Chapter 4).

## Chapter IV A multi-scale analytical study of the effects of conservation treatments on the aging of model painted metal surfaces

This chapter addresses the question of the protection efficiency of common conservation treatments used on painted metal artifacts in a museum storage climate. Strategies for the treatment of painted metals are already in place in the conservation-restoration field, although they are typically adapted from treatment protocols for the paint or the metal alone. They often include treating the observed alteration, such as stabilizing corrosion on the metal support or consolidating the paint layer, as well as reducing future alteration by applying protective surface coatings. Taking into account the main environmental factors present in museum storage facilities that can alter the painted metal system, namely, fluctuations in relative humidity and temperature as well as exposure to light, a testing protocol was devised in order to study the protection efficiency of selected conservation treatments against controlled artificial aging degradation of the painted metal system.

Model painted metal coupons were prepared with coatings consisting of either lead white or chrome green oxide pigments (hereafter, LW and CrGO, respectively) in a linseed oil binder (LO). Two conservation treatments were tested that are already employed by conservation and restoration specialists: a 0.05 M solution of sodium tetradecanoate ( $\text{NaC}_{14}$ ), a long-chain carboxylate salt with corrosion inhibiting properties, and a resin-wax mixture composed of 30:10 wt% Regalrez 1126<sup>®</sup>-Cosmoloid H80<sup>®</sup> that provides a protective surface barrier against environmental degradation factors. The evolution of the painted metal coupons with and without treatment was monitored using a multi-technique analytical methodology in order to determine the effect of the presence of the treatments in different experimental conditions. The following results show the evolution of the model coupons from the macro to the micro-scale, beginning with a photographic study of the replicate sets and followed by microscopic observations of the surface of the model coupons. The evolution of the chemical structure of the paint coating throughout aging was investigated by FTIR spectroscopy and X-ray absorption spectroscopy. A summary of the observed differences between the untreated and treated zones at the end of the chapter allows to conclude on the observed effectiveness of the conservation treatments against the aging of the model painted metal system.



## IV.1 Photographic study of the model coupons

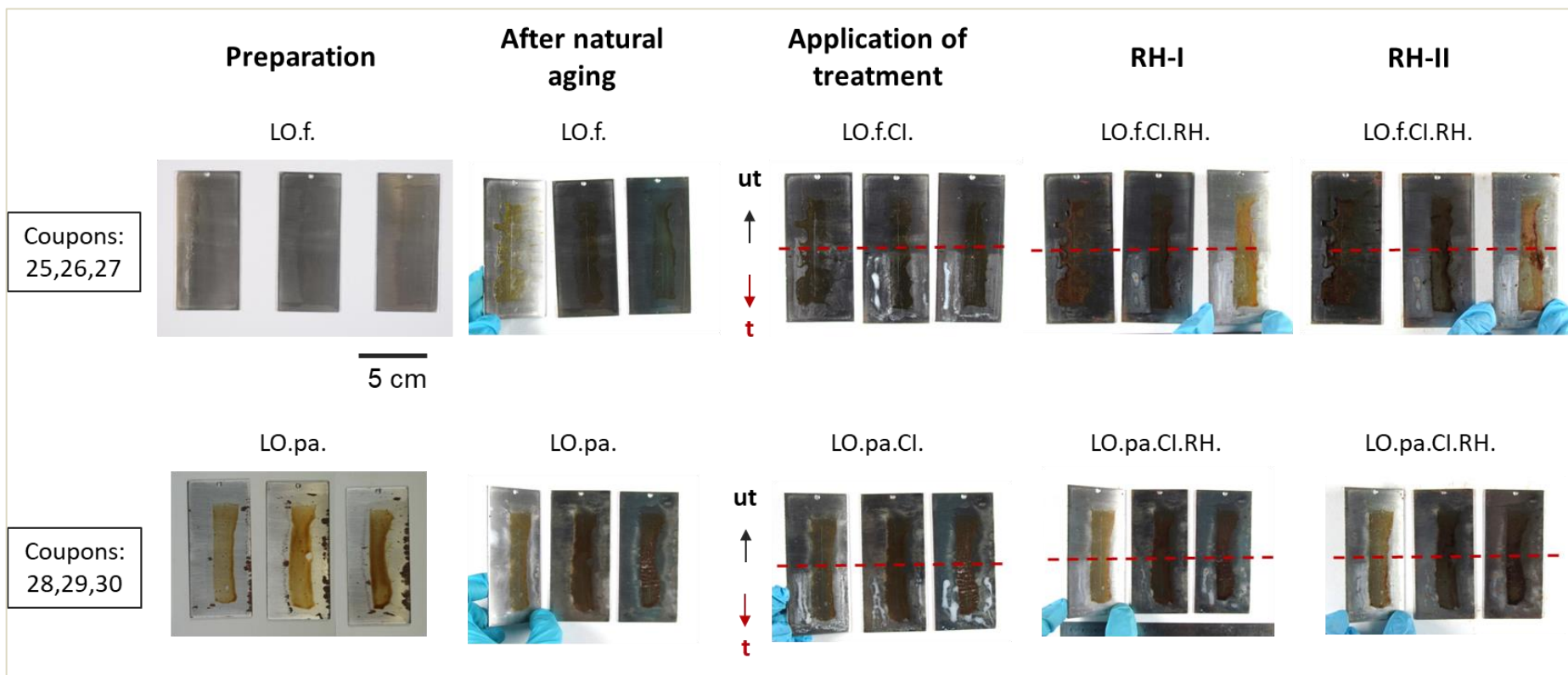
The following photographic study documents the macroscopic state of the surface of the three replicate coupons in each experimental combination throughout the steps of the testing protocol. The photographs are grouped by type of conservation treatment and artificial aging the coupons experienced. Within each experimental group, the fresh (f) and pre-aged (pa) cases are grouped together for direct visual comparison. See “II.II.VII Summary of experimental design for Axe II” for a reminder of the experimental parameter abbreviations.

### IV.1.1 Linseed oil-coated metal coupons

The initial aspect of the linseed oil applied to the metal coupons is almost transparent and colourless. This appearance makes the observation of visual changes by photography difficult. As seen in Figure IV-1, coupons have been tilted to improve the visibility of the surface. After the artificial pre-aging treatment, the linseed oil darkened and developed a red-brown colour. Some areas are still transparent while others are opaque. Corrosion products are observed on the uncoated metal surrounding the binder. These were removed mechanically before continuing the protocol. After 1.5 years of natural aging (storage at ambient air and temperature, non-exposed to light), the fresh coupons have darkened and resemble the colour of the pre-aged coupons. The applied conservation treatments are not invisible: the corrosion inhibitor treatment leaves a white colour that is opaque in areas where an excess of product has pooled, while the resin-wax mixture is more transparent but can still be observed in areas where the application is thicker (e.g., the edges of brushstrokes).

After relative humidity aging (Figure IV-1, Figure IV-2), the fresh samples have darkened and become slightly redder, while the pre-aged coupons do not present a significant colour change. The treated zones do not appear to have aged differently than the untreated zone for either of the applied conservation treatments, except in the case of the pre-aged coupons treated with the resin-wax mixture where the treated zone is more saturated in colour after aging than the untreated zone.

The artificial aging by light exposure had a fading effect: the colour of the oil coating is less saturated than before exposure. The corrosion inhibitor-treated zones do not appear to have aged differently than the untreated binder (Figure IV-3), in contrast to the resin-wax-treated zones that have retained the saturation of the binder from before aging (Figure IV-4).



Coupons:  
25,26,27

Coupons:  
28,29,30

Figure IV-1 Photographs of fresh (f) and pre-aged (pa) linseed oil (LO) coated metal coupons throughout treatment with  $\text{NaC}_{14}$  corrosion inhibitor (CI) and relative humidity (RH) aging cycles (RH-I: phase I, 3 weeks; RH-II: phase II, 6 weeks). Dotted lines separate the untreated (ut) and treated (t) zones.

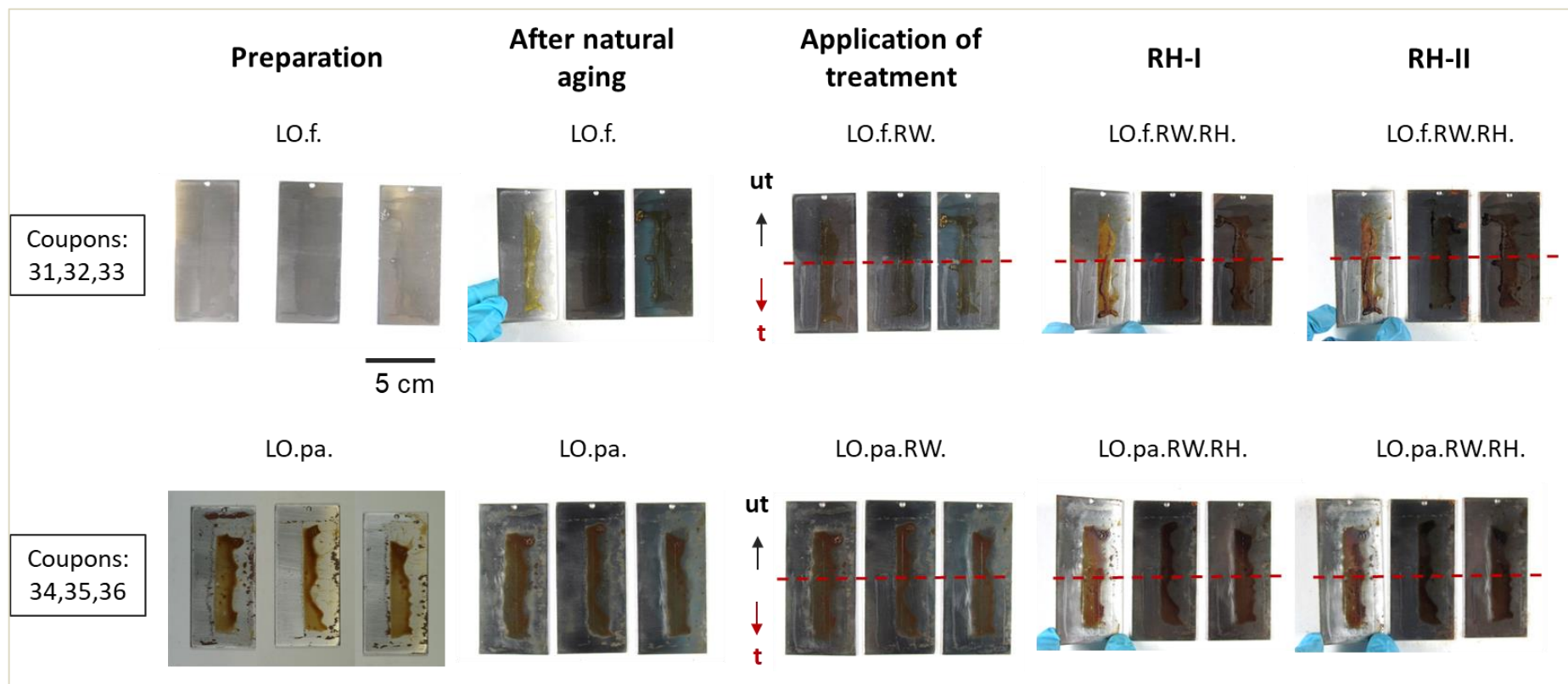


Figure IV-2 Photographs of fresh (f) and pre-aged (pa) linseed oil (LO) coated metal coupons throughout treatment with resin-wax (RW) mixture (30:10 wt% Regalrez 1126:Cosmoloid H80) and relative humidity (RH) aging cycles (RH-I: phase I, 3 weeks; RH-II: phase II, 6 weeks). Dotted lines separate the untreated (ut) and treated (t) zones.

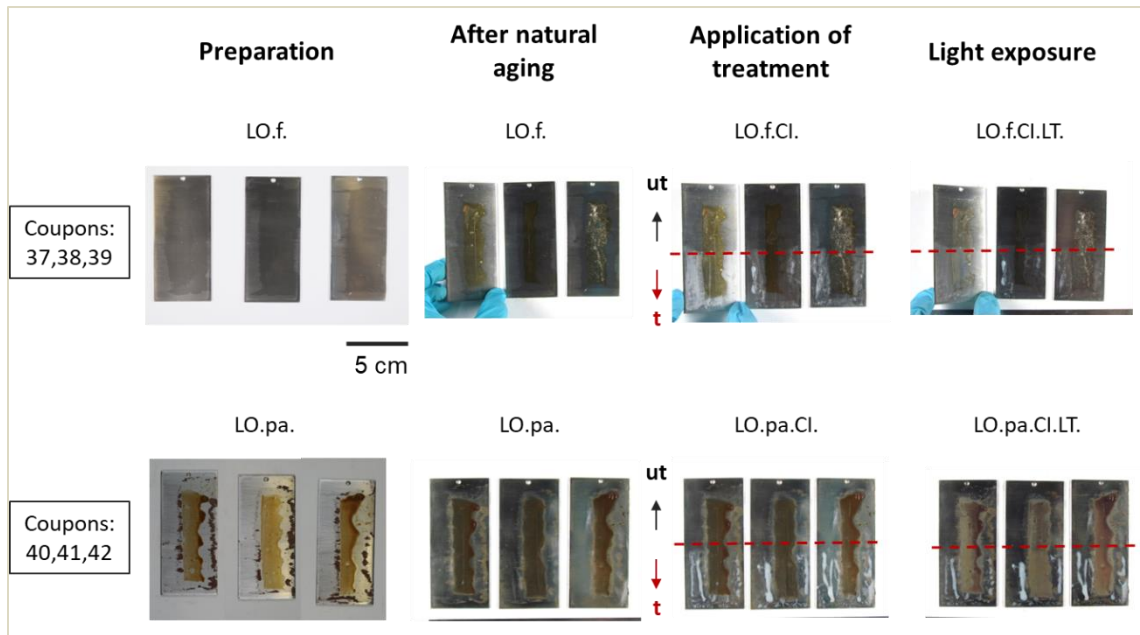


Figure IV-3 Photographs of fresh (f) and pre-aged (pa) linseed oil (LO) coated metal coupons throughout treatment with NaC<sub>14</sub> corrosion inhibitor (CI) and light (LT) exposure aging. Dotted lines separate the untreated (ut) and treated (t) zones.

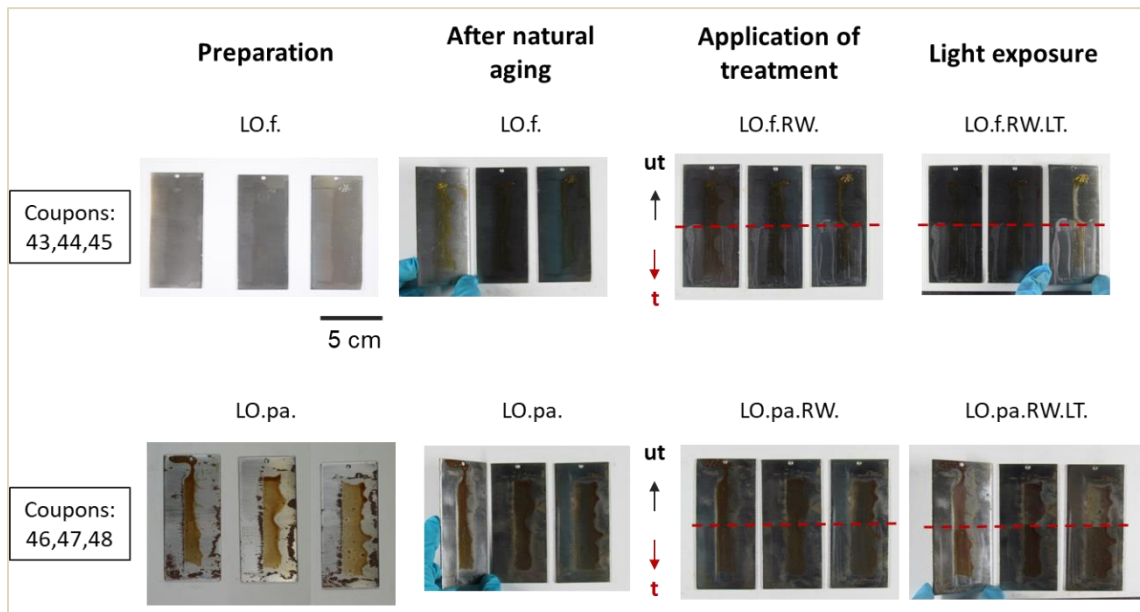


Figure IV-4 Photographs of fresh (f) and pre-aged (pa) linseed oil (LO) coated metal coupons throughout treatment with resin-wax (RW) mixture (30:10 wt% Regalrez 1126:Cosmoloid H80) and light (LT) exposure aging. Dotted lines separate the untreated (ut) and treated (t) zones.

## IV.1.II Lead white-painted metal coupons

The lead white-based paint coating was initially a pure white after application and drying on the metal coupon. After the pre-aging cycle, the paint became more yellow. After 1.5 years of natural aging, some yellowing of the fresh lead white paint is observed but not to the same extent as the artificially pre-aged lead white paint. The initial application of the conservation treatments does not change the appearance of the paint coating.

An increase in yellow colour of the painted surface is observed after aging by relative humidity cycles for both the fresh and pre-aged coupons. In the case of both conservation treatments, no difference between the untreated and treated zones is observed after Phase I or II of relative humidity cycles (with a duration of 3 and 6 weeks respectively), inferring that neither of the conservation treatments have an inhibiting effect on the observed yellowing of the paint.

Exposure to light is observed to bleach (whiten) the paint coating. The fresh coupons display almost the same level of whiteness as in their initial state, while the pre-aged coupons still appear slightly yellow. The remaining yellowness of the sample appears to be dependent on the intensity of the yellow colour before light exposure, as the pre-aged coupons were more yellow than the fresh samples prior to aging. The coupons treated with NaC<sub>14</sub> do not show a difference between the untreated and treated zones after aging (Figure IV-7), suggesting that the presence of the corrosion inhibitor does not impede the bleaching of the painted surface. The coupons treated with the resin-wax mixture do show a difference in colour between the untreated and treated zones after light exposure (Figure IV-8). The untreated zone has whitened more than the treated zone which still retains some yellow colour, although with a lesser intensity than before aging. This suggests that the resin-wax mixture had a protective effect on the original paint coating by blocking the bleaching effects of the light exposure.



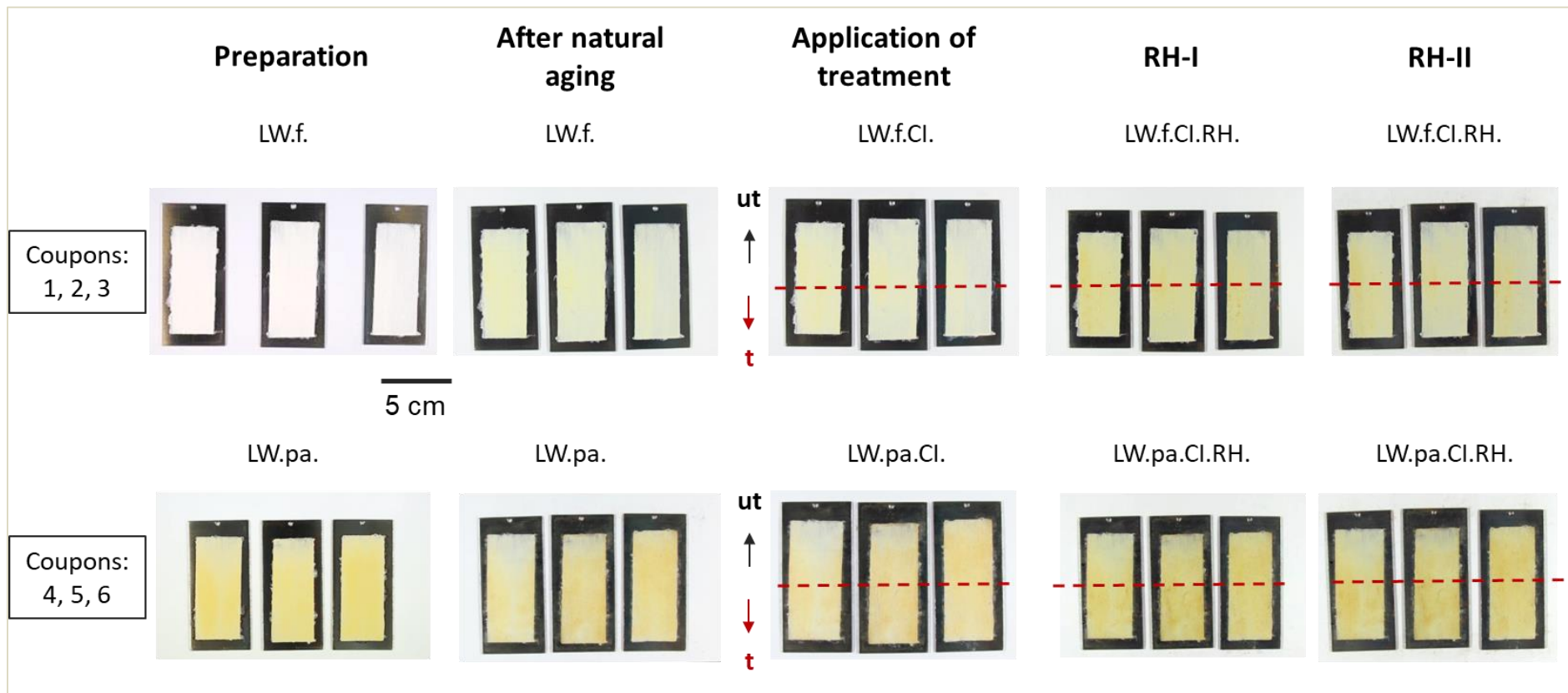


Figure IV-5 Photographs of fresh (f) and pre-aged (pa) lead white (LW)-painted metal coupons throughout treatment with  $\text{NaC}_{14}$  corrosion inhibitor (CI) and relative humidity (RH) aging cycles (RH-I: phase I, 3 weeks; RH-II: phase II, 6 weeks). Dotted lines separate the untreated (ut) and treated (t) zones.

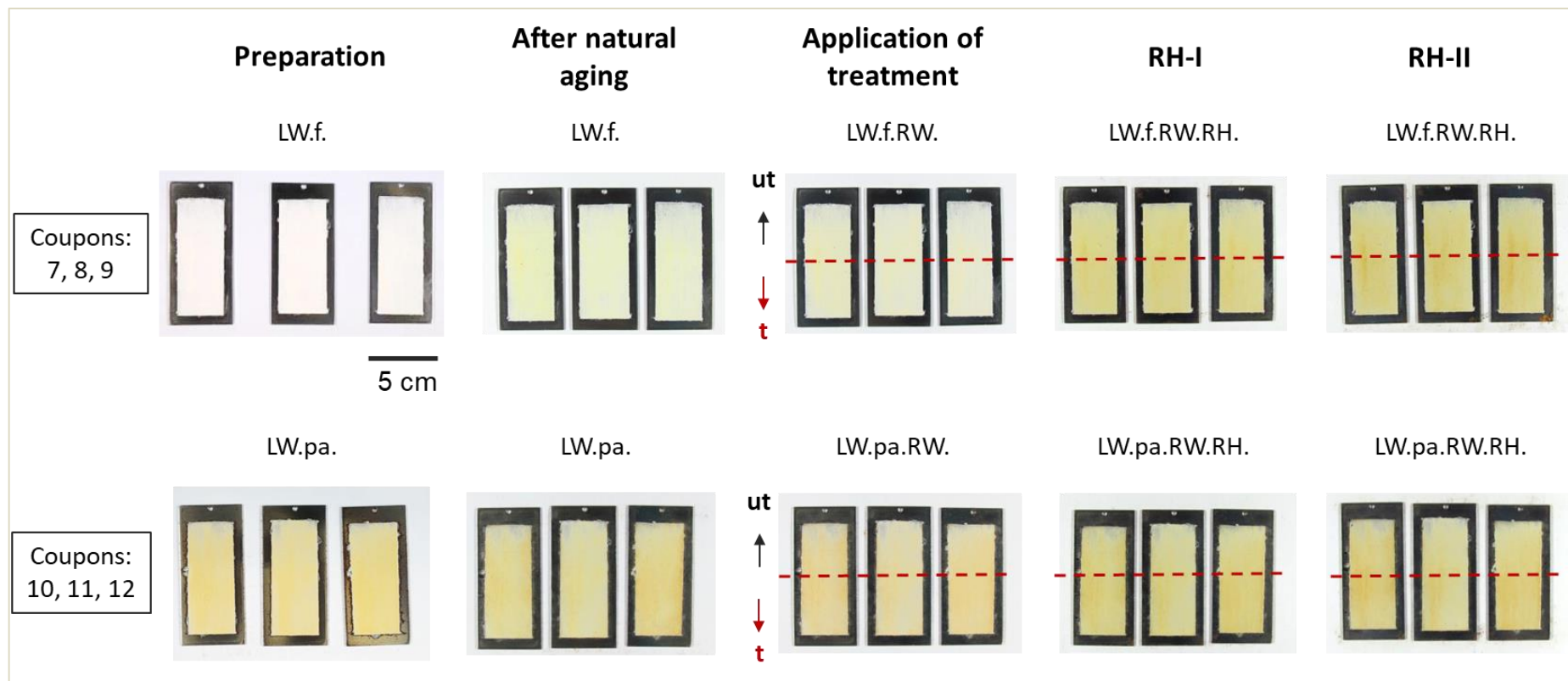


Figure IV-6 Photographs of fresh (f) and pre-aged (pa) lead white (LW)-painted metal coupons throughout treatment with resin-wax (RW) mixture (30:10 wt% Regalrez 1126:Cosmoloid H80) and relative humidity (RH) aging cycles (RH-I: phase I, 3 weeks; RH-II: phase II, 6 weeks). Dotted lines separate the untreated (ut) and treated (t) zones.

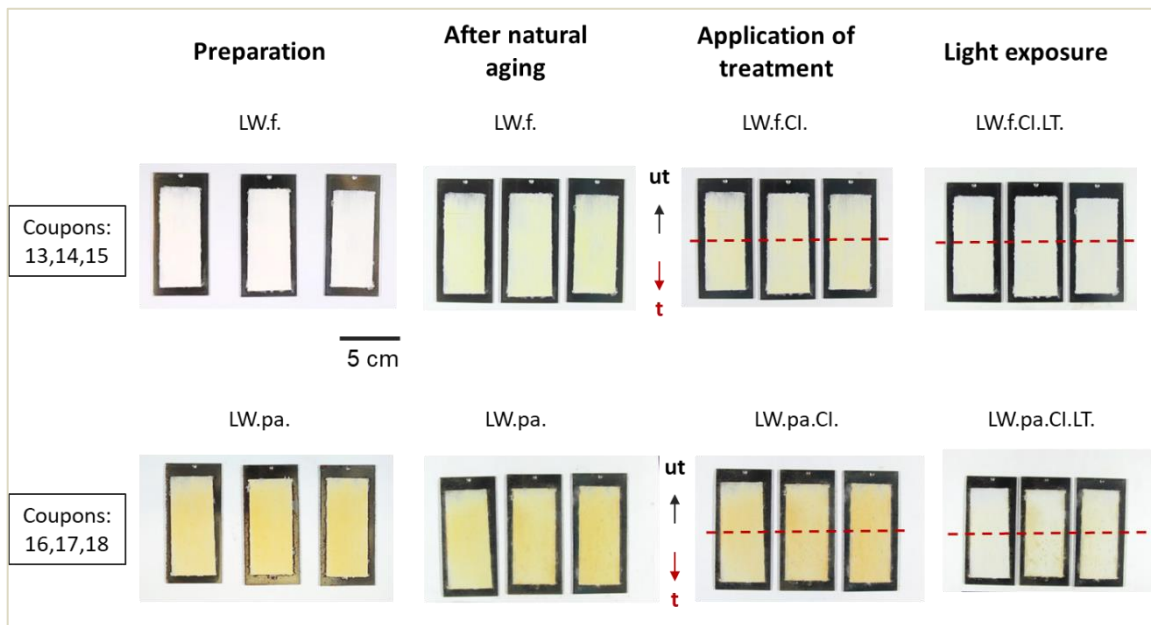


Figure IV-7 Photographs of fresh (f) and pre-aged (pa) lead white (LW)-painted metal coupons throughout treatment with  $\text{NaC}_{14}$  corrosion inhibitor (CI) and light (LT) exposure aging. Dotted lines separate the untreated (ut) and treated (t) zones.

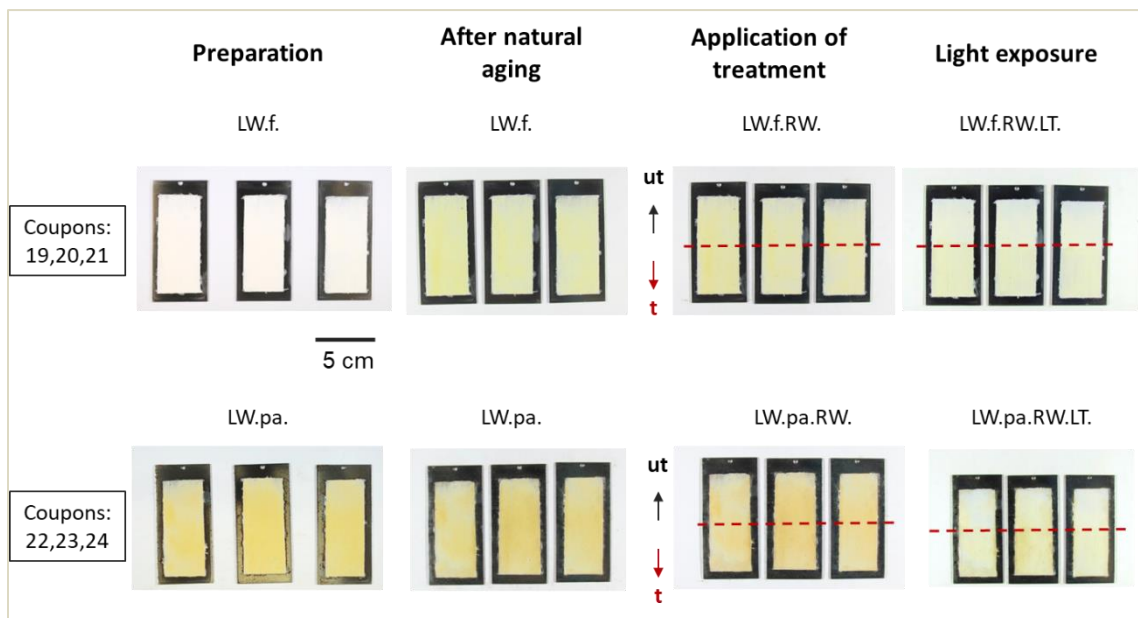


Figure IV-8 Photographs of fresh (f) and pre-aged (pa) lead white (LW)-painted metal coupons throughout treatment with resin-wax (RW) mixture (30:10 wt% Regalrez 1126:Cosmoloid H80) and light (LT) exposure aging. Dotted lines separate the untreated (ut) and treated (t) zones.

### IV.I.III Chrome green oxide-painted metal coupons

In the following photographic study, the state of the chrome green oxide-painted metal coupons aged by relative humidity cycles or light exposure is documented. The initial aspect of the fresh paint directly after drying is shown for comparison (Figure IV-9), although only pre-aged full sized chrome green oxide-painted coupons were submitted to the aging protocols. Extra coupons (61, 62, 63) had been prepared with swatches of each coating type (Figure IV-10); the chrome green oxide-painted swatches on these samples were used as the fresh version of the paint during the aging protocol.

The fresh chrome green oxide paint appears brighter and more yellow before the artificial pre-aging treatment. After pre-aging, the paint coating is darker in colour. After 1.5 years of natural aging, no visible differences are noticeable. Before artificial aging, the conservation treatments were applied either to the bottom half of the painted surface (in the case of the full sized pre-aged samples) or to the right half of the painted swatch (in the case of the fresh CrGO paint on coupons 62 and 63). Neither of the treatments are visible on the fresh paint coatings. For the pre-aged samples, treatment with corrosion inhibitor did not change the appearance of the coating but treatment with the resin-wax mixture darkened the aspect of the paint coating.

After Phase I of relative humidity cycles (Figure IV-10, Figure IV-11), minimal changes are visible for both the fresh and pre-aged paint coatings, although some lighter-coloured streaks are apparent on the pre-aged coupons. After Phase II however, the fresh and pre-aged paint coatings have darkened, and the streaks on the pre-aged coupons are more visible. No difference is observed between the untreated paint and the corrosion inhibitor-treated paint, while the painted surfaces treated with the resin-wax mixture appears less altered, suggesting that the resin-wax mixture may have limited the aging effects of the relative humidity cycles.

The light exposure aging appears to have had a lightening/fading effect on the painted surface (Figure IV-12). No difference is observed between the untreated and corrosion inhibitor treated zones. Conversely, the zones treated with the resin-wax mixture appear slightly darker than the untreated paint coating, demonstrating that the presence of the resin-wax mixture decreased the fading effect of the light exposure.

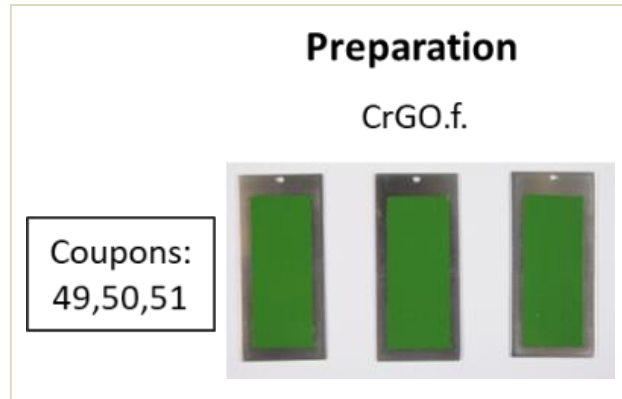


Figure IV-9 Chrome green oxide (CrGO)-painted metal coupons (coupons 49, 50, 51). Photograph of the samples in their fresh (f) state (8 days after preparation).

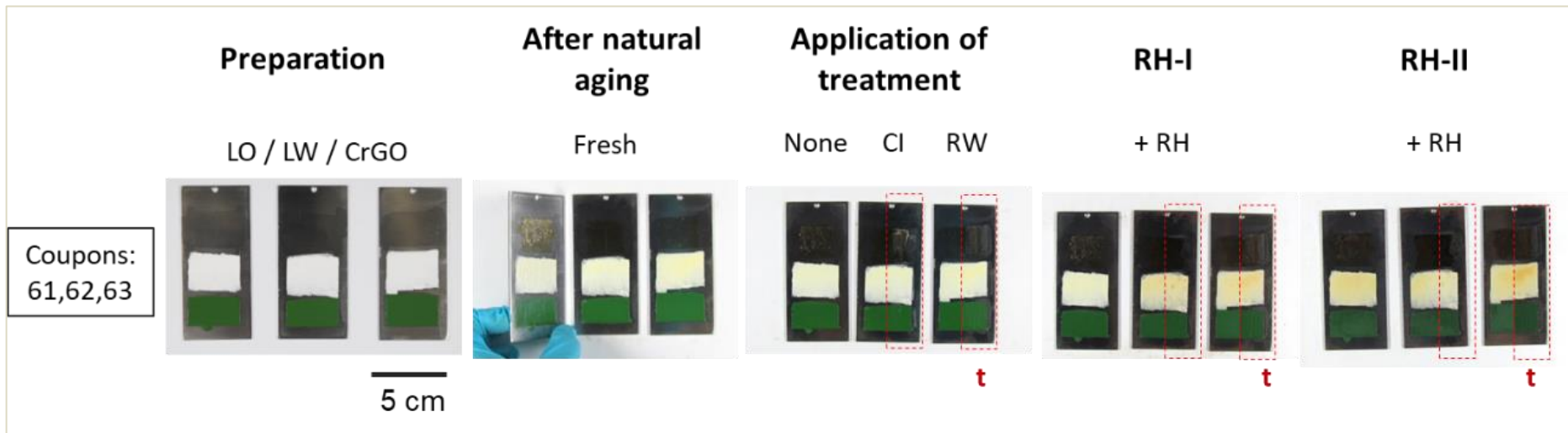


Figure IV-10 Extra coupons (61, 62, 63) prepared with swatches of each coating: linseed oil binder (LO), lead white (LW) paint, chrome green oxide (CrGO) paint. Treated (t) zones using NaC<sub>14</sub> corrosion inhibitor (CI) (coupon 62) or resin-wax mixture (RW) (coupon 63) are indicated by red dotted lines.

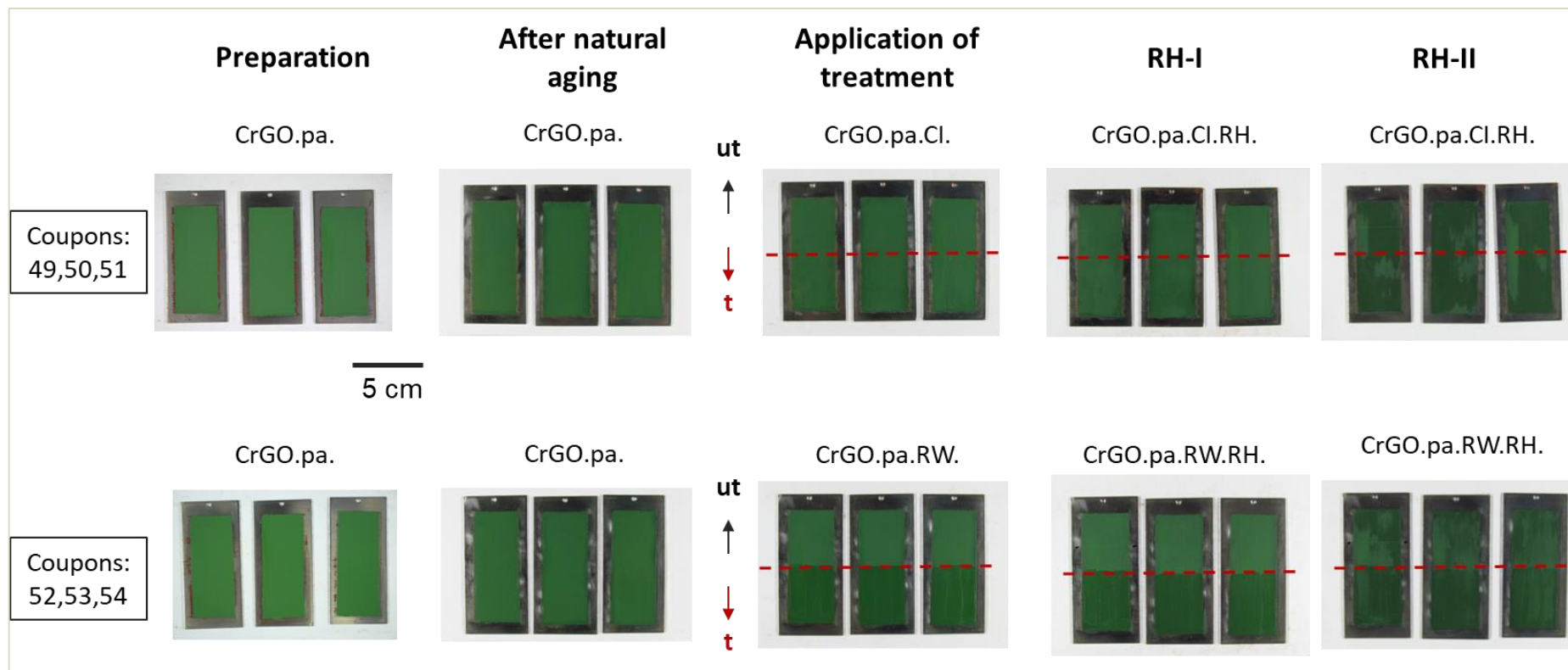


Figure IV-11 Photographs of pre-aged (pa) Chrome green oxide (CrGO)-painted metal coupons throughout treatment with NaC<sub>14</sub> corrosion inhibitor (Cl) (top row) and resin-wax (RW) mixture (bottom row) and relative humidity (RH) aging cycles (RH-I: phase I, 3 weeks; RH-II: phase II, 6 weeks). Dotted lines separate the untreated (ut) and treated (t) zones.

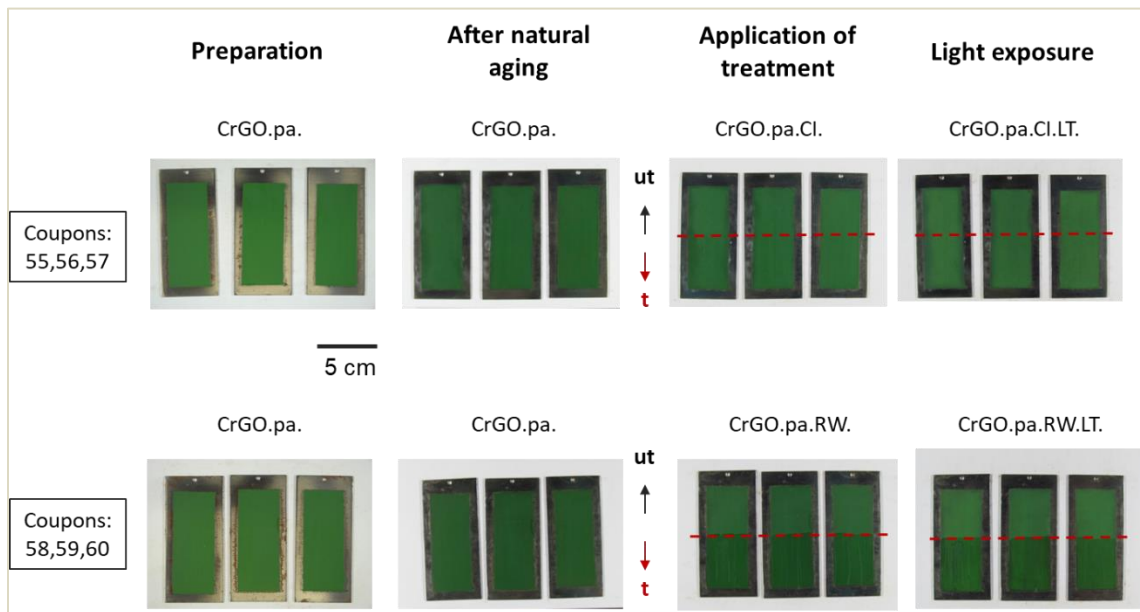


Figure IV-12 Photographs of chrome green oxide (CrGO)-painted metal coupons throughout treatment with NaCl<sub>4</sub> corrosion inhibitor (Cl) (top row) and resin-wax (RW) mixture (bottom row) and aged by light (LT) exposure. Dotted lines separate the untreated (ut) and treated (t) zones.

## IV.II Colorimetric study of the painted metal surfaces

### IV.II.I Initial materials

Colorimetry measurements for the painted metal coupons were collected at each stage of aging. Their initial state was first documented eight days after the application of the paint coatings and immediately after the pre-aging cycles (see Table IV-1). This measurement was repeated 1.5 years later upon reprisal of the experiment (see Table IV-2). The tables list the colorimetric values and the calculated difference in colour ( $\Delta E^*$ ) between the fresh and pre-aged coupons for each series (LO, LW, CrGO).

**Table IV-1 Comparison of the colorimetric measurements obtained on fresh (f) and pre-aged (pa) painted coupons directly after preparation. Values are either a unique measurement or an average of measurements obtained on different coupons.**

Coating	Initial state	Num. samples	L*	a*	b*	$\Delta E^*$
LO (binder)	f	1	66.81	0.02	1.46	24.52
	pa	4	50.69	3.20	19.66	
LW	f	1	91.64	-2.97	8.00	25.51
	pa	4	82.90	-0.11	31.80	
CrGO	f	1	41.37	-18.01	13.34	2.05
	pa	4	39.51	-17.28	12.87	

**Table IV-2 Comparison of the colorimetric measurements obtained on fresh (f) and pre-aged (pa) painted coupons after 1.5 years of natural aging. Values are an average of measurements obtained on different coupons.**

Coating	Initial state	Num. samples	L*	a*	b*	$\Delta E^*$
LO (binder)	f	2	55.38	0.26	24.77	13.62
	pa	2	43.17	6.26	25.19	
LW	f	2	89.46	-5.56	20.78	6.70
	pa	2	84.90	-2.70	24.78	
CrGO	f	2	37.07	-22.37	17.64	4.72
	pa	2	36.17	-18.84	14.65	

The difference in colorimetric values between the fresh and pre-aged initial states both after preparation and after 1.5 years of natural aging are represented visually for each series in Figure IV-13. The LO and LW-painted coupons are less different after the period of natural aging (as seen by a decrease in  $\Delta E^*$ ), while the CrGO-painted coupons show a greater difference (observed increase in  $\Delta E^*$ ).



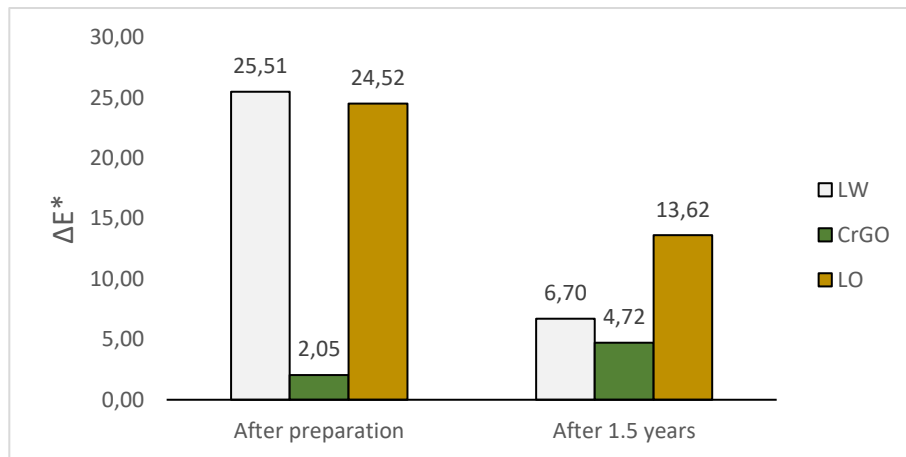


Figure IV-13  $\Delta E^*$  values (representing the difference in colorimetric measurements between the fresh and pre-aged types of each series of model coupon) after preparation of coupons and after 1.5 years of natural aging.

The **LO-coated series** shows a decrease in  $\Delta E^*$  from 24.52 after preparation to 13.62 after 1.5 years. Both the fresh and pre-aged LO coupons show a decrease in  $L^*$ , indicating a darkening of colour, while the fresh LO coupons show a large increase in  $b^*$ , bringing it closer in yellowness to the pre-aged sample. The pre-aged LO coupon has a larger  $a^*$  value after the natural aging period which is representative of a greater redness contribution. The increase in  $b^*$  over time which is observed in these measurements could be linked to the yellowing that occurs naturally with the aging of linseed oil (Townsend et al., 2011).

For the **LW-painted series**, the initial difference in colour between the fresh and pre-aged paint was significant with a  $\Delta E^*$  of 25.51. The comparison of the  $L^*a^*b^*$  values show a decrease in lightness, a slight increase in redness and an increase in yellowness for the pre-aged coupon. After 1.5 years, the colour difference between the fresh and pre-aged coupons decreased to a  $\Delta E^*$  of 6.70. This is still a perceptible colour difference, but less so than when the coupons were originally prepared. This is mainly linked to a positive  $b^*$  shift for the fresh LW coupon, indicating that the lead white-based paint will tend towards a yellow colour over time. The  $L^*$  values have remained stable while the  $a^*$  values have decreased, indicating a shift towards greenness.

The **CrGO-painted series** is more colour-stable to both the artificial pre-aging treatment and to natural aging. This is evidenced by a non-perceptible colour difference of  $\Delta E^* = 2.05$  after preparation of the coupons, which increased to a slightly perceptible difference of  $\Delta E^* = 4.72$  after 1.5 years of natural aging. The  $L^*$  value has decreased over time for both the fresh and pre-aged coupons, representing a darkening of colour. A decrease in  $a^*$  and an increase in  $b^*$  is seen for both coupons, although to a greater extent in the fresh coupon. These shifts indicate an increase in greenness and yellowness, respectively.

## IV.II.II Colour monitoring throughout testing of conservation treatments

Colorimetric measurements were acquired on the untreated and treated zones of the model coupons after each step in the conservation treatment testing protocol and the difference in colour between the zones was calculated ( $\Delta E^*$ ). The colorimetric data and  $\Delta E^*$  values for the linseed oil-coated metal coupons can be found in Appendix H for reference but will not be discussed here as we are mainly interested in studying the changes on the pigmented coating system. The following results are presented by paint coating type.

### IV.II.II.i Lead White-painted metal coupons

The  $L^*a^*b^*$  measurements for the lead white-painted metal coupons are found in the Appendix (see Appendix H). For all combinations of fresh and pre-aged paint treated with either the NaC<sub>14</sub> corrosion inhibitor (CI) solution or the resin-wax (RW) mixture, the  $\Delta E^*$  values for the colour difference between the untreated and treated zones before artificial aging are below the threshold for a perceptible colour difference (a just noticeable difference is set at the threshold of  $\Delta E^* > 2.3$ ), indicating that the application of the treatments did not have an initial influence on the colour appearance of the lead white-based paint.

After Phase I aging by relative humidity cycles, the overall trend for the lead white-painted coupons is a shift towards red and yellow, as well as a darkening of the paint ( $-L^*$ ). The coupons treated with corrosion inhibitor show a perceptible colour difference between the treated and untreated zones, as does the fresh-painted sample treated with the resin-wax mixture. The pre-aged coupon treated with the resin-wax mixture does not show a difference in colour. The same observations are made after Phase II of relative humidity cycles; however, for both types of conservation treatment, the fresh-painted coupons show a slight decrease in the difference between the two zones. In the case of the fresh-painted coupon treated with the resin-wax mixture, the  $\Delta E^*$  decreased to a value under the threshold of perception. The differences shown by the  $\Delta E^*$  values for the lead white-painted coupons treated with corrosion inhibitor can be linked to a higher  $b^*$  value for the treated zone. This infers that the treated zone has yellowed more than the untreated zone throughout the artificial aging by relative humidity cycles. A visual comparison of the measured colour difference for each type of coupon throughout the relative humidity cycles is seen in Figure IV-14.

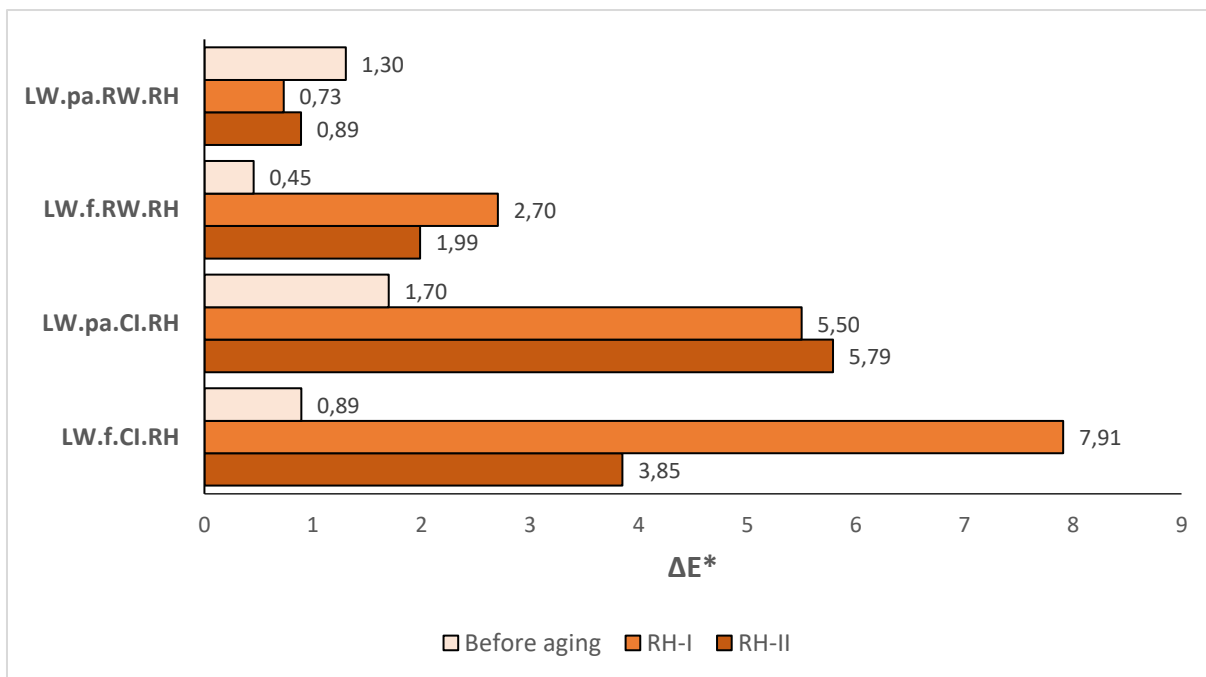


Figure IV-14 Difference in colorimetric measurements ( $\Delta E^*$ ) obtained on untreated and treated zones of lead white (LW)-painted coupons through artificial aging (relative humidity (RH) cycles).

The lead white-painted coupons aged by light exposure show colorimetric differences representative of a lightening of the paint and a shift towards red and blue. Apart from the pre-aged coupon treated with the corrosion inhibitor  $\text{NaC}_{14}$  (LW.pa.CI.LT), all the coupon types show a difference between the untreated and treated zone after aging by light exposure. Calculated colour differences between the untreated and treated zones of the light-aged lead white-painted coupons are graphed in Figure IV-15. The  $L^*a^*b^*$  data (Appendix H) shows that these differences are mainly linked to a high  $\Delta b^*$ . The untreated zones have a greater  $-b^*$  shift compared to the treated zones after light exposure, indicating a shift towards blue on the yellow-blue axis. A decrease in the yellow colour of the lead white-based paint after light exposure was also noticeable in the photographic study, but a difference between the untreated and treated zones was not perceptible on initial observation. These results suggest that the conservation treatments maintain the initial colour to an extent, but the data should be considered with respect to the visual and photographic observations.

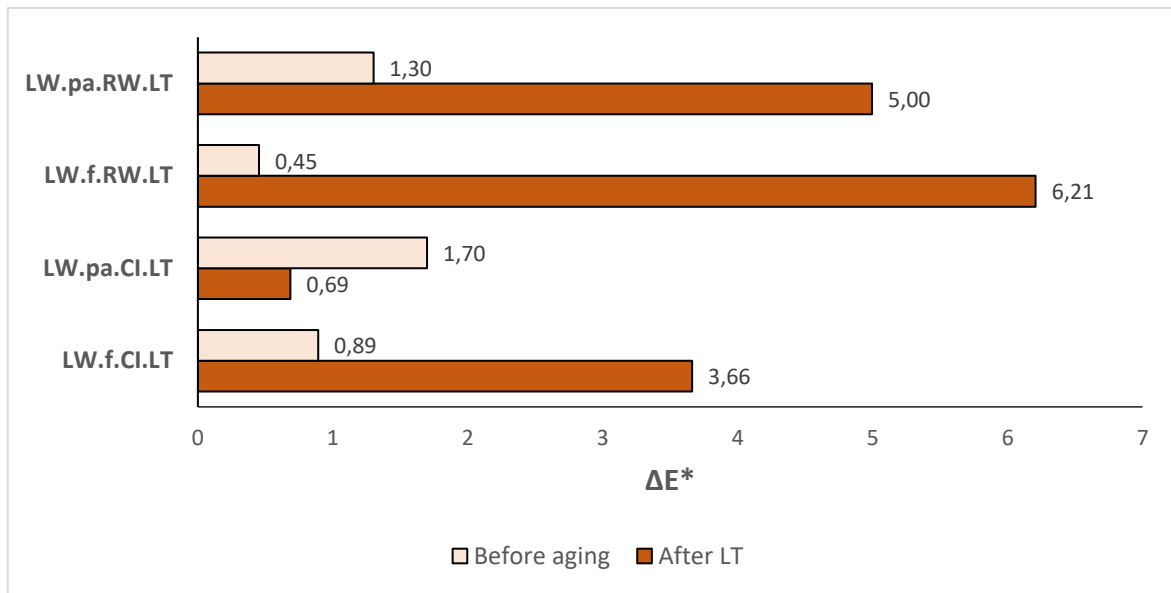


Figure IV-15 Difference in colorimetric measurements ( $\Delta E^*$ ) obtained on untreated and treated zones of lead white (LW)-painted coupons before and after artificial aging by light (LT) exposure.

#### IV.II.II.ii Chrome green oxide-painted metal coupons

The  $\Delta E^*$  values for the untreated and treated zones of the chrome green oxide-painted metal coupons aged by relative humidity cycles are displayed in Figure IV-16.

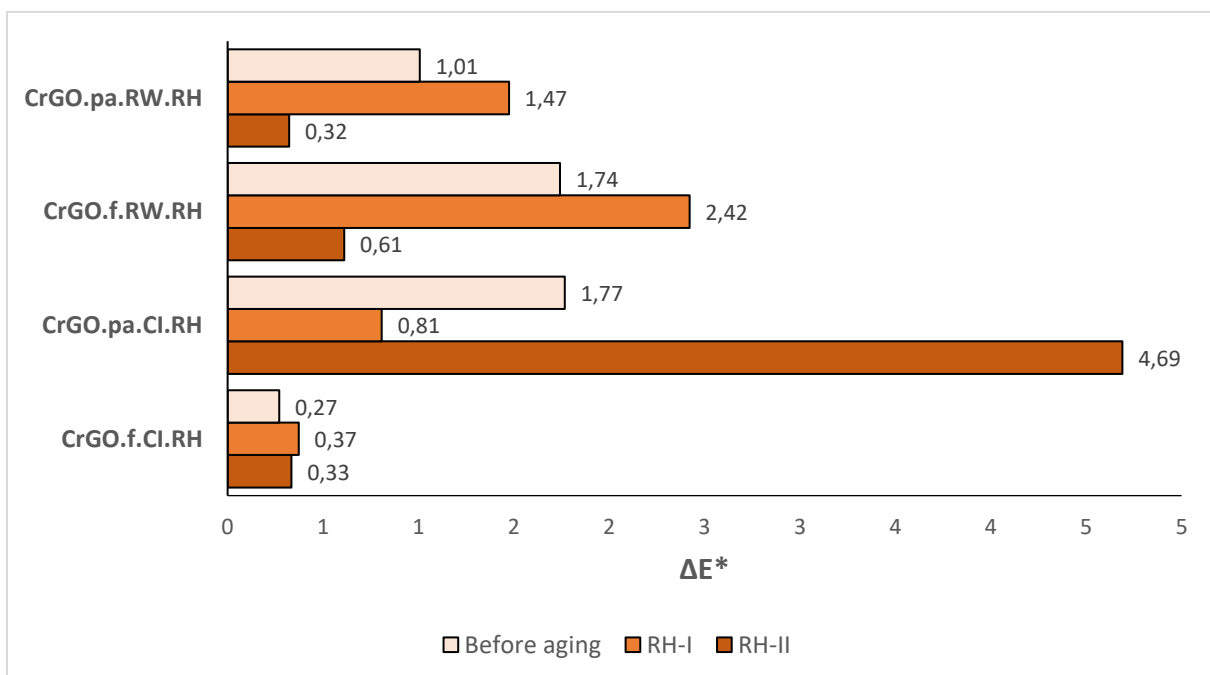


Figure IV-16 Difference in colorimetric measurements ( $\Delta E^*$ ) obtained on untreated and treated zones of chrome green oxide (CrGO)-painted coupons through artificial aging (relative humidity (RH) cycles).

After application of the conservation treatments and before aging, none of the measured differences between the untreated and treated paint are above the perception threshold. This suggests that the treatments do not initially influence the colour aspect of the painted surface.

After Phase I of relative humidity cycles, the  $L^*a^*b^*$  values (Appendix H) show that in general, the CrGO-painted coupons increased or stayed at the same level of lightness  $L^*$ , the  $a^*$  slightly decreased (shift towards green) and the  $b^*$  slightly increased (shift towards yellow) or stayed the same. The coupons treated with corrosion inhibitor do not show a difference between the untreated and treated painted surfaces. The coupons treated with the resin-wax mixture have slightly higher values of  $\Delta E^*$ , but only the fresh-painted coupon has a  $\Delta E^* > 2.3$ . However, the differences in the  $L^*a^*b^*$  values for this case are marginal.

After Phase II of relative humidity cycles, the colorimetric values for the CrGO paint coating show an overall trend of darkening. The fresh coupons show an increase in  $a^*$  (shift towards red) and a decrease in  $b^*$  (shift towards blue), while the  $a^*$  and  $b^*$  values for the pre-aged coupons remain similar to the values measured after Phase I. Only the pre-aged coupon treated with corrosion inhibitor has a  $\Delta E^*$  above the perception threshold; however, given the heterogeneity of the surface (light and dark streaks) seen in the photographs (see Figure IV-11), not enough measurements were acquired to properly represent the variance in colour. The colour differences for the untreated and treated zones throughout aging are graphed in Figure IV-16.

After light aging of the pre-aged CrGO-painted coupons (fresh coupons were not aged by light exposure), the  $\Delta E^*$  between the untreated and treated zones increases to just around a perceptible level for both treatment types, seen visually in Figure IV-17. The  $L^*a^*b^*$  values indicate that the influence of the light aging on the untreated pre-aged CrGO paint is an increase in lightness and a shift towards red and yellow. The coupon treated with corrosion inhibitor shows a greater shift towards red and yellow in the treated zone than in the untreated zone, indicating a different colour evolution in the presence of the treatment compared to the untreated paint. On the coupon treated with the resin-wax mixture, where the  $\Delta E^*$  is higher, the  $L^*a^*b^*$  values show that the difference is mainly due to a greater increase of the  $L^*$  value in the untreated zone than in the treated zone. This suggests that the resin-wax mixture preserved the initial paint colour against the lightening effects of the light exposure.

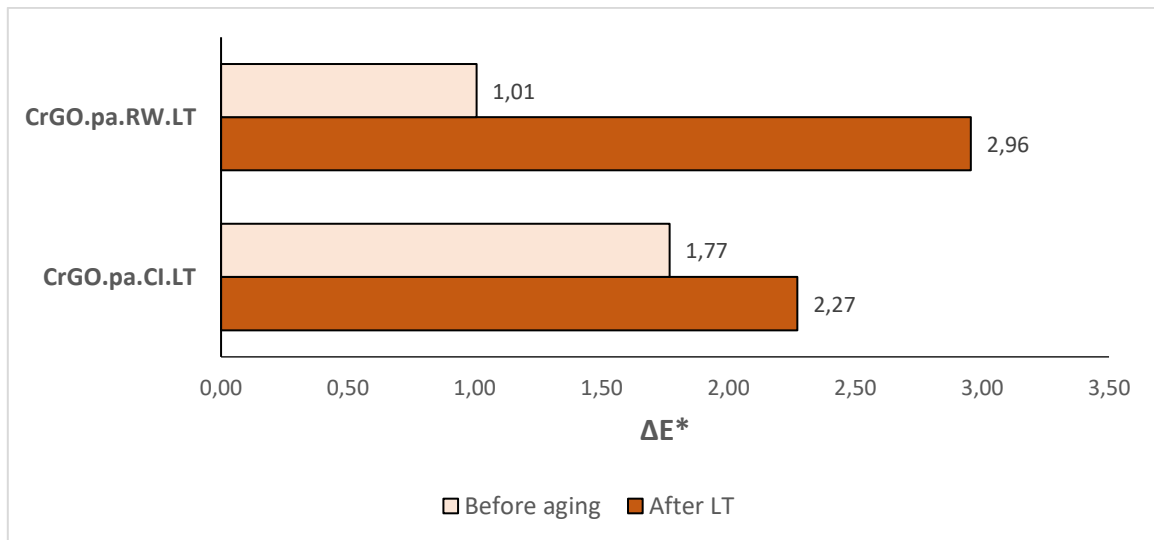


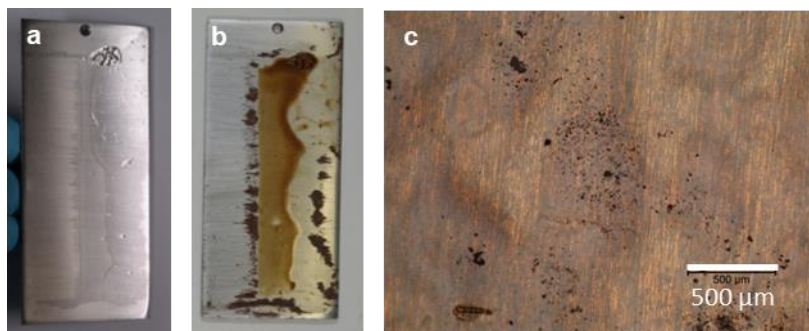
Figure IV-17 Difference in colorimetric measurements ( $\Delta E^*$ ) obtained on untreated and treated zones of chrome green oxide (CrGO)-painted coupons before and after artificial aging by light (LT) exposure.

### IV.III Microscopic study of the painted metal surfaces

In addition to macroscopic observations of the model coupons which provide general information about the overall aesthetic changes occurring mainly on the painted surface, optical microscopic observation can yield complementary insight into the state of alteration by revealing the presence of alterations occurring at a smaller scale. An improved understanding of the state of the surface will also aid in the interpretation of more advanced characterisation techniques such as FTIR and XANES spectroscopy that provide localized information of the chemistry of the sample surfaces at the micro-scale.

#### IV.III.I Linseed oil-coated metal coupons

The linseed oil-coated coupon is seen in its fresh and pre-aged states in Figure IV-18. Corrosion products appeared around the coated areas on the bare metal after the pre-aging process; these were removed mechanically before continuing the testing protocol. The microscope image of the pre-aged coating demonstrates the transparent aspect of the oil coating as the metal coupon can be seen underneath. Furthermore, some dark products are seen within the coating which may be corrosion products.



**Figure IV-18 Photographs of the linseed oil-coated metal coupons: fresh (a); pre-aged (b) and microscope image of pre-aged coating (c). Coupons measure 100 mm x 45 mm.**

After Phase I of relative humidity aging cycles, the surfaces of the linseed oil coated-metal coupons were once again observed under the microscope for signs of alteration. The untreated coatings (Figure IV-19 a,b,c) show uneven discoloration, differences in transparency, and formation of dark brown products that appear to have grown underneath the coating and have broken through the coating in some areas.



Figure IV-19 Microscope images of the surface of untreated (a, b, c) linseed oil coated-metal coupons after phase I of relative humidity aging cycles.

### IV.III.II Lead white-painted metal coupons

Macro and microscopic images of examples of lead white-painted metal coupons in the fresh and pre-aged state are seen in Figure IV-20. The photographs of the full coupons (described more fully in IV.I Photographic study of the model coupons) show that the coating is white before pre-aging and becomes yellow afterwards. The microscope images show a more heterogeneous aspect, where the fresh lead white paint coating (Figure IV-20c) contains a mix of lighter and darker shades of white in general, and also presents darker marks or grains of about 50-100 μm in size. The pre-aged lead white paint coating is mainly yellow in colour but also presents darker and lighter heterogeneities, notably around the pigment grains where the grain itself appears whiter but the area surrounding the grain appears darker in colour.

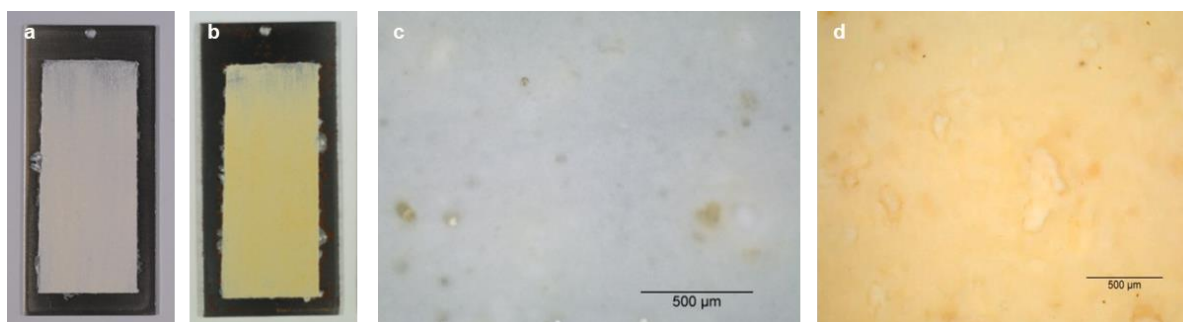


Figure IV-20 Photographs of the fresh (a) and pre-aged (b) lead white-painted metal coupons and microscope image of the fresh (c) pre-aged (d) coatings. Coupons measure 100 mm x 45 mm.

After Phase I of relative humidity cycles, microscope images were acquired on the untreated fresh and pre-aged lead white paint coatings, centered on the scratch that had been traced through the middle of the paint coating before aging (Figure IV-21). Apart from the difference in colour, the coatings do not



present signs of alteration. The size of the pigment grains is more evident in these images as a multi-image acquisition mode was used to create focused images of the uneven surface.

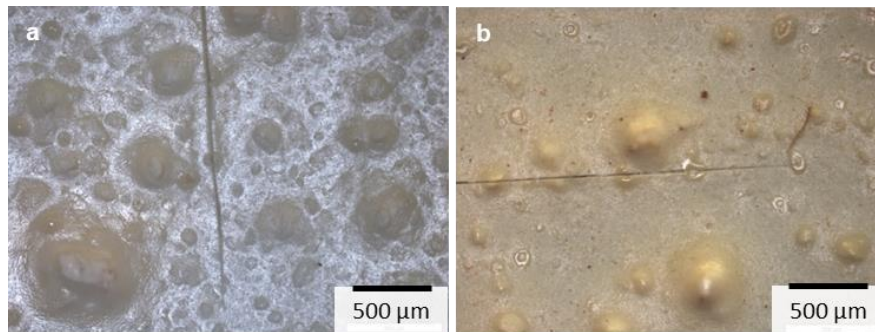


Figure IV-21 Microscope images of the surface of untreated fresh (a) and pre-aged (b) lead white painted-metal coupons after phase I of relative humidity aging cycles.

### IV.III.III Chrome green oxide-painted metal coupons

The chrome green oxide-painted metal coupons showed a slight darkening of the coating by macro-observation; this difference is less obvious when the coating is observed by microscope. The fresh paint coating shows a fine granular aspect with a mainly green colour with some darker particles dispersed without (Figure IV-22c). After pre-aging, the coating appears slightly streaked and some bright orange corrosion products are visible within the paint coating (Figure IV-22d).

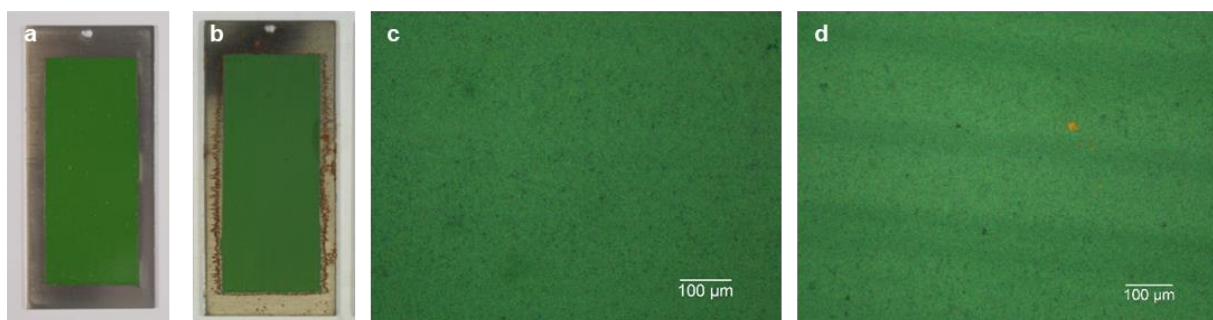


Figure IV-22 Photographs of the fresh (a) and pre-aged (b) chrome green oxide-painted metal coupons and microscope images of the fresh (c) and pre-aged (d) coatings. Coupons measure 100 mm x 45 mm.

In Figure IV-23, microscope images of some surface alterations that formed on the untreated coatings after Phase I of relative humidity cycles are shown. Streaks of varying reflectivity are observed on the fresh paint coating, possibly along the edges of brush strokes from the application of the paint (Figure IV-23a). The pre-aged paint coating showed some cases of fissuring, revealing the metal coupon underneath (see Figure IV-23b). Furthermore, a white/reflective product is present in a general manner

Chapter IV A multi-scale analytical study of the effects of conservation treatments on the aging of model painted metal surfaces

over the entirety of the surface. It is also observed that the edges of the paint surface have receded from the “scratch” that was applied to the coating before aging (Figure IV-23c).

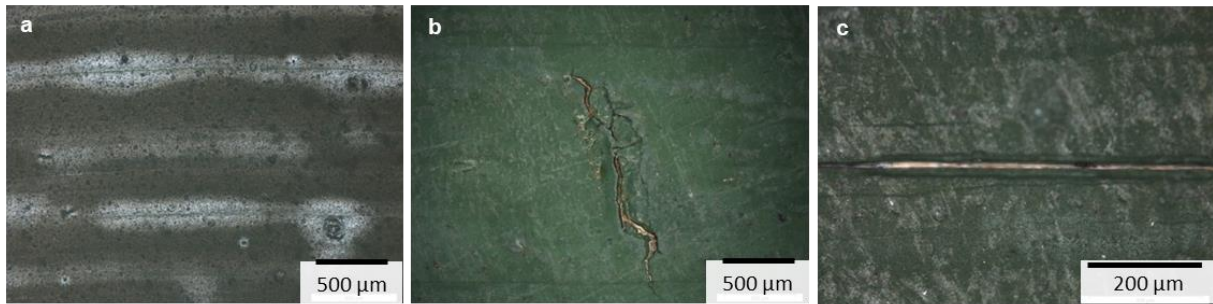


Figure IV-23 Microscope images of the surface of chrome green oxide painted-metal coupons after phase I of relative humidity aging cycles: fresh paint coating (a); fissure in pre-aged paint coating (b); scratch in pre-aged paint coating (c).

## IV.IV FTIR study of the paint coatings

The objective of using FTIR spectroscopy in this study is to monitor changes in the paint coating throughout the artificial aging processes and to compare the evolution of the paint in the untreated and treated zones. Specifically, changes in the FTIR absorption spectrum are used to understand what chemical modifications may be occurring. Differences in the evolution of the untreated and treated zones help to clarify the effect that the conservation treatments have on the aging of the paint. The FTIR spectra acquired on our model painted metal coupons contain absorption bands corresponding to vibrational modes related to the structure of the organic linseed oil binder, the pigments (basic lead (II) carbonate or chrome (III) oxide), the conservation treatments (corrosion inhibitor NaC<sub>14</sub> or resin-wax mixture 30:10 wt% Regalrez 1126®:Cosmoloid H80®) as well as molecular structures formed due to interactions between the components. Despite the complexity of the system, each structure has characteristic absorption bands that can be used to understand which chemical processes are associated with changes observed in the FTIR spectra throughout aging.

### IV.IV.I FTIR absorption bands of interest

As discussed in the literature review (see I.I.II.ii Binders), linseed oil is a drying oil composed mainly of triacylglycerides (TAGs), a structure composed of three fatty acids joined by ester linkages to a glycerol backbone. The fatty acids present may be saturated or unsaturated. The double bonds of the unsaturated acids act as reactive sites for oxidation and polymerisation and are responsible for the siccative properties of the oil. During drying and hardening of the paint film, modifications in the position and/or intensity of absorption bands in the FTIR spectra are indicative of the occurrence of chemical changes. The mechanisms involved in the drying and aging of the oil are complex and involve various transformations of the chemical structure.

Notable changes in the aging of linseed oil include (Meilunas et al., 1990):

- the loss of the *cis* olefinic C-H stretch ( $3010\text{ cm}^{-1}$ ) due to the polymerisation and oxidation of the unsaturated fatty acid chains,
- the formation of oxidation products (including free fatty acids) as evidenced by an increase in absorption in the hydroxyl OH region between  $3600\text{-}3000\text{ cm}^{-1}$  and a broadening of the carbonyl C=O stretch between  $1850\text{-}1600\text{ cm}^{-1}$ . Band formation at  $1418\text{ cm}^{-1}$  along with a shoulder at  $1715\text{ cm}^{-1}$  is characteristic of free fatty acids.

In addition to the characteristic oil absorption bands, other bands associated to the pigment used are present in the FTIR spectra of the paint system; these are identified and discussed in the following

results sections (by paint type). In this study we are interested in the observation of specific products resulting from interactions or reactions occurring within the paint system during aging. These are mainly carbonyl and hydroxyl-containing products contained within the polymer network as well as free fatty acids produced from the aging of the oil. The free fatty acids may also interact with metal ions in the pigments to form metal carboxylates (soaps). Metal soaps are a topic of popular interest in the field of conservation science and the reader is referred to the literature review (see I.I.III.iii Pigment-binder interaction) for more detailed studies on their behaviour and characterisation. Lead soaps are expected to form in our model painted metal coupons as they have often been observed in oil paint systems containing lead-based pigments, while chrome soaps have not been reported in oil paints to our knowledge. For the purposes of this study, the main characteristic FTIR absorption bands for metal soaps reported in the literature will be used to monitor for their presence during the artificial aging of the painted metal coupons. In general, the asymmetric and symmetric carboxylate group (COO) stretches of metal soaps appear around 1550 and 1400  $\text{cm}^{-1}$ , respectively. The frequency of these absorptions will vary depending on the nature of the metal cation. Pure lead soaps have sharp characteristic absorption bands (ex. 1506, 1415  $\text{cm}^{-1}$  for neutral lead palmitate), while in paint samples the absorption region is broadened and shifted to higher wavelengths (between 1500-1600  $\text{cm}^{-1}$ ). This broadening is explained by the presence of various molecular species present in the paint which can give rise to an overlap of characteristic absorption bands or to different coordination modes of the fatty acids to the lead ion (J. Hermans et al., 2014). A summary of the characteristic absorption bands that shall be used to diagnose the state of alteration of the paint coatings of the model coupons throughout artificial aging are listed in Table IV-3.

Table IV-3 Diagnostic species for the state of alteration of paint coatings on model metal coupons and characteristic FTIR absorption bands.

State of alteration and diagnostic species	Characteristic absorption bands (cm <sup>-1</sup> ) used for diagnosis	Band Assignment <sup>1</sup>
Uncured oil paint: Triglyceride ester linkages	1746 1239, 1164, 1101	v C=O v C-O (Meilunas et al., 1990)
Uncured oil paint: Unsaturated fatty acid chains	3010 1652 722	v C-H (cis-type alkene) v C=C (cis-type alkene) C-H bending (cis-type alkene) (Meilunas et al., 1990)
Aged oil paint: Free fatty acids	3600-3000 1714, 1418	v OH v C=O, v C-O (COOH) (Maia et al., 2013; Meilunas et al., 1990)
Aged oil paint: Other oxidation products	3600-3000 1850-1600	v OH v C=O (Meilunas et al., 1990)
Aged oil paint: Metal soaps	~1550, ~1400	v <sub>as</sub> COO, v <sub>s</sub> COO (Robinet & Corbeil, 2003)
Aged oil paint: Lead soaps	1500-1600 (broad)	v <sub>as</sub> COO (J. Hermans et al., 2014)
Pure species (for reference): Lead palmitate (Pb(C <sub>16</sub> ) <sub>2</sub> )	1506, 1415	v <sub>as</sub> COO, v <sub>s</sub> COO (J. Hermans et al., 2014)

<sup>1</sup>v<sub>as</sub> = asymmetric stretch, v<sub>s</sub> = symmetric stretch

The application of conservation treatments to the painted surfaces introduces additional absorption bands into the acquired FTIR spectra.

The first treatment consists of a resin-wax mixture and is composed of 30:10 wt% Regalrez 1126:Cosmoloid H80. Regalrez 1126® (a resin) and Cosmoloid H80® (a microcrystalline wax) both contain saturated hydrocarbons (see I.II.II Remedial conservation regarding their composition) and their characteristic FTIR spectra should reflect this composition, albeit with slight differences due to their specific individual chemical structures. A previous study (Vega, 2016) measured the FTIR spectra of pure Regalrez 1126 and a microcrystalline wax independently, as well as a 4:1 wax:resin mixture of the two (Figure IV-24). The resulting spectrum of the mixture (labeled KTW5\_R2) is shown to be a combination of the spectra of the pure products, with band intensities proportional to the quantity of the components in the mixture.

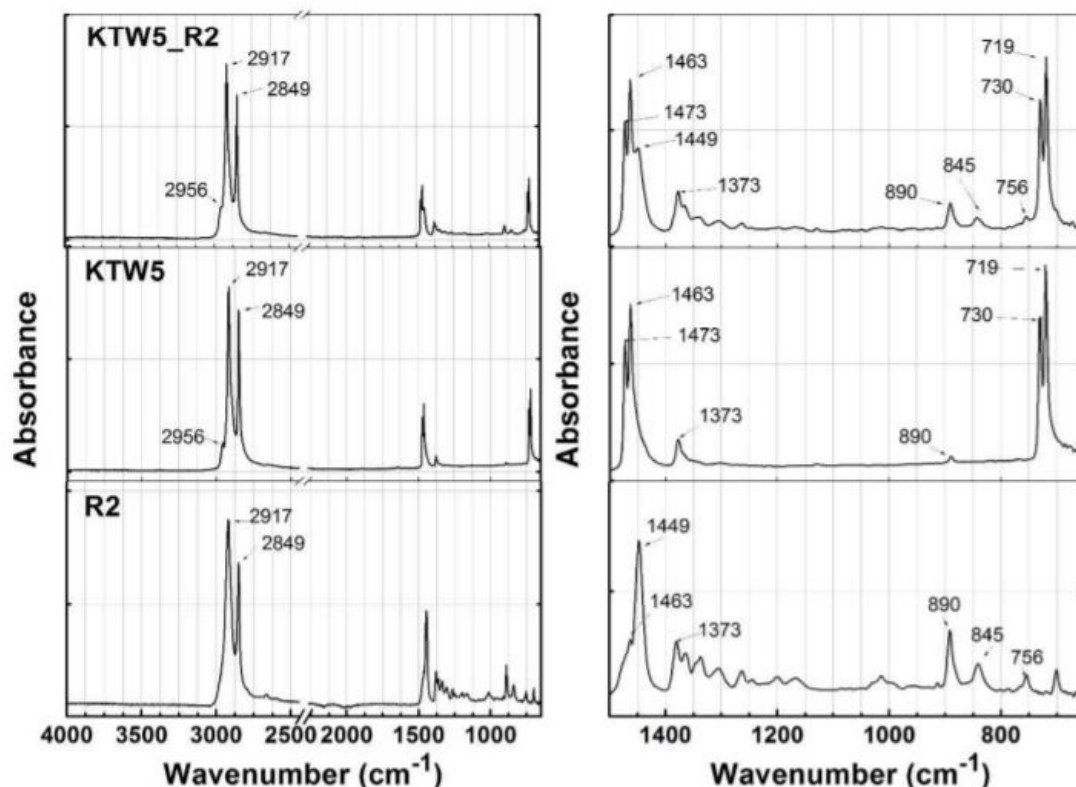


Figure IV-24 FTIR spectra of pure Regalrez 1126 (R2) resin, pure microcrystalline wax (KTW5) and a 4:1 wax:resin mixture (KTW5\_R2) (from (Vega, 2016)). The left figure shows the entire spectrum while the right figure shows a magnification of the region from 1500-650  $\text{cm}^{-1}$ .

The second conservation treatment, a 0.05 M solution of  $\text{NaC}_{14}$ , contains the sodium salt of a 14-carbon chain fatty acid. Absorption bands corresponding to the carboxylate head group and alkyl groups of the hydrocarbon chain should appear in the characteristic FTIR spectrum. Vibrational changes are expected to occur after application due to possible interactions between the applied carboxylate and the surface components. In a previous study that explored the use of carboxylic acid-based treatments as corrosion inhibitors for the conservation of iron heritage, iron carboxylates were synthesized ( $\text{FeC}_n$  with  $n = 7, 8, 10, 12,$  and  $14$ ) and characterised by FTIR spectroscopy (Hollner, 2009). The asymmetric and symmetric carboxylate stretches for iron carboxylates were observed at 1582 and 1418  $\text{cm}^{-1}$ , respectively. The bands associated to the alkyl  $\text{CH}_2$  stretching absorptions (2924 and 2852  $\text{cm}^{-1}$ ) were observed to increase in intensity with the increase in length of the alkyl chain. Other bands of interest are a series of sharp peaks (progression bands) between 1330 and 1200  $\text{cm}^{-1}$ , assigned to the bending modes of the methylene groups in the alkyl chain. The number of these bands is dependent on the length of the carbon chain; 7 bands were observed for  $\text{FeC}_{14}$ . Bands appearing in the lower wavenumber region (700-400  $\text{cm}^{-1}$ ) are assigned to the stretching and bending modes of the metal-oxygen bonds and are characteristic of the presence of Fe. The study also compared the FTIR spectra of the starting acid  $\text{HC}_{10}$ , the sodium carboxylate  $\text{NaC}_{10}$  and the iron carboxylate  $\text{FeC}_{10}$  (Figure IV-25). The wavenumber position

of the asymmetric COO stretching band (around  $1580\text{ cm}^{-1}$ ) is seen to increase slightly between the  $\text{NaC}_{10}$  spectrum and the  $\text{FeC}_{10}$  spectrum. This will be an important consideration when observing the model coupons treated with  $\text{NaC}_{14}$  in this current study.

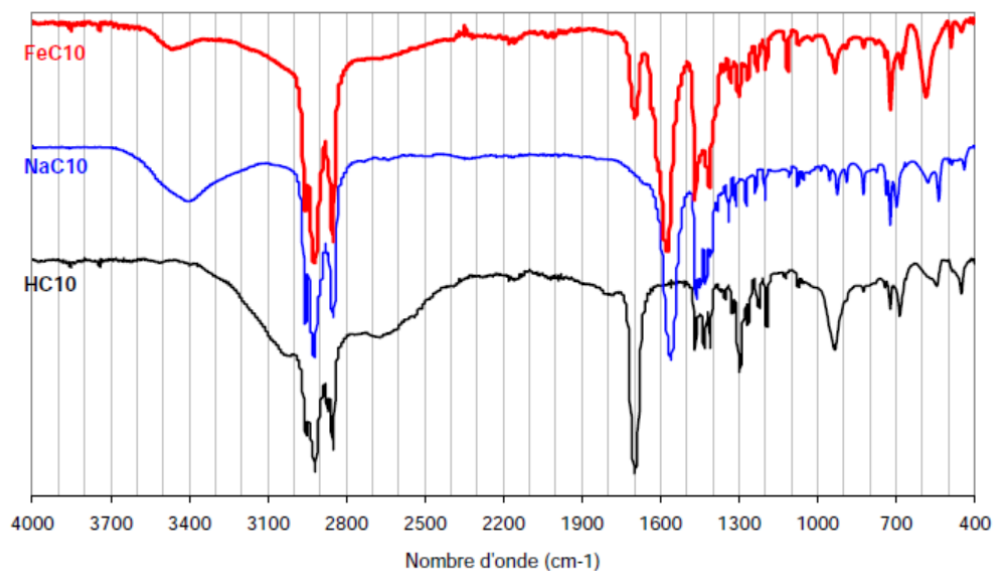


Figure IV-25 FTIR spectra of decanoic acid ( $\text{HC}_{10}$ ), sodium decanoate ( $\text{NaC}_{10}$ ) and iron decanoate ( $\text{FeC}_{10}$ ). From: (Hollner, 2009).

## IV.IV.II Reference spectra of linseed oil binder

The evolution of the reference linseed oil-coated metal coupons throughout treatment and artificial aging will not be presented systematically as many sources exist in the literature that have studied the aging processes of linseed oil (see I.I.III.ii Binder aging and degradation). The linseed oil spectra from this study will be shown when necessary in order to improve the interpretation of the evolution of the paint coating spectra. The bands of interest corresponding to the linseed oil binder as well as diagnostic vibrational changes for the aging of linseed oil are discussed in the introduction of this section (see IV.IV.I FTIR absorption bands of interest).

## IV.IV.III Reference spectra of conservation treatments

Reference FTIR spectra of the conservation treatments were acquired before and after aging. While ATR mode was used for analysis of collected samples of the dried films before aging, specular reflectance (RS) mode was used to measure the aged conservation treatments directly on the metal coupons. This choice was made primarily for the preference of analysing the material directly on the coupon without sampling or contact. Eventually, this measurement mode could also be used for non-invasive investigations of the surface of painted metal objects. However, since the quality of the FTIR-RS spectra is highly dependent on the physical aspects of the surface, testing this method on model coupons with known materials allows to investigate the applicability of the technique for different surface characteristics. In the following cases, the lack of deformation of the reflectance spectra allows for their qualitative comparison with spectra obtained in FTIR-ATR mode.

### IV.IV.III.i FTIR spectra of resin-wax (RW) mixture

During application of the conservation treatments to the model coupons, a swatch of the resin-wax mixture (30:10 wt% Regalrez 1126<sup>®</sup>:Cosmoloid H80<sup>®</sup>) was applied to a glass slide for a later analysis. A small amount of material was sampled using a scalpel and analysed by FTIR in ATR mode. The resulting spectrum is displayed in Figure IV-26.

The strongest absorption bands present in the FTIR-ATR spectrum of the resin-wax mixture are listed in Table IV-4. Vega (Vega, 2016) reported the same characteristic absorption bands for their wax-resin mixture containing microcrystalline wax and Regalrez 1126 (see Figure IV-24). In Figure IV-26, the Regalrez 1126 band at 1448 cm<sup>-1</sup> is more intense than the 1463 cm<sup>-1</sup> band of the wax and is indicative of the higher proportion of resin used in our mixture compared to that of Vega's study. Similarly, the lack of a band at 2956 cm<sup>-1</sup> (CH<sub>3</sub> stretch of microcrystalline wax) indicates a lower amount of wax present



in the mixture. The bands in the spectrum are representative of a composition containing saturated hydrocarbon features.

**Table IV-4 Vibrational assignments for the FTIR-ATR spectrum of the unaged resin-wax mixture treatment. (Assignments based on: (Maia et al., 2013; Robinet & Corbeil, 2003; Vega, 2016)).**

Wavenumber (cm <sup>-1</sup> )	Band Assignment <sup>1</sup>
2919	v <sub>as</sub> CH <sub>2</sub>
2851	v <sub>s</sub> CH <sub>2</sub>
1463	δ CH <sub>2</sub>
1448	δ CH <sub>2</sub>
1380-1180	δ CH <sub>2</sub>
892	δ CH <sub>3</sub> + v C-C
841	ρ CH <sub>2</sub> rocking?
721	ρ CH <sub>2</sub>

<sup>1</sup>v<sub>as</sub> = asymmetric stretch, v<sub>s</sub> = symmetric stretch, δ = scissoring, ρ = rocking

After aging, the resin-wax mixture was analysed by FTIR-RS directly on the metal coupon in areas without the paint or binder layer. The comparison of the spectra (Figure IV-27) shows important differences depending on the aging method. Notably, bands at 3450, 1729, 1715 and 1418 cm<sup>-1</sup> are only present in the spectrum of the resin-wax mixture aged by light exposure. The band at 3450 cm<sup>-1</sup> is associated with an O-H stretching vibration, the band at 1729 cm<sup>-1</sup> is associated with the C=O vibration, and the pair of bands at 1715 cm<sup>-1</sup> and 1418 cm<sup>-1</sup> correspond to the C=O and C-O stretches of carboxylic acids (Meilunas et al., 1990). The presence of these bands suggests the formation of photo-oxidation products containing carbonyl, carboxyl, and hydroxyl groups. Furthermore, the FTIR-RS spectrum of the resin-wax mixture aged by relative humidity cycles does not present major differences in absorption to the FTIR-ATR spectrum of the resin-wax mixture before aging (Figure IV-26). It can be concluded that the resin-wax mixture is more stable when submitted to relative humidity cycles than to light exposure.

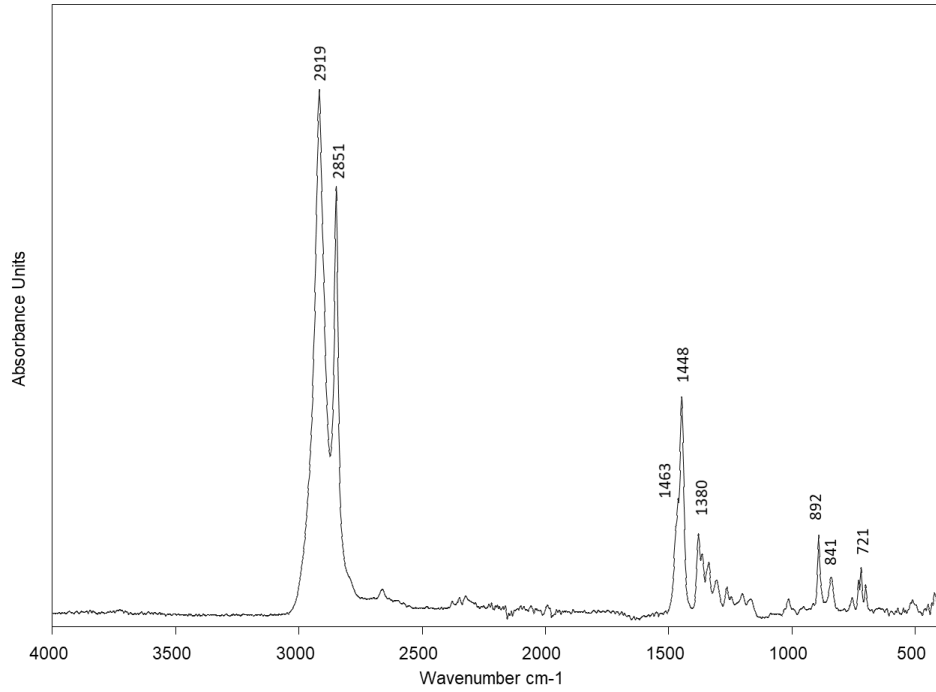


Figure IV-26 FTIR-ATR spectrum (baseline corrected) of the resin-wax mixture (30:10 wt% Regalrez 1126:Cosmoloid H80) before artificial aging.

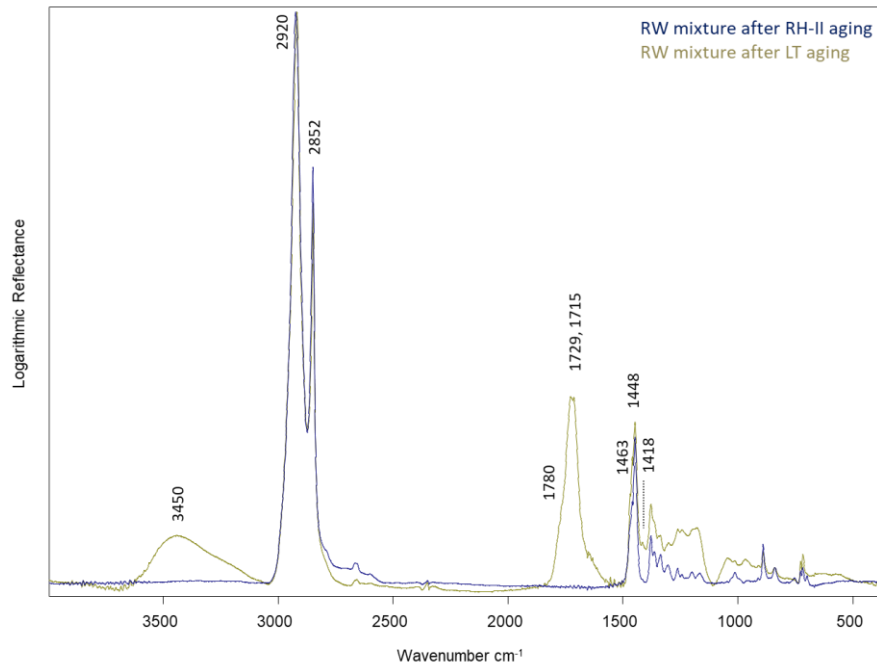


Figure IV-27 FTIR-RS representative spectra (baseline corrected) of the resin-wax (RW) mixture on bare metal after phase II of relative humidity (RH-II) aging cycles and light (LT) exposure.

#### IV.IV.III.ii FTIR spectra of corrosion inhibitor (CI)

Similarly to the reference of the resin-wax mixture, the 0.05 M solution of NaC<sub>14</sub> was applied to a glass slide and left to dry. A sample of the dry film was analysed by FTIR-ATR to obtain a reference spectrum of NaC<sub>14</sub> before aging (Figure IV-28).

The absorption bands and their assignment (Table IV-5) correspond to the expected structural features of a long-chain carboxylate molecule. The presence of strong bands at 1560 and 1423 cm<sup>-1</sup> correspond to asymmetric and symmetric COO absorptions, respectively. The intense absorption bands at 2955, 2919, 2876 and 2848 cm<sup>-1</sup> are related to the stretching vibrations of the CH<sub>3</sub> and CH<sub>2</sub> groups of the alkyl chain.

**Table IV-5 Vibrational assignments for the FTIR-ATR spectrum of the corrosion inhibitor NaC<sub>14</sub> before aging. (Assignments based on: (J. Hermans et al., 2014; Otero et al., 2014; E. L. Smith, 1992)).**

Wavenumber (cm <sup>-1</sup> )	Band Assignment <sup>1</sup>
2955	v <sub>as</sub> CH <sub>3</sub>
2919	v <sub>as</sub> CH <sub>2</sub>
2876	v <sub>s</sub> CH <sub>3</sub> ?
2848	v <sub>s</sub> CH <sub>2</sub>
1560	v <sub>as</sub> COO <sup>-</sup>
1466	δ CH <sub>2</sub>
1445	δ CH <sub>2</sub> / v <sub>s</sub> COO <sup>-</sup>
1423	v <sub>s</sub> COO <sup>-</sup>
1380	ω CH <sub>2</sub>
1380-1180	δ CH <sub>2</sub>
924	ρ CH <sub>2</sub>
725	ρ CH <sub>2</sub>
700	?

<sup>1</sup>v<sub>as</sub> = asymmetric stretch, v<sub>s</sub> = symmetric stretch, δ = scissoring, ω = wagging, ρ = rocking

After aging, FTIR-RS spectra were acquired directly on the metal coupons in areas where the corrosion inhibitor had been applied on the metal support and are displayed in Figure IV-29. While the spectrum of NaC<sub>14</sub> on coupons aged by relative humidity cycles is noisy and has a deformed baseline (probably due to the very thin layer of material analysed), some differences related to the aging method used are observed. The band at 2920 cm<sup>-1</sup> in the light-aged spectrum is slightly shifted to 2916 cm<sup>-1</sup> in the RH-aged spectrum. A decrease in intensity of the asymmetric carboxylate COO absorption band at 1570 cm<sup>-1</sup> in the RH-aged spectrum is also observed. Apart from these differences, the band positions are all the same above 1500 cm<sup>-1</sup>; below this point, the deformation of the RH-aged spectrum does not permit a comparison.

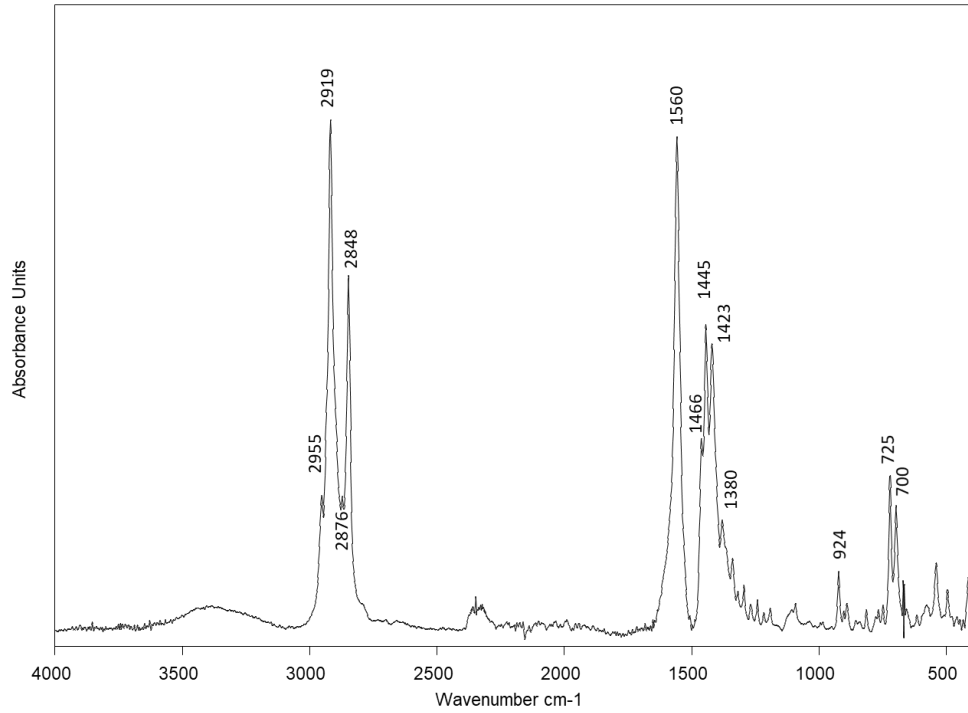


Figure IV-28 FTIR-ATR spectrum (baseline corrected) of corrosion inhibitor  $\text{NaC}_{14}$ , sampled from a film dried on a glass slide. The noise in the background is most likely related to the low quantity of sample analysed.

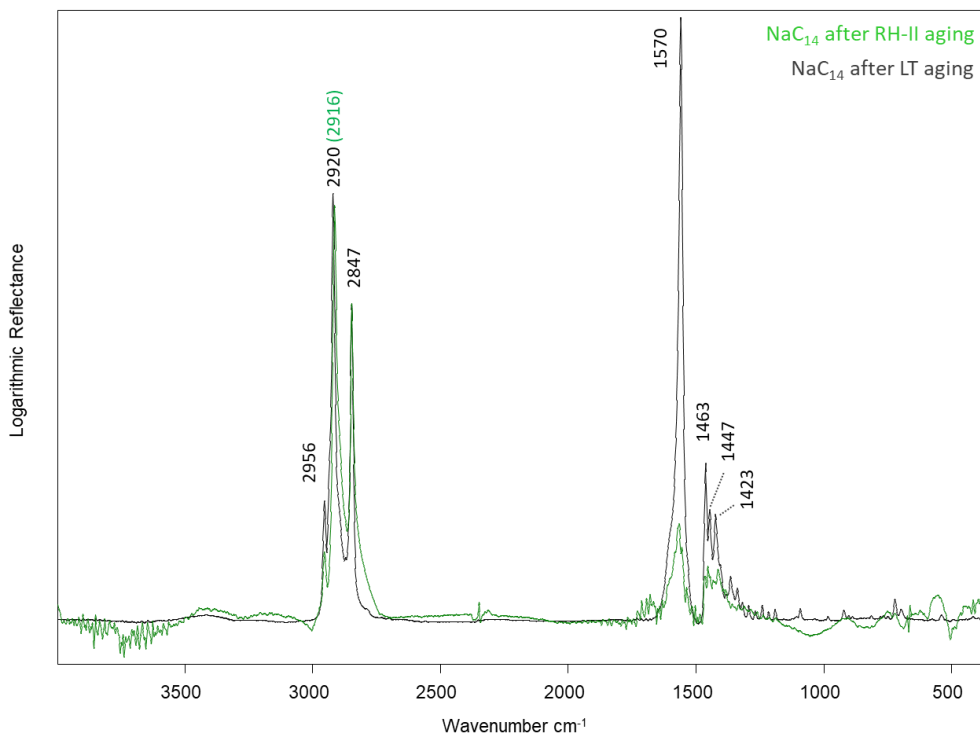


Figure IV-29 FTIR-RS spectra (baseline corrected) of corrosion inhibitor  $\text{NaC}_{14}$  applied to bare metal coupon after phase II of relative humidity (RH-II) cycles (green) or light (LT) exposure (black). The noise in the background is most likely related to the low quantity of sample analysed.

When the two FTIR-RS spectra of RH and LT aged samples are compared to the FTIR-ATR spectrum of the corrosion inhibitor before aging, some differences are also noted. For both types of aging, the asymmetric COO absorption at  $1560\text{ cm}^{-1}$  in the spectrum before aging has shifted to  $1570\text{ cm}^{-1}$  in the spectrum of the aged  $\text{NaC}_{14}$ -treated metal coupon. This shift is most likely associated to a modification of the binding interaction of the carboxylate group than to an aging effect. Indeed, when the carboxylate is applied to the iron surface, its characteristic frequency will shift due to a change in the nature of the coordinated metal ion (Palacios-Beas et al., 2004). In Hollner's study (Hollner, 2009), an increase in the frequency of the asymmetric COO stretch was also observed between the FTIR-ATR spectra of  $\text{NaC}_{10}$  and  $\text{FeC}_{10}$  (see, Figure IV-25). Moreover, the bonding between the carboxylate and the metal was studied by XAS at the Fe K edge and the metal ion was identified as the  $\text{Fe}^{3+}$  ion (Hollner, 2009). In the FTIR-RS spectrum of  $\text{NaC}_{14}$ -treated zones on coupons aged by light exposure, the ratio of intensities of the asymmetric COO stretching band ( $1570\text{ cm}^{-1}$ ) to the symmetric COO stretching band ( $1423\text{ cm}^{-1}$ ) has increased, while in the relative humidity-aged spectrum the ratio has stayed roughly the same as before aging. Finally, a decrease in the intensity of the bands at  $924$  and  $725\text{ cm}^{-1}$  ( $\text{CH}_2$  rocking deformations) is observed in the spectrum of  $\text{NaC}_{14}$  on the light-aged coupon.

### **Summary of spectral changes observed after artificial aging of the conservation treatments**

The characteristic absorption bands for the conservation treatments before and after artificial aging are listed in Table IV-6. The analysis of the resin-wax mixture revealed a mainly alkane-based composition that remains stable after aging by relative humidity cycles but shows signs of oxidation after light exposure. The comparison of the corrosion inhibitor before and after aging mainly shows differences related to the change in the coordination mode of the carboxylate complex when applied to the bare iron metal coupon; no major changes related to aging were observed.

Table IV-6 Summary of FTIR absorption bands (in  $\text{cm}^{-1}$ ) observed in spectra of conservation treatments before and after aging. Important aspects are indicated by the following: bold = formation of new band; ↓ = decrease in intensity; n.i.: not interpretable due to deformation of spectrum; - = absent in spectrum. ATR denotes spectra acquired by FTIR-ATR mode while RS refers to spectra acquired by FTIR-RS mode.

Resin-wax mixture (30:10 wt% Regalrez 1126-Cosmoloid H80)			
<i>Unaged (ATR)</i>	<i>Aged by RH cycles (RS)</i>	<i>Aged by Light (RS)</i>	<i>Assignments</i>
-	-	<b>3450</b>	$\nu$ OH
2919	2920	2920	$\nu_{\text{as}}$ CH <sub>2</sub>
2851	2852	2852	$\nu_{\text{s}}$ CH <sub>2</sub>
-	-	<b>1780 (sh)</b>	$\nu$ C=O
-	-	<b>1729</b>	$\nu$ C=O
-	-	<b>1715</b>	$\nu$ C=O (COOH)
1463	1463	1463	$\delta$ CH <sub>2</sub>
1448	1449	1449	$\delta$ CH <sub>2</sub>
-	-	<b>1418</b>	$\nu$ C-O (COOH)
1380-1180	1380-1180	1380-1180	$\delta$ CH <sub>2</sub>
892	892	892	$\delta$ CH <sub>3</sub> + $\nu$ C-C
841	841	841	$\rho$ CH <sub>2</sub> ?
721	721	721	$\rho$ CH <sub>2</sub>
Corrosion inhibitor (0.05 M solution of NaC <sub>14</sub> )			
<i>Unaged (ATR)</i>	<i>Aged by RH cycles (RS)</i>	<i>Aged by Light (RS)</i>	<i>Assignments</i>
2955	2956	2956	$\nu_{\text{as}}$ CH <sub>3</sub>
2919	2916	2920	$\nu_{\text{as}}$ CH <sub>2</sub>
2876	-	2872	$\nu_{\text{s}}$ CH <sub>3</sub> ?
2848	2847	2847	$\nu_{\text{s}}$ CH <sub>2</sub>
1560	1570	1570	$\nu_{\text{as}}$ COO <sup>-</sup>
1466	n.i.	1463	$\delta$ CH <sub>2</sub>
1445	n.i.	1447 ↓	$\delta$ CH <sub>2</sub> / $\nu_{\text{s}}$ COO <sup>-</sup>
1423	n.i.	1423 ↓	$\nu_{\text{s}}$ COO <sup>-</sup>
1380	n.i.	1382	$\omega/\delta$ CH <sub>2</sub>
1380-1180	n.i.	1380-1180	$\delta$ CH <sub>2</sub>
924	n.i.	924 ↓	$\rho$ CH <sub>2</sub>
725	n.i.	723 ↓	$\rho$ CH <sub>2</sub>
700	n.i.	700	?

## IV.IV.IV Lead white-painted metal coupons

### IV.IV.IV.i Starting materials

In Figure IV-30, the FTIR-ATR spectra of the initial lead white pigment, the fresh linseed oil reference coating and the fresh and pre-aged lead white paint coatings are shown. Note that the linseed oil and paint coatings were analysed 1.5 years after preparation, so some natural aging has already occurred.

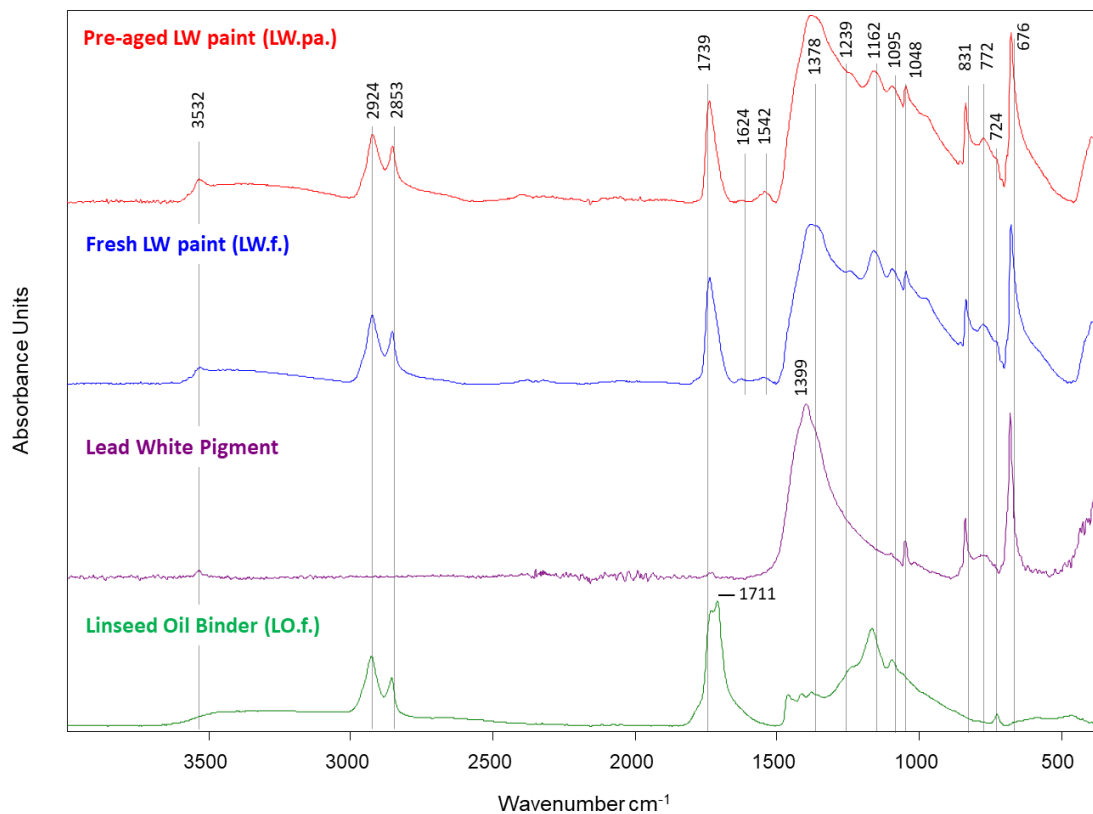


Figure IV-30 FTIR-ATR spectra of: Linseed oil coating (green); Lead white (LW) pigment reference (violet); Fresh LW paint (blue); Pre-aged LW paint (red).

The comparison of the individual spectra allows for the identification of bands originating from the binder or from the pigment, as well as which bands result from the combination of the components. The bands at 2924, 2853, 1239, 1162, 1095 and 724  $\text{cm}^{-1}$  that are present in the paint coatings correspond to the absorptions of alkyl and ester groups of the binder. The main bands associated to the lead white pigment are 1399, 1048, 831, 772 and 676  $\text{cm}^{-1}$ . The absorption at 1399  $\text{cm}^{-1}$  broadens in the paint coating spectra while the other bands remain unchanged. 676  $\text{cm}^{-1}$  was therefore selected in the following paint spectra comparisons as the normalization band. The formation of new weak bands in the paint coating spectra at 1624 and 1542  $\text{cm}^{-1}$  are assigned to the asymmetric COO stretch of metal carboxylates  $\text{M}(\text{RCOO})_n$  (B. Smith, 1998; van der Weerd et al., 2005). Specifically, the broad absorption

at 1541  $\text{cm}^{-1}$  has previously been attributed to lead carboxylates (van der Weerd 2005, Hermans et al. 2014). The symmetric COO stretch should appear around 1400  $\text{cm}^{-1}$  but is most likely masked by the large pigment absorption. The presence of these groups can be associated to the interaction of the pigment and binder upon mixing. Table IV-7 lists the characteristic vibrations for the starting materials (linseed oil and lead white pigment) as well as the fresh and pre-aged lead white paint coatings.

**Table IV-7 Absorption bands (in  $\text{cm}^{-1}$ ) and vibrational assignments for the FTIR-ATR spectra of the starting materials (linseed oil (LO) binder and lead white (LW) pigment) and the fresh and pre-aged model lead white-based paint coatings before artificial aging. FTIR spectra of the LO binder and the paint samples were acquired after 1.5 years of natural aging. (Assignments based on: (Meilunas et al., 1990; van der Weerd et al., 2005)).**

LO binder	LW pigment	Fresh LW paint (+1.5 years)	Pre-aged LW paint (+1.5 years)	Assignments <sup>1</sup>
-	3532	3532	3532	$\nu_s$ OH
2924	-	2924	2924	$\nu_{as}$ CH <sub>2</sub>
2853	-	2853	2853	$\nu_s$ CH <sub>2</sub>
1739	1736, 1730	1739	1739	$\nu_s$ C=O (ester, LW pigment)
1711	-	-	-	$\nu$ C=O (COOH)
-	-	1624	1624	$\nu$ COO <sup>-</sup>
-	-	1542	1542	$\nu_{as}$ COO <sup>-</sup>
1462	-	-	-	alkyl CH <sub>3</sub> and CH <sub>2</sub> bending
1414	-	-	-	$\nu$ C-O (COOH)
-	1399	-	-	$\nu_{as}$ CO <sub>3</sub>
-	-	1385	1385	$\nu_{as}$ CO <sub>3</sub>
1378	-	1378	1378	CH <sub>3</sub> symmetric bending
1239	-	1239	1239	$\nu$ C-O (ester)
1162	-	1162	1162	$\nu$ C-O (ester)
1095	1095	1095	1095	$\nu$ C-O (ester)
-	1048	1048	1048	$\nu_s$ CO <sub>3</sub>
-	-	976	976	<i>trans</i> C=C-H bending
-	831	831	831	Neutral PbCO <sub>3</sub>
-	772	772	772	OH bending
724	-	724	724	<i>cis</i> C=C-H bending $\rho$ CH <sub>2</sub>
-	676	676	676	$\rho$ CO <sub>3</sub>

<sup>1</sup>  $\nu_{as}$  = asymmetric stretch,  $\nu_s$  = symmetric stretch,  $\rho$  = rocking.

#### Lead white paint studied by FTIR in reflectance mode

As discussed in the section “IV.IV.III Reference spectra of conservation treatments”, the measurement of FTIR spectra in reflectance mode (RS) is an interesting application for eventual non-invasive analysis on historical painted metal objects. FTIR-RS spectra were acquired on model coupons with fresh and pre-aged lead white-based paint, as seen in Figure IV-31. The deformation of the baseline and some of the vibrational bands of the spectra is most likely due to the physical characteristics of the surface of the lead white-based paint coating, which presents an uneven surface due to large grains of pigment and could result in scattering of the incident light. This is especially seen in the zone of the CH<sub>2</sub> bands



(2960-2850  $\text{cm}^{-1}$ ) which are bands of interest for the interpretation of the evolution of the paint. The quality of the spectra obtained complicates the observation of small changes in intensity or band positions throughout the aging steps. For these reasons it was decided to only study the evolution of the model lead white paint coatings by FTIR-ATR measurements.

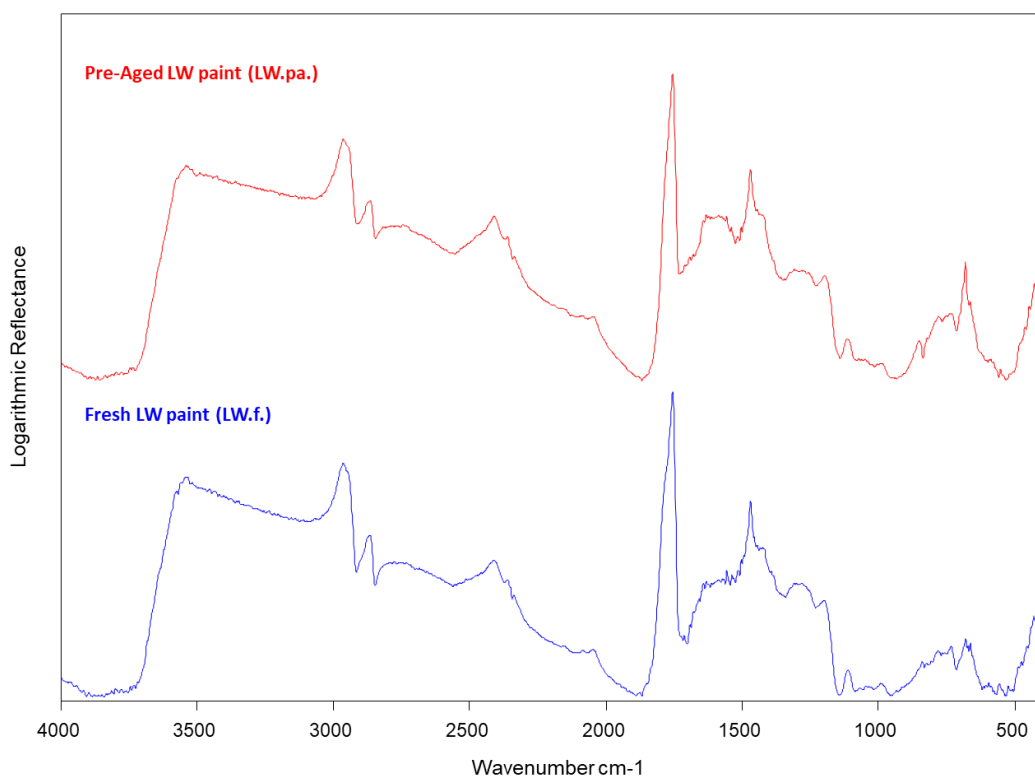


Figure IV-31 FTIR-RS spectra (baseline corrected) of lead white (LW) paint samples: Fresh LW paint (blue); Pre-aged LW paint (red).

#### IV.IV.IV.ii Fresh and pre-aged lead white-painted coupons treated with corrosion inhibitor and aged by relative humidity cycles (LW.f/pa.CI.RH)

In the following series of spectra, the lead white-painted metal coupons have been treated with the corrosion inhibitor and then undergone artificial aging by relative humidity (RH) cycles. The aged spectra were measured after Phase II of RH cycles and so have endured 9 weeks total of artificial aging. The FTIR-ATR spectra for the fresh lead white paint before aging and the untreated and corrosion inhibitor (0.05 M NaC<sub>14</sub>)-treated paint after RH aging are compared in Figure IV-32.

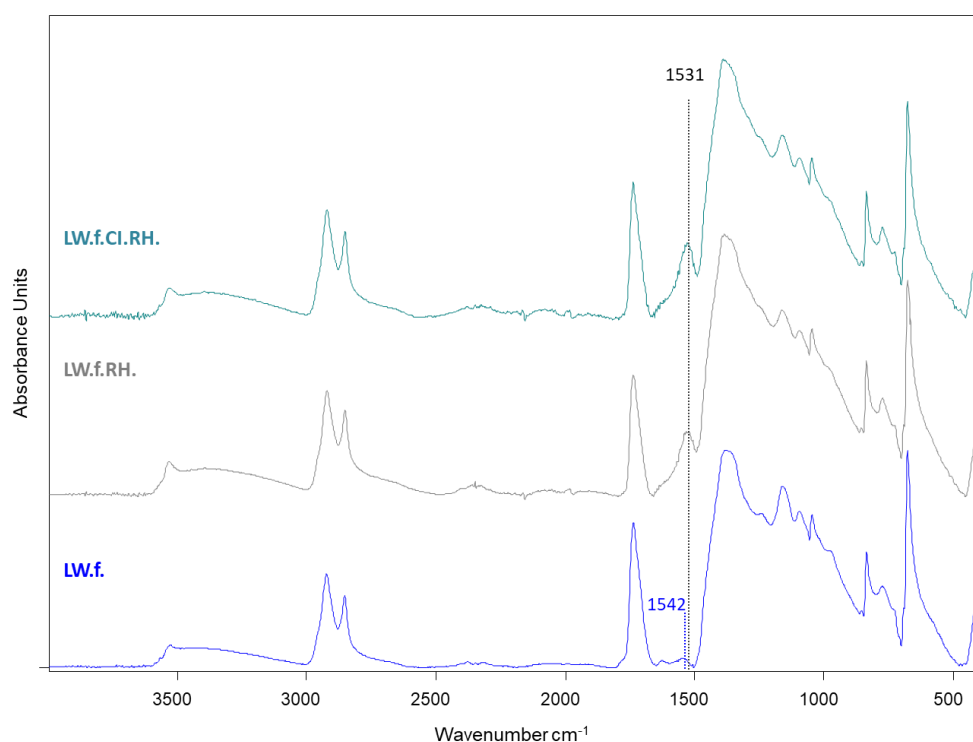
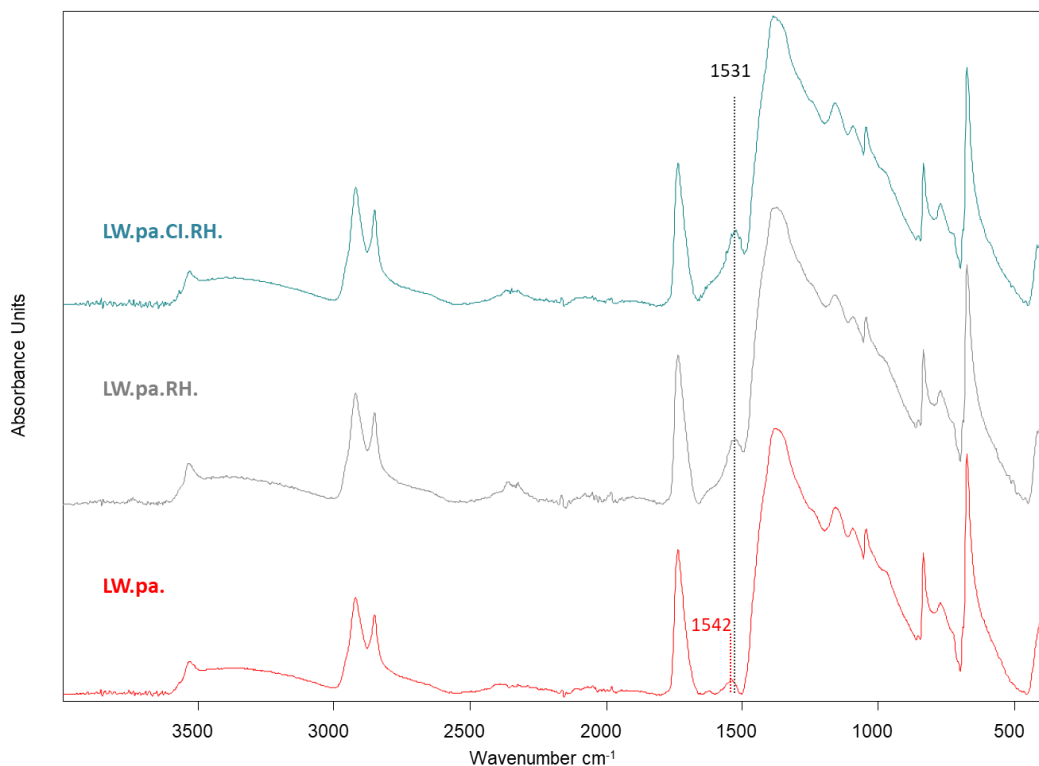


Figure IV-32 FTIR-ATR spectra (baseline corrected) of lead white (LW) paint samples, intensities normalised to LW pigment band at 676 cm<sup>-1</sup>: fresh paint (LW.f.); untreated fresh paint aged by relative humidity cycles (LW.f.RH); treated paint (Corrosion Inhibitor, CI) aged by relative humidity cycles (LW.f.CI.RH).

The major change observed in the spectra of the RH-aged lead white paint coatings is the growth and shift of the carboxylate asymmetric stretching absorption at 1542 to 1531 cm<sup>-1</sup>. This modification is observed for both the untreated and treated coatings. The shift could infer a change in the types of structures of the lead carboxylates present. In addition, the presence of the corrosion inhibitor treatment may influence the position of the carboxylate absorption band in the spectrum of the treated sample. It does not appear to be the main carboxylate species present because its characteristic carboxylate absorption at 1560 cm<sup>-1</sup> is not the maximum of the observed band. Furthermore, since there is not a significant difference in the carboxylate band positions in the spectra of the untreated and

treated samples, this does not seem to be a major process. Besides the carboxylate band, no major differences are observed.

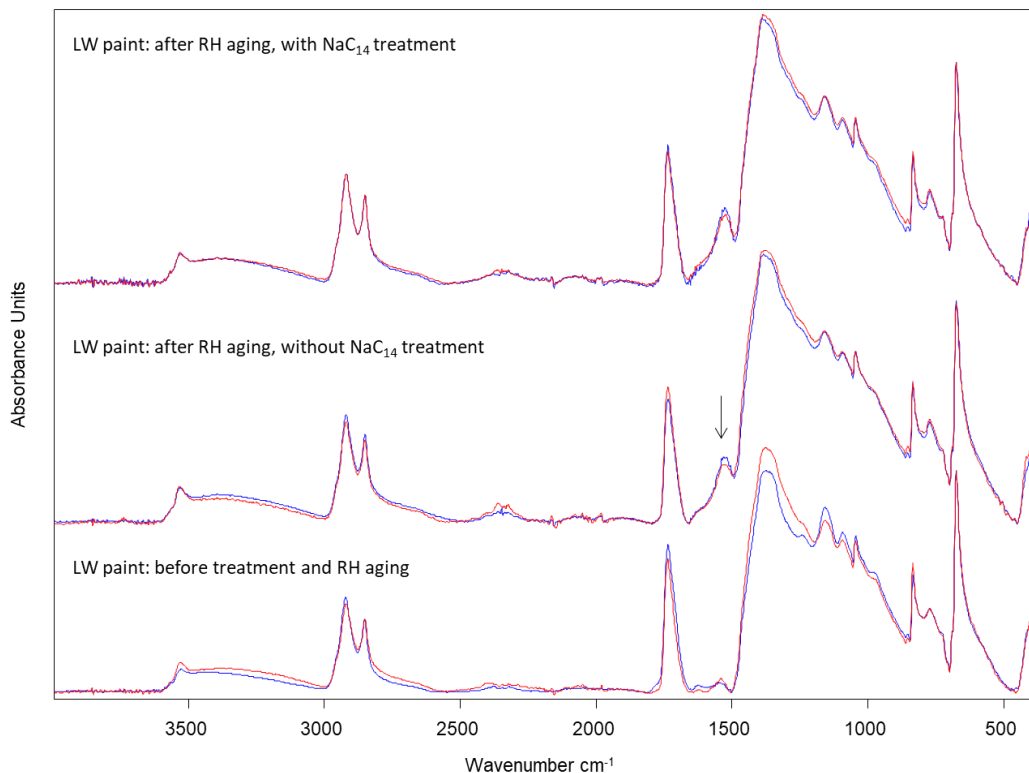
The same experimental conditions were tested on pre-aged lead white painted coupons and the FTIR-ATR spectra acquired after each step are compared in Figure IV-33.



**Figure IV-33 FTIR-ATR spectra (baseline corrected) of lead white (LW) paint samples, intensities normalised to LW pigment band at  $676\text{ cm}^{-1}$ : pre-aged paint (LW.pa.); untreated pre-aged paint aged by relative humidity cycles (LW.pa.RH); treated pre-aged paint (Corrosion Inhibitor, CI) aged by relative humidity cycles (LW.pa.Cl.RH).**

The evolution of the pre-aged lead white coating under relative humidity cycles follows the same changes as the fresh samples: notably, the shift of the maximum of the carboxylate absorption band from  $1542\text{ cm}^{-1}$  in the spectrum of the coating prior to aging to  $1531\text{ cm}^{-1}$  in the spectra obtained after aging. This was observed for both the untreated and treated areas of the aged coating. Besides the carboxylate band, no major differences are observed.

In order to compare the evolution of the fresh and pre-aged lead white paint coatings that otherwise experienced the same experimental conditions, the spectra are superimposed for each step in Figure IV-34.



**Figure IV-34 Comparison of FTIR-ATR spectra of fresh (blue) and pre-aged (red) lead white paint samples from the following steps: before treatment and artificial aging; after RH aging without NaC<sub>14</sub>; after RH aging with NaC<sub>14</sub>.**

A qualitative comparison of the spectra in each step does not show a difference in the position of the absorption bands. However, some slight differences in the intensity of certain bands are noticeable, such as the 1531 cm<sup>-1</sup> band in the spectra of the untreated aged samples, but are likely too small a change to be significant.

Overall, the results of the above comparison indicate that:

- 1) The state of the initial starting material (fresh or pre-aged) does not have a significant effect on the evolution of the paint in these experimental conditions.
- 2) The presence of the corrosion inhibitor NaC<sub>14</sub> does not delay the formation of lead soaps under the applied RH conditions, as seen by the growth and shift of the lead carboxylate absorption band at 1541 cm<sup>-1</sup> in both the treated and untreated samples.
- 3) Treatment with the corrosion inhibitor does not induce a detectable formation of reaction products in these experimental conditions.

#### IV.IV.IV.iii Fresh and pre-aged lead white-painted coupons treated with resin-wax mixture and aged by relative humidity cycles (LW.f/pa.RW.RH)

In the following series of spectra, the lead white-painted metal coupons have been treated with the resin-wax mixture and then undergone artificial aging by relative humidity (RH) cycles. The aged spectra were measured after Phase II of RH cycles and so have endured 9 weeks total of artificial aging. The FTIR-ATR spectrum for the fresh lead white paint before aging is compared to the untreated and RW-treated fresh lead white paint spectra after RH aging in Figure IV-35.

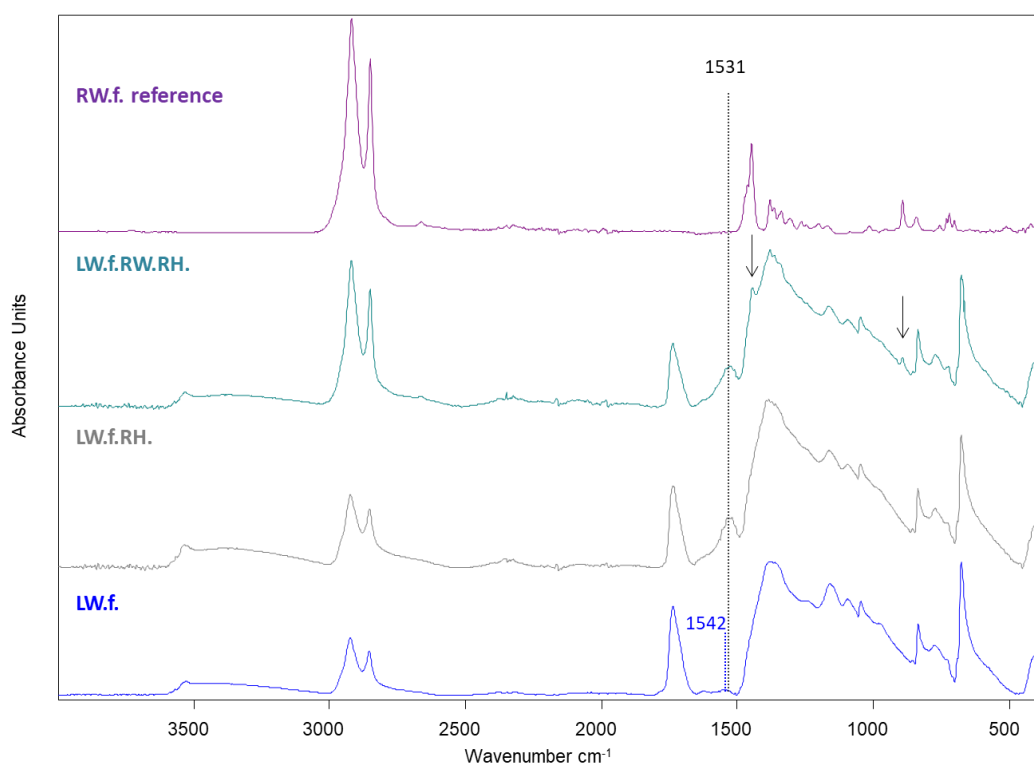


Figure IV-35 FTIR-ATR spectra (baseline corrected) of lead white (LW) paint samples, intensities normalised to LW pigment band at  $676\text{ cm}^{-1}$ : fresh paint (LW.f.); untreated fresh paint aged by relative humidity cycles (LW.f.RH); treated paint (Resin-Wax mixture, RW) aged by relative humidity cycles (LW.f.RW.RH); reference spectrum for the fresh RW mixture (RW.f.). Arrows indicate bands in the treated sample spectrum that originate from the RW spectrum.

The major change for this series of spectra is the increase and shift of the band at  $1542\text{ cm}^{-1}$  to  $1531\text{ cm}^{-1}$ , corresponding to the formation of lead carboxylates, in both the untreated and treated samples. This is the same as was seen in the previous case with the treatment using the  $\text{NaC}_{14}$  corrosion inhibitor. An increase in the  $\text{CH}_2$  bands ( $2960\text{--}2850\text{ cm}^{-1}$ ) is observed and can be attributed to the methylene groups present in the components of the RW mixture. Additionally, new bands at  $1445$  and  $895\text{ cm}^{-1}$  are present in the spectrum of the treated sample; these can be assigned to the RW mixture as well, as indicated by

the arrows from the reference spectrum in Figure IV-35. The rest of the spectrum remains relatively unchanged throughout the experimental steps.

Figure IV-36 presents the evolution of the pre-aged lead white paint under the same experimental conditions (relative humidity cycles, with or without treatment with the RW mixture).

It is reminded that whenever possible, both the external and internal faces of the collected microsample of paint coating were analysed. This was not always easy to implement as the microsample sometimes fragmented after analysis of the first face, mainly due to the applied pressure during the measurement. In this case, it is seen that despite the intention to analyse both faces, the resulting spectra do not show the expected spectral differences: the spectrum of the external face shows a more intense absorption in the region of the CH<sub>2</sub> stretching bands (as expected), but the resin-wax bands at 1445 and 895 cm<sup>-1</sup> are missing. This could be explained by either a low quantity of resin-wax treatment present on the external face of the collected microsample (which should not be the case as the surfaces were prepared as homogeneously as possible) or that fragmentation of the sample prevented a distinct analysis of the external face and that the resulting spectrum is rather a mixture of the external and internal faces of the microsample. Both spectra have been included for interest's sake.

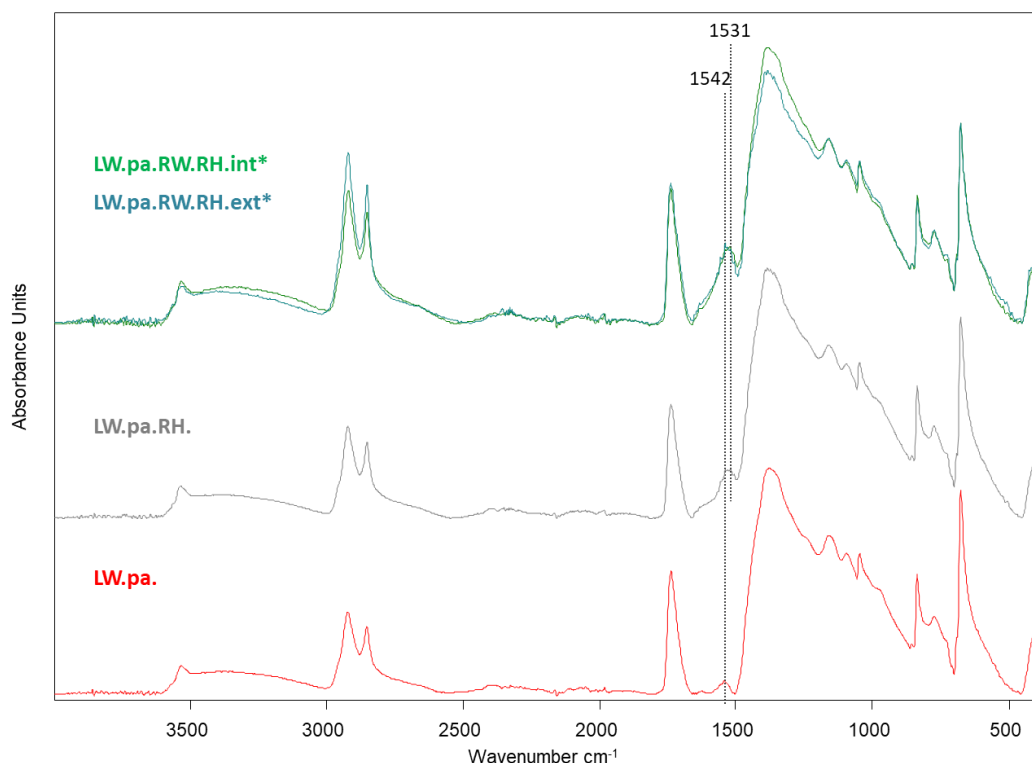
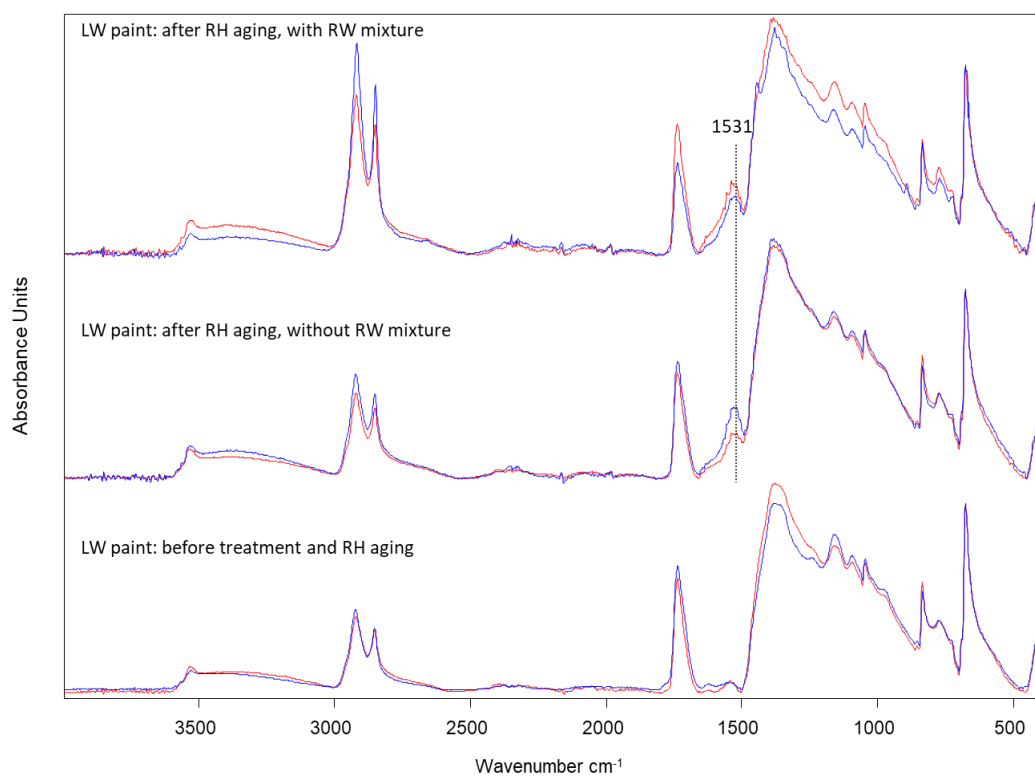


Figure IV-36 FTIR-ATR spectra (baseline corrected) of lead white (LW) paint samples, intensities normalised to LW pigment band at 676 cm<sup>-1</sup>: pre-aged paint (LW.pa.); untreated pre-aged paint aged by relative humidity cycles (LW.pa.RH); treated pre-aged paint (RW = resin-wax mixture) aged by relative humidity cycles, exterior face\* (LW.pa.RH.ext); treated pre-aged paint (RW = resin-wax mixture) aged by relative humidity cycles, interior face (LW.pa.RH.int). \*face identification uncertain.

In this series of spectra, the lead carboxylate band remains centered at  $1542\text{ cm}^{-1}$  as it increases in the aged samples, contrarily to the previous cases where a shift of the band maximum was observed. The band at  $1531\text{ cm}^{-1}$  seen in the previous cases forms as well. This could indicate the presence of two major lead carboxylate species in equal proportion. The rest of the spectrum remains relatively unchanged throughout the experimental steps.

In order to compare the evolution of the fresh and pre-aged lead white paint coatings that otherwise experienced the same experimental conditions, the spectra are superimposed for each step in Figure IV-37.



**Figure IV-37 Comparison of spectra of fresh (blue) and pre-aged (red) lead white samples through the following steps: before treatment and artificial aging; after RH aging without RW treatment; after RH aging with RW treatment.**

A qualitative comparison of the spectra in each step does not show a difference in absorption bands. Some differences in the intensity of certain bands are noticeable, such as the  $1531\text{ cm}^{-1}$  band for the aged coatings without treatment. The fresh spectrum (blue) shows a more intense absorption at this position than the pre-aged spectrum (red). This suggests that more lead carboxylates formed during aging in the fresh paint than in the pre-aged paint. The observed variations in intensity in the spectra of the treated and aged coatings are related to both the presence of the RW mixture and possibly to slight variations in the pigment:binder ratio of the analysed samples.

The evolution of the lead white paint coating aged by RH cycles in the presence or not of the RW mixture is briefly summarized by the following points:

- 1) The initial state of the paint coating (fresh or pre-aged) may influence the amount of lead soaps formed after the artificial aging, as observed by the more intense carboxylate band in the spectrum of the fresh untreated RH-aged paint coating compared to the equivalent spectrum for the pre-aged paint.
- 2) The presence of the RW mixture does not delay the formation of lead soaps under the applied RH conditions, as seen by the growth and shift of the lead carboxylate absorption band at  $1541\text{ cm}^{-1}$  in both the treated and untreated samples.
- 3) Treatment with the RW mixture does not induce a detectable formation of reaction products with the paint coating under these experimental conditions.

#### **IV.IV.IV.iv Fresh and pre-aged lead white-painted coupons treated with corrosion inhibitor and aged by light exposure (LW.f/pa.CI.LT)**

The FTIR-ATR spectra for the fresh lead white paint before aging, after light aging without treatment, and after light aging with the corrosion inhibitor (0.05 M NaC<sub>14</sub>) treatment are compared in Figure IV-38.



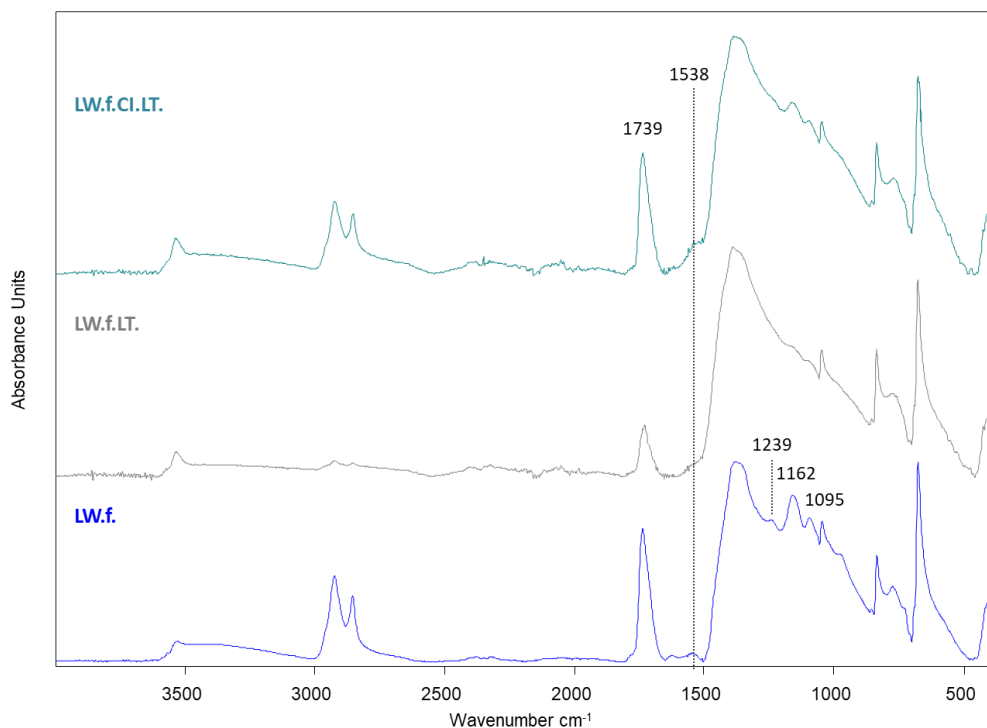


Figure IV-38 FTIR-ATR spectra (baseline corrected) of lead white (LW) paint samples, intensities normalised to LW pigment band at  $676\text{ cm}^{-1}$ : fresh paint (LW.f.); untreated fresh paint aged by light exposure (LW.f.LT.); treated paint (Corrosion Inhibitor, CI) aged by light exposure (LW.f.CI.LT.).

A major loss of absorption bands related to the organic components of the paint is observed in the spectrum of the untreated light-aged sample, including the  $\text{CH}_2$  bands ( $2960\text{--}2850\text{ cm}^{-1}$ ) and the carbonyl and ester stretches of the triglyceride structure ( $1739$  and  $1239, 1162, 1095\text{ cm}^{-1}$ , respectively). The remaining bands are mainly associated to the lead white pigment. The organic bands have been retained in the treated sample, although the intensity of the ester bands have decreased. An increase in the lead carboxylate band is seen at  $1538\text{ cm}^{-1}$  for both the untreated and treated aged samples, although to a lesser extent than seen in the samples aged by RH cycles.

The same experimental conditions were tested on a pre-aged lead white paint coating; the FTIR-ATR spectra acquired throughout the testing are compared in Figure IV-39.

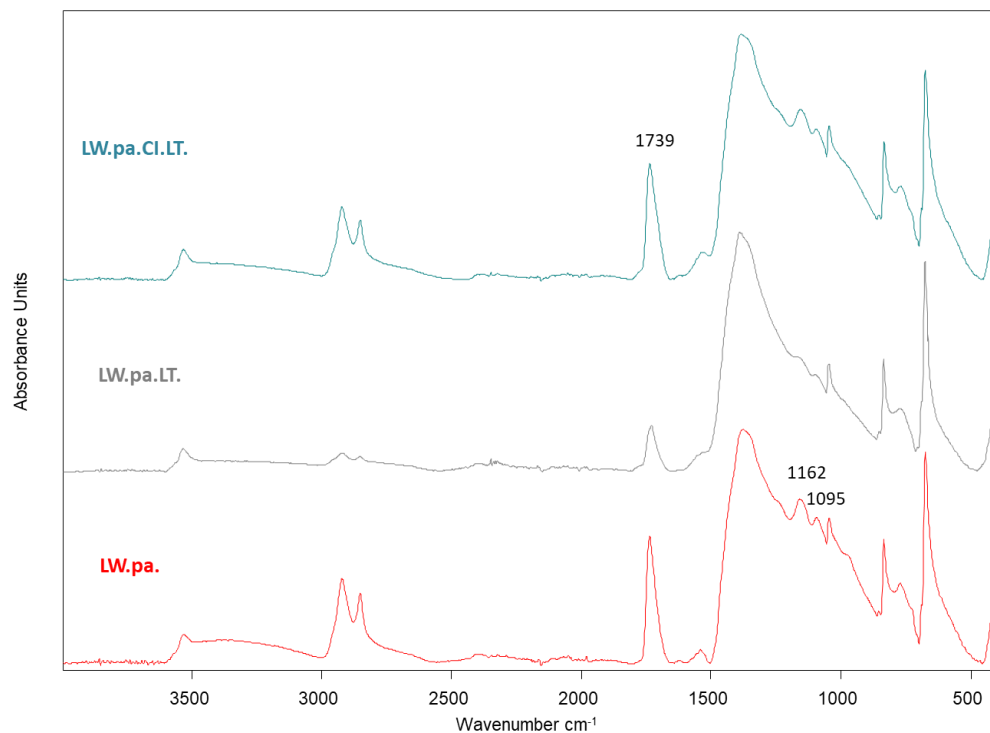
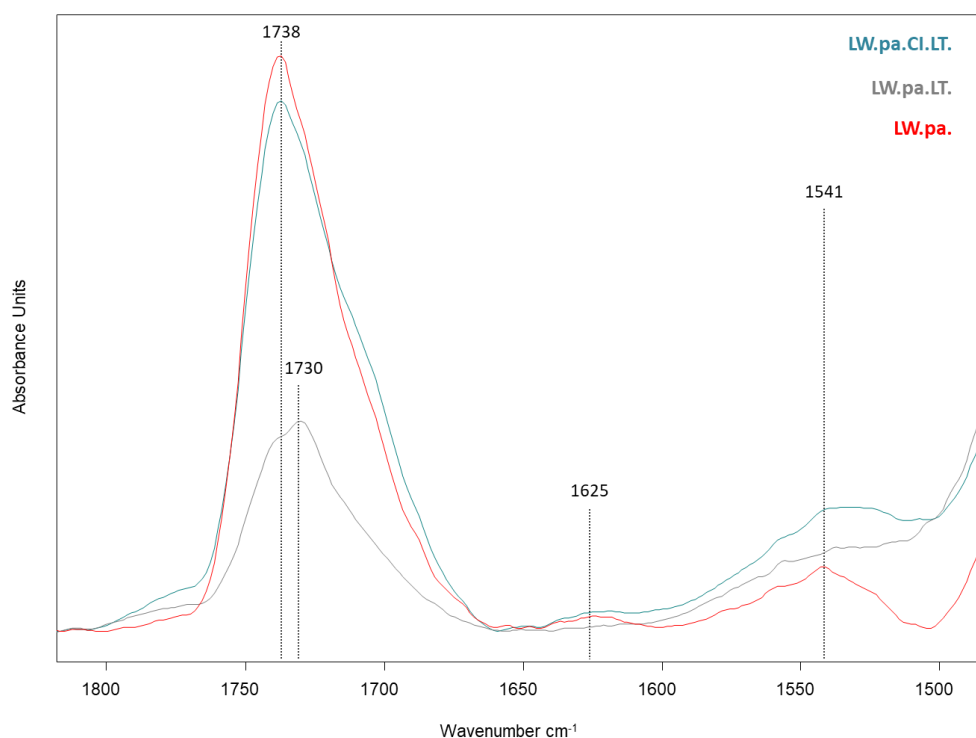


Figure IV-39 FTIR-ATR spectra (baseline corrected) of lead white (LW) paint samples, intensities normalised to LW pigment band at 676 cm<sup>-1</sup>: pre-aged paint (LW.pa.); untreated pre-aged paint aged by light exposure (LW.pa.LT.); treated pre-aged paint (Corrosion Inhibitor, CI) aged by light exposure (LW.pa.CI.LT.).

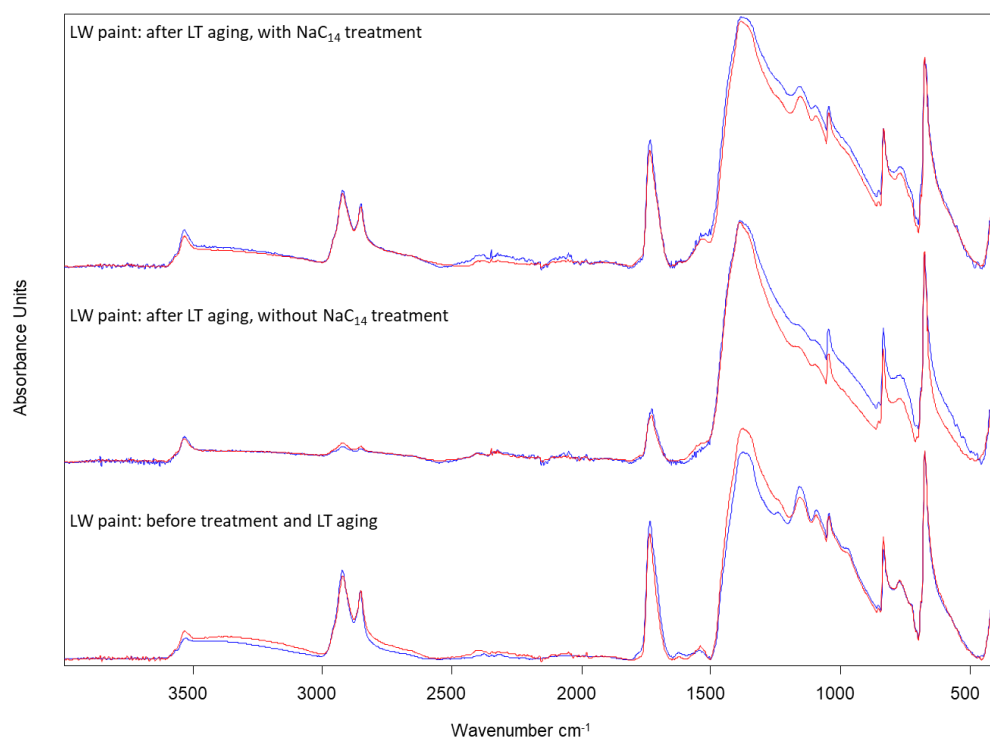
The same loss of organic absorption bands in the spectrum corresponding to the untreated and light-aged lead white paint coating as was seen in the fresh paint case is observed. The organic features have been retained in the spectrum corresponding to the corrosion inhibitor-treated zone. A magnification of the 1810-1480 cm<sup>-1</sup> region in Figure IV-40 compares the changes in the carbonyl and carboxylate absorption bands.



**Figure IV-40 Magnification of the spectral region of 1810-1480  $\text{cm}^{-1}$  from Figure IV-39. Pre-aged paint (LW.pa.); untreated pre-aged paint aged by light exposure (LW.pa.LT.); treated pre-aged paint (Corrosion Inhibitor, CI) aged by light exposure (LW.pa.CI.LT.).**

The comparison of the spectra in this region clearly shows that the corrosion inhibitor-treated paint coating retains a similar absorption behaviour after light aging to the initial pre-aged paint coating before aging, while the spectrum of the untreated light-aged paint coating shows loss of structural aspects. In the spectrum of the untreated aged coating (LW.pa.LT), the band at  $1625 \text{ cm}^{-1}$  has disappeared and the band at  $1541 \text{ cm}^{-1}$  has broadened into a shoulder of the large carbonate absorption starting at  $1490 \text{ cm}^{-1}$ . In the spectrum of the treated and aged coating (LW.pa.CI.LT), the bands at  $1625 \text{ cm}^{-1}$  and  $1541 \text{ cm}^{-1}$  have been retained, although the  $1541 \text{ cm}^{-1}$  band also shows some broadening. This increase in absorption between  $1540\text{-}1500 \text{ cm}^{-1}$ , the absorption range for the asymmetric COO stretch of lead carboxylates, suggests the formation of new carboxylate species after light exposure. The carbonyl band at  $1738 \text{ cm}^{-1}$  in the spectrum of the treated and aged paint coating (LW.pa.CI.LT), corresponding to the C=O stretch of esters, has kept the same position and intensity throughout aging, while the carbonyl band in the spectrum of the untreated and aged sample (LW.pa.LT) has lowered in intensity and furthermore shows a shift towards  $1730 \text{ cm}^{-1}$ . The band at  $1730 \text{ cm}^{-1}$  is most likely directly related to the characteristic C=O stretch of the lead white pigment; the disappearance of the ester C=O stretch at  $1738 \text{ cm}^{-1}$  confirms that much of the organic content of the untreated and aged sample has been degraded.

The evolution of the fresh and pre-aged samples under the same experimental conditions is compared by superimposing the spectra from equivalent steps of aging in Figure IV-41.



**Figure IV-41 Comparison of FTIR-ATR spectra of fresh (blue) and pre-aged (red) lead white (LW) paint samples through the following steps: before treatment and artificial aging; after light (LT) aging without NaC<sub>14</sub>; after LT aging with NaC<sub>14</sub>.**

A qualitative comparison of the spectra in each step does not show a difference in absorption bands. Some differences in intensity are observed between the spectra of the fresh and pre-aged lead white paint coatings that are most likely due to differences in the pigment to binder ratios of the analysed paint samples. It can be concluded that the initial state of the paint does not influence the subsequent evolution of the paint when treated with the corrosion inhibitor NaC<sub>14</sub> and submitted to light exposure aging.

The evolution of the lead white paint coating treated with the NaC<sub>14</sub> corrosion inhibitor and aged by light exposure is briefly summarized by the following points:

- 1) The state of the initial starting material (fresh or pre-aged) does not have a significant effect on the evolution of the paint in these experimental conditions.
- 2) Light aging of the untreated lead white-based paint shows significant degradation of the organic content, but an increase in absorption in the zone characteristic of lead carboxylates is observed (shoulder between 1540-1500 cm<sup>-1</sup>). The same shoulder is observed in the treated sample spectrum.

- 3) The absorption bands of the organic functional groups ( $\text{CH}_2$ ,  $\text{C}=\text{O}$  and  $\text{C}-\text{O}$  of esters) are more retained in the sample treated with  $\text{NaC}_{14}$  than in the untreated sample.
- 4) Treatment with  $\text{NaC}_{14}$  followed by light aging does not induce a detectable formation of reaction products in these experimental conditions.

#### **IV.IV.IV.v Fresh and pre-aged lead white painted coupons treated with resin-wax mixture and aged by light exposure (LW.f/pa.RW.LT)**

The FTIR-ATR spectra for the fresh lead white paint before aging, untreated fresh lead white paint after light aging, and resin-wax (RW)-treated fresh lead white paint after light aging are compared in Figure IV-42.

Both the external and internal faces of the sample collected in the treated zone were analysed. The acquired spectra are not equivalent: this can be attributed mainly to the presence of the resin-wax treatment on the external face, but also to a possibly different state of alteration. In fact, the spectrum of the internal face is very similar to the spectrum of the lead white paint before aging (LW.f.). This suggests that the organic structure of the paint at the paint-metal interface did not degrade to the same extent as the untreated sample. This is particularly apparent in the  $\text{C}-\text{H}$  ( $2960\text{-}2850\text{ cm}^{-1}$ ) and  $\text{C}=\text{O}$  regions ( $1780\text{-}1700\text{ cm}^{-1}$ ) where the intensities of these bands have greatly reduced in the spectrum of the untreated sample. However, it is difficult to determine the extent of degradation of the paint on the external face due to overlap of the  $\text{C}-\text{H}$  and  $\text{C}=\text{O}$  absorption bands by the bands belonging to the resin-wax mixture. In the region of the  $\text{C}-\text{O}$  ester stretches ( $1164, 1101\text{ cm}^{-1}$ ), the relative intensities of the bands are seen to be better retained in the spectra of the treated sample (both external and internal faces) than in the untreated sample, suggesting that the external and internal faces may have a similar state of alteration.

It is observed that the lead carboxylate absorption maximum of  $1541\text{ cm}^{-1}$  has been retained in both the untreated and treated samples, but that absorption has also increased between  $1540\text{-}1500\text{ cm}^{-1}$ . As mentioned before, this suggests the formation of new carboxylate species. The presence of the resin-wax treatment does not appear to influence the changes observed in this region.

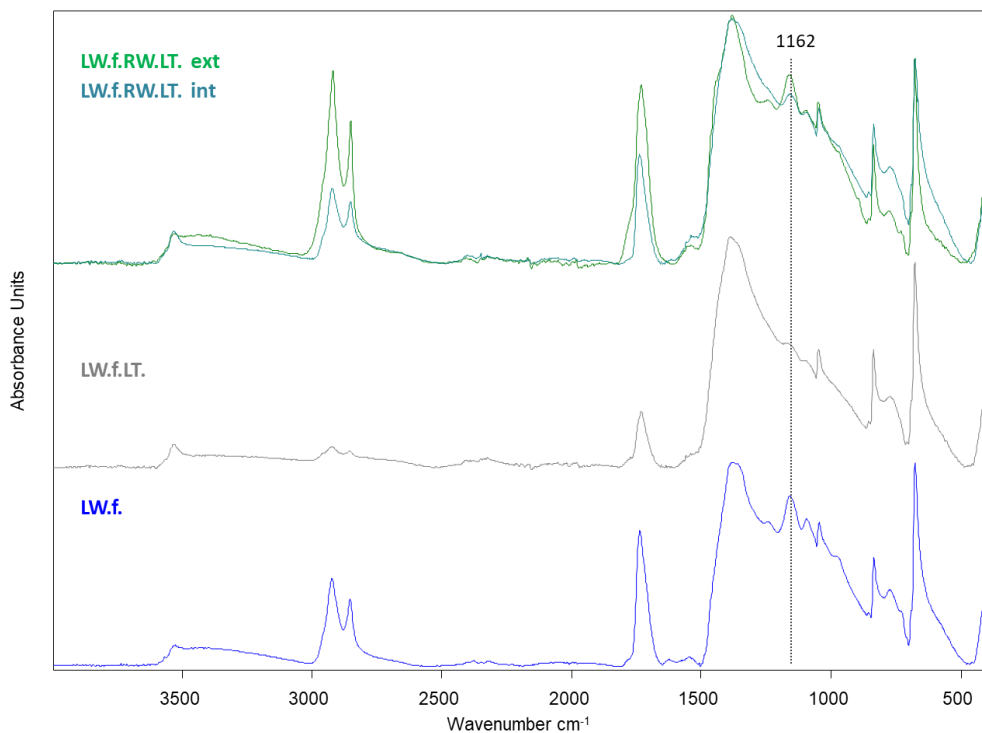


Figure IV-42 FTIR-ATR spectra (baseline corrected) of lead white (LW) paint samples, intensities normalised to LW pigment band at  $676\text{ cm}^{-1}$ : fresh paint (LW.f.); untreated fresh paint aged by light exposure (LW.f.LT.); treated (RW = resin-wax mixture) fresh paint aged by light exposure, *interior face* of microsample (LW.f.RW.LT. int); treated fresh paint aged by light exposure, *exterior face* of microsample (LW.f.RW.LT. ext).

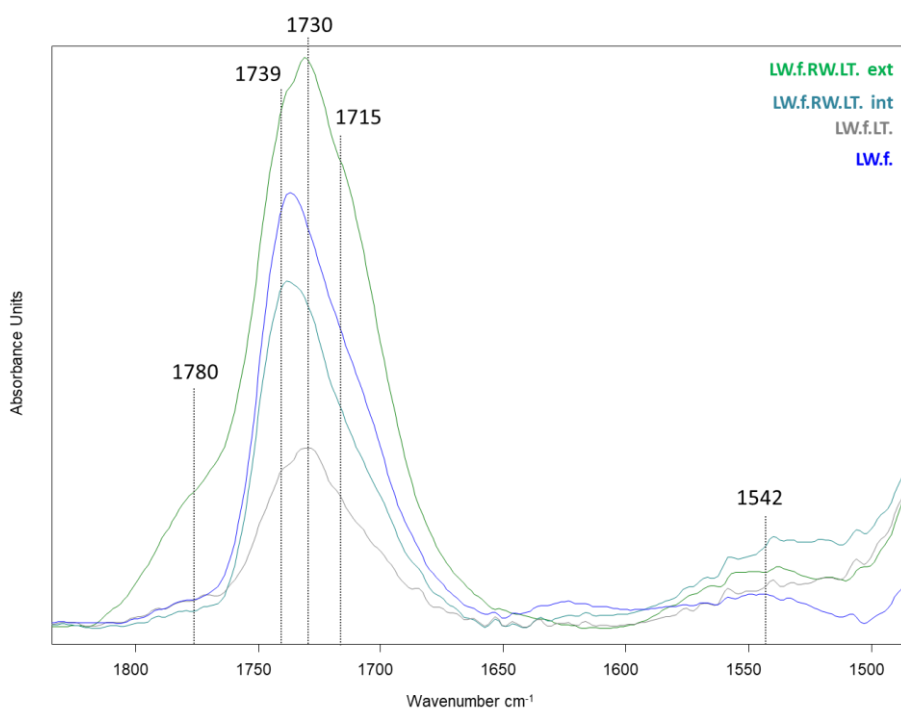


Figure IV-43 Magnification of the spectral region of  $1830\text{--}1480\text{ cm}^{-1}$  from Figure IV-42. Fresh paint (LW.f.); untreated fresh paint aged by light exposure (LW.f.LT.); treated fresh paint (RW = resin-wax mixture) aged by light exposure, *interior face* of microsample (LW.f.RW.LT. int); treated fresh paint aged by light exposure, *exterior face* of microsample (LW.f.RW.LT. ext).

Looking more closely at the region from 1830-1480  $\text{cm}^{-1}$  (Figure IV-43) reveals some variations in the absorption spectra of the different samples. The carbonyl absorption band between 1780-1700  $\text{cm}^{-1}$  shows some differences between the measured samples. The band at 1739  $\text{cm}^{-1}$  present in the fresh paint sample (LW.f.) is retained after light aging in the spectra of the treated samples (LW.f.RW.LT. int and ext) while the band for the untreated sample (LW.f.LT.) has decreased at 1739  $\text{cm}^{-1}$  and increased at 1730  $\text{cm}^{-1}$ . The form of the latter spectrum resembles that of the C=O absorption bands of the pure lead white pigment. This agrees with the previous statements that much of the organic binder structure of the paint was lost during the light exposure and that the remaining paint has a higher proportion of pigment than in its initial state. The spectrum of the exterior face of the treated sample (LW.f.RW.LT.ext) contains a larger band at 1730  $\text{cm}^{-1}$  and shoulders 1780 and 1715  $\text{cm}^{-1}$  that are not present on the sample of the interior face; these bands correspond to the absorption band at 1780/1729/1715  $\text{cm}^{-1}$  that was observed to form in the sample of pure resin-wax mixture aged by light exposure (see Figure IV-27).

The FTIR-ATR spectra for the pre-aged lead white paint before and after light aging, with or without the resin-wax treatment, are compared in Figure IV-44. It was only possible to analyse one face of the treated sample, which was the internal face. Therefore, the characteristic RW bands at 1448 and 892  $\text{cm}^{-1}$  and increased intensity of the  $\text{CH}_2$  bands are not present in the spectrum of the treated sample. Similarly to the previous examples, a decrease in the intensity of the organic absorption bands after light exposure is observed, but less so in the treated sample than in the untreated sample. Additionally, a shoulder at 1780  $\text{cm}^{-1}$  forms in the spectra of both the untreated and treated samples. A shift of the carbonyl band from 1739 to 1730  $\text{cm}^{-1}$  is observed for both the untreated and treated samples after aging; this is shown more closely in Figure IV-45.

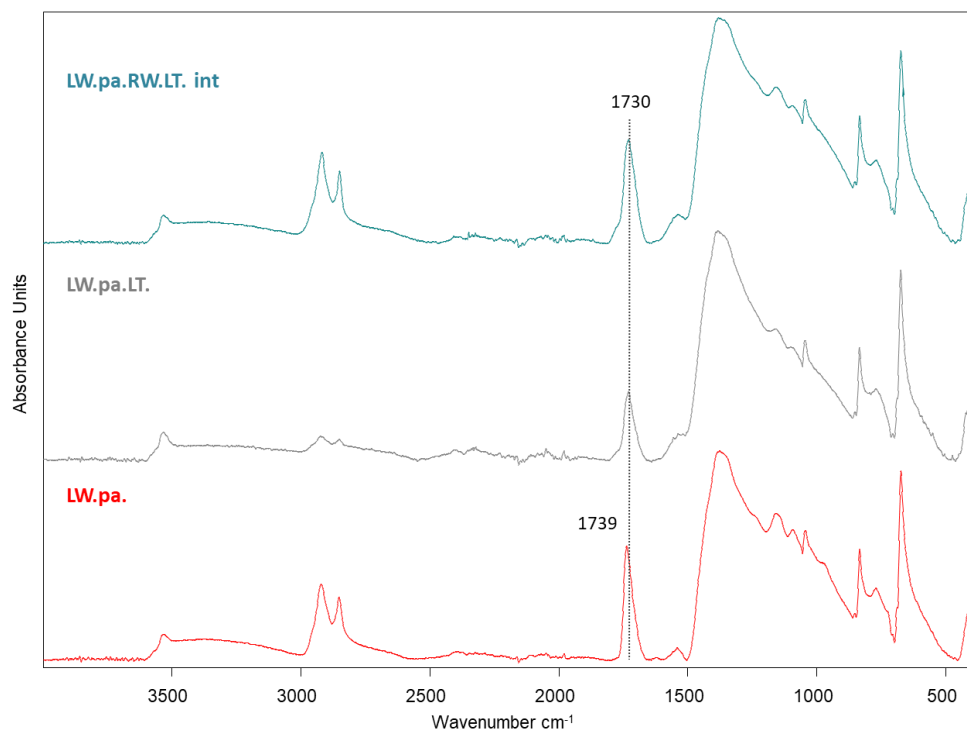
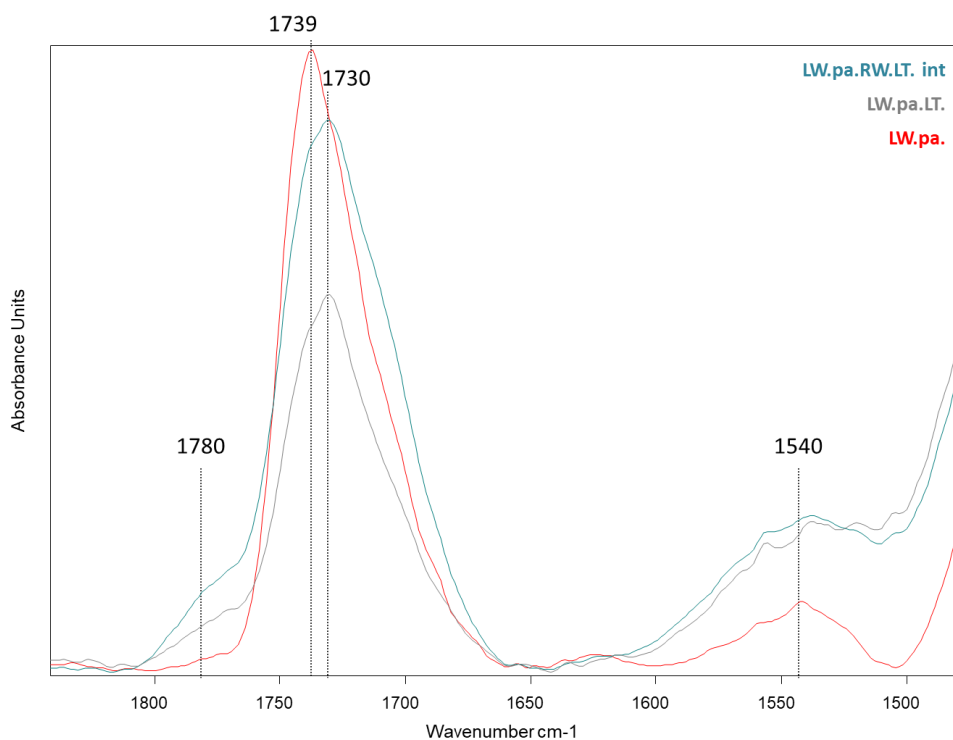


Figure IV-44 FTIR-ATR spectra (baseline corrected) of lead white (LW) paint samples, intensities normalised to LW pigment band at 676 cm<sup>-1</sup>: pre-aged paint (LW.pa.); untreated pre-aged paint aged by light exposure (LW.pa.LT.); treated pre-aged paint (RW = resin-wax mixture) aged by light exposure, *internal face* of microsample (LW.pa.RW.LT. int).

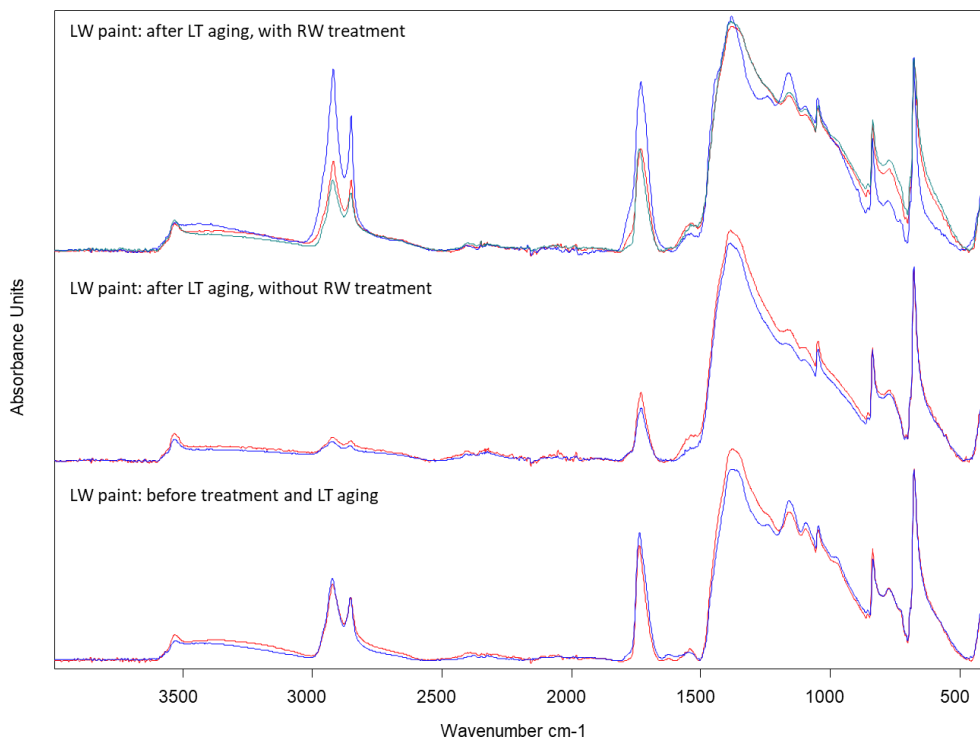




**Figure IV-45** Magnification from Figure IV-44 of the spectral region of 1900-1500  $\text{cm}^{-1}$ . Pre-aged paint (LW.pa.); untreated pre-aged paint aged by light exposure (LW.pa.LT.); treated pre-aged paint (RW = resin-wax mixture) aged by light exposure, *internal face* of microsample (LW.pa.RW.LT. int).

The maximum at 1739  $\text{cm}^{-1}$  for the pre-aged paint sample is present as a shoulder in the untreated and treated aged sample spectra, along with new bands at 1780 and 1730  $\text{cm}^{-1}$ . The presence of the shoulder at 1780  $\text{cm}^{-1}$  in both the untreated and treated samples could suggest the formation of other carbonyl compounds after light exposure. The band at 1730  $\text{cm}^{-1}$  in the treated sample spectrum may be assigned to general formation of carbonyl-containing products, but also to a greater proportion of pigment to binder in the paint composition due to degradation of the organic material by light exposure. It appears to be in a medium state of alteration between the initial material (LW.pa.) and the highly altered state of the untreated and aged paint (LW.pa.LT.). As in the previous light-aged cases, the lead carboxylate band has been retained at 1540  $\text{cm}^{-1}$  regardless of treatment and shows an increase in absorption between 1540-1500  $\text{cm}^{-1}$ .

In order to compare the evolution of the fresh and pre-aged samples that otherwise experienced the same experimental conditions, the spectra are superimposed for each step in Figure IV-46.



**Figure IV-46 Comparison of FTIR-ATR spectra of fresh (blue, turquoise) and pre-aged (red) lead white (LW) paint samples through the following steps: before treatment and artificial aging; after LT aging without RW mixture; after LT aging with RW mixture (turquoise spectrum = internal face of LW.f.RW.LT sample).**

A qualitative comparison of the fresh and pre-aged spectra in each step does not show a difference in absorption bands, although some variations in intensity are observed. In the untreated sample spectra, the variations are more likely linked to differences in the pigment:binder ratio of the analysed samples. In the treated sample spectra, the observed differences are linked to which face of the microsample was analysed. Overall, it can be concluded that the initial state of the paint does not influence the subsequent evolution of the paint when treated with the resin-wax mixture and submitted to light exposure aging.

The evolution of the lead white paint coating treated with the resin-wax mixture and aged by light exposure is briefly summarized by the following points:

- 1) The state of the initial starting material (fresh or pre-aged) does not have a significant effect on the evolution of the paint in these experimental conditions.
- 2) Light aging of the untreated lead white-based paint coating shows significant degradation of the organic content.
- 3) The intensities of the absorption bands of the organic functional groups ( $\text{CH}_2$ ,  $\text{C}=\text{O}$  and  $\text{C}-\text{O}$  of esters) are more retained in the spectra of the interior face of the treated samples. Determination of the state of alteration of the paint on the exterior face (in contact with the

resin-wax mixture) is difficult due to overlap of diagnostic bands by the spectrum of the resin-wax treatment.

- 4) The formation of a shoulder at  $1780\text{ cm}^{-1}$  and a strong band at  $1730\text{ cm}^{-1}$  in the treated sample spectra are associated to the degradation of the RW mixture in the case when the exterior face of the paint coating sample was analysed. When the interior face was analysed, these bands correspond to the formation of carbonyl-containing products within the paint system.

## IV.IV.V Chrome green oxide-painted metal coupons

### IV.IV.V.i Starting materials

#### Chrome green oxide pigment

Figure IV-47 displays the FTIR spectrum obtained in ATR mode for the chrome green oxide pigment. It contains characteristic absorption bands at 608, 525, 441 and 409  $\text{cm}^{-1}$ . This is consistent with the reference spectrum reported in the literature, except for the band at 525  $\text{cm}^{-1}$  which was reported at 504  $\text{cm}^{-1}$  (Vahur et al., 2016). The baseline is quite intense in the region from 700-400  $\text{cm}^{-1}$ .

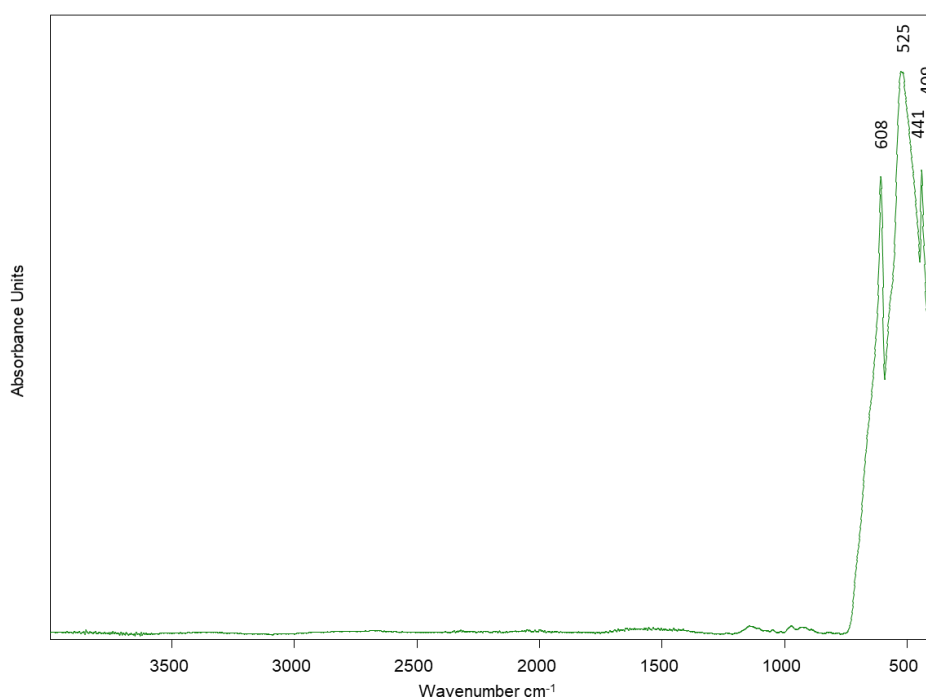


Figure IV-47 FTIR-ATR spectrum (baseline corrected) of chrome green oxide pigment (Kremer).

#### Chrome green oxide-based paint: ATR vs reflectance modes

The fresh chrome green oxide (CrGO)-based paint coating was analysed in both ATR and reflectance modes and the spectra are shown in Figure IV-48. Note that the spectra were acquired 1.5 years after preparation of the model coupons so some natural aging had already occurred. In the FTIR-ATR spectrum the baseline and vibrational bands are partly deformed while the FTIR-RS spectrum presents the expected spectral shape (Figure IV-48). The deformation of the ATR spectrum occurs due to the optical principles behind an ATR measurement. To have an attenuated total reflection, the material being analysed must have a lower refractive index than the ATR crystal (here, diamond). However, chromium oxide ( $\text{Cr}_2\text{O}_3$ ) has a refractive index of 2.5 which is greater than the refractive index of the

diamond crystal ( $n_i = 2.418$ ), causing an imperfect total reflection of the IR beam and hence deformations of the resulting absorbance spectrum (Vahur et al., 2010). Because of this particular characteristic of the CrGO pigment, monitoring of the evolutions in the paint coating by FTIR analysis was conducted solely in reflectance mode.

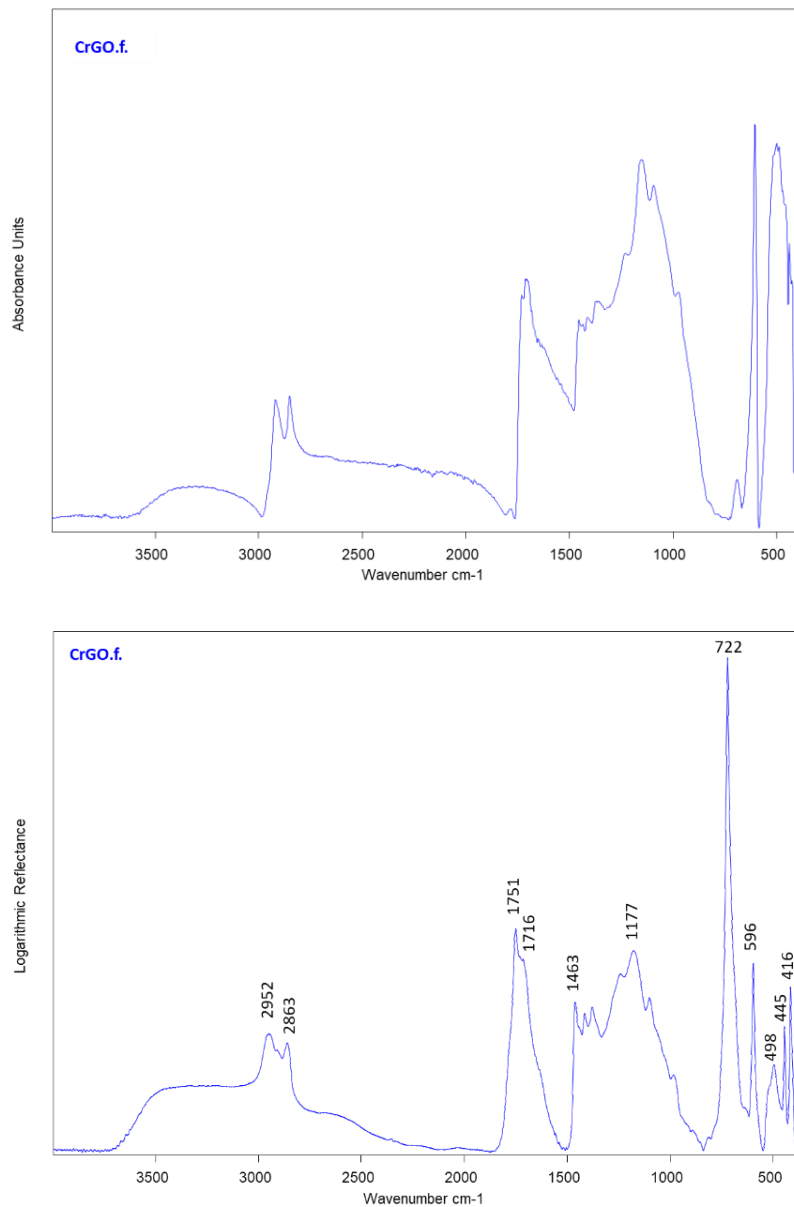


Figure IV-48 FTIR-ATR (top) and FTIR-RS (bottom) spectra (baseline corrected) of fresh chrome green oxide paint.

#### Chrome green oxide-based paint: before aging

In Figure IV-49, the FTIR-RS spectra of the fresh and pre-aged CrGO-paint samples are compared. The equivalent fresh and pre-aged samples of linseed oil binder are also included. The absorption spectra of the paint coatings contain bands associated to both the binder and the pigment.

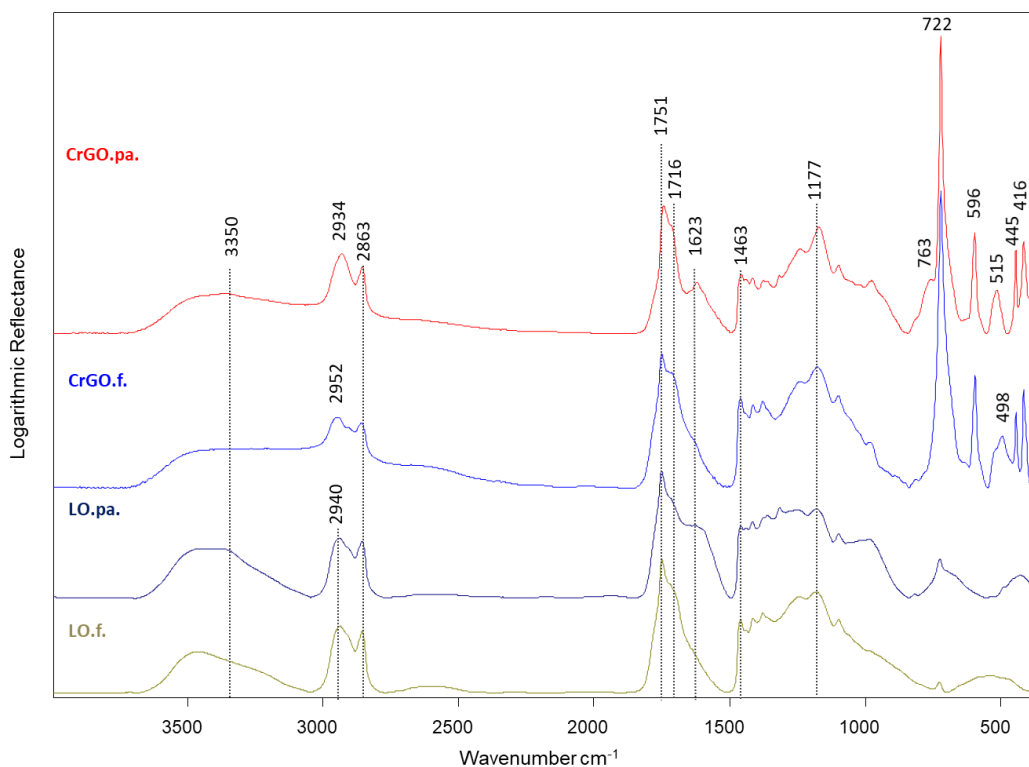


Figure IV-49 FTIR-RS spectra of: fresh linseed oil, naturally aged 1.5 years (LO.f.); pre-aged linseed oil, naturally aged 1.5 years (LO.pa.); fresh CrGO paint, naturally aged 1.5 years (CrGO.f.); pre-aged CrGO paint, naturally aged 1.5 years (CrGO.pa.).

The bands associated to the CrGO pigment are 596, 498, 445 and 416  $\text{cm}^{-1}$ . These are slightly different positions than were observed in the FTIR-ATR spectrum of the pure pigment (see Figure IV-47). Due to the deformation of the pigment spectrum in ATR mode, it is difficult to conclude whether the differences between the bands in the pure pigment and the paint are significant. The band maximum at 498  $\text{cm}^{-1}$  observed in the fresh sample has shifted to 515  $\text{cm}^{-1}$  in the pre-aged paint sample. The shift is significant but the molecular modification responsible for the change is unclear. The remaining bands belong to the absorption of the organic groups in the linseed oil binder. Some differences in these bands are observed in the pre-aged CrGO paint coating spectrum compared to the fresh coating spectrum. These include an increase at 763  $\text{cm}^{-1}$  (unassigned) as a shoulder of the 722  $\text{cm}^{-1}$  absorption, the formation of a band at 1623  $\text{cm}^{-1}$  (assigned to either an asymmetric carboxylate absorption or to the OH bending vibration of water molecules within the crystal lattice), a shift in the asymmetric  $\text{CH}_2$  stretching vibration from 2952  $\text{cm}^{-1}$  to 2934  $\text{cm}^{-1}$ , and an increase in absorption at 3350  $\text{cm}^{-1}$  (OH stretch, linked to the formation of oxidation products of the linseed oil binder). The increase in absorption at 1623  $\text{cm}^{-1}$  is also observed in the pre-aged linseed oil spectrum. Due to the physical particularity of  $\text{Cr}_2\text{O}_3$  (see IV.IV.V.i Starting materials), spectra obtained from the analysis of materials containing this pigment using either of the measurement modes of FTIR analysis (ATR or specular reflectance) may be affected by optical

phenomena, giving results that are difficult to interpret. The main absorption bands for each spectrum are listed and assigned in Table IV-8.

Table IV-8 Absorption bands (in  $\text{cm}^{-1}$ ) and vibrational assignments for the FTIR-RS spectra of the fresh and pre-aged model chrome green oxide (CrGO)-based paint coating samples and reference linseed oil binder (+1.5 years of natural aging). Important aspects are indicated by the following: bold = formation of new band;  $\uparrow$  = increase in intensity; - = absent in spectrum (assignments based on: (Meilunas et al., 1990; Vahur et al., 2010; van der Weerd et al., 2005)).

Linseed oil (fresh)	Linseed oil (pre-aged)	Fresh CrGO paint (+1.5 years)	Pre-aged CrGO paint (+1.5 years)	Assignments
3350-3470	3350 $\uparrow$ - 3470	3350 - 3470	<b>3350 <math>\uparrow</math> -3470</b>	$\nu$ - OH
2940	2940	2952	<b>2934</b>	$\nu_{\text{as}}$ - $\text{CH}_2$
2863	2863	2863	2863	$\nu_{\text{s}}$ - $\text{CH}_2$
1751	1751	1751	1751	$\nu_{\text{s}}$ - C=O
1716	1716	1716	1716	$\nu_{\text{s}}$ - C=O (COOH)
1627 (sh)	1627 $\uparrow$	1623 (sh)	<b>1623 <math>\uparrow</math></b>	? $\delta$ OH ( $\text{H}_2\text{O}$ ) ? $\nu_{\text{as}}$ - $\text{COO}^-$
1463	1463	1463	1463	$\delta$ $\text{CH}_2$
1177	1177	1177	1177	$\nu$ C-O (ester)
-	-	-	<b>763</b>	?
728 (w)	728 (m)	722 (s)	722 (s)	$\rho$ $\text{CH}_2$ / $\nu$ C=C
-	-	596	596	$\text{Cr}_2\text{O}_3$ vib. modes
-	-	498	<b>515</b>	$\text{Cr}_2\text{O}_3$ vib. modes
-	-	445	445	$\text{Cr}_2\text{O}_3$ vib. modes
-	-	416	416	$\text{Cr}_2\text{O}_3$ vib. modes

<sup>1</sup>  $\nu_{\text{as}}$  = asymmetric stretch,  $\nu_{\text{s}}$  = symmetric stretch,  $\delta$  = scissoring,  $\rho$  = rocking.

#### IV.IV.V.ii Fresh and pre-aged chrome green oxide painted coupons treated with corrosion inhibitor and aged by relative humidity cycles (CrGO.f/pa.CI.RH)

The first two cases investigate the evolution of the CrGO paint coating in the presence or not of the corrosion inhibitor treatment composed of 0.05 M NaC<sub>14</sub>. The aged spectra were measured after Phase II of RH cycles, meaning they have endured 9 weeks total of artificial aging.

In Figure IV-50, the FTIR-RS spectra of fresh CrGO paint, untreated RH-aged CrGO paint and corrosion inhibitor (NaC<sub>14</sub>)-treated RH-aged CrGO paint are compared.

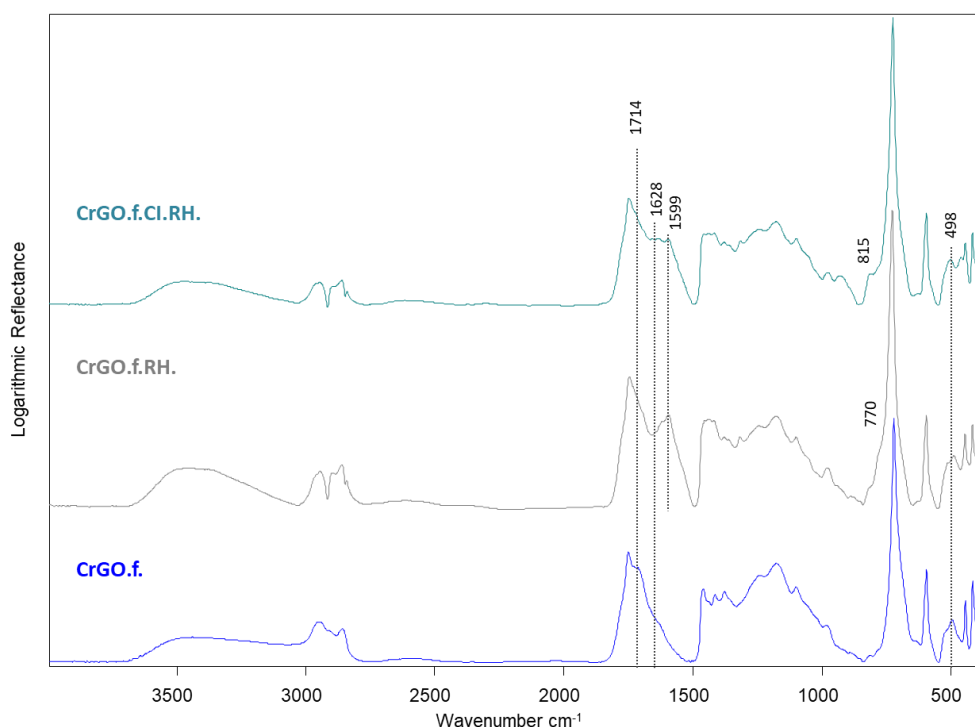


Figure IV-50 FTIR-RS spectra (baseline corrected) of chrome green oxide (CrGO) paint coatings, intensities normalised to CrGO pigment band at 596 cm<sup>-1</sup>: fresh paint (CrGO.f.); untreated fresh paint aged by relative humidity cycles (CrGO.f.RH); treated paint (Corrosion Inhibitor, CI) aged by relative humidity cycles (CrGO.f.CI.RH).

The main changes are seen in the region between 1650-1600 cm<sup>-1</sup>. Before aging, the fresh CrGO paint coating shows an absorption at 1628 cm<sup>-1</sup> as a shoulder on the broad carbonyl absorption band. In the RH-aged untreated sample, the absorption in the region increases and shifts to a maximum at 1599 cm<sup>-1</sup>. In the RH-aged sample treated with the corrosion inhibitor, the absorption in the region also increases but the bands at 1628 and 1599 cm<sup>-1</sup> are equally intense. This suggests that the presence of the corrosion inhibitor inhibited the formation of the species associated to the band at 1599 cm<sup>-1</sup>. Absorption between 1650-1540 cm<sup>-1</sup> is characteristic of the asymmetric carboxylate stretch of metal carboxylates (B. Smith, 1998) and so it can be suggested that chromium carboxylates have formed



during the RH aging cycles. The decrease in absorption at  $1714\text{ cm}^{-1}$  in the aged coating spectra, a characteristic band of free fatty acids, corroborates the suggestion that metal carboxylates have formed by consuming free carboxylic acids. An IR study of pure chromium (III) carboxylates with short fatty acid chains (maximum three carbons) showed two characteristic asymmetric carboxylate absorptions at around  $1610$  and  $1550\text{ cm}^{-1}$  (Kapoor & Sharma, 1983) due to the presence of non-equivalent carboxylate groups around the Cr atom. The difference in frequency compared to the bands in our paint coatings is most likely due to a difference in chemical environment of the chromium carboxylate species in the paint system compared to the pure carboxylate products. Additionally, a shoulder at  $770\text{ cm}^{-1}$  has formed in the untreated RH-aged coating that is similar to the shoulder at  $763\text{ cm}^{-1}$  seen to form in the pre-aged CrGO coating before aging (see Table IV-8); the shoulder appears at  $815\text{ cm}^{-1}$  in the corrosion inhibitor-treated RH-aged spectrum. The band at  $498\text{ cm}^{-1}$  that was seen to shift to  $515\text{ cm}^{-1}$  after pre-aging does not change after the RH aging cycles.

The same experimental conditions were tested on the pre-aged CrGO paint coating. The FTIR-RS spectra acquired on the pre-aged CrGO paint coating before aging (CrGO.pa.), after RH aging without treatment (CrGO.pa.RH), and after RH aging with the corrosion inhibitor treatment (CrGO.pa.Cl.RH) are compared in Figure IV-51.

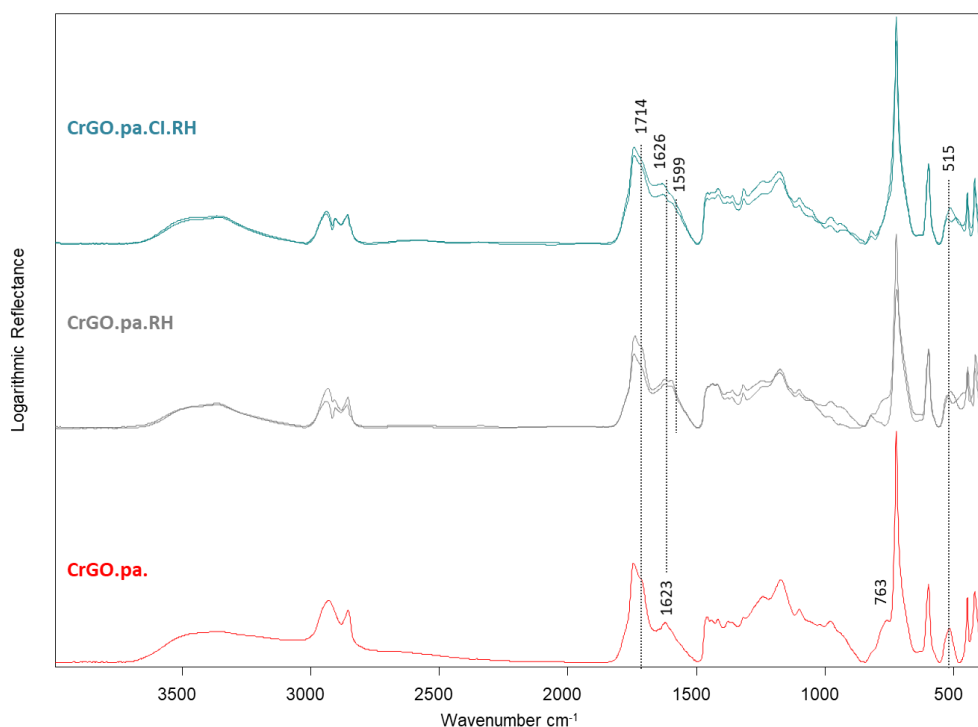
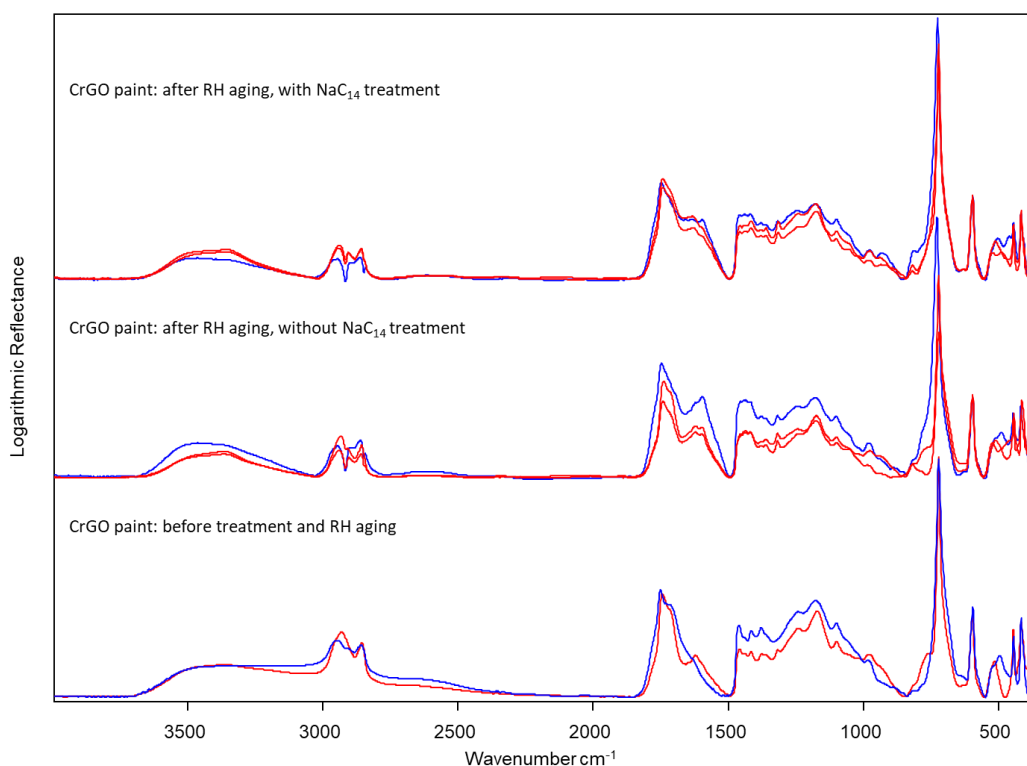


Figure IV-51 FTIR-RS spectra (baseline corrected) of chrome green oxide (CrGO) paint coatings, intensities normalised to CrGO pigment band at  $596\text{ cm}^{-1}$ : pre-aged paint (CrGO.pa.); untreated pre-aged paint aged by relative humidity cycles (CrGO.pa.RH); treated paint (Corrosion Inhibitor, Cl) aged by relative humidity cycles (CrGO.pa.Cl.RH). The spectra acquired on the aged samples showed some variability between points of analysis (3 points per zone) and so multiple spectra have been included for comparison.

In the pre-aged CrGO-paint sample, the absorption in the 1650-1600  $\text{cm}^{-1}$  region has a maximum at 1623  $\text{cm}^{-1}$ . This peak remains unchanged after the RH aging cycles in the spectra of both the untreated and treated paint coatings. However, an increase in absorption is seen at 1599  $\text{cm}^{-1}$  in the untreated sample and to a lesser extent in the treated sample. As in the case of the fresh coating, this suggests that the application of the corrosion inhibitor inhibited the RH-induced formation of the species associated to the 1599  $\text{cm}^{-1}$  band. The intensity of the band at 1714  $\text{cm}^{-1}$  stays constant throughout aging, suggesting that the amount of free fatty acids in the pre-aged CrGO paint coating did not change during the RH aging cycles. No change in the band at 515  $\text{cm}^{-1}$  is observed after the RH aging cycles.

In order to compare the evolution of the fresh and pre-aged samples that otherwise experienced the same experimental conditions, the spectra are superimposed for each step in Figure IV-52.



**Figure IV-52 Comparison of FTIR-RS spectra of fresh (blue) and pre-aged (red) chrome green oxide (CrGO) samples through the following steps: before treatment and artificial aging; After RH aging without  $\text{NaC}_{14}$ ; after RH aging with  $\text{NaC}_{14}$ . Replicate spectra of the pre-aged coating samples are shown to demonstrate variability of absorption intensity in certain regions.**

As discussed above, the comparison of the spectra (Figure IV-52) acquired on the fresh (blue) and pre-aged (red) CrGO paint coatings shows some differences in aging under these experimental conditions. Before aging, the spectrum of the fresh paint coating shows a shoulder around 1628  $\text{cm}^{-1}$  while in the spectrum of the pre-aged paint coating, the same band is fully resolved and present with a greater intensity. After RH aging cycles, an increase at 1599  $\text{cm}^{-1}$  is seen in the spectrum of the untreated fresh

coating compared to the spectrum of the untreated pre-aged coating, which contains the bands at 1623 and 1599  $\text{cm}^{-1}$  in equal intensity. The free fatty acid absorption band at 1714  $\text{cm}^{-1}$  stays relatively constant throughout aging in the pre-aged samples, as opposed to the decrease in intensity seen in the fresh samples. The decrease at 1714  $\text{cm}^{-1}$  and increase at 1599  $\text{cm}^{-1}$  suggests the formation of chromium carboxylates. The observation of a greater increase in intensity of the band at 1599  $\text{cm}^{-1}$  after the RH aging cycles in the fresh paint coating spectrum compared to the pre-aged coating spectrum suggests that the latter is more stable against the RH-induced formation of the species that absorbs at 1599  $\text{cm}^{-1}$ . This stability may be linked to the composition of the paint coating after the pre-aging process. Notably, the formation of the band at 1623  $\text{cm}^{-1}$  after pre-aging could indicate the presence of a chromium carboxylate species with a different coordination environment around the Cr atom than that present in the carboxylate species associated with the absorption at 1599  $\text{cm}^{-1}$ . Regardless of the initial state of the paint coating, the RH-aged samples treated with  $\text{NaC}_{14}$  show less of an increase at 1599  $\text{cm}^{-1}$  than in the untreated RH-aged samples.

Overall, the results of the investigation indicate that:

- 1) An absorption peak at 1599  $\text{cm}^{-1}$  is observed to form in the spectra of the RH-aged CrGO paint coatings and was deduced to be associated to the formation of a chromium carboxylate species.
- 2) The state of the initial starting material (fresh or pre-aged) has an effect on the evolution of the paint in these experimental conditions: the band at 1599  $\text{cm}^{-1}$  forms to a lesser extent in the pre-aged paint than in the fresh paint.
- 3) The presence of the  $\text{NaC}_{14}$  corrosion inhibitor treatment seems to reduce the RH-induced formation of the carboxylate absorption at 1599  $\text{cm}^{-1}$ .
- 4) Treatment with  $\text{NaC}_{14}$  does not induce a detectable formation of reaction products with the paint coating under these experimental conditions.

#### IV.IV.V.iii Fresh and pre-aged chrome green oxide painted coupons treated with resin-wax mixture and aged by relative humidity cycles (CrGO.f/pa.RW.RH)

The next two cases investigate the effect of treatment with the resin-wax (RW) mixture on the evolution of the CrGO paint coating throughout artificial aging by relative humidity cycles. Figure IV-53 shows the FTIR-RS spectra of the fresh CrGO paint coating before aging, the untreated fresh CrGO paint coating aged by RH cycles, and the RW-treated fresh CrGO paint coating aged by RH cycles.

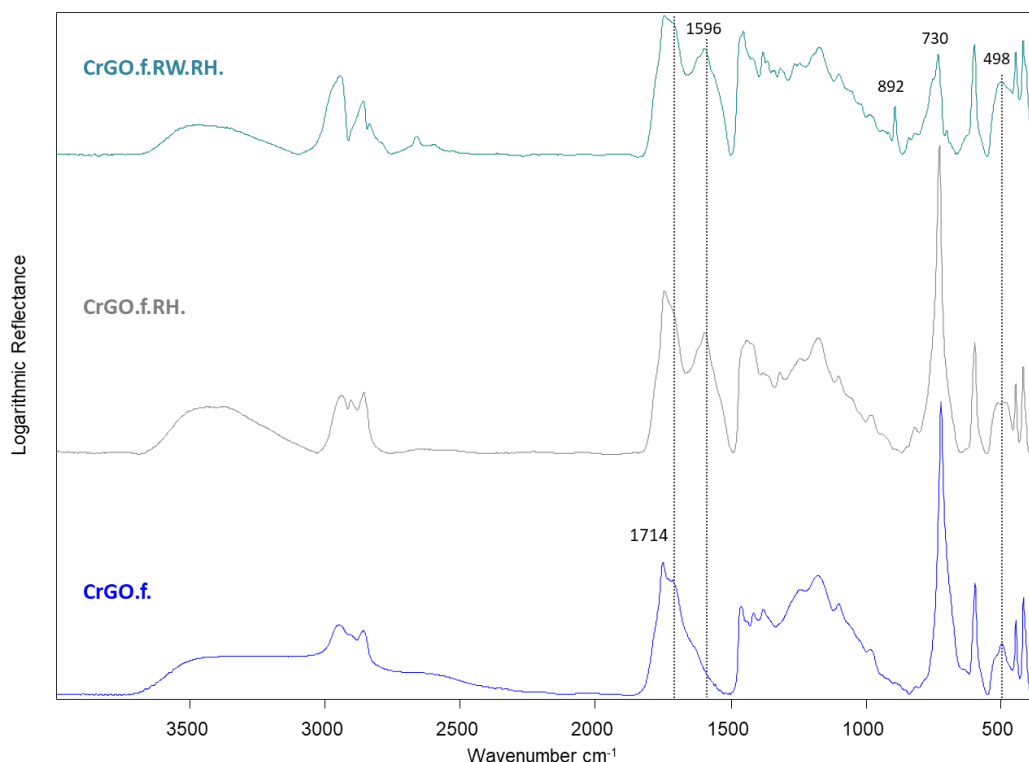


Figure IV-53 FTIR-RS spectra (baseline corrected) of chrome green oxide (CrGO) paint coatings, intensities normalised to CrGO pigment band at 596  $\text{cm}^{-1}$ : fresh paint (CrGO.f.); untreated fresh paint aged by relative humidity (RH) cycles (CrGO.f.RH); treated paint (Resin-Wax mixture, RW) aged by relative humidity cycles (CrGO.f.RW.RH).

As seen in the series treated with the corrosion inhibitor, an increase at 1596  $\text{cm}^{-1}$  and decrease at 1715  $\text{cm}^{-1}$  is observed with RH aging. The band at 1596  $\text{cm}^{-1}$  is present in both the untreated and treated paint coating spectra and suggests the formation of chromium carboxylates. The new band at 892  $\text{cm}^{-1}$  in the spectrum of the treated and aged sample is a characteristic absorption of the resin-wax mixture. The decrease in intensity of the band at 722  $\text{cm}^{-1}$  (associated to the  $\text{CH}_2$  rocking of the hydrocarbon chains of the binder in the paint coating) compared to the other spectra suggests that the absorption signal of the paint coating is attenuated due to the presence (and absorption) of the resin-wax mixture.

The same experimental treatment was applied to a pre-aged CrGO paint; the FTIR-RS spectra are displayed in Figure IV-54.

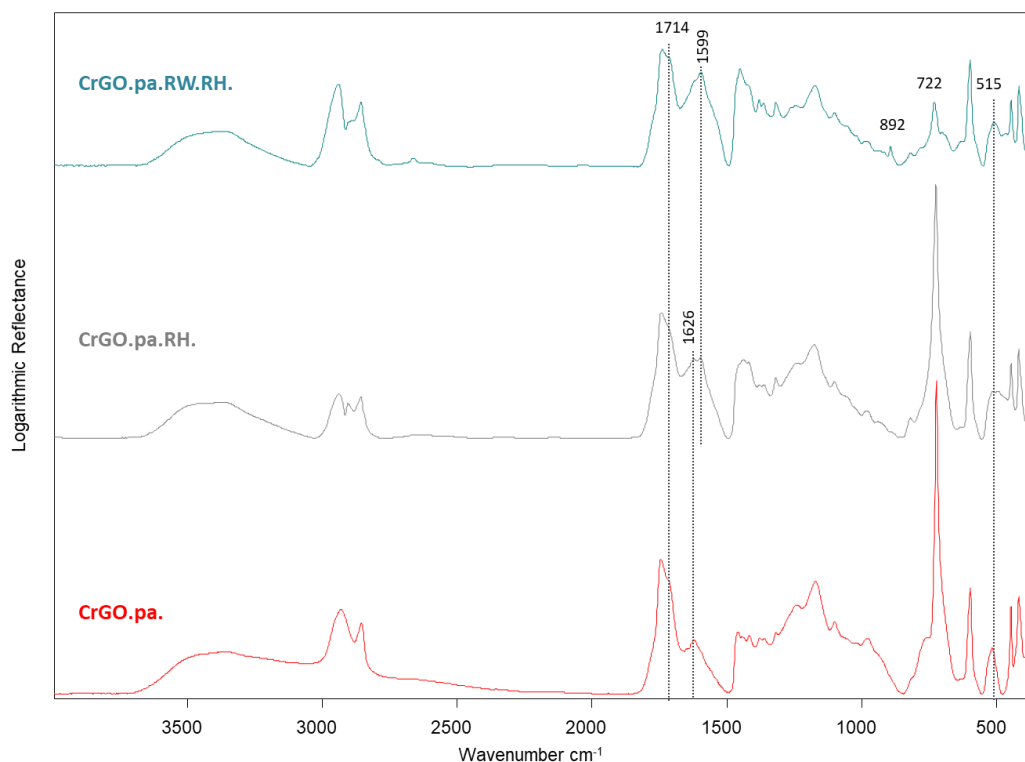
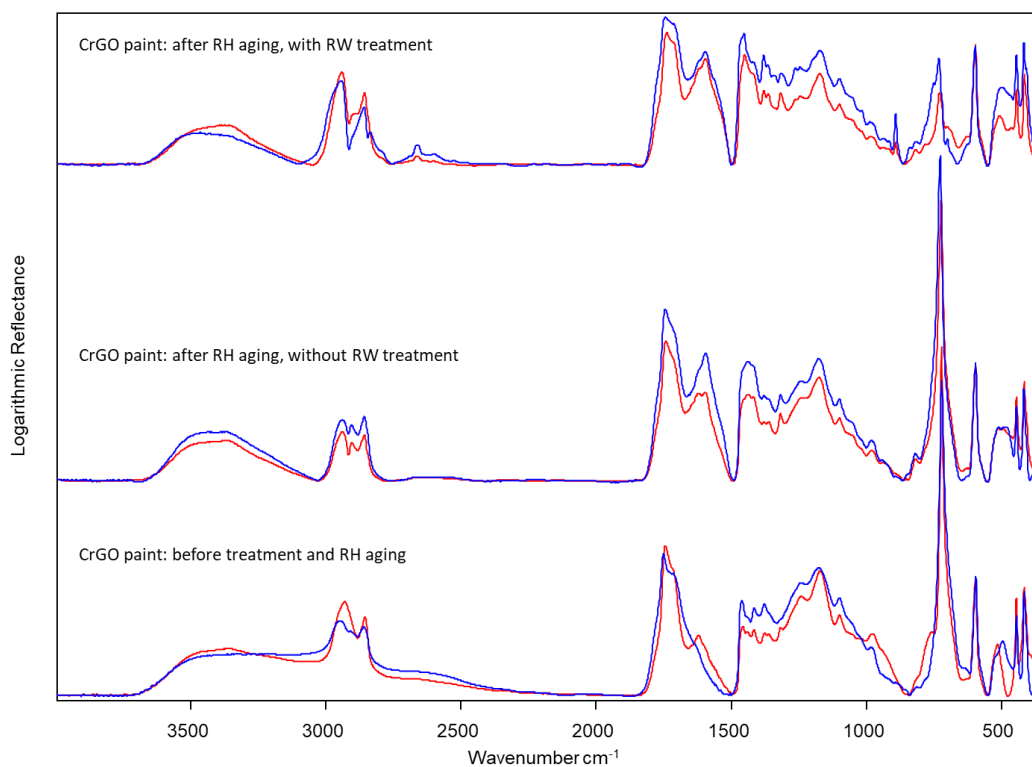


Figure IV-54 FTIR-RS spectra (baseline corrected) of chrome green oxide (CrGO) paint coatings, intensities normalised to CrGO pigment band at  $596\text{ cm}^{-1}$ : pre-aged paint (CrGO.pa.); untreated pre-aged paint aged by relative humidity cycles (CrGO.pa.RH); treated paint (Resin-Wax mixture, RW) aged by relative humidity cycles (CrGO.pa.RW.RH).

As seen in the previous case of pre-aged CrGO paint coating aged by RH cycles, the intensities of the  $1714$  and  $1626\text{ cm}^{-1}$  bands stay relatively unchanged after RH-aging. An increase in absorption at  $1599\text{ cm}^{-1}$  is observed with RH aging, and more so in the treated sample than in the untreated sample, which is not consistent with previous observations. In this case it seems that the formation of the species associated to the band at  $1599\text{ cm}^{-1}$  increases with the presence of the resin-wax mixture. Again, the presence of the band at  $892\text{ cm}^{-1}$  (characteristic of RW mixture) and the decrease in intensity of absorption at  $722\text{ cm}^{-1}$  (attenuation of characteristic absorption feature of paint sample) infer that the absorption of the paint layer is attenuated by the presence of the RW mixture.

In order to compare the evolution of the fresh and pre-aged samples that otherwise experienced the same experimental conditions, the spectra are superimposed for each step in Figure IV-55.



**Figure IV-55 Comparison of FTIR-RS spectra of fresh (blue) and pre-aged (red) chrome green oxide (CrGO) samples through the following steps: before treatment and artificial aging; after RH aging without RW treatment; after RH aging with RW treatment.**

As discussed earlier, the comparison of the fresh and pre-aged paint coating shows some differences in aging under these experimental conditions, particularly in the spectra of the paint coatings before aging (bottom) and after RH-aging without treatment (middle). In the treated sample, the differences between the fresh and pre-aged samples are more subtle. They mainly differ in intensity, which may be related to the thickness of the resin-wax surface treatment. Both the fresh and pre-aged coating spectra show peaks associated to the resin-wax mixture, such as  $892\text{ cm}^{-1}$ , and attenuation of the band at  $722\text{ cm}^{-1}$ , characteristic of the paint coating composition. The presence of the resin-wax mixture may interfere with analysis of the underlying paint coating, making it difficult to compare the spectra of the treated paint coatings with the untreated paint coatings.

Overall, the results of the investigation indicate that:

- 1) An absorption peak at  $1599\text{ cm}^{-1}$  is observed to form in the RH-aged CrGO paint.
- 2) The state of the initial starting material (fresh or pre-aged) influences the evolution of the paint in these experimental conditions: the band at  $1599\text{ cm}^{-1}$  forms to a lesser extent in the pre-aged paint than in the fresh paint.
- 3) The presence of the resin-wax mixture on the treated samples attenuates the absorption signal of the underlying paint sample, making it difficult to assess changes in intensity of the absorption bands characteristic of the paint. A reasonable comparison with the untreated sample spectra cannot be conducted.
- 4) A conclusion on the effects of the presence of the resin-wax mixture on the evolution of the CrGO paint in these experimental conditions cannot be reached.

#### IV.IV.V.iv Pre-aged chrome green oxide painted coupons treated with corrosion inhibitor and aged by light exposure (CrGO.pa.CI.LT)

The evolution of the pre-aged chrome green oxide (CrGO) paint coating aged by light exposure in the presence or not of the corrosion inhibitor solution composed of 0.05 M NaC<sub>14</sub> is investigated. The FTIR-RS spectra of the samples before and after aging are displayed in Figure IV-56.

The main change observed in the spectrum of the untreated pre-aged CrGO paint coating after light exposure is a decrease in intensity of the band at 722 cm<sup>-1</sup>. The rest of the spectrum remains the same. The untreated and treated sample spectra do not present major differences either, indicating that the presence of the corrosion inhibitor treatment did not have an observable influence on the evolution of the pre-aged CrGO paint coating.

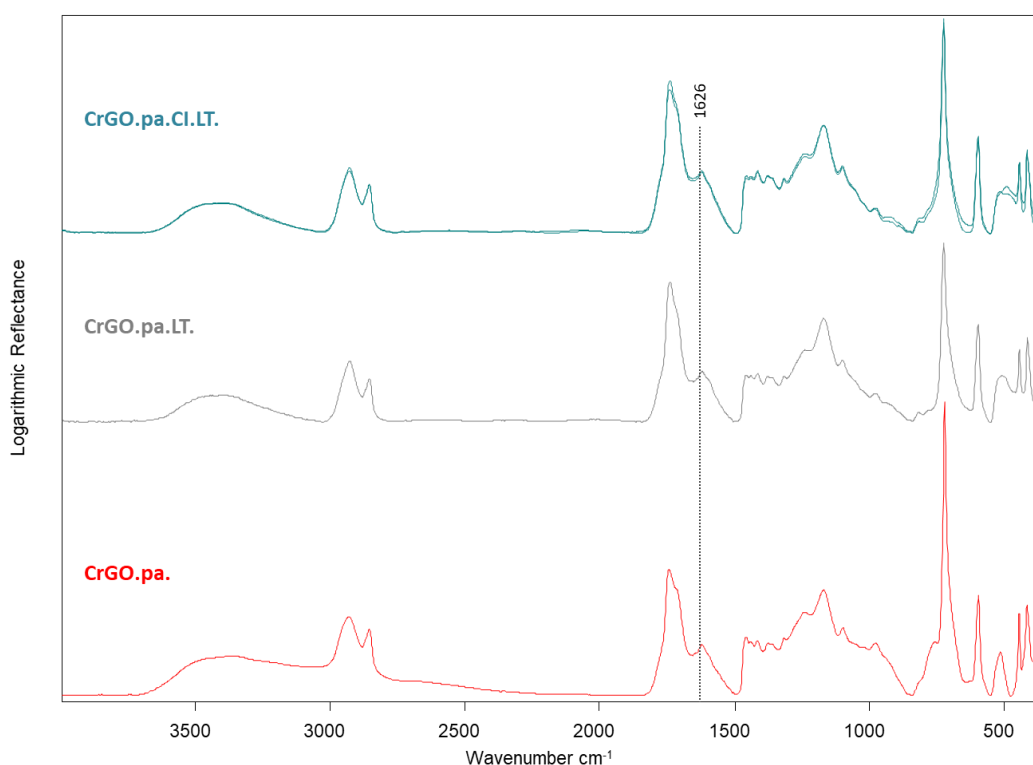


Figure IV-56 FTIR-RS spectra (baseline corrected) of chrome green oxide (CrGO) paint coatings, intensities normalised to CrGO pigment band at 596 cm<sup>-1</sup>: pre-aged paint (CrGO.pa.); untreated pre-aged paint aged by light exposure (CrGO.pa.LT); treated paint (Corrosion Inhibitor, CI) aged by light exposure (CrGO.pa.CI.LT) - two replicate spectra are shown in this case to demonstrate slight variations in intensity.



#### IV.IV.V.v Pre-aged chrome green oxide painted coupons treated with resin-wax mixture (CrGO.pa.RW.LT)

In this case, the pre-aged chrome green oxide (CrGO) paint coating has been treated with the resin-wax (RW) mixture and undergone aging by light exposure. The FTIR-RS spectra of the paint coatings before and after aging are displayed in Figure IV-57.

As in the previous case, no major differences are observed in the spectra acquired after light aging apart from a decrease in intensity of the band at  $722\text{ cm}^{-1}$ . Some differences are observed in the spectrum of the treated paint coating between  $1500\text{--}900\text{ cm}^{-1}$ , most likely due to absorption by the treatment. The band at  $1450\text{ cm}^{-1}$  is a characteristic absorption of the resin-wax mixture. Some variations in intensity are also observed for the bands below  $800\text{ cm}^{-1}$ . This suggests that this region of the treated sample spectrum may be more sensitive to optical perturbations due either to the presence of the resin-wax treatment or to the physical characteristics of  $\text{Cr}_2\text{O}_3$ , implying that the variations are not necessarily associated to a modification of the chemical structure.

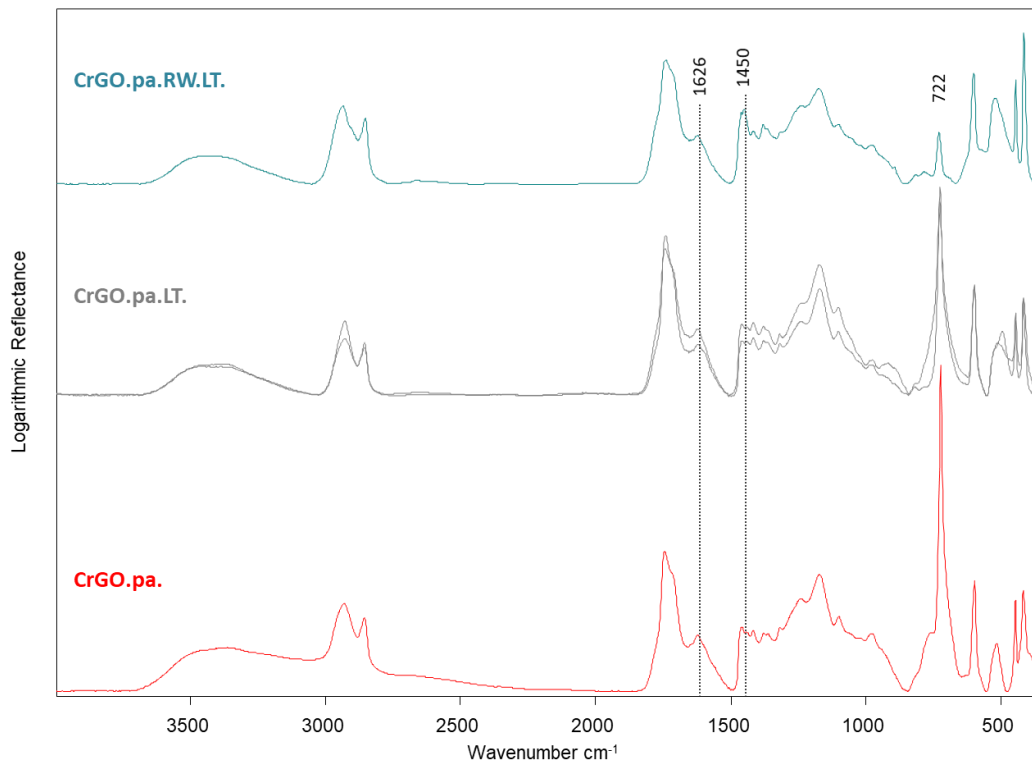


Figure IV-57 FTIR-RS spectra (baseline corrected) of Chrome Oxide Green paint samples, intensities normalised to CrGO pigment band at  $596\text{ cm}^{-1}$ : pre-aged paint (CrGO.pa.); untreated pre-aged paint aged by light exposure (CrGO.pa.LT) - two replicate spectra are shown in this case to demonstrate slight variations in intensity; treated paint (Resin-Wax mixture, RW) aged by light exposure (CrGO.pa.RW.LT).

## IV.IV.VI Discussion of the FTIR analysis of the paint coatings

For the **lead white**-based paint coatings on model coupons aged by **relative humidity cycles**, the main characteristics that were observed were changes related to the lead carboxylate absorption at  $1542\text{ cm}^{-1}$  and changes in the intensity of the  $\text{CH}_2$  stretching vibrations between  $2960\text{--}2850\text{ cm}^{-1}$ . No other new bands were observed in the FTIR spectra after aging. The comparison of these diagnostic changes between the untreated and treated samples after relative humidity aging cycles are listed in Table IV-9.

Table IV-9 Summary of observations of FTIR spectral changes of the untreated and treated model lead white-based paint coating after aging by relative humidity cycles.

		Artificial aging model: relative humidity cycles		
Main observations		<i>No treatment</i>	<i>Corrosion inhibitor</i>	<i>Resin-wax mixture</i>
Fresh paint	<i>Lead carboxylate absorption at <math>1542\text{ cm}^{-1}</math></i>	Growth + shift of $1542 \rightarrow 1531\text{ cm}^{-1}$	Growth + shift of $1542 \rightarrow 1531\text{ cm}^{-1}$	Growth + shift of $1542 \rightarrow 1531\text{ cm}^{-1}$
	<i>Change in intensity of the <math>\text{CH}_2</math> bands</i>	No change	No change	Not conclusive due to overlap by RW absorption
	<i>Formation of new absorption bands</i>	None	None	None
Pre-aged paint	<i>Lead carboxylate absorption at <math>1542\text{ cm}^{-1}</math></i>	2 cases: Growth + shift of $1542 \rightarrow 1531\text{ cm}^{-1}$ ; Growth of $1542$ and $1531\text{ cm}^{-1}$ equally	Growth + shift of $1542 \rightarrow 1531\text{ cm}^{-1}$	Growth of $1542$ and $1531\text{ cm}^{-1}$ equally
	<i>Change in intensity of the <math>\text{CH}_2</math> bands</i>	No change	No change	Not conclusive due to overlap by RW absorption
	<i>Formation of new absorption bands</i>	None	None	None

No major differences are noticed between the states of the untreated or treated lead white paint samples after aging by relative humidity cycles. Lead carboxylates are observed to form in both the untreated and treated paint coatings, inferring that neither of the conservation treatments prevent their formation. This is a logical result as the formation of lead soaps in a lead white-pigmented oil paint is an intrinsic process due to the catalytic effect of the lead white pigment on the aging mechanisms of oil (Meilunas et al., 1990). In one case (the untreated and RW-treated pre-aged paint coatings), a

difference in the behaviour of the lead carboxylate band is observed in comparison to the other experimental cases. Instead of the generally observed growth and shift from 1542 to 1531  $\text{cm}^{-1}$ , in this particular case both bands at 1542 and 1531  $\text{cm}^{-1}$  appear to have grown to an equal level of intensity. This suggests a slightly different process in the formation of lead carboxylates during the relative humidity aging, but as it is observed equally in the untreated and RW-treated samples it cannot be associated to the presence of the RW mixture treatment. It is rather related to some variability between the prepared model coupons.

In the case of the **lead white**-based paint coatings aged by **light exposure**, the main spectral modifications observed after aging were a decrease in the intensity of absorption bands related to the organic features of the paint and the appearance of new bands. The occurrence of these changes for the untreated and treated samples after light exposure aging is described in Table IV-10.

**Table IV-10 Summary of observations of FTIR spectral changes of the untreated and treated model lead white-based paint coating after aging by light exposure.**

		Artificial aging model: light exposure		
Main observations		<i>No treatment</i>	<i>Corrosion Inhibitor</i>	<i>Resin-Wax mixture</i>
Fresh paint	<i>Change in intensity of bands related to organic groups in binder (CH<sub>2</sub>, C=O and C-O of esters)</i>	Large decrease	Retained (slight decrease)	C-O bands retained (slight decrease)  CH <sub>2</sub> and C=O bands overlapped by RW absorption
	<i>Formation of new absorption bands</i>	Growth + shift of 1542 → 1538 $\text{cm}^{-1}$ (shoulder)  Increase at 1780 $\text{cm}^{-1}$	Growth + shift of 1542 → 1538 $\text{cm}^{-1}$ (shoulder)	Growth + shift of 1542 → 1538 $\text{cm}^{-1}$ (shoulder)  Increase at 1780/1739/1715 $\text{cm}^{-1}$ related to aging of RW treatment
Pre-aged paint	<i>Change in intensity of bands related to organic groups in binder (CH<sub>2</sub>, C=O and C-O of esters)</i>	Large decrease	Retained (slight decrease)	Retained (slight decrease)*
	<i>Formation of new absorption bands</i>	Growth + shift of 1542 → 1538 $\text{cm}^{-1}$ (shoulder)  Increase at 1780 $\text{cm}^{-1}$	Growth + shift of 1542 → 1538 $\text{cm}^{-1}$ (shoulder)	Growth + shift of 1542 → 1538 $\text{cm}^{-1}$ (shoulder)*  Increase at 1780 $\text{cm}^{-1}$ *

\*Interior face was measured (RW treatment not present).

Comparison of the FTIR spectra show that after light exposure, the organic functional bands (CH<sub>2</sub>, C=O, C-O ester bands) were more retained in the treated samples than the untreated samples. The formation of a carbonyl band at 1780  $\text{cm}^{-1}$  in the untreated samples appears to be inhibited by the presence of the corrosion inhibitor treatment; the effect in the RW-treated paint samples cannot be determined

due to absorption at the same position by the RW mixture. Finally, the presence of either treatment does not inhibit the increase of a shoulder at  $1538\text{ cm}^{-1}$  in the spectra after light aging; this band is interpreted as the formation of new lead carboxylate species.

The main changes observed in the FTIR spectra of the **chrome green oxide**-based paint coatings after **relative humidity cycles** occurred in the region of  $1630\text{-}1500\text{ cm}^{-1}$ , although a decrease was also seen in the intensity of the carboxylic acid C=O stretch at  $1715\text{ cm}^{-1}$  and various changes were observed between  $815\text{-}700\text{ cm}^{-1}$ , the region corresponding to  $\text{CH}_2$  bending vibrations. The occurrence of (or lack thereof) these changes for the untreated and treated samples are described in Table IV-11.

Table IV-11 Summary of observations of FTIR spectral changes of the untreated and treated model chrome green oxide-based paint coating after aging by relative humidity cycles.

		Artificial aging model: relative humidity cycles		
Main observations		<i>No treatment</i>	<i>Corrosion inhibitor</i>	<i>Resin-wax mixture</i>
Fresh paint	<i>Formation of band at <math>1599\text{ cm}^{-1}</math></i>	Yes	Yes	Yes
	<i>Intensity (I) of bands at <math>1628</math> and <math>1599\text{ cm}^{-1}</math></i>	$I_{1628} < I_{1599}$	$I_{1628} = I_{1599}$	$I_{1628} < I_{1599}$
	<i>Intensity of carboxylic acid band (<math>1715\text{ cm}^{-1}</math>)</i>	Decrease	Decrease	Decrease
	<i>Changes in region <math>815\text{-}700\text{ cm}^{-1}</math></i>	Formation of $770\text{ cm}^{-1}$ (shoulder)	Formation of $815\text{ cm}^{-1}$ (shoulder)	Decrease in intensity of $722\text{ cm}^{-1}$ (attenuated signal due to RW layer)
Pre-aged paint	<i>Formation of band at <math>1599\text{ cm}^{-1}</math></i>	Yes	Yes	Yes
	<i>Intensity (I) of bands at <math>1628</math> and <math>1599\text{ cm}^{-1}</math></i>	$I_{1628} = I_{1599}$	$I_{1628} > I_{1599}$	$I_{1628} < I_{1599}$
	<i>Intensity of carboxylic acid band (<math>1715\text{ cm}^{-1}</math>)</i>	Constant	Constant	Constant
	<i>Changes in region <math>815\text{-}700\text{ cm}^{-1}</math></i>	Variation between spectra; change is not clear	Decrease in intensity at $763\text{ cm}^{-1}$	Decrease in intensity at $722\text{ cm}^{-1}$ (attenuated signal due to RW layer)

Before aging, a band at  $1623\text{ cm}^{-1}$  is present in the pre-aged sample but not in the fresh sample. After RH aging, this band appears in the spectrum of the fresh sample but stays constant in the pre-aged samples. A band at  $1599\text{ cm}^{-1}$  also forms in the spectra of both the fresh and pre-aged samples after RH aging. These bands are assigned to the asymmetric carboxylate stretches of chromium carboxylates. The intensity of the band at  $1599\text{ cm}^{-1}$  with respect to the band at  $\sim 1623\text{ cm}^{-1}$  seems to depend on the initial state of the paint coating: in the fresh samples,  $1599\text{ cm}^{-1}$  is more intense than  $1623\text{ cm}^{-1}$ , but

they are of approximately equal intensity in the pre-aged samples. The simultaneous decrease of the C=O stretch of carboxylic acids at  $1715\text{ cm}^{-1}$  in the fresh samples suggests that more chromium carboxylates are formed in the fresh samples after RH aging than in the pre-aged samples. In the samples treated with the corrosion inhibitor, the presence of the treatment appears to inhibit the formation of the band at  $1599\text{ cm}^{-1}$ . Conversely, the presence of the resin-wax mixture does not appear to limit the formation of this band. In fact, in the RW-treated pre-aged paint coating the band is present with a higher intensity than in the untreated paint coating, suggesting that the presence of the RW treatment promoted the formation of the carboxylate species. Other changes are observed in the lower wavenumber region, but no clear trends can be deduced.

The spectra of the CrGO-based paint coatings aged by **light exposure** show minimal changes compared to before aging (Table IV-12). The main change is a slight decrease in intensity of the band at  $722\text{ cm}^{-1}$ . The spectrum of the paint coating treated with the corrosion inhibitor does not differ from the untreated sample spectrum, indicating that it did not have an effect on the evolution of the chemical structure of the pre-aged CrGO paint coating under the applied light exposure aging conditions. The analysis of the pre-aged paint coating treated with RW mixture shows a major decrease in intensity of the band at  $722\text{ cm}^{-1}$  as well as other variations in intensity below  $800\text{ cm}^{-1}$ ; these changes are attributed more so to attenuation of the paint coating signal by the absorption of the RW treatment and possibly other optical phenomena related to the physical characteristics of the CrGO pigment than to chemical modifications within the paint coating.

**Table IV-12 Summary of observations of FTIR spectral changes of the untreated and treated pre-aged model chrome green oxide-based paint coating after aging by light exposure.**

		Artificial aging model: light exposure		
Main observations		<i>No treatment</i>	<i>Corrosion inhibitor</i>	<i>Resin-wax mixture</i>
Pre-aged paint	<i>Formation of band at <math>1599\text{ cm}^{-1}</math></i>	No	No	No
	<i>Decrease of band at <math>722\text{ cm}^{-1}</math></i>	Yes - slight	Yes - slight	Yes - major

#### IV.IV.VII Conclusions on the FTIR study of the paint coatings

The evolution of the treated painted metal model systems was monitored throughout artificial aging using several techniques, including by FTIR spectroscopy. This technique was used specifically as a diagnostic tool for understanding the aging processes endured by the paint coatings and the efficiency of protection of the conservation treatments against these processes. The use of both attenuated total reflectance (ATR) and specular reflectance (RS) modes during the study provided an interesting comparison in terms of the quality of information gained from each technique. FTIR-RS is a promising technique for non-invasive characterisation of painted metal surfaces, but as its applicability is limited by physical aspects of the paint coating, the analysis of some of the surfaces of the studied samples was found to be problematic. This was observed for the lead white-based paint coating where the presence of an uneven surface (caused by a large granulometry of the pigment in the paint coating) was found to degrade and distort the spectra acquired in reflectance mode. Although the granulometry of the pigments is much finer on real objects, the presence of other conditions that might lead to uneven surfaces (corrosion, surface pollution, or mechanical alterations) may still be encountered. The FTIR-RS spectra obtained on the chrome green oxide-based paint coatings, which have a smooth surface, were of sufficient quality to be able to evaluate changes in the absorption bands. ATR mode, a standard for material analysis due to its simple operation (no specific sample preparation, and small quantity necessary), gave good results for the lead white-based paint but this measurement mode was not suitable for the chrome green oxide-based paint because of its refractive index which hinders the attenuated total reflection. Both acquisition modes are shown to have some limitations related either to the roughness of the analyzed surfaces, or to the nature of the pigment present. Another methodological complication was that since FTIR analysis in both ATR and RS modes has a small depth of penetration, the observations are only for the "near surface" of the samples. For example, the spectra acquired on treated zones showed overlap of the signal of the conservation treatments with the signal of the underlying paint coating. For this reason, micro-sampling (and in some cases, preparation of thin sliced (microtomed) cross sections) is still an important strategy for understanding the full stratigraphy of the aged paint system. In general however, the conservation treatment layer was thin enough to still observe changes in the bands attributed to the paint sample, allowing to draw some conclusions on the protection efficiency of the treatments.

The FTIR study of the evolution of the model lead white-based paint coating throughout artificial aging conditions provided a systematic description of changes in the molecular structure of the paint system induced by either relative humidity cycles or light exposure. Furthermore, the comparison of the changes observed in the spectra of the untreated paint coatings with the paint coatings treated with

either the corrosion inhibitor NaC<sub>14</sub> or the resin-wax mixture composed of 30:10 wt% Regalrez 1126®-Cosmoloid H80® allowed to assess whether the presence of the conservation treatments had an effect of the evolution of the paint system under the applied artificial aging conditions.

The main change observed in the spectra of the paint samples aged by relative humidity cycles was the shift and increase in intensity of the lead carboxylate absorption from 1542 to 1531 cm<sup>-1</sup>. This change was observed regardless of the presence or not of a conservation treatment. This shows that neither of the conservation treatments inhibited the formation of lead soaps, which is not a surprising result given the reactivity of the lead white pigment in the linseed oil paint system. It is also possible that the applied RH aging conditions were not extreme enough to create a state of degradation where the protective effect of the conservation treatments could be observed.

In contrast to the RH-aged samples, aging by light exposure was found to have a degrading effect on the organic structure of the lead white-based paint coating, as evidenced by a major decrease in intensity of the organic absorption bands. Despite the main function of the solution of NaC<sub>14</sub> treatment being a corrosion inhibitor, it also shows a protective behaviour for the lead white-based paint against the aging effects of light exposure: NaC<sub>14</sub>-treated zones were observed to retain the initial intensity of organic absorption bands better than in the untreated zones. The effect of the resin-wax mixture could not be assessed due to overlap of the treatment absorption bands with the diagnostic bands for aging in the paint coating spectra. Neither of the treatments were observed to inhibit the formation of lead carboxylates, as seen by the shift and growth of the band at 1541 to 1538 cm<sup>-1</sup> in the both of the light-aged paint samples.

An increase in intensity of the lead carboxylate absorption is observed under both of the applied artificial aging conditions, although to a lesser extent in the light-aged coupons than the RH-aged samples. A shift of the corresponding band is also observed under relative humidity aging conditions, while under light exposure the band position remains almost unchanged. Due to the degradation of the organic content under light exposure it is possible that there are fewer potential species of metal carboxylates that can be formed, thus explaining the lesser increase and shift of the carboxylate absorption band.

The chrome green oxide-based paint is more stable under the imposed light exposure conditions than under the relative humidity cycles. In the latter case, bands suggestive of chromium carboxylates appeared in the spectra after nine weeks total of RH aging. The presence of the corrosion inhibitor treatment appears to limit the development of a chromium carboxylate band, while the resin-wax mixture was found to have no effect (or in one case, a stimulating effect) on the formation of the same band. Under the light exposure aging, the presence of the corrosion inhibitor NaC<sub>14</sub> did not have an

Chapter IV A multi-scale analytical study of the effects of conservation treatments on the aging of model painted metal surfaces

effect on the evolution of the CrGO paint coating, while the effect of the resin-wax mixture could not be determined due to optical phenomena that caused deformation of the resulting spectra.



## IV.V XANES study of the Pb-L<sub>3</sub> edge of the lead white-based paint coating

In the present section the results of a study by X-ray Absorption Near Edge Structure (XANES) spectroscopy are presented. XANES at the Pb L<sub>3</sub> edge was used to evaluate changes in the local environment of lead in the lead white-based paint coating of model painted metal coupons throughout the conservation treatment testing protocol. The analysis of lead-based reference compounds will first be presented, followed by the results obtained on the painted metal coupons, and the section will conclude with a synthesis and discussion of the observed trends.

### IV.V.I Reference compounds

The XANES spectra of the following lead reference compounds were acquired: a lead metal sheet, minium (Pb<sub>3</sub>O<sub>4</sub>), lead oxide (PbO), lead acetate (Pb(CH<sub>3</sub>COO)<sub>2</sub>), lead salts of palmitic (16-carbon chain) and azelaic (9-carbon chain) acids, lead sulfate (PbSO<sub>4</sub>) and basic lead carbonate (2PbCO<sub>3</sub>·Pb(OH)<sub>2</sub>, the lead white pigment used for preparation of the lead white-based paint on the model coupons).

The coordination geometry of the lead complexes is dependent upon the metal's oxidation state and the coordination number (number of ligands). The reference compounds contain lead in either the 0, +2 or +4 oxidation states (see Table IV-14). Pb(II) can form a variety of coordination complexes, explained in part by its electronic configuration of [Xe]4f<sup>14</sup>5d<sup>10</sup>6s<sup>2</sup>. The 6s<sup>2</sup> lone pair has been found to be stereochemically active in some cases which affects the organization of the ligands around the metal centre and gives rise to various coordination geometries as seen in Figure IV-58.

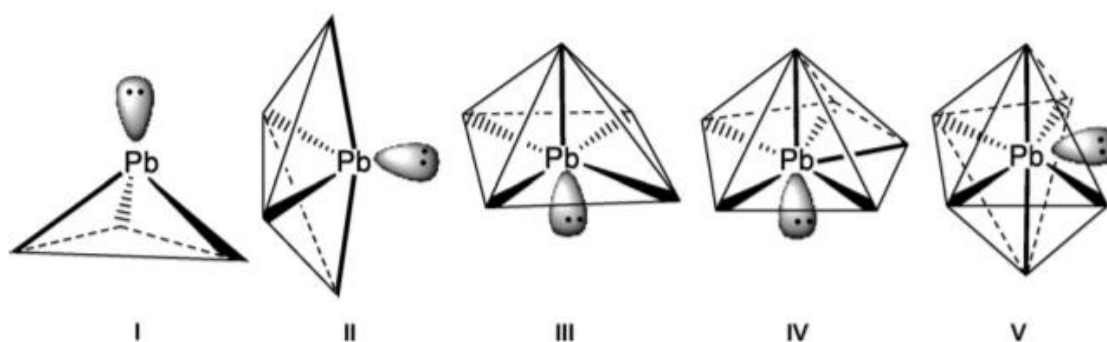


Figure IV-58 Spatial arrangements of the Pb(II) ion with varying numbers of oxygen-donating ligands. From: (Davidovich et al., 2009).

The coordination geometry of Pb(II) complexes have been found to be “*holodirected*”, in which the bonds to ligand atoms are directed throughout the surface of an encompassing globe” and “*hemidirected*”, in which the bonds to ligand atoms are directed throughout only part of the globe, that is, there is an

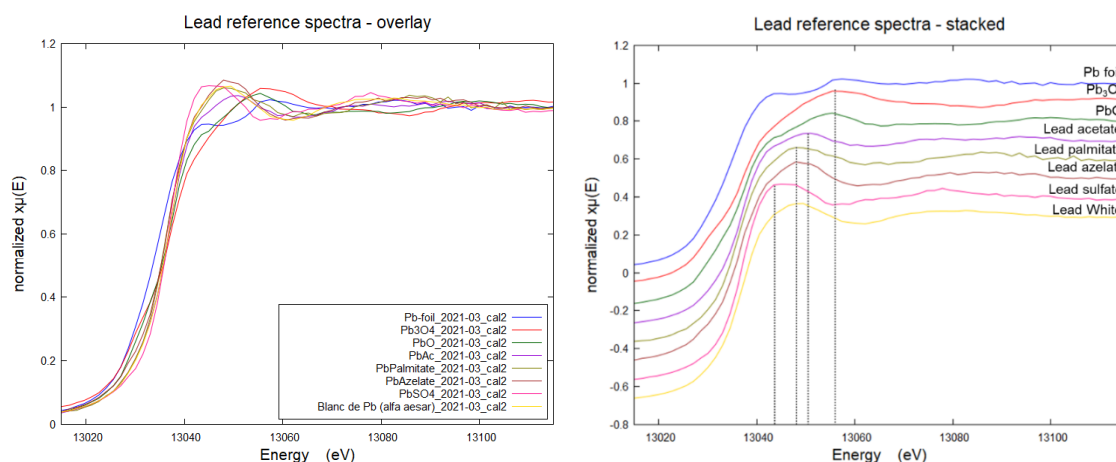
identifiable void (or gap) in the distribution of bonds to the ligands” (Davidovich et al., 2009). In Table IV-13 it is seen that the environment of Pb(II) changes depending on the coordination number of the species.

**Table IV-13 Coordination geometry of Pb(II) ions depending on their coordination number.**

Lead ion	Coordination number	Coordination geometry
Pb(II)	2-5	Hemidirected
Pb(II)	Intermediate: 6-8	Hemi and holo-directed
Pb(II)	9-10	Holodirected

In contrast, Pb(IV) complexes (electronic configuration:  $[\text{Xe}]4f^{14}5d^{10}$ ) have no lone pair and therefore the coordination geometry of the ligands around the metal centre is holodirected and less diverse.

Figure IV-59 shows the Pb  $L_3$ -edge XANES spectra of each reference compound. The overlaid spectra permit a better visibility of variations in the absorption edge while the stacked spectra demonstrate the variations in position of the white line and of the subsequent oscillations. Variations of the absorption edge position are indicative mainly of differences in oxidation state of the metal centre, while variations of shape and position of the white line indicate more so differences in the coordination geometry. The complexes containing Pb(II) (see Table IV-14) have different spectral forms, inferring that the compounds present different coordination geometries.



**Figure IV-59 XANES Pb  $L_3$ -edge spectra of lead reference compounds, overlaid (left) and stacked (right) for comparison. Dotted lines indicate positions of white lines for various compounds.**

The energy positions of the absorption edge and the white line of each reference spectra are listed in Table IV-14. The Pb carboxylates' lower absorption edge (13035.9 eV) allows them to be differentiated from the rest of the compounds (edge position  $\sim$ 13037 eV). Several groups of white line positions are

present, as shown by the dotted lines in Figure IV-59. Lead sulfate has a white line at 13045 eV. Lead white and the Pb carboxylates cannot be differentiated based on their white line position, although the shape of the lead white spectrum is slightly different from that of the soaps. Lead acetate is the only compound with a white line at 13050 eV, and furthermore has a small shoulder just before at 13045 eV. PbO and Pb<sub>3</sub>O<sub>4</sub> have similar white line positions at 13054.9 eV and 13056.8 eV, respectively. These results show that most of the Pb species can be differentiated by their white line position and shape, with the exception of the Pb carboxylates that present almost identical shapes.

**Table IV-14 Energy positions of the absorption edge and white line from XANES spectra of Pb reference compounds.**

Reference compounds	Oxidation state of Pb	Coordination number (CN)	Edge E (eV)	White line (eV) position of the maximum
Pb foil (metal sheet)	0	-	13035	13044.7; 13057.7
Red lead/minium: Pb <sub>3</sub> O <sub>4</sub>	+2, +4	CN 6 (Pb(IV)) (Dickens, 1965)	13037.5	13056.8
Lead oxide: PbO	+2	CN 4 ( <i>Materials Data on PbO by Materials Project, 2020</i> )	13037.4	13054.9
Lead acetate: Pb(CH <sub>3</sub> COO) <sub>2</sub>	+2	CN 7 (Martínez-Casado et al., 2016)	13037.6	13050.0
Lead palmitate: Pb(CH <sub>3</sub> (CH <sub>2</sub> ) <sub>14</sub> COO) <sub>2</sub>	+2	CN 7 (Martínez-Casado et al., 2019)	13035.9	13048.5
Lead azelate: Pb(OOC(CH <sub>2</sub> ) <sub>7</sub> COO) <sub>2</sub>	+2	CN 7 (Plater et al., 2003)	13035.9	13048.5
Lead sulphate: PbSO <sub>4</sub>	+2	CN 10 ( <i>Materials Data on PbSO<sub>4</sub> by Materials Project, 2020</i> )	13037.3	13045.0
Lead white: 2PbCO <sub>3</sub> ·Pb(OH) <sub>2</sub>	+2	CN 7 (Gonzalez, 2016)	13037.4	13049.0

Chen-Wiegart *et al.* (Chen-Wiegart et al., 2017) reported the following white line positions in their XANES study of Pb-containing references: 13054.3 ± 1.0 eV for lead white, 13055.5 ± 1.0 eV for lead azelate, 13056.2 ± 1.0 eV for lead palmitate, and 13060.7 ± 1.0 eV for red lead. While the values are slightly higher in energy, they follow the same trend as our data with the lead oxides having higher energy white line positions than the carbonates and soaps. They suggest that the spectra of lead white and the Pb carboxylates collected in fluorescence mode may be hard to distinguish potentially due to effects of self-absorption which is particularly high for materials containing Pb.

## IV.V.II Initial state of materials

In Figure IV-60, the XANES spectra of the lead white pigment as well as the lead white-based paint in its fresh and pre-aged form are shown.

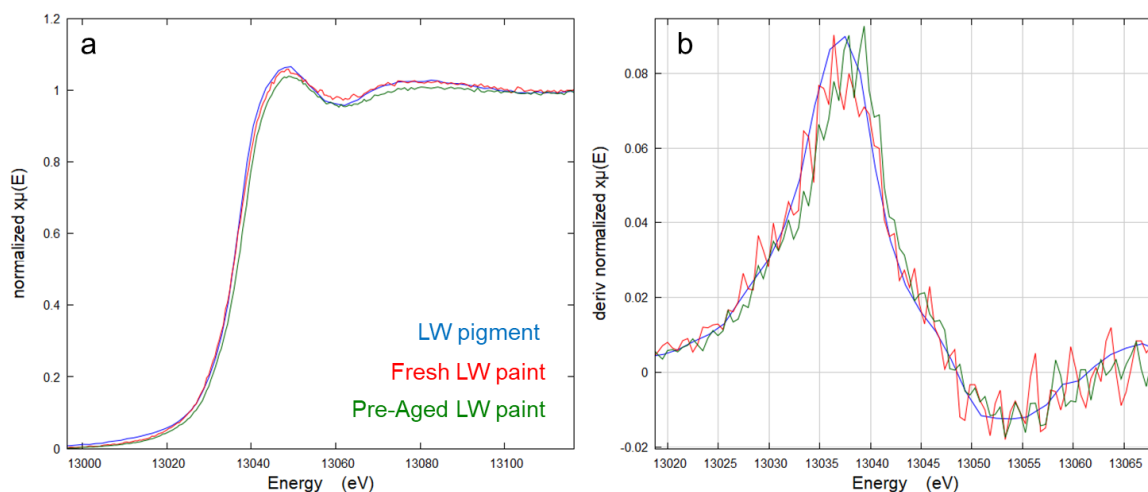


Figure IV-60 (a) Normalized XANES spectra at the Pb-L<sub>3</sub> edge; (b) First derivative of the normalized spectra, for the initial starting materials: lead white (LW) pigment (blue), fresh LW paint (red) and pre-aged LW paint (green).

The positions of the absorption edge and white line for each spectrum have been identified from the maximum and post-edge zero-crossing of the first derivatives and are listed in Table IV-15. The absorption edges for the lead white pigment and the fresh lead white paint are the same ( $13037.0 \pm 0.5$  eV and  $13037.4 \pm 0.5$  eV) while the pre-aged lead white paint shows a positive shift to  $13038.4 \pm 0.5$  eV. This suggests that the pre-aging climatic cycles had an oxidising effect on the lead white paint system. The position of the white line remains unchanged between the three spectra, but the shape of each spectrum is slightly different (oscillations are dampened).

Table IV-15 Absorption edge and white line positions from XANES spectra of lead white pigment and lead white-based paints.

Compound/sample	Absorption edge (eV)	White line (eV)
Lead white pigment	$13037.0 \pm 0.5$	$13049.0 \pm 0.5$
Fresh lead white paint	$13037.4 \pm 0.5$	$13048.5 \pm 0.5$
Pre-aged lead white paint	$13038.4 \pm 0.5$	$13048.5 \pm 0.5$

### IV.V.III Fresh and pre-aged lead white paint from coupons treated with corrosion inhibitor and aged by relative humidity cycles (LW-f-CI-RH and LW-pa-CI-RH)

Fresh and pre-aged lead white-painted coupons have been aged by relative humidity (RH) cycles in the presence or not of the corrosion inhibitor NaC<sub>14</sub>. Figure IV-61 shows the XANES spectra of the paint in its initial fresh/pre-aged state, after Phase I of aging, and after Phase II of aging. The spectra of the untreated and treated zones are superimposed in each step for comparison.

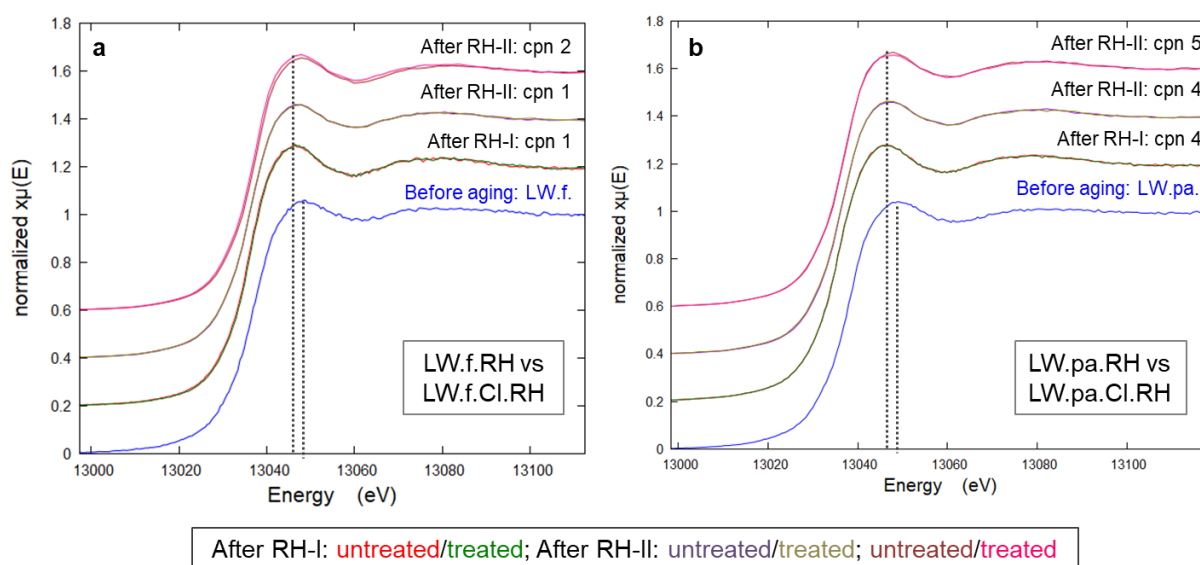


Figure IV-61 Normalized XANES spectra of fresh (a) and pre-aged (b) lead white (LW) painted coupons untreated/treated with corrosion inhibitor (CI) and aged by relative humidity (RH) cycles (RH-I: phase I, 3 weeks; RH-II: phase II, 6 weeks). Measurements were acquired on one coupon (cpn) after RH-I and on two coupons after RH-II. Dotted lines indicate position of maximum of white lines.

The edge positions for each spectrum as well as the difference in edge position for the untreated and treated areas after each aging step are shown in Table IV-16 for fresh and pre aged coupons, respectively. Given that the energy resolution is about 0.5 eV, no significant difference is observed between the absorption edge positions of the untreated and treated zones at any point during the artificial aging process, whatever the initial state. However, a slight shift in energy is observed in the position of the white line between the spectra of the initial and RH-aged lead white-painted coupons. A small difference in the shape of the oscillations is also noted between the spectra from the untreated and treated zones of the fresh lead white paint (coupon 2) after Phase II of RH aging. The presence of the corrosion inhibitor does not appear to influence the local environment of Pb in the lead white paint during the artificial RH aging cycles.

While replicate coupons (coupons 1 and 2 in the fresh paint; 4 and 5 in the pre-aged paint) show the same relationship between the untreated and treated zones, some variability is present between the coupons themselves. Table IV-16 shows that after Phase II aging, the shift of the edge position with respect to the initial material for coupon 1 is -1.5 eV, while no shift occurred for coupon 2. Similarly, coupon 4 shows an edge shift of -2.3 eV with respect to the initial pre-aged paint after Phase II aging while coupon 5 has an edge shift of around -1.5 eV (average between the untreated and treated edge shifts). In both cases the second replicate coupon has a higher edge position.

**Table IV-16 Edge positions for the untreated and corrosion inhibitor-treated zones of fresh and pre-aged lead white paint throughout RH aging process (left column); absolute value of the difference in edge position between spectra from the treated and untreated zones (middle column); edge shift with respect to initial state throughout RH aging process (right column). Cpn: coupon.**

	Edge position E (eV)		$\Delta E =  treated-untreated $ (eV)	$\Delta E = E-E_{initial}$ (eV)	
	Untreated	Treated		Untreated	Treated
Initial (fresh)	13037.4	13037.4	0	0	0
Phase I (cpn1)	13036.1	13036.4	0.3	-1.3	-1
Phase II (cpn 1)	13035.9	13035.9	0	-1.5	-1.5
Phase II (cpn 2)	13037.5	13037.4	0.1	0.1	0
Initial (pre-aged)	13038.4	13038.4	0	0	0
Phase I (cpn4)	13035.9	13035.7	0.2	-2.5	-2.7
Phase II (cpn 4)	13036.1	13036.1	0	-2.3	-2.3
Phase II (cpn 5)	13037	13036.8	0.2	-1.4	-1.6

#### IV.V.IV Fresh and pre-aged lead white paint from coupons treated with resin-wax mixture and aged by relative humidity cycles (LW-f-RW-RH and LW-pa-RW-RH)

Fresh and pre-aged lead white paint samples were aged by climatic cycles in the presence or not of the resin-wax (RW) mixture (30:10 wt% Regalrez 1126®-Cosmoloid H80®). Figure IV-62 shows the XANES spectra of the paint in its initial fresh/pre aged state, after Phase I of aging, and after Phase II of aging. The spectra of the untreated and treated zones are superimposed in each step for comparison.

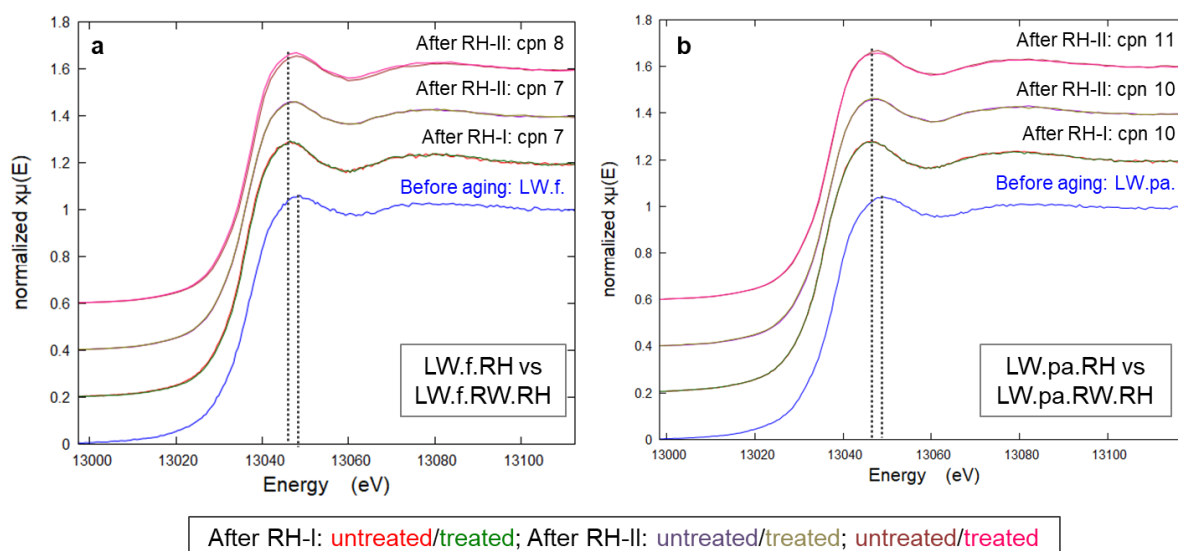


Figure IV-62 Normalized XANES spectra of fresh (a) and pre-aged (b) lead white (LW) paint untreated/treated with resin-wax mixture (RW) and aged by relative humidity (RH) cycles (RH-I: phase I, 3 weeks; RH-II: phase II, 6 weeks). Measurements were acquired on one coupon (cpn) after RH-I and on two coupons after RH-II. Dotted lines indicate position of maximum of white lines.

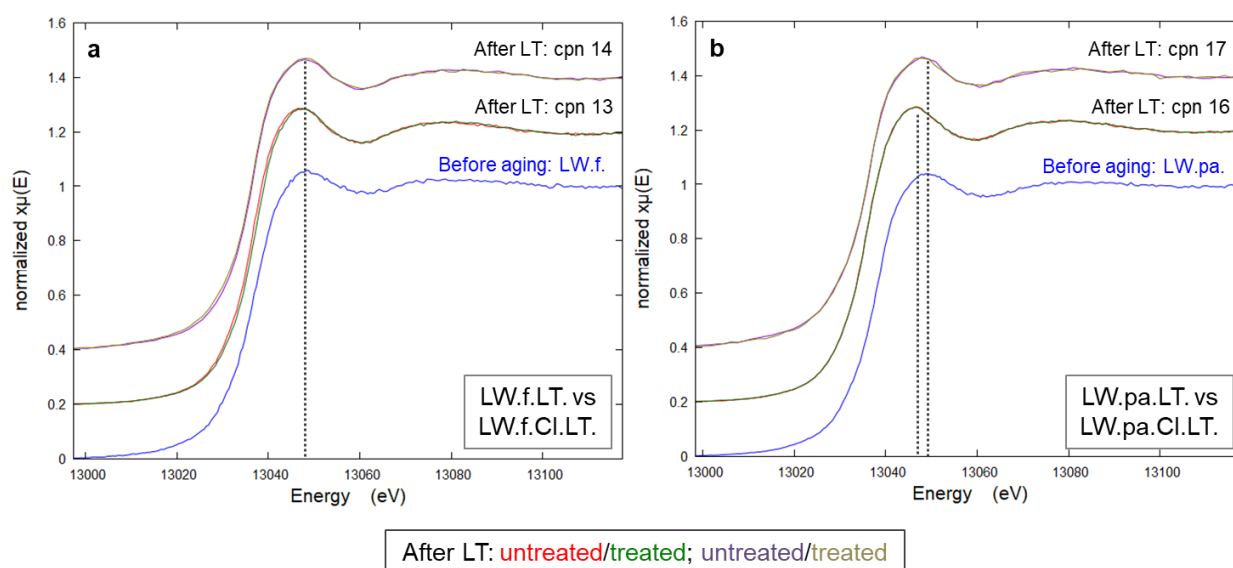
The edge positions for each spectrum as well as the difference in edge position for the untreated and treated areas after each aging step are shown in Table IV-17. The results indicate no significant difference between the untreated and the RW-treated zones in any of the aging steps, regardless of the initial state of the paint coating. The shape of the spectra after Phase I present a slightly narrower absorption maximum peak compared to the spectra in the initial state and after Phase II aging. Furthermore, less variability is observed between the replicate coupons after Phase II.

Table IV-17 Edge positions for untreated and RW-mixture treated zones of fresh and pre-aged lead white paint throughout RH aging process (left column); absolute value of the difference in edge position between spectra from the treated and untreated zones (middle column); edge shift with respect to initial state throughout RH aging process (right column). Cpn: coupon.

	Edge position E (eV)		$\Delta E =  treated-untreated $ (eV)	$\Delta E = E-E_{initial}$ (eV)	
	Untreated	Treated		Untreated	Treated
Initial (fresh)	13037.4	13037.4	0	0	0
Phase I (cpn7)	13036.1	13036.5	0.4	-1.3	-0.9
Phase II (cpn 7)	13036.6	13036.5	0.1	-0.8	-0.9
Phase II (cpn 8)	13037	13036.8	0.2	-0.4	-0.6
Initial (pre-aged)	13038.4	13038.4	0	0	0
Phase I (cpn10)	13036.1	13035.9	0.2	-2.3	-2.5
Phase II (cpn 10)	13036.7	13036.6	0.1	-1.7	-1.8
Phase II (cpn 11)	13036.9	13036.8	0.1	-1.5	-1.6

### IV.V.V Fresh and pre-aged lead white paint from coupons treated with corrosion inhibitor and aged by light exposure (LW-f-CI-LT and LW-pa-CI-LT)

Fresh and pre-aged lead white-based paint coatings were aged by light exposure with or without treatment with the corrosion inhibitor NaC<sub>14</sub>. Figure IV-63 shows the XANES spectra of the paint in its initial state and after light exposure. The spectra of the untreated and treated zones are superimposed in each step for comparison.



**Figure IV-63 Normalized XANES spectra of fresh (a) and pre-aged (b) lead white (LW) paint untreated/treated with corrosion inhibitor (CI) and aged by light (LT) exposure. Measurements were acquired on two replicate coupons (cpn). Dotted lines indicate position of maximum of white lines.**

The edge positions for each spectrum as well as the difference in edge position for the untreated and treated areas after each aging step are listed in Table IV-18. The results indicate no significant difference in terms of edge position between the untreated and the NaC<sub>14</sub>-treated zones in any of the aging steps. However, differences in the position of the white line and the shape of the spectra are observed after aging. This is especially evident in the pre-aged paint samples (Figure IV-63 b). Coupon 16 shows a shift after aging of about -2.4 eV while coupon 17 shows a shift of -1.8 eV, giving a difference of about 0.6 eV between the two. In addition, their respective white lines are slightly different around the maximum (in position and shape). This difference may be explained by a possible change in the Pb local environment as time passes post-light exposure since XANES measurements were performed on coupon 16 one month after light exposure aging while coupon 17 was analysed one year and four months after the end of the light aging.



Table IV-18 Edge positions for the untreated and NaC<sub>14</sub> treated zones of fresh and pre-aged lead white paint before and after light exposure (left column); absolute value of the difference in edge position between spectra from the treated and untreated zones (middle column); edge shift with respect to initial state throughout RH aging process (right column). Cpn: coupon.

	Edge position E (eV)		$\Delta E =  treated-untreated $ (eV)	$\Delta E = E-E_{initial}$ (eV)	
	Untreated	Treated		Untreated	Treated
Initial (fresh)	13037.4	13037.4	0	0	0
Phase I (cpn13)	13037	13037.4	0.4	-0.4	0
Phase I (cpn 14)	13036.8	13036.7	0.1	-0.6	-0.7
Initial (pre-aged)	13038.4	13038.4	0	0	0
Phase I (cpn16)	13036	13035.9	0.1	-2.4	-2.5
Phase I (cpn 17)	13036.6	13036.6	0	-1.8	-1.8

#### IV.V.VI Fresh and pre-aged lead white paint treated with resin-wax mixture and aged by light exposure (LW-f-RW-LT and LW-pa-RW-LT)

Fresh and pre-aged lead white paint was aged by light exposure in the presence or not of the resin-wax mixture. Figure IV-64 shows the XANES spectra of the paint in its initial state and after light aging. The spectra of the untreated and treated zones are superimposed in each step for comparison.

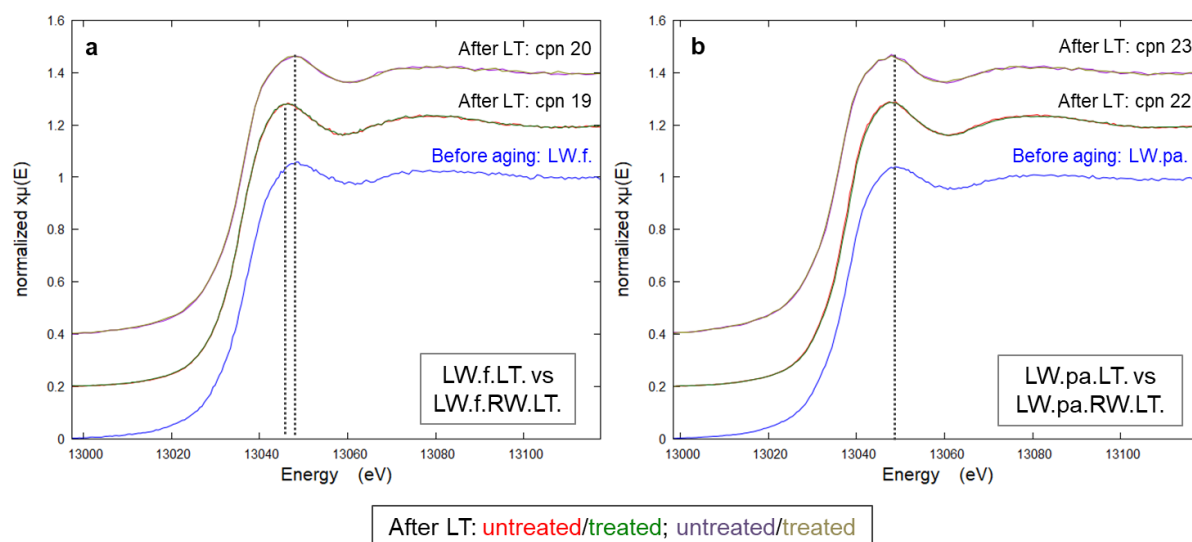


Figure IV-64 Normalized XANES spectra of fresh (a) and pre-aged (b) lead white (LW) paint untreated/treated with resin-wax mixture (RW) and aged by light (LT) exposure. Measurements were acquired on two replicate coupons (cpn). Dotted lines indicate position of maximum of white lines.

The edge positions for each spectrum as well as the difference in edge position for the untreated and treated areas after each aging step are shown in Table IV-19. No difference is detected between the untreated and treated zones at any point of aging, although some variability between replicate coupons

is observed. A small difference of about +0.5 eV is measured between the edge positions of coupon 20 and coupon 19 (fresh paint) and there is a difference in the shape around the maximum of the white line (max 13046.3 eV for coupon 19 and 13047.7 for coupon 20). In the pre-aged paint case, coupon 22 does not show a significant shift from the initial state, while coupon 23 shows an edge shift of -2.4 eV. Furthermore, the shape of the white lines and first oscillations are different.

**Table IV-19** Edge positions for the untreated and RW-treated zones of fresh and pre-aged lead white paint before and after light exposure (left column); absolute value of the difference in edge position between spectra from the treated and untreated zones (middle column); edge shift with respect to initial state throughout RH aging process (right column). Cpn: coupon.

	Edge position E (eV)		$\Delta E =  treated-untreated $ (eV)	$\Delta E = E-E_{initial}$ (eV)	
	<i>Untreated</i>	<i>Treated</i>		<i>Untreated</i>	<i>Treated</i>
Initial (fresh)	13037.4	13037.4	0	0	0
Phase I (cpn19)	13035.9	13035.8	0.1	-1.5	-1.6
Phase I (cpn 20)	13036.4	13036.2	0.2	-1	-1.2
Initial (pre-aged)	13038.4	13038.4	0	0	0
Phase I (cpn22)	13038.2	13038.1	0.1	-0.2	-0.3
Phase I (cpn 23)	13036	13036	0	-2.4	-2.4

## IV.V.VII Conclusions on the XANES analyses of the lead white-based paint coatings

The XANES spectra acquired on the lead white-based paint coatings show very small differences (close to the energy resolution). However, some trends were noticed and are listed here:

- A significant change in the edge position between the fresh and pre-aged initial states.
- Very small changes in the absorption edge energy position during the artificial aging experiments.
- Occasionally, the spectra present differences in the shape and amplitude of the white line and first EXAFS oscillation.
- No significant difference between the untreated and treated zones at any point during the aging experiments.

Additionally, some variability was observed between replicate sample measurements. It is possible that the aging conditions were not endured in a homogeneous way for all model coupons. In the case of the coupons aged by light exposure, the replicate coupons were not measured at the same time and the resulting XANES spectra show structural differences. This suggests that the structure of the paint coatings changed as time elapsed after the artificial aging processes, so that replicate samples measured at different times after aging were not comparable. It would be interesting to continue this study by measuring the painted coupons at set intervals (ex. every six months) to monitor for possible changes that may occur due to natural aging.

The changes observed may be explained by some modification of the Pb local environment or that new Pb alteration products have formed; however, the differences are too small to reach a definitive conclusion. In addition, due to the similarity of the characteristic XANES spectra of different Pb(II) compounds, it is difficult to characterise new phases unless they have formed in sufficient quantity to significantly change the shape of the measured XANES spectra. This suggests that more time or more intense aging conditions are required to change the Pb environment in our model painted metal coupons.

## IV.VI Summary of the evolution of untreated and treated painted metal coupons throughout artificial aging

In the following tables, the difference between the results obtained on the treated and untreated zones of the paint coatings are summarised for each technique. This assessment of differences permits to evaluate the effect of the presence of the applied treatment.

### IV.VI.I Aging by relative humidity

The comparisons of the untreated and treated zones on the linseed oil-coated coupons are listed in Table IV-20. The treated zones on the linseed oil-coated metal coupons present a different aspect (white colour, visible brush strokes) to the untreated zones after application of the treatment and before aging; a colour difference is also perceptible by colorimetry. After Phases I and II of relative humidity aging, the treated zones do not appear visually different from the untreated zones, except for in the case of the pre-aged linseed oil coating treated with the resin-wax mixture. However, a colour difference was detected by colorimetry in all cases after Phase II of aging.

The comparison of the treated zones to the untreated zones on the lead white-painted metal coupons after each step of RH aging (Table IV-21) shows that no major differences were detected. The colorimetry analysis indicates a colour difference after Phase I and II of RH aging for the lead white-painted coupons treated the corrosion inhibitor, as well as for the fresh lead white-painted coupon treated with the resin-wax mixture. However, these colorimetric differences were not visible by macro-observation (photography) and must therefore not be representative of the entire painted surfaces.

The visual observations of the chrome green oxide-painted metal coupons after RH aging (Table IV-22) show no difference between the untreated and corrosion inhibitor-treated zones. In one case (CrGO.pa.Cl.RH), the colorimetric measurements indicated a noticeable difference in colour. The FTIR results reveal that the zone treated by the corrosion inhibitor has not aged in the same way as the untreated paint coating: the treatment appears to inhibit the formation of a carboxylate species. The CrGO-painted coupons treated with the RW mixture show a visible difference between the untreated and treated zones both before and after the RH aging phases: the treated zones appear darker/more saturated in colour than the untreated zones. However, the measured differences in colour of the zones are less pronounced and below the threshold of perception. This may be due to the heterogeneity of the sample surface and the number of measurements acquired; we can assume that the calculated colour differences will become more representative of the painted surface with more measurements.

Due to overlap of the absorption of the RW treatment on diagnostic aging bands of paint in the acquired FTIR spectra, a difference in the chemical structure between the two zones cannot be determined.

**Table IV-20 Observed differences between the untreated and treated zones for linseed oil-coated coupons aged by RH cycles.**

	Experimental coupon series (LO-binder reference coupons)			
Technique	LO-f-CI-RH	LO-pa-CI-RH	LO-f-RW-RH	LO-pa-RW-RH
Photography	<p><b>Before aging:</b> visible differences (treated zone has white colour)</p> <p><b>After Phase I aging:</b> no visible difference</p> <p><b>After Phase II aging:</b> no visible difference</p>	<p><b>Before aging:</b> visible differences (treated zone has white colour)</p> <p><b>After Phase I aging:</b> no visible difference</p> <p><b>After Phase II aging:</b> no visible difference</p>	<p><b>Before aging:</b> visible differences (treated zone is opaque in thicker areas)</p> <p><b>After Phase I aging:</b> no visible difference</p> <p><b>After Phase II aging:</b> no visible difference</p>	<p><b>Before aging:</b> visible differences (treated zone is opaque in thicker areas)</p> <p><b>After Phase I aging:</b> visible difference (treated zone is more saturated)</p> <p><b>After Phase II aging:</b> visible difference (treated zone is more saturated)</p>
Colorimetry	<p><b>Before aging:</b> above noticeable difference threshold</p> <p><b>After Phase I aging:</b> above noticeable difference threshold</p> <p><b>After Phase II aging:</b> above noticeable difference threshold</p>	<p><b>Before aging:</b> above noticeable difference threshold</p> <p><b>After Phase I aging:</b> below noticeable difference threshold</p> <p><b>After Phase II aging:</b> above noticeable difference threshold</p>	<p><b>Before aging:</b> above noticeable difference threshold</p> <p><b>After Phase I aging:</b> above noticeable difference threshold</p> <p><b>After Phase II aging:</b> above noticeable difference threshold</p>	<p><b>Before aging:</b> above noticeable difference threshold</p> <p><b>After Phase I aging:</b> below noticeable difference threshold</p> <p><b>After Phase II aging:</b> above noticeable difference threshold</p>

Chapter IV A multi-scale analytical study of the effects of conservation treatments on the aging of model painted metal surfaces

Table IV-21 Observed differences between the untreated and treated zones for lead white (LW)-painted coupons aged by RH cycles.

	Experimental coupon series (LW-painted metal coupons)			
Technique	LW-f-CI-RH	LW-pa-CI-RH	LW-f-RW-RH	LW-pa-RW-RH
Photography	<p><b>Before aging:</b> no visible difference.</p> <p><b>After Phase I aging:</b> no visible difference.</p> <p><b>After Phase II aging:</b> no visible difference.</p>	<p><b>Before aging:</b> no visible difference.</p> <p><b>After Phase I aging:</b> no visible difference.</p> <p><b>After Phase II aging:</b> no visible difference.</p>	<p><b>Before aging:</b> no visible difference.</p> <p><b>After Phase I aging:</b> no visible difference.</p> <p><b>After Phase II aging:</b> no visible difference.</p>	<p><b>Before aging:</b> no visible difference.</p> <p><b>After Phase I aging:</b> no visible difference.</p> <p><b>After Phase II aging:</b> no visible difference.</p>
Colorimetry	<p><b>Before aging:</b> below noticeable difference threshold</p> <p><b>After Phase I aging:</b> above noticeable difference threshold</p> <p><b>After Phase II aging:</b> above noticeable difference threshold</p>	<p><b>Before aging:</b> below noticeable difference threshold</p> <p><b>After Phase I aging:</b> above noticeable difference threshold</p> <p><b>After Phase II aging:</b> above noticeable difference threshold</p>	<p><b>Before aging:</b> below noticeable difference threshold</p> <p><b>After Phase I aging:</b> above noticeable difference threshold</p> <p><b>After Phase II aging:</b> below noticeable difference threshold</p>	<p><b>Before aging:</b> below noticeable difference threshold</p> <p><b>After Phase I aging:</b> below noticeable difference threshold</p> <p><b>After Phase II aging:</b> below noticeable difference threshold</p>
FTIR	<p><b>Before aging:</b> not measured.</p> <p><b>After Phase I aging:</b> no difference (data not shown).</p> <p><b>After Phase II aging:</b> No observable difference.</p>	<p><b>Before aging:</b> not measured.</p> <p><b>After Phase I aging:</b> no difference (data not shown).</p> <p><b>After Phase II aging:</b> No observable difference.</p>	<p><b>Before aging:</b> not measured.</p> <p><b>After Phase I aging:</b> no difference (data not shown).</p> <p><b>After Phase II aging:</b> No observable difference.</p>	<p><b>Before aging:</b> not measured.</p> <p><b>After Phase I aging:</b> no difference (data not shown).</p> <p><b>After Phase II aging:</b> No observable difference.</p>
XANES Pb L <sub>3</sub> -edge	<p><b>Before aging:</b> not measured.</p> <p><b>After Phase I aging:</b> no significant difference.</p> <p><b>After Phase II aging:</b> no significant difference.</p>	<p><b>Before aging:</b> not measured.</p> <p><b>After Phase I aging:</b> no significant difference.</p> <p><b>After Phase II aging:</b> no significant difference.</p>	<p><b>Before aging:</b> not measured.</p> <p><b>After Phase I aging:</b> no significant difference.</p> <p><b>After Phase II aging:</b> no significant difference.</p>	<p><b>Before aging:</b> not measured.</p> <p><b>After Phase I aging:</b> no significant difference.</p> <p><b>After Phase II aging:</b> no significant difference.</p>

Table IV-22 Observed differences between the untreated and treated zones for chrome green oxide-painted coupons aged by RH cycles.

	Experimental coupon series (CrGO-painted metal coupons)			
Technique	CrGO-f-CI-RH (cpn 62)	CrGO-pa-CI-RH	CrGO-f-RW-RH (cpn 63)	CrGO-pa-RW-RH
Photography	<p><b>Before aging:</b> no visible difference</p> <p><b>After Phase I aging:</b> no visible difference</p> <p><b>After Phase II aging:</b> no visible difference</p>	<p><b>Before aging:</b> no visible difference</p> <p><b>After Phase I aging:</b> no visible difference</p> <p><b>After Phase II aging:</b> no visible difference</p>	<p><b>Before aging:</b> no visible difference</p> <p><b>After Phase I aging:</b> visible difference</p> <p><b>After Phase II aging:</b> visible difference</p>	<p><b>Before aging:</b> visible difference</p> <p><b>After Phase I aging:</b> visible difference</p> <p><b>After Phase II aging:</b> visible difference (but less than in previous steps)</p>
Colorimetry	<p><b>Before aging:</b> below noticeable difference threshold</p> <p><b>After Phase I aging:</b> below noticeable difference threshold</p> <p><b>After Phase II aging:</b> below noticeable difference threshold</p>	<p><b>Before aging:</b> below noticeable difference threshold</p> <p><b>After Phase I aging:</b> below noticeable difference threshold</p> <p><b>After Phase II aging:</b> above noticeable difference threshold</p>	<p><b>Before aging:</b> below noticeable difference threshold</p> <p><b>After Phase I aging:</b> (just) noticeable difference.</p> <p><b>After Phase II aging:</b> below noticeable difference threshold</p>	<p><b>Before aging:</b> below noticeable difference threshold</p> <p><b>After Phase I aging:</b> below noticeable difference threshold</p> <p><b>After Phase II aging:</b> below noticeable difference threshold</p>
FTIR	<p><b>Before aging:</b> Not measured.</p> <p><b>After Phase I aging:</b> no difference (data not shown).</p> <p><b>After Phase II aging:</b> different</p>	<p><b>Before aging:</b> Not measured.</p> <p><b>After Phase I aging:</b> no difference (data not shown).</p> <p><b>After Phase II aging:</b> different</p>	<p><b>Before aging:</b> Not measured.</p> <p><b>After Phase I aging:</b> no difference (data not shown).</p> <p><b>After Phase II aging:</b> cannot be deduced</p>	<p><b>Before aging:</b> Not measured.</p> <p><b>After Phase I aging:</b> no difference (data not shown).</p> <p><b>After Phase II aging:</b> cannot be deduced</p>

## IV.VI.II Aging by light exposure

The comparisons of the untreated and treated zones on the linseed oil-coated coupons are listed in Table IV-23. The treated zones on the linseed oil-coated metal coupons present a different aspect (white colour, visible brush strokes) to the untreated zones after application of the treatment and before aging; a colour difference is also perceptible by colorimetry. The results show that light exposure had a bleaching effect on the linseed oil coating, although this effect was observed to a lesser extent for the zones treated with the RW mixture. The zones treated with the corrosion inhibitor do not appear to have aged differently to the untreated zones, although a “noticeable” difference was measured by colorimetry.

**Table IV-23 Observed differences between the untreated and treated zones for linseed oil coated coupons aged by light (LT) exposure.**

	Experimental coupon series (LO-binder reference coupons)			
Technique	LO-f-CI-LT	LO-pa-CI-LT	LO-f-RW-LT	LO-pa-RW-LT
Photography	<b>Before aging:</b> visible differences (treated zone has white colour) <b>After aging:</b> no visible difference	<b>Before aging:</b> visible differences (treated zone has white colour) <b>After aging:</b> no visible difference	<b>Before aging:</b> visible differences (treated zone is opaque in thicker areas) <b>After aging:</b> visible difference (treated zone is more saturated)	<b>Before aging:</b> visible differences (treated zone is opaque in thicker areas) <b>After aging:</b> visible difference (treated zone is more saturated)
Colorimetry	<b>Before aging:</b> above noticeable difference threshold <b>After aging:</b> above noticeable difference threshold	<b>Before aging:</b> above noticeable difference threshold <b>After aging:</b> above noticeable difference threshold	<b>Before aging:</b> above noticeable difference threshold <b>After aging:</b> below noticeable difference threshold	<b>Before aging:</b> above noticeable difference threshold <b>After aging:</b> above noticeable difference threshold

Before light aging, the treated zones on the lead white-painted coupons do not appear visually different from the untreated zones; the same result is obtained in the colorimetric measurements (see Table IV-24). After aging, differences are mainly seen in the RW-treated zones which retained the original yellow hue in contrast to the untreated zones that were bleached by the light exposure. This colour difference is confirmed by colorimetry. A colorimetric difference is also detected in the case of the fresh paint treated with corrosion inhibitor, although this was not observed during the visual assessment. The FTIR analysis shows a difference in composition after aging between the two zones in all cases: the treatments were found to prevent the degradation of the organic structure of the paint. Finally, the XANES analysis of the lead environment at the Pb L<sub>3</sub>-edge did not show any significant difference in aging between the untreated and treated zones.



Table IV-24 Observed differences between the untreated and treated zones for lead white-painted coupons aged by light (LT) exposure.

	Experimental coupon series (LW-painted metal coupons)			
Technique	LW-f-CI-LT	LW-pa-CI-LT	LW-f-RW-LT	LW-pa-RW-LT
Photography	<b>Before aging:</b> no visible difference <b>After aging:</b> no visible difference	<b>Before aging:</b> no visible difference <b>After aging:</b> no visible difference	<b>Before aging:</b> no visible difference <b>After aging:</b> visible difference (untreated zone has become whiter, treated zone has retained yellow colour)	<b>Before aging:</b> no visible difference <b>After aging:</b> visible difference (untreated zone has become whiter, treated zone has retained yellow colour)
Colorimetry	<b>Before aging:</b> below noticeable difference threshold <b>After aging:</b> above noticeable difference threshold	<b>Before aging:</b> below noticeable difference threshold <b>After aging:</b> below noticeable difference threshold	<b>Before aging:</b> below noticeable difference threshold <b>After aging:</b> above noticeable difference threshold	<b>Before aging:</b> below noticeable difference threshold <b>After aging:</b> above noticeable difference threshold
FTIR	<b>Before aging:</b> not measured. <b>After aging:</b> difference in intensity of bands is observed.	<b>Before aging:</b> not measured. <b>After aging:</b> Difference in intensity of bands is observed.	<b>Before aging:</b> not measured. <b>After aging:</b> Difference in intensity of bands is observed.	<b>Before aging:</b> not measured. <b>After aging:</b> difference in intensity of bands is observed.
XANES Pb L <sub>3</sub> -edge	<b>Before aging:</b> not measured. <b>After aging:</b> no significant difference	<b>Before aging:</b> not measured. <b>After aging:</b> no significant difference	<b>Before aging:</b> not measured. <b>After aging:</b> no significant difference	<b>Before aging:</b> not measured. <b>After aging:</b> no significant difference

The comparisons (Table IV-25) of the results obtained on the pre-aged chrome green oxide-painted coupons (fresh versions were not tested) show no differences in aging between the two zones in the case of treatment with the corrosion inhibitor. For the coupons treated with RW, a visible difference is observed, where the treated zone appears darker than the untreated zone. Based on the comparison of the acquired FTIR spectra, no difference in the chemical structure after light aging was observed for either type of treatment.

Table IV-25 Observed differences between the untreated and treated zones for chrome green oxide-painted coupons aged by light (LT) exposure.

	Experimental coupon series (CrGO-painted metal coupons)			
Technique	CrGO -f-CI-LT	CrGO-pa-CI-LT	CrGO-f-RW-LT	CrGO-pa-RW-LT
Photography		<p><b>Before aging:</b> no visible difference</p> <p><b>After Phase I aging:</b> no visible difference</p>		<p><b>Before aging:</b> visible difference (treated zone darker than untreated zone)</p> <p><b>After Phase I aging:</b> visible difference (treated zone darker than untreated zone)</p>
Colorimetry		<p><b>Before aging:</b> below noticeable difference threshold</p> <p><b>After aging:</b> (just) noticeable difference.</p>		<p><b>Before aging:</b> below noticeable difference threshold</p> <p><b>After aging:</b> (just) noticeable difference.</p>
FTIR		<p><b>Before aging:</b> not measured.</p> <p><b>After aging:</b> no difference of bands is observed.</p>		<p><b>Before aging:</b> not measured.</p> <p><b>After aging:</b> no difference of bands is observed.</p>

## IV.VII Discussion on the effects of the conservation treatments on the aging of model painted metal coupons

The results of the complementary analytical studies give insight into the modifications endured by the model painted metal coupons, both visually and chemically during the artificial aging processes. FTIR spectroscopy proved to be a powerful tool for comparing changes in the chemical structure of the paint coating, although some limitations related to the physical aspects of the analysed materials were encountered. Finally, the XANES study of the Pb environment in the lead white-painted coupons did not show any differences between the untreated and treated zones, explained most likely by the formation of only a low quantity of degradation products that did not permit their differentiation from the bulk material.

An important result is that neither of the conservation treatments were observed to interact with the paint coatings in a way that altered the paint composition. This gives a good indication at this stage of the study for their use as safe, non-reactive products for application on painted metal surfaces. In general, the corrosion inhibitor NaC<sub>14</sub> appears to have less of a protective effect on the aging of the paint coating, as expected. Treatment with the resin-wax mixture was found to protect the original aspect of the painted surface against the bleaching effects of light exposure. However, the detected formation of oxidation products in the light-aged resin-wax mixture suggests a limited lifetime for its protective properties. No significant change was observed in the composition of the resin-wax mixture after relative humidity cycles, inferring stability under the applied artificial RH aging conditions. Despite the inferred stability, its presence was not shown to have an inhibiting effect on the formation of metal carboxylates during the relative humidity cycles. This is explained by the inherent behaviour of the (specifically, lead white) paint coating to form lead soaps due to the reactivity of the pigment with the oil binder. Continued ageing by the application of further phases of climatic cycles could induce a state of degradation of the paint coating in which the effect of the treatments on aging might be observed.

Some questions remain from the results obtained in this study that are worth exploring to improve the understanding of the effect of the conservation treatments on the aging of the painted metal coupons. First, the formation of carboxylate bands in the FTIR spectra acquired on the CrGO-painted coupons after relative humidity aging is observed. This was attributed to a possible formation of chromium carboxylate species. The formation appears to be dependent on the initial state of the paint (fresh or pre-aged) and the presence of treatment appears to have an influence as well. To bring more insight to these observations, complementary analyses should be acquired to study the composition of the CrGO-paint coating during RH cycles. For example, XANES measurements at the Cr K edge could be acquired to probe possible changes in the local environment of Cr. GC-MS analysis of the paint coating would

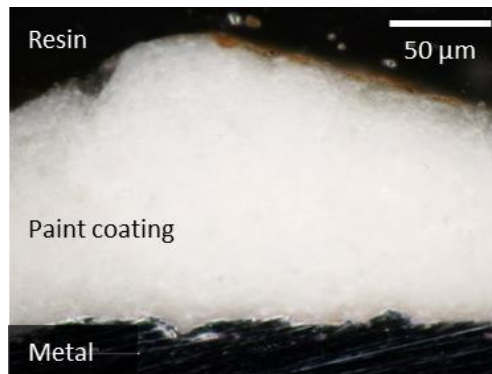
enhance the information acquired from the FTIR study: in particular, it could reveal the precise molecular composition of the organic components in the paint before and after aging (such as concentration and nature of free fatty acids) which would help to understand the aging processes. A past study on the water sensitivity of oil paints from the 20<sup>th</sup> century used GC-MS to show that the nature of the pigment has a strong effect on the curing of the binder and that the resulting composition will determine the paint coatings' sensitivity to moisture (Lee et al., 2018). In this study, they reported that an oil paint sample from 1945 containing chromium oxide was observed to be water sensitive and that this was linked to a high content of dicarboxylic acids; lead white-based paints, which were associated with high metal soap formation and low dicarboxylic acid content, were observed to be more stable to water. Additionally, GC-MS analysis of the resin-wax mixture after light exposure aging could be used to fully describe the oxidation products that were observed to form during the FTIR study.

With regards to the stability of the metal substrate underlying the paint coatings, only slight alterations were observed. First signs of corrosion were present in small, localized features such as cracks or fissures within the paint layer. As previously discussed, the applied aging conditions were most likely not enough to provoke a high level of degradation of the entire system, which may present itself as lifting of the paint due to under-layer corrosion processes or staining due to ferric ion migration. Therefore, we cannot comment on the effect of the presence of the conservation treatments on the evolution of the metal substrate based on the current state of the model coupons. Eventually with further aging of the coupons (either naturally or artificially), the influence of the applied treatments may become more apparent.

Eventually, more complex aging experiments that more closely resemble real conditions should be used to introduce other aging factors into the study of the protective effects of the conservation treatments. For example, one important factor that was not addressed in this study is the influence of environmental pollutants (of particulate or gaseous nature). It is crucial to understand what effect their presence may have on the protective abilities of the treatments. Glass slides have been placed in the storage facilities of the Musée des Arts et Métiers to collect particulate pollutants which will eventually be characterised in order to implement them into a future artificial aging study. As for gaseous pollutants, sensors will need to be installed to detect specific species.

To improve our understanding of the painted metal system as a whole, cross-sections of the model coupons should be obtained in order to acquire localized measurements within the stratigraphy. This would provide insight into changes occurring at the interface of the paint and the conservation treatment, within the bulk of the paint layer, and at the paint-metal interface. This approach was tested on a model coupon. Figure IV-65 shows a microscope image of the cross-section of the model coupon

with a lead white-based paint coating that was exposed to relative humidity cycles. Red-brown products are observed on the surface of the paint coating and most likely correspond to deposition of corrosion products during removal of the corrosion that formed on the unpainted edges of the coupons. Minimal amounts of corrosion are observed at the paint-metal interface, inferring that the coupons have not yet reached a high level of alteration under the imposed artificial climatic aging conditions. Moreover, this highlights the protective nature of the paint coating against the corrosive environmental conditions. The artificial aging should be continued before retrying this approach.



**Figure IV-65 Microscope image of the cross-section of the untreated zone of a pre-aged lead white painted-metal coupon after phase II of relative humidity aging cycles.**

Another aspect that should be addressed is the reversibility of the conservation treatments. To validate the use of these treatments on painted metal artifacts, their ease of removal from the artifact will need to be tested. The treated and aged painted metal coupons present an exemplary set of samples on which to conduct reversibility testing that mimics the removal of conservation treatments from historic painted metal objects. Once the different criteria for an ideal conservation treatment have been tested and proven, these strategies will be validated from a chemical inertness and practicality point of view, improving the confidence of their use for the conservation and restoration of painted metal artifacts.

# General conclusions and perspectives



This thesis addresses the question of the conservation of painted metals of industrial and technical heritage that are often found in museum collections. The presence of these objects in everyday life and for various applications greatly increased when improvements in the efficiency of their production began during the Industrial Revolution of the 18<sup>th</sup>-19<sup>th</sup> centuries. Depending on the nature of the metal, the structure is more or less susceptible to corrosion processes which can lead to degradation and loss of function. Iron and steel, which are often used as metallic substrates for technical applications, are prone to spontaneous oxidation, leading to the formation of a surface layer of corrosion products. To prevent corrosion, paint coatings have long been applied to metal substrates to act as a protective barrier against environmental factors such as moisture, oxygen, and pollutants. In addition to the protective role of the paint coating, it can also have a decorative function which can be seen in the choice of colour, artistic detailing, or inscriptions on the surface of the object. However, the paint coating itself is a complex system of inorganic and organic components that can lose its protective and/or aesthetic properties over time due to either its own degradation phenomena, or due to the degradation of the underlying metallic substrate. The complicated and intertwined alteration processes of the paint coating and the metal exacerbate the possible structural and material states of the painted metal system over time.

Given the composite and variable nature of the aged painted metal system, the approach taken towards their conservation is challenging because it must consider the sensitivities of all the components present. The current strategies in place in the conservation-restoration field often include treating the origin of the observed alteration, such as stabilizing corrosion products on the metal support or consolidating the degraded paint layer, as well as reducing future alteration by applying a protective transparent coating (varnish). However, these strategies are often adapted from conservation treatments used on either metal or paint alone and have not been extensively investigated to validate their implementation on the full painted metal system.

Based on the challenges presented above, this thesis work was designed to improve the current understanding of historic painted metal artefacts dating from the 19<sup>th</sup>-early 20<sup>th</sup> centuries and to investigate strategies for their conservation through two main research themes, or axes. The first axis addresses the general lack of documentation and research into the historical formulations and techniques used for paint coatings on metallic objects of technical heritage, and on their characteristic alteration phenomena; the study is presented in Chapter 3. This was accomplished by conducting a multi-scale description of historic painted metal objects from the collections of the Musée des Arts et Métiers in Paris, France. The material composition and state of conservation of the objects were described from a global perspective before completing an analytical characterisation of micro-samples of paint and corrosion products collected from altered areas on a corpus of nine painted iron objects.



The most representative samples were prepared as cross-sections to observe their layer structure. The samples show a variety of stratigraphic structures: some have only one paint layer, but most contain multiple layers that can vary in thickness and in colour. In some cases, it was difficult to determine the role of the paint coatings (protective, decorative) and whether they were original or repainted based only on these initial observations. Due to the complex structure and composition of the samples, a combination of analytical techniques was employed to collect complementary information at different scales of observation: the morphology of the layers was studied using light and fluorescence microscopy, scanning electron microscopy (SEM), and synchrotron deep-UV photoluminescence (DUV-PL) imaging; the elemental composition was determined using synchrotron micro-X Ray Fluorescence (XRF) and Energy Dispersive X-ray Spectroscopy coupled to SEM (SEM-EDS); and finally, the structural characterisation of the components was accomplished using micro-Raman spectroscopy, micro-X-Ray Absorption Near-Edge Structure Spectroscopy (XANES), and Gas Chromatography coupled to Mass Spectrometry (GC-MS). The use of imaging modes and point analysis allowed to obtain specific information about the distribution of the components within the stratigraphy.

The comparison of the complementary data acquired from this methodology allowed for the successful identification of the pigments and additives present as well as their location within the paint coating stratigraphy. The identified compounds are mainly traditional pigments that are typical of the historical period of study. The most modern pigments identified were phthalocyanine blue and green, which were introduced in the mid-1930s. They were identified on an artefact dating from circa 1945, which is slightly later than our intended period of study. Of particular interest was the detection of pigments with anticorrosive properties, such as red lead, lithopone, and other lead and zinc-containing pigments, which were found mainly in layers directly in contact with the metal substrate. These observations give evidence of the historical techniques used for the preparation of protective primer coatings for iron substrates. Finally, it should be noted that many of the pigments contain heavy metals like lead, chromium and mercury which have been progressively phased out since the mid-20<sup>th</sup> century due to their toxicity.

The characterisation of the binders revealed a mixture of fatty acids, including palmitic, stearic, and azelaic acids. Additionally, some samples also contain components related to the composition of resins (in particular, oxidation products of abietic acid). The fatty acids suggest the presence of an oxidised drying oil and the abietic acid derivatives suggest a resin from the *Pinaceae* family, such as colophony or Venice turpentine. From this we can deduce that the paint coatings have a mainly oil-based composition, where the oil is most likely a linseed oil based on historical references. The presence of resin biomarkers raises the question of its intended role in the acquired paint samples, as it may have been included as a component of the binder or as a varnish. No varnish layer of significant thickness was

observed in the studied cross-sections, but this does not exclude the possible presence of thin or degraded varnish layers. This information is important for understanding the historical techniques used in producing and conserving these types of objects, and therefore more conclusive studies on the nature and distribution of the organic components in the paint layers should be conducted in the future, as was discussed in Chapter 3.

The analytical characterisation study also allowed for the description and investigation of the alteration phenomena involved in the degradation of the painted iron system. Some identifications could immediately be associated to alteration processes, such as the identification of azelaic acid, a marker of an oxidised drying oil. Similarly, corrosion products, when present in the collected micro-sample, are indicative of the oxidation of the iron-based substrate underlying the paint coating. The identified phases (in majority, iron oxyhydroxides goethite and lepidocrocite) are typical of the composition of a corrosion layer formed by indoor atmospheric corrosion conditions. The analytical investigation of the corrosion layer is limited in the studied samples by the lack of the full painted metal stratigraphy: without the metal-corrosion layer interface, the full extent of the corrosion processes occurring under the paint layers cannot be apprehended in a representative way. However, some effects on the paint coating due to the formation of a corrosion layer were still observed. In a few cases, paint layers were noted to have bent out of their planar form due to the mechanical stress exerted by the increase in volume of the corrosion products. Formation of corrosion products within the paint layer, linked to the migration of iron ions in areas of lower ionic resistance, led sometimes to visual alterations such as staining in lighter-coloured paint layers. These preliminary observations demonstrate the idea that the alteration of the painted metal system is an interrelated series of processes and underline the need for a characterisation of the processes occurring at the metal substrate-corrosion layer-paint layer interfaces.

Based on the initial characterisations of the pigment and binder components of the paint layer, it was hypothesized that samples containing red lead pigment (or other pigments known to form metal soap aggregates in oil paint) may present signs of metal soap aggregation or other forms of associated degradation phenomena. Some of the studied paint layers composed of red lead oil paint do indeed present a heterogeneous morphology in which aggregate-like shapes were observed, suggesting the formation of metal soap clusters. It is important to verify the nature and reactivity of metal soap aggregates in the paint layers for metallic heritage due to their known risk for paint degradation. Furthermore, the structural changes induced in the paint coating by metal soap aggregation will undoubtedly influence the barrier properties of the paint layers, in particular red lead-containing primers whose primary role on iron substrates is corrosion control. More research will need to be

devoted to the effect that metal soap aggregation in paint layers may have on the degradation of the painted metal system.

The second research axe of this thesis work addresses conservation strategies used for painted metal artefacts. The aim is to replace the most commonly used approaches, which have often been borrowed from treatments used for metals or paints alone and are not always adapted to the needs of the full painted metal system. The study, presented in Chapter 4, investigated the protective properties of two types of conservation treatments that fulfill the requirements for use on painted metal artefacts and have shown promising protective and aesthetic qualities when used on historic artefacts. The treatments tested in this study were also chosen because they have different protection mechanisms. The first, a solution of 0.05 M NaC<sub>14</sub> sodium carboxylate solution, stabilizes the metal substrate by creating a thin passivation layer against further corrosion, while the second is a mixture of resin and wax (30:10 wt% Regalrez 1126®-Cosmoloid H80®) and acts as a transparent barrier coating against environmental degradation factors. In practice, the object will first be treated locally with the corrosion inhibitor before applying a general transparent surface coating for overall protection. To improve the confidence in the use of these treatments, they must be shown to be inert towards the painted metal system both at the moment of application and in the long term. The first step towards fully understanding the long-term efficiency of the treatments was to study a simplified system through the use of model samples and controlled aging conditions. Model painted iron coupons were prepared on which different experimental parameters could be tested, including pigment type, initial state of alteration, type of conservation treatment and specific aging conditions. The paint coatings chosen for our study consist of either lead white pigment or chrome green oxide pigment in a linseed oil binder; the pigments were chosen in order to represent light and dark-coloured paint coatings so that different types of visual alterations could be observed. The coupons were subjected to one of two artificial aging methods chosen for our study: relative humidity cycles or light exposure. The visual and structural evolution of the painted metal coupons in the presence or absence of treatment was monitored using several complementary analytical techniques, including photography, colorimetry, FTIR spectroscopy and micro-XANES.

The comparison of the complementary data allowed to evaluate the protective effect of the treatments on the painted metal system. Neither of the treatments were observed to interact with the paint coatings in a detectable manner, both upon application and after artificial aging, which improves the confidence in their ability to be used as inert and potentially reversible treatments for painted metals. The corrosion inhibitor NaC<sub>14</sub> was not observed to have a protective effect on aging of paint, as expected since its main role is to treat corroded areas of the metal support. The transparent resin-wax mixture was observed to protect the original visual aspect of the paint coating against the bleaching effects of

light exposure; this appears to be a sacrificial mode of protection due to the detection of oxidation products in the resin-wax mixture coating after aging by light exposure. This also implies a limited lifetime for its protective abilities since it degrades in the presence of light. In contrast, no degradation of the resin-wax mixture was observed under the applied relative humidity cycles. Despite its stability in the imposed aging conditions, its presence did not have a significant protective effect on the aging processes of the paint coatings. This is most likely due to the fact that the observed aging phenomena (formation of metal carboxylates) are partly inherent (i.e. independent of imposed climatic aging conditions). Moreover, the applied aging parameters and duration may not have been enough to degrade the paint to an extent in which a difference in aging linked to the presence of the resin-wax coating could be revealed. To further the investigation of the protective ability of the resin-wax mixture under relative humidity cycles, the aging experiments should continue to be applied to the model coupons to maximize their alteration.

This methodological approach provided new insights about the chemical behaviour and the protective effect of the tested conservation treatments for painted metal surfaces exposed to controlled aging conditions. However, it is acknowledged that model systems are not directly comparable to the complicated material composition of real, naturally aged artefacts. In the future, tests will need to be repeated on increasingly complex systems that more closely resemble the structural and compositional aspects of the historical samples characterised in the first research axe of this thesis. A first proposal is to introduce more accurate environmental conditions during the aging of the model samples. This includes introducing a parameter that was not addressed during this work: the presence of gaseous and particulate pollutants in the atmospheric environment. The nature and concentration of these species are specific to the environment of interest and studies will need to be developed that collect, identify, and quantify the characteristic species. This information can then be used to design artificial aging experiments that are more representative of the actual environmental conditions and to help elucidate the degrading effect of the pollutants on both the original materials and on the conservation treatments. The collection step of this proposed study has already been initiated during the course of this work by placing glass slides in the storage facilities of the Musée des Arts et Métiers in order to collect particulate matter. Alternative methods for the detection of gaseous pollutants, such as the installation of sensors, will need to be put in place. Eventually, this study should be expanded to include other types of metal substrates, such as copper and aluminum-based alloys. The conservation strategies may need to be adapted to better suit the properties of these other painted metal systems.

A final validation phase must be completed during which the proposed treatments will be tested on naturally altered historic objects to study the aesthetic compatibility, the protective effect, and the reversibility. This final step of treatment must be carried out under the supervision of conservation-

restoration professionals and the objects must be monitored in their normal environment (museum collections or storage facilities). Regular condition reports should be carried out using the same model as introduced in the first research axe of this thesis in close collaboration between physicochemists and conservation-restoration professionals. This process will allow the final validation of the protocol.

This work has established an analytical approach towards improving the strategies for the indoor conservation of painted metals artefacts. It has provided an extensive compilation of characteristic materials identified on painted iron objects of technical heritage, as well as a description and reflection on the historical techniques used for the production of the studied objects. It has also proposed hypotheses for possible alteration phenomena that could present a concern for the future conservation of the artefacts. While the focus of this work was on objects manufactured before the early 20<sup>th</sup> century, the analytical characterisation strategy should continue to be applied to more modern artefacts in order to expand the available documentation of historic manufacturing techniques used over the course of the 20<sup>th</sup> century. These objects will most likely present different paint coating formulations and structures, due notably to the developments in polymer chemistry over the 20<sup>th</sup> century which led to a greater variety of available synthetic binders. Furthermore, equivalent studies will need to be conducted for other types of painted metals in order to compare the results and understand how the materials and their associated alterations differ. Following the characterisation of these other types of objects, the studies conducted on the behaviour and efficiency of the conservation treatments will need to be continued on these new material systems to determine their suitability for conserving the full range of types of painted metal systems that can be found on artefacts in museum collections.

# Reference List

- 8 mai 1842: [Estampe] *Accident sur le chemin de fer de Versailles, Rive gauche*. (n.d.). s.n. Retrieved January 6, 2022, from <http://gallica.bnf.fr/ark:/12148/btv1b8414950k>
- Albini, M., Ridolfi, S., Giuliani, C., Pascucci, M., Staccioli, M. P., & Riccucci, C. (2020). Multi-Spectroscopic Approach for the Non-invasive Characterization of Paintings on Metal Surfaces. *Frontiers in Chemistry*, *8*, 289. <https://doi.org/10.3389/fchem.2020.00289>
- Appelbaum, B. (1987). Criteria for Treatment: Reversibility. *Journal of the American Institute for Conservation*, *26*(2), 65–73.
- Argyropoulos, V., Boyatzis, S. C., Giannoulaki, M., Guilminot, E., & Zacharopoulou, A. (2021). Organic Green Corrosion Inhibitors Derived from Natural and/or Biological Sources for Conservation of Metals Cultural Heritage. In E. Joseph (Ed.), *Microorganisms in the Deterioration and Preservation of Cultural Heritage* (pp. 341–367). Springer International Publishing. [https://doi.org/10.1007/978-3-030-69411-1\\_15](https://doi.org/10.1007/978-3-030-69411-1_15)
- Artesani, A., Gherardi, F., Nevin, A., Valentini, G., & Comelli, D. (2017). A Photoluminescence Study of the Changes Induced in the Zinc White Pigment by Formation of Zinc Complexes. *Materials*, *10*(4), 340. <https://doi.org/10.3390/ma10040340>
- Aze, S., Vallet, J.-M., Detalle, V., Grauby, O., & Baronnet, A. (2008). Chromatic alterations of red lead pigments in artworks: A review. *Phase Transitions*, *81*(2), 145–154. <https://doi.org/10.1080/01411590701514326>
- Bell, I. M., Clark, R. J. H., & Gibbs, P. J. (1997). Raman spectroscopic library of natural and synthetic pigments (Pre-1850 AD). *Spectrochimica Acta Part A: Molecular and Biomolecular Spectroscopy*, *53*, 2159–2179.
- Bellot-Gurlet, L., Neff, D., Réguer, S., Monnier, J., Saheb, M., & Dillmann, P. (2009). Raman Studies of Corrosion Layers Formed on Archaeological Irons in Various Media. *Journal of Nano Research*, *8*, 147–156. <https://doi.org/10.4028/www.scientific.net/JNanoR.8.147>
- Berrie, B. H., Feller, R. L., Roy, A., & FitzHugh, E. W. (2007). *Artists' Pigments: A Handbook of Their History and Characteristics* (B. H. Berrie, Ed.; Vol. 4). National Gallery of Art.
- Bierwagen, G. P. (1996). Reflections on corrosion control by organic coatings. *Progress in Organic Coatings*, *28*(1), 43–48. [https://doi.org/10.1016/0300-9440\(95\)00588-9](https://doi.org/10.1016/0300-9440(95)00588-9)
- Bonaduce, I., Carlyle, L., Colombini, M. P., Duce, C., Ferrari, C., Ribechini, E., Selli, P., & Tiné, M. R. (2012). New Insights into the Ageing of Linseed Oil Paint Binder: A Qualitative and Quantitative Analytical Study. *PLoS ONE*, *7*(11), e49333. <https://doi.org/10.1371/journal.pone.0049333>
- Bruggerhoff, S. (2007). Coatings for Industrial Heritage Surfaces—Between the Poles of Aesthetics and Durability. In S. Bruggerhoff (Ed.), *BigStuff '07: Beyond Conservation—Industrial Heritage Management* (pp. 27–29). <http://www.bergbaumuseum.de/web/aktuelles-veranstaltungen-2007-bigstuff>
- Burgio, L., & Clark, R. J. (2001). Library of FT-Raman spectra of pigments, minerals, pigment media and varnishes, and supplement to existing library of Raman spectra of pigments with visible

- excitation. *Spectrochimica Acta. Part A, Molecular and Biomolecular Spectroscopy*, 57(7), 1491–1521. [https://doi.org/10.1016/s1386-1425\(00\)00495-9](https://doi.org/10.1016/s1386-1425(00)00495-9)
- Burgio, L., Clark, R. J., & Firth, S. (2001). Raman spectroscopy as a means for the identification of plattnerite (PbO<sub>2</sub>), of lead pigments and of their degradation products. *The Analyst*, 126(2), 222–227. <https://doi.org/10.1039/b008302j>
- Buxbaum, E. G., & Pfaff, G. (2005). *Industrial Inorganic Pigments* (3rd ed.). WILEY-VCH.
- Caggiani, M. C., Cosentino, A., & Mangone, A. (2016). Pigments Checker version 3.0, a handy set for conservation scientists: A free online Raman spectra database. *Microchemical Journal*, 129, 123–132. <https://doi.org/10.1016/j.microc.2016.06.020>
- Canadian Conservation Institute. (2017, September 14). *Care of Paintings on Ivory, Metal and Glass – CCI Notes 10/14*. <https://www.canada.ca/en/conservation-institute/services/conservation-preservation-publications/canadian-conservation-institute-notes/care-paintings-ivory-metal-glass.html>
- Cano, E., & Lafuente, D. (2013). Corrosion inhibitors for the preservation of metallic heritage artefacts. In P. Dillmann, D. Watkinson, E. Angelini, & A. Adriaens (Eds.), *Corrosion and conservation of cultural heritage metallic artefacts* (pp. 570–594). Woodhead Publishing.
- Carlyle, L. (1999). Paint driers discussed in 19th-century British oil painting manuals. *Journal of the American Institute for Conservation*, 38(1), 69–82.
- Carlyle, L. (2001). *The Artist's Assistant: Oil painting instruction manuals and handbooks in Britain, 1800-1900, with reference to selected eighteenth-century sources*. Archetype Publications.
- Casadio, F., Keune, K., Noble, P., Van Loon, A., Hendriks, E., Centeno, S. A., & Osmond, G. (Eds.). (2019). *Metal Soaps in Art: Conservation and Research*. Springer.
- Castorina, E., Ingall, E. D., Morton, P. L., Tavakoli, D. A., & Lai, B. (2019). Zinc K-edge XANES spectroscopy of mineral and organic standards. *Journal of Synchrotron Radiation*, 26, 1302–1309. <https://doi.org/10.1107/S160057751900540X>
- Chen-Wiegart, Y. K., Catalano, J., Williams, G. J., Murphy, A., Yao, Y., Zumbulyadis, N., Centeno, S. A., Dybowski, C., & Thieme, J. (2017). Elemental and Molecular Segregation in Oil Paintings due to Lead Soap Degradation. *Scientific Reports*, 7, 11656. <https://doi.org/10.1038/s41598-017-11525-1>
- Chua, L. (2019). Whitish haze, soapy globules: Micro-analysis of degraded burmese paintings on zinc supports. *Heritage Science*, 7(1), 46. <https://doi.org/10.1186/s40494-019-0287-5>
- Coccatto, A., Moens, L., & Vandenabeele, P. (2017). On the stability of mediaeval inorganic pigments: A literature review of the effect of climate, material selection, biological activity, analysis and conservation treatments. *Heritage Science*, 5(1), 12. <https://doi.org/10.1186/s40494-017-0125-6>
- Colombini, M. P., Modugno, F., Fuoco, R., & Tognazzi, A. (2002). A GC-MS study on the deterioration of lipidic paint binders. *Microchemical Journal*, 73(1–2), 175–185. [https://doi.org/10.1016/S0026-265X\(02\)00062-0](https://doi.org/10.1016/S0026-265X(02)00062-0)

## Reference List

- Corr, S. (2018). *Conservation-Restoration of Cultural Heritage in less than 1000 words*. Council of Europe. <https://rm.coe.int/strategy-21-conservation-restoration-of-cultural-heritage-in-less-than/16807bfbba>
- Cotte, M., Checroun, E., De Nolf, W., Taniguchi, Y., De Viguerie, L., Burghammer, M., Walter, P., Rivard, C., Salomé, M., Janssens, K., & Susini, J. (2017). Lead soaps in paintings: Friends or foes? *Studies in Conservation*, 62(1), 2–23. <https://doi.org/10.1080/00393630.2016.1232529>
- Daher, C. (2012). *Analyse par spectroscopies Raman et infrarouge de matériaux naturels organiques issus d'objets du patrimoine: Méthodologies et applications* [PhD Dissertation, Université Pierre et Marie Curie]. <https://tel.archives-ouvertes.fr/tel-00742851>
- Davidovich, R. L., Stavila, V., Marinin, D. V., Voit, E. I., & Whitmire, K. H. (2009). Stereochemistry of lead(II) complexes with oxygen donor ligands. *Coordination Chemistry Reviews*, 253(9–10), 1316–1352. <https://doi.org/10.1016/j.ccr.2008.09.003>
- Defeyt, C., Van Pevenage, J., Moens, L., Strivay, D., & Vandenabeele, P. (2013). Micro-Raman spectroscopy and chemometrical analysis for the distinction of copper phthalocyanine polymorphs in paint layers. *Spectrochimica Acta Part A: Molecular and Biomolecular Spectroscopy*, 115, 636–640. <https://doi.org/10.1016/j.saa.2013.04.128>
- Degrigny, C. (2011). *Protection temporaire d'Objets métalliques base fer et cuivre à l'aide d'Inhibiteurs de corrosion Non Toxiques: Application aux objets patrimoniaux techniques et scientifiques de grandes dimensions exposés en atmosphère non contrôlée* [Technical Report]. HE-Arc CR. <http://rgdoi.net/10.13140/RG.2.1.1057.6242>
- Degrigny, C., Argyropoulos, V., Pouli, P., Grech, M., Kreislova, K., Harith, M. A., Mirambet, F., Haddadh, N., Angelini, E., Cano, E., Hajjaji, N., Çilingiroğlu, A., Almansour, A., & Mahfoud, L. (2007). The methodology for the PROMET project to develop / test new non-toxic corrosion inhibitors and coatings for iron and copper alloy objects housed in Mediterranean museums. *METAL2007*, 5, 31–37.
- Degrigny, C., Morel, O., Morvan, J., Maire, J. M., & Boucard, S. (1995). Nettoyage et stabilisation de surfaces métalliques peintes: Application a la restauration d'une voiture autochenille. *Studies in Conservation*, 40(4), 227–236. <https://doi.org/10.2307/1506497>
- Dickens, B. (1965). The bonding in Pb<sub>3</sub>O<sub>4</sub> and structural principles in stoichiometric lead oxides. *Journal of Inorganic and Nuclear Chemistry*, 27, 1509–1515. [https://doi.org/10.1016/0022-1902\(65\)80011-2](https://doi.org/10.1016/0022-1902(65)80011-2)
- Dillmann, P., Leroy, S., Disser, A., Bauvais, S., Vega, E., & Fluzin, P. (2015). Dernières avancées des études sur la production, la circulation et la datation des métaux ferreux archéologiques. *Les nouvelles de l'archéologie*, 138, 28–34. <https://doi.org/10.4000/nda.2723>
- Erhardt, D., Tumosa, C. S., & Mecklenburg, M. F. (2005). Long-Term Chemical and Physical Processes in Oil Paint Films. *Studies in Conservation*, 50(2), 143–150. <https://doi.org/10.2307/25487732>
- Feller, R. L. (1994). *Accelerated Aging: Photochemical and Thermal Aspects*. <http://www.getty.edu/publications/virtuallibrary/0892361255.html>
- Feller, R. L., Roy, A., FitzHugh, E. W., & Berrie, B. H. (1986). *Artists' pigments: A handbook of their history and characteristics* (R. L. Feller, Ed.; Vol. 1). National Gallery of Art.



- Fink, F. (1922). *Nouveau manuel complet de peinture et vernissage des métaux et du bois* (M. S. Lacombe, Ed.). Roret. <https://gallica.bnf.fr/ark:/12148/bpt6k939526j>
- FitzHugh, E. W., Feller, R. L., Roy, A., & Berrie, B. H. (1997). *Artists' Pigments: A Handbook of Their History and Characteristics* (E. W. FitzHugh, Ed.; Vol. 3). National Gallery of Art.
- Garrappa, S., Kočí, E., Švarcová, S., Bezdička, P., & Hradil, D. (2020). Initial stages of metal soaps` formation in model paints: The role of humidity. *Microchemical Journal*, *156*, 104842. <https://doi.org/10.1016/j.microc.2020.104842>
- Germinario, G., Werf, I. D. van der, & Sabbatini, L. (2015). Pyrolysis gas chromatography mass spectrometry of two green phthalocyanine pigments and their identification in paint systems. *Journal of Analytical and Applied Pyrolysis*, *115*, 175–183. <https://doi.org/10.1016/j.jaap.2015.07.016>
- Gervais, C., Languille, M.-A., Reguer, S., Gillet, M., Pelletier, S., Garnier, C., Vicenzi, E., & Bertrand, L. (2013). Why does Prussian blue fade? Understanding the role(s) of the substrate. *Journal of Analytical Atomic Spectrometry*, *28*(10), 1600–1609. <https://doi.org/10.1039/C3JA50025J>
- Gettens, R. J., Kühn, H., & Chase, W. T. (1967). Lead White. *Studies in Conservation*, *12*(4), 125–139. <https://doi.org/10.2307/1505410>
- Giuliani, A., Jamme, F., Rouam, V., Wien, F. F., Giorgetta, J.-L., Lagarde, B., Chubar, O., Bac, S., Yao, I., Rey, S., Herbeaux, C., Marlats, J.-L., Zerbib, D., Polack, F., & Réfrégiers, M. (2009). DISCO: A low-energy multipurpose beamline at synchrotron SOLEIL. *Journal of Synchrotron Radiation*, *16*(Pt 6), 835–841. <https://doi.org/10.1107/S0909049509034049>
- Goergen, P. (2007). Autour de la conservation et de la valorisation du patrimoine métallique de l'industrie en Guyane: Un projet de rencontres scientifiques et techniques. *InSitu*, *8*. <https://journals.openedition.org/insitu/3427>
- Goltz, D., McClelland, J., Schellenberg, A., Attas, M., Cloutis, E., & Collins, C. (2003). Spectroscopic Studies on the Darkening of Lead White. *Applied Spectroscopy*, *57*(11), 1393–1398. <https://doi.org/10.1366/000370203322554563>
- Gonzalez, V. (2016). *Caractérisation micro-structurale et luminescence des carbonates de plomb: Apport à la discrimination des pigments blancs de plomb des oeuvres peintes* [These de doctorat en chimie, UPMC - Université Paris 6 Pierre et Marie Curie]. <https://hal.archives-ouvertes.fr/tel-01621352>
- Graphic Communications Open Textbook Collective. (2015). Lab Colour Space and Delta E Measurements. In *Graphic Design and Print Production Fundamentals*. BCcampus. <https://opentextbc.ca/graphicdesign/chapter/4-4-lab-colour-space-and-delta-e-measurements/>
- Greenspan, L. (1977). Humidity Fixed Points of Binary Saturated Aqueous Solutions. *Journal of Research of the National Bureau of Standards - A. Physics and Chemistry*, *81A*(1), 89–96.
- Hansen, A. K., Christiansen, M. B., Sanyova, J., & Simonsen, K. P. (2018). Analysis of Poul Gernes' painted folding doors at Herlev Hospital. *Heritage Science*, *6*(1), 29. <https://doi.org/10.1186/s40494-018-0196-z>

## Reference List

- Hermans, J., Keune, K., van Loon, A., & Iedema, P. (2016). The crystallization of metal soaps and fatty acids in oil paint model systems. *Phys. Chem. Chem. Phys.*, *18*, 10896. <https://doi.org/10.1039/C6CP00487C>
- Hermans, J., Keune, K., van Loon, A., Stols, M., Corkery, R., & Iedema, P. (2014). The synthesis of new types of lead and zinc soaps: A source of information for the study of oil paint degradation. *ICOM-CC 17th Triennial Conference Preprints, Melbourne, 15–19 September 2014*, 8 pp.
- Hermans, Joen. J., Baij, L., Koenis, M., Keune, K., Iedema, P. D., & Woutersen, S. (2019). 2D-IR spectroscopy for oil paint conservation: Elucidating the water-sensitive structure of zinc carboxylate clusters in ionomers. *Science Advances*, *5*(6), aaw3592. <https://doi.org/10.1126/sciadv.aaw3592>
- Higgitt, C., Spring, M., & Saunders, D. (2003). Pigment-medium Interactions in Oil Paint Films containing Red Lead or Lead-tin Yellow. *National Gallery Technical Bulletin*, *24*, 75–95.
- Hollner, S. (2009). *Développement de nouveaux traitements de protection à base d'acide carboxylique pour la conservation d'objets en fer du patrimoine culturel* [PhD Dissertation]. Université Henri-Poincaré Nancy I.
- IARC. (1989). Occupational exposures in paint manufacture and painting. In *IARC monographs on the evaluation of carcinogenic risks to humans* (Vol. 47, pp. 329–425). International Agency for Research on Cancer, World Health Organization. <https://www.ncbi.nlm.nih.gov/books/NBK524899/>
- Iezzi, R. A. (2011, August 1). Corrosion Mechanisms of Painted Metal. *U.S. Department of Defense Corrosion 2011 Conference*. U.S. Department of Defense Corrosion 2011 Conference.
- Izzo, F. C. (2011). *20th Century Artist's Oil Paints; A Chemical-Physical Survey* [PhD Dissertation]. Università Ca' Foscari Venezia.
- Izzo, F. C., Kratter, M., Nevin, A., & Zendri, E. (2021). A Critical Review on the Analysis of Metal Soaps in Oil Paintings. *ChemistryOpen*, *10*(9), 904–921. <https://doi.org/10.1002/open.202100166>
- Jouet, J. (2020). « *En voiture!* » *Etude et conservation-restauration d'une voiture à pédales Euréka: Le modèle Touriste 203 (1933-1936, Mulhouse, Cité de l'Automobile-Collection Schlumpf). Evaluation de différents adhésifs en vue du refixage d'un revêtement peint nitrocellulosique sur alliage ferreux* [Mémoire pour le diplôme de restaurateur du patrimoine, Spécialité Arts du feu - Metal]. Institut National du Patrimoine.
- Kapoor, R., & Sharma, R. (1983). Anhydrous Chromium(III) Carboxylates: Reactions of CrO<sub>3</sub> with Carboxylic Acid Anhydrides. *Zeitschrift Für Naturforschung B*, *38*, 42–44. <https://doi.org/10.1515/znb-1983-0110>
- Kendig, M., & Mills, D. J. (2017). An historical perspective on the corrosion protection by paints. *Progress in Organic Coatings*, *102*, 53–59. <https://doi.org/10.1016/j.porgcoat.2016.04.044>
- Keune, K. (2005). *Binding medium, pigments and metal soaps characterised and localised in paint cross-sections* [PhD Dissertation]. FOM Institute for Atomic and Molecular Physics.
- Keune, K., & Boon, J. J. (2007). Analytical imaging studies of cross-sections of paintings affected by lead soap aggregate formation. *Studies in Conservation*, *3*, 161–176.

- Keune, K., Ferreira, E., & Boon, J. (2005). Characterization and localization of the oil-binding medium in paint cross-sections using imaging secondary ion mass spectrometry. *The 14th Triennial Meeting The Hague Preprints*, 2, 796–802.
- Keune, K., Kramer, R. P., Huijbregts, Z., Schellen, H. L., Stappers, M. H. L., & Hommes, M. H. van E. (2016). Pigment Degradation in Oil Paint Induced by Indoor Climate: Comparison of Visual and Computational Backscattered Electron Images. *Microscopy and Microanalysis*, 22(2), 448–457. <https://doi.org/10.1017/S1431927616000076>
- La Nasa, J., Modugno, F., Aloisi, M., Lluveras-Tenorio, A., & Bonaduce, I. (2018). Development of a GC/MS method for the qualitative and quantitative analysis of mixtures of free fatty acids and metal soaps in paint samples. *Analytica Chimica Acta*, 1001, 51–58. <https://doi.org/10.1016/j.aca.2017.11.017>
- Lauridsen, C. B., Sanyova, J., & Simonsen, K. P. (2015). Raman analysis of complex pigment mixtures in 20th century metal knight shields of the Order of the Elephant. *Spectrochimica Acta Part A: Molecular and Biomolecular Spectroscopy*, 150, 54–62. <https://doi.org/10.1016/j.saa.2015.04.117>
- Lawson, A. (2016). *Assessment of the performance of three clear coatings for use in heritage conservation by an oxygen consumption technique* [PhD Dissertation]. Cardiff University.
- Lazzari, M., & Chiantore, O. (1999). Drying and oxidative degradation of linseed oil. *Polymer Degradation and Stability*, 65(2), 303–313. [https://doi.org/10.1016/S0141-3910\(99\)00020-8](https://doi.org/10.1016/S0141-3910(99)00020-8)
- Leaded zinc oxide. (2016). In *CAMEO: Conservation and Art Materials Encyclopedia Online*. [http://cameo.mfa.org/wiki/Leaded\\_zinc\\_oxide](http://cameo.mfa.org/wiki/Leaded_zinc_oxide)
- Leclercq, N., Berthault, J., Langlois, F., Le, S., Poirier, S., Bisou, J., Blache, F., Medjoubi, K., & Mocuta, C. (2016). Flyscan: A fast and multi-technique data acquisition platform for the SOLEIL beamlines. In K. Riches (Ed.), *Proceedings of the 15th International Conference on Accelerator and Large Experimental Physics Control Systems ICALEPCS 2015* (p. 1225).
- Lee, J., Bonaduce, I., Modugno, F., La Nasa, J., Ormsby, B., & van den Berg, K. J. (2018). Scientific investigation into the water sensitivity of twentieth century oil paints. *Microchemical Journal*, 138, 282–295. <https://doi.org/10.1016/j.microc.2018.01.017>
- Leidheiser, H. (1982). Corrosion of Painted Metals—A Review. *CORROSION*, 38(7), 374–383. <https://doi.org/10.5006/1.3581899>
- Li, D., & Leroux, P. (2016). *Corrosion resistance of coating after scratch testing*. Nanovea.
- Lin, L. (Ed.). (1998). Extender pigments. *Pigment & Resin Technology*, 27(2). <https://doi.org/10.1108/prt.1998.12927baf.010>
- Lussier, S. M., & Smith, G. D. (2007). A review of the phenomenon of lead white darkening and its conversion treatment. *Studies in Conservation*, 52(sup1), 41–53. <https://doi.org/10.1179/sic.2007.52.Supplement-1.41>
- Lyon, S. B., Bingham, R., & Mills, D. J. (2017). Advances in corrosion protection by organic coatings: What we know and what we would like to know. *Progress in Organic Coatings*, 102, 2–7. <https://doi.org/10.1016/j.porgcoat.2016.04.030>

## Reference List

- Maia, M., Barros, A. I. R. N. A., & Nunes, F. M. (2013). A novel, direct, reagent-free method for the detection of beeswax adulteration by single-reflection attenuated total reflectance mid-infrared spectroscopy. *Talanta*, *107*, 74–80. <https://doi.org/10.1016/j.talanta.2012.09.052>
- Martínez-Casado, F. J., Ramos-Riesco, M., Rodríguez-Cheda, J. A., Cucinotta, F., Matesanz, E., Miletto, I., Gianotti, E., Marchese, L., & Matěj, Z. (2016). Unraveling the Decomposition Process of Lead(II) Acetate: Anhydrous Polymorphs, Hydrates, and Byproducts and Room Temperature Phosphorescence. *Inorganic Chemistry*, *55*(17), 8576–8586. <https://doi.org/10.1021/acs.inorgchem.6b01116>
- Martínez-Casado, F. J., Rodríguez-Cheda, J. A., Ramos-Riesco, M., Redondo-Yélamos, M. I., Cucinotta, F., & Fernández-Martínez, A. (2019). Physicochemistry of Pure Lead(II) Soaps: Crystal Structures, Solid and Liquid Mesophases, and Glass Phases – Crystallographic, Calorimetric, and Pair Distribution Function Analysis. In F. Casadio, K. Keune, P. Noble, A. Van Loon, E. Hendriks, S. A. Centeno, & G. Osmond (Eds.), *Metal Soaps in Art: Conservation and Research* (pp. 227–239). Springer International Publishing. [https://doi.org/10.1007/978-3-319-90617-1\\_13](https://doi.org/10.1007/978-3-319-90617-1_13)
- Materials Data on PbO by Materials Project* (mp-19921). (2020). Lawrence Berkeley National Lab. (LBNL), Berkeley, CA (United States). LBNL Materials Project. <https://doi.org/10.17188/1195107>
- Materials Data on PbSO4 by Materials Project* (mp-3472). (2020). Lawrence Berkeley National Lab. (LBNL), Berkeley, CA (United States). LBNL Materials Project. <https://doi.org/10.17188/1183758>
- Mayne, J. E. O. (1973). The Mechanism of the Protection of Iron and Steel by Paint. *Anti-Corrosion Methods and Materials*, *20*(10), 3–8. <https://doi.org/10.1108/eb006930>
- Meilunas, R. J., Bentsen, J. G., & Steinberg, A. (1990). Analysis of Aged Paint Binders by FTIR Spectroscopy. *Studies in Conservation*, *35*(1), 33–51. <https://doi.org/10.2307/1506280>
- Messerschmidt, L. (2014). Wuhu iron paintings: Basic research and conservation of a four-sided lantern. *Studies in Conservation*, *59*(sup1), S111–S114. <https://doi.org/10.1179/204705814X13975704318434>
- Mirambet, F., Reguer, S., Rocca, E., Hollner, S., & Testemale, D. (2010). A complementary set of electrochemical and X-ray synchrotron techniques to determine the passivation mechanism of iron treated in a new corrosion inhibitor solution specifically developed for the preservation of metallic artefacts. *Applied Physics A*, *99*(2), 341–349. <https://doi.org/10.1007/s00339-010-5674-4>
- Mirambet, F., Rocca, E., & Steinmetz, J. (2004). Protection of iron artefacts of the cultural heritage: Use of the sodium carboxylates as corrosion inhibitors. *Eurocorr 2004*, 71. <https://www.lrmh.fr/Default/doc/SYRACUSE/138852/protection-of-iron-artefacts-of-the-cultural-heritage-use-of-the-sodium-carboxylates-as-corrosion-in>
- Mirambet-Paris, A., & Mirambet, F. (2011). La conservation-restauration du patrimoine technique et industriel dans le cadre de la loi sur les Musées de France, une mission impossible ? *La Lettre de l'OCIM*, *135*, 27–35. <https://doi.org/10.4000/ocim.874>
- Modugno, F., Di Gianvincenzo, F., Degano, I., van der Werf, I. D., Bonaduce, I., & van den Berg, K. J. (2019). On the influence of relative humidity on the oxidation and hydrolysis of fresh and aged oil paints. *Scientific Reports*, *9*(1), 1–16. <https://doi.org/10.1038/s41598-019-41893-9>

- Moghaddam, R. F., Chen, S., Hedjam, R., & Cheriet, M. (2013). A maximal-information color to gray conversion method for document images: Toward an optimal grayscale representation for document image binarization. *ArXiv, Computer Science*(Computer Vision and Pattern Recognition), 1306.6058.
- Monico, L., Van der Snickt, G., Janssens, K., De Nolf, W., Miliani, C., Verbeeck, J., Tian, H., Tan, H., Dik, J., Radepon, M., & Cotte, M. (2011). Degradation Process of Lead Chromate in Paintings by Vincent van Gogh Studied by Means of Synchrotron X-ray Spectromicroscopy and Related Methods. 1. Artificially Aged Model Samples. *Analytical Chemistry*, 83(4), 1214–1223. <https://doi.org/10.1021/ac102424h>
- Monnier, J. (2008). *Corrosion atmosphérique sous abri d'alliages ferreux historiques: Caractérisation du système, mécanismes et apport à la modélisation* [PhD Dissertation]. Université Paris-Est.
- Monnier, J., Bellot-Gurlet, L., Baron, D., Neff, D. D., Guillot, I., & Dillmann, P. (2011). A methodology for Raman structural quantification imaging and its application to iron indoor atmospheric corrosion products. *Journal of Raman Spectroscopy*, 42(4), 773–781. <https://doi.org/10.1002/jrs.2765>
- Monnier, J., Réguer, S., Vantelon, D., Dillmann, P., Neff, D., & Guillot, I. (2010). X-rays absorption study on medieval corrosion layers for the understanding of very long-term indoor atmospheric iron corrosion. *Applied Physics A: Materials Science and Processing*, 99, 399–406. <https://doi.org/10.1007/s00339-010-5638-8>
- Noble, P. (2019). A Brief History of Metal Soaps in Paintings from a Conservation Perspective. In F. Casadio, K. Keune, P. Noble, A. Van Loon, E. Hendriks, S. A. Centeno, & G. Osmond (Eds.), *Metal Soaps in Art: Conservation and Research* (pp. 1–22). Springer International Publishing. [https://doi.org/10.1007/978-3-319-90617-1\\_1](https://doi.org/10.1007/978-3-319-90617-1_1)
- Ocim. (2021). *Les acteurs du Patrimoine et de la Culture scientifiques, techniques et industriels*. Ocim - Observatoire du Patrimoine et de la Culture scientifiques et techniques. <https://www.calameo.com/books/005777060e643868e55ec>
- Olender, J., & Wantuch-Jarkiewicz, K. (2019). Extraction of Zinc Corrosion from Beneath a Paint Layer: A Case Study. *Studies in Conservation*, 64(3), 146–158. <https://doi.org/10.1080/00393630.2018.1530900>
- Otero, V., Sanches, D., Montagner, C., Vilarigues, M., Carlyle, L., Lopes, J. A., & Melo, M. J. (2014). Characterisation of metal carboxylates by Raman and infrared spectroscopy in works of art. *Journal of Raman Spectroscopy*, 45(11–12), 1197–1206. <https://doi.org/10.1002/jrs.4520>
- Palacios-Beas, E., Juárez-López, G., & Monhemius, J. (2004). Infrared spectroscopy of metal carboxylates: II. Analysis of Fe(III), Ni and Zn carboxylate solutions. *Hydrometallurgy*, 72, 139–148. [https://doi.org/10.1016/S0304-386X\(03\)00137-3](https://doi.org/10.1016/S0304-386X(03)00137-3)
- Pavlopoulou, L.-C., & Watkinson, D. (2006). The degradation of oil painted copper surfaces. *Studies in Conservation*, 51(sup1), 55–65. <https://doi.org/10.1179/sic.2006.51.Supplement-1.55>
- Penner-Hahn, J. E. (2003). X-ray Absorption Spectroscopy. In *Comprehensive Coordination Chemistry II* (Vol. 2). Elsevier.

## Reference List

- Plater, M. J., De Silva, B., Gelbrich, T., Hursthouse, M. B., Higgitt, C. L., & Saunders, D. R. (2003). The characterisation of lead fatty acid soaps in 'protrusions' in aged traditional oil paint. *Polyhedron*, 22(24), 3171–3179. [https://doi.org/10.1016/S0277-5387\(03\)00461-3](https://doi.org/10.1016/S0277-5387(03)00461-3)
- Pliny the Elder. (1855). Book XXXIV. The Natural History of Metals, Chapter 43—Methods of Preventing Rust. In J. Bostock & H. T. Riley (Trans.), *The Natural History*. Taylor and Francis, Red Lion Court, Fleet Street.  
<http://www.perseus.tufts.edu/hopper/text?doc=urn:cts:latinLit:phi0978.phi001.perseus-eng1:34.43>
- Pöllnitz, G., Schreiner, M., Vetter, W., Pichler, B., & Jastrzębiowski, A. (2019). Uncovering the illegible: Multi-analytical approach to reveal paint stratigraphy of corroded signposts from the Auschwitz-Birkenau State Museum. *Heritage Science*, 7(1), 98. <https://doi.org/10.1186/s40494-019-0339-x>
- Prochaska, S., & Tordonato, D. (2017). *Review of Corrosion Inhibiting Mechanisms in Coatings*. U.S. Department of the Interior Bureau of Reclamation Research and Development Office.
- Radepont, M. (2013). *Understanding of chemical reactions involved in pigment discoloration, in particular in mercury sulfide (HgS) blackening* [PhD Dissertation]. Universiteit Antwerpen; Université Pierre et Marie Curie.
- Ravel, B., & Newville, M. (2005). ATHENA, ARTEMIS, HEPHAESTUS: Data analysis for X-ray absorption spectroscopy using IFEFFIT. *Journal of Synchrotron Radiation*, 12(Pt 4), 537–541. <https://doi.org/10.1107/S0909049505012719>
- Robinet, L., & Corbeil, M.-C. (2003). The Characterization of Metal Soaps. *Studies in Conservation*, 48(1), 23–40. <https://doi.org/10.1179/sic.2003.48.1.23>
- Rocca, E., & Mirambet, F. (2007). Corrosion inhibitors for metallic artefacts: Temporary protection. In P. Dillmann, G. Béranger, P. Piccardo, & H. Matthiesen (Eds.), *Corrosion of Metallic Heritage Artefacts* (pp. 308–334). Woodhead Publishing. <https://doi.org/10.1533/9781845693015.308>
- Roy, A. (Ed.). (1993). *Artists' pigments: A handbook of their history and characteristics* (Vol. 2). National gallery of art.
- Saunders, D. (2000). Pollution and the National Gallery. *National Gallery Technical Bulletin*, 21, 77–94.
- Saunders, D., & Kirby, J. (2001). A comparison of light-accelerated ageing regimes in some galleries and museums. *The Conservator*, 25(1), 95–104. <https://doi.org/10.1080/01410096.2001.9995168>
- Saunders, D., & Kirby, J. (2004). The Effect of Relative Humidity on Artists' Pigments. *National Gallery Technical Bulletin*, 25, 62–72.
- Schanda, J. (2007). *Colorimetry: Understanding the CIE System*. Wiley. <https://www.wiley.com/en-us/Colorimetry%3A+Understanding+the+CIE+System-p-9780470049044>
- Scherrer, N. C., Stefan, Z., Francoise, D., Annette, F., & Renate, K. (2009). Synthetic organic pigments of the 20th and 21st century relevant to artist's paints: Raman spectra reference collection. *Spectrochimica Acta Part A: Molecular and Biomolecular Spectroscopy*, 73(3), 505–524. <https://doi.org/10.1016/j.saa.2008.11.029>
- Schroter, J. (2008). *Etude comparative de systèmes de protection transparents pour le patrimoine en fer peint* [Internship report]. Université Paris 1 Panthéon Sorbonne.

- Schroter, J. (2009). *L'étude et la conservation-restauration du fer peint: Le cas d'une croix tombale en fer forgé peint au Musée des Arts Appliqués de Vienne, Autriche* [Master's thesis, in Conservation and Restoration of Cultural Heritage]. Université Paris I Panthéon Sorbonne.
- Sharma, B. K. (Ed.). (2006). *Industrial Chemistry* (15th ed.). GOEL Publishing House.
- Sharma, G., & Bala, R. (2017). *Digital Color Imaging Handbook*. CRC Press.
- Shashoua, Y., & Matthiesen, H. (2010). Protection of iron and steel in large outdoor industrial heritage objects. *Corrosion Engineering, Science and Technology*, 45(5), 357–361. <https://doi.org/10.1179/147842210X12710800383648>
- Šima, J. (2015). (Non)luminescent properties of iron compounds. *Acta Chimica Slovaca*, 8(2), 126–132. <https://doi.org/10.1515/acs-2015-0022>
- Skoog, D. A., Holler, F. J., & Crouch, S. R. (2017). *Principles of instrumental analysis* (7th Edition). Cengage Learning.
- Smith, B. (1998). *Infrared Spectral Interpretation: A Systematic Approach* (1st ed.). CRC Press. <https://doi.org/10.1201/9780203750841>
- Smith, C. A. (1981). Early protective coatings. Part I: Oils, fats & paints. *Anti-Corrosion Methods and Materials*, 28(3), 12–15. <https://doi.org/10.1108/eb010189>
- Smith, E. L. (1992). *Characterization of self-assembled carboxylate monolayers and multilayers at copper and silver* [PhD Dissertation, Iowa State University]. <https://lib.dr.iastate.edu/rtd/10389/>
- Smith, G. D., & Clark, R. J. H. (2002). The role of H<sub>2</sub>S in pigment blackening. *Journal of Cultural Heritage*, 3(2), 101–105. [https://doi.org/10.1016/S1296-2074\(02\)01173-1](https://doi.org/10.1016/S1296-2074(02)01173-1)
- Spoerl, J. S. (2004). *A Brief History of Iron and Steel Production*. [https://www.academia.edu/31060927/A\\_Brief\\_History\\_of\\_Iron\\_and\\_Steel\\_Production](https://www.academia.edu/31060927/A_Brief_History_of_Iron_and_Steel_Production)
- Spring, M., & Grout, R. (2002). The Blackening of Vermilion: An Analytical Study of the Process in Paintings. *National Gallery Technical Bulletin*, 23, 50–61.
- Stewart, C. (2019, February 14). *The Composition of a Paint Coating*. Corrosionpedia. <https://www.corrosionpedia.com/the-composition-of-a-paint-coating/2/3247>
- Stoye, D., Marwald, B., & Plehn, W. (2010). Paints and Coatings, 1. Introduction. In *Ullmann's Encyclopedia of Industrial Chemistry*. WILEY-VCH. [https://doi.org/10.1002/14356007.a18\\_359.pub3](https://doi.org/10.1002/14356007.a18_359.pub3)
- Sutter, J. (2013). *Aux trois rois: Étude et conservation-restauration d'une enseigne en alliage ferreux, peinte sur ses deux faces, Evaluation de l'impact de deux traitements inhibiteurs de corrosion sur une couche picturale à l'huile composée de pigments à bases d'oxydes métalliques* [Mémoire pour le diplôme de restaurateur du patrimoine de l'INP, Spécialité Peinture]. Institut National du Patrimoine.
- Sutter, J. (2017). *Retour d'expérience: Restauration de couches picturales sur support métallique*. Journée ICOM Métal France 2017, Institut National du Patrimoine.
- Tator, K. B. (2015). Coating Deterioration. In K. B. Tator (Ed.), *Protective Organic Coatings* (pp. 462–473). ASM International. <https://doi.org/10.31399/asm.hb.v05b.a0006073>

## Reference List

- Thoury, M., Van Loon, A., Keune, K., Hermans, J. J., Réfrégiers, M., & Berrie, B. H. (2019). Photoluminescence Micro-imaging Sheds New Light on the Development of Metal Soaps in Oil Paintings. In F. Casadio, K. Keune, P. Noble, A. Van Loon, E. Hendriks, S. A. Centeno, & G. Osmond (Eds.), *Metal Soaps in Art: Conservation and Research* (pp. 211–225). Springer International Publishing. [https://doi.org/10.1007/978-3-319-90617-1\\_12](https://doi.org/10.1007/978-3-319-90617-1_12)
- Tissot, I., Fonseca, J. F., Tissot, M., Lemos, M., Carvalho, M. L., & Manso, M. (2020). Discovering the colours of industrial heritage characterisation of paint coatings from the powerplant at the Levada de Tomar. *Journal of Raman Spectroscopy*, *52*(1), 208–216. <https://doi.org/10.1002/jrs.5924>
- Townsend, J., Carlyle, L., Cho, J.-H., & Félix Campos, M. (2011). The yellowing/bleaching behaviour of oil paint: Further investigations into significant colour change in response to dark storage followed by light exposure. *ICOM Committee for Conservation 16th Triennial Meeting Preprints, Lisbon, 19-23 September 2011*. ICOM Committee for Conservation 16th Triennial Meeting, Lisbon, Portugal.
- Uo, M., Wada, T., & Sugiyama, T. (2015). Applications of X-ray fluorescence analysis (XRF) to dental and medical specimens. *Japanese Dental Science Review*, *51*(1), 2–9. <https://doi.org/10.1016/j.jdsr.2014.07.001>
- Vagnini, M., Vivani, R., Viscuso, E., Favazza, M., Brunetti, B. G., Sgamellotti, A., & Miliani, C. (2018). Investigation on the process of lead white blackening by Raman spectroscopy, XRD and other methods: Study of Cimabue's paintings in Assisi. *Vibrational Spectroscopy*, *98*, 41–49. <https://doi.org/10.1016/j.vibspec.2018.07.006>
- Vahur, S., Teearu, A., & Leito, I. (2010). ATR-FT-IR spectroscopy in the region of 550–230cm<sup>-1</sup> for identification of inorganic pigments. *Spectrochimica Acta Part A: Molecular and Biomolecular Spectroscopy*, *75*(3), 1061–1072. <https://doi.org/10.1016/j.saa.2009.12.056>
- Vahur, S., Teearu, A., Peets, P., Joosu, L., & Leito, I. (2016). ATR-FT-IR spectral collection of conservation materials in the extended region of 4000-80 cm<sup>-1</sup>. *Analytical and Bioanalytical Chemistry*, *408*(13), 3373–3379. <https://doi.org/10.1007/s00216-016-9411-5>
- van den Berg, J. D. J. (2002). *Analytical chemical studies on traditional linseed oil paints* [PhD Dissertation]. Universiteit van Amsterdam.
- van den Berg, K. J. (2003). Analysis of diterpenoid resins and polymers in paint media and varnishes with an atlas of mass spectra. *MOLART Report, FOM Institute AMOLF, Amsterdam*, *10*, 1–97.
- van der Graaf, J. A. (1972). Development of Oil-Paint and the Use of Metal-Plates as a Support. *Studies in Conservation*, *17*(sup1), 139–151. <https://doi.org/10.1179/sic.1972.17.s1.004>
- van der Weerd, J., van Loon, A., & Boon, J. (2005). FTIR Studies of the Effects of Pigments on the Aging of Oil. *Studies in Conservation*, *50*, 3–22. <https://doi.org/10.1179/sic.2005.50.1.3>
- Vecco, M. (2010). A definition of cultural heritage: From the tangible to the intangible. *Journal of Cultural Heritage*, *11*(3), 321–324. <https://doi.org/10.1016/j.culher.2010.01.006>
- Vega, D. (2016). *Oil painting on copper: Characterization of the copper support and the feasibility of using pigmented wax resin infills for paint loss reintegration*. [Master's thesis, in Conservation



and Restoration, Universidade Nova de Lisboa].  
[https://run.unl.pt/bitstream/10362/20339/1/Vega\\_2016.pdf](https://run.unl.pt/bitstream/10362/20339/1/Vega_2016.pdf)

- Veiga, A. R. (2010). Oil painting on tinplate by Francisco José Resende. Techniques, materials and degradation of three nineteenth century paintings. *CeROArt, EGG-2010-Horizons*.  
<https://doi.org/10.4000/ceroart.1775>
- Veiga, A., Teixeira, D. M., Candeias, A. J., Mirão, J., Manhita, A., Miguel, C., Rodrigues, P., & Teixeira, J. G. (2015). Micro-analytical study of two 17th century gilded miniature portraits on copper. *Microchemical Journal*, 123, 51–61. <https://doi.org/10.1016/j.microc.2015.05.015>
- Walker, R. (1982). The corrosion and preservation of iron antiques. *Journal of Chemical Education*, 59(11), 943–947. <https://doi.org/10.1021/ed059p943>
- Westland, S. (2016). The CIE system. In *Handbook of Visual Display Technology*.  
[https://doi.org/10.1007/978-3-319-14346-0\\_11](https://doi.org/10.1007/978-3-319-14346-0_11)
- Wheeler, D. H. (1950). The chemistry of drying oils. *Journal of the American Oil Chemists Society*, 27(11), 440–445. <https://doi.org/10.1007/BF02637760>

# Appendix



# Appendix A. Environmental conditions in the storage facilities of the Musée des Arts et Métiers (CNAM), October 2016-April 2017

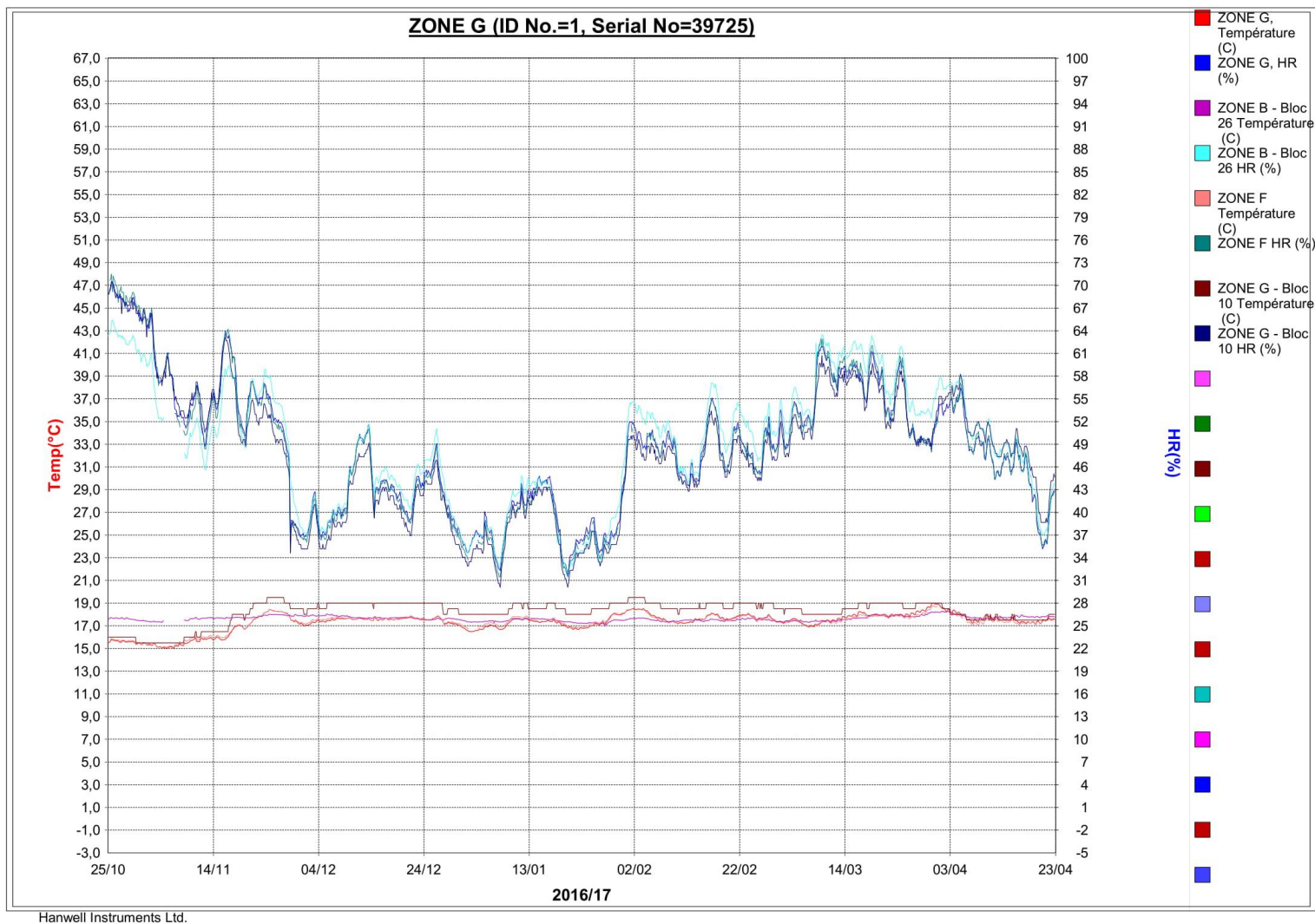


Figure Appendix A-1 Environmental conditions in the storage facilities of the Musée des Arts et Métiers (CNAM), October 2016-April 2017

## Appendix B. Summary of findings from consultation of restoration reports from the Musée des Arts et Métiers (CNAM)

Les rapports de restauration des objets à base de métal peint présents dans les collections du CNAM ont été dépouillés. L'objectif était de relever les altérations constatées et les interventions réalisées pour y remédier.

Table Appendix B-1 Summary of findings from the consultation of restoration reports from the Musée des Arts et Métiers (CNAM).

Altérations (Issues des constats d'état)	Nettoyage	Consolidation / Stabilisation	Retouches	Protection
Empoussièrément	Pinceau fin, micro-aspiration			
Touche collante à la surface/matière grasse.	Compresse de cyclohexane.			
Peinture encrassée/terne/ traces blanchâtres.	Nettoyage avec éthanol, isopropanol, acétone, white spirit, tensioactif selon solubilité de la peinture.		Lustrée avec « poudre de tripoli » en solution aqueuse.	
Couche picturale fragile (soulèvements, perte d'adhésion, fissures, lacunaire)		Consolidant : Paraloïd B72 7% dans éthanol/acétone. Spatule chauffante pour mise en place des soulèvements. Seringue utilisé pour infiltrer fluide.  Plextol B500, tenu avec aimants.  Résine Regalrez dans white spirit.	Lacunes retouchées avec Gamblin (résine Laropal A81 dans isopropanol/ essence F) et pigments.  Résine époxy Araldite 2011 teintée dans la masse avec pigments.  Application de peinture acrylique au-dessous pour diminuer brillance.  Mélange huile de lin et pigments similaires aux couleurs d'origine.	Cire microcristalline dans white spirit/cyclohexane sur zones non-fragiles.
Oxydes de fer sur la peinture.	Micro-brossage. Nettoyage avec solution huile et inhibiteur.	Stabilisation des oxydes de fer avec solution d'acide tannique*.		

## Appendix

Altérations (Issues des constats d'état)	Nettoyage	Consolidation / Stabilisation	Retouches	Protection
Corrosion du support métallique dans zones de peinture mis à nu (i.e. lacunes)	Elimination avec scalpel, brosse en fibre de verre, laine d'acier fin.	Stabilisation des oxydes de fer avec solution d'acide tannique*.  Neutralisation avec Bactifer (bio- convertisseur de l'oxyde de fer de EMDEX-Biochimie).		« Imperméabilisation » des lacunes de peinture.  Vernis acrylique réversible Paraloïd B72 puis couche de cire microcristalline.  Mélange 60:40 résine Regalrez avec cire Cosmoloid H80 dans cyclohexane.  Cire microcristalline dans white spirit appliqué à chaud.  L'huile VD 40 contenant un inhibiteur de corrosion.

\* La réaction de l'acide tannique avec les oxydes de fer donne un produit noir (le tannate de fer) – à prendre en compte quant à l'esthétique de la couche picturale.

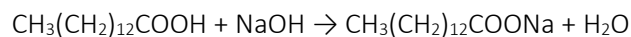
Quelques notes :

- Ce résumé fait le bilan de 23 rapports consultés. Les interventions datent de 1993-2019. Le travail de 8 professionnels est représenté, mais 18 des 23 rapports ont été réalisés par une même personne.
- Tous les restaurateurs auteurs des rapports consultés sont spécialistes du métal : cela à un effet sur leur présentation de l'objet (souvent concentrée sur le métal, où la couche picturale est soit non évoquée, soit qualifiée comme « revêtement » tout simplement) et leurs choix d'interventions.
- En raison du manque d'un format de rapport standardisé, les rapports consultés ne contenaient pas toujours les détails permettant de renseigner les catégories abordées dans le tableau ci-dessus.

## Appendix C. Protocol: preparation of sodium tetradecanoate (NaC<sub>14</sub>) solution

Objective: Preparation of 0.05 M sodium tetradecanoate solution

Balanced equation:



Molecular weight of tetradecanoic acid (myristic acid): 228.3709 g/mol

Concentration of final sodium tetradecanoate (sodium myristate) solution required: 0.05 M

Volume of solution to prepare: 250 mL

Mass of tetradecanoic acid (myristic acid) required: 2.8546 g

Approximate time: 2 hours

Procedure:

1. In a beaker, heat 150 mL of 2:1 ethanol:water solution to 40°C on a hotplate.
2. While stirring, add 2.8546 g (0.0125 mol) of myristic acid to the solution, rinse weigh boat with deionised water into the beaker. HC<sub>14</sub> should partially dissolve but solution will remain cloudy.
3. Using a burette, add 0.5 M sodium hydroxide solution dropwise to the solution. Check the pH periodically using pH indicator paper until it reaches a pH of approximately 7 (around 25 mL of NaOH). HC<sub>14</sub> should be completely dissolved.
4. Insert pH meter into solution.
5. Continue adding 0.5 M NaOH until the solution reaches a pH between 8.5 and 9.5. Solution should be clear and homogeneous.
6. Note final volume of NaOH used and final pH attained.
7. Remove beaker from heat.
8. Top up solution with deionized water to a total volume of 250 mL.
9. Store in sealed bottle.
10. Allow pH to stabilize one week. Adjust accordingly to range of 8.5-9.5.

## Appendix D. Protocol: Preparation of Resin-Wax mixture

This protocol was adapted from the Master Thesis (2007-2009) of J. Schröter (Schroter, 2008).

Objective: Preparation of a mixture containing 30% Regalrez 1126<sup>®</sup> (resin) and 10 % Cosmoloid 80H<sup>®</sup> (wax). Mass percents are with respect to a total volume of 100 g of solution after mixing (i.e. 30 g resin, 10 g wax, 60 g solvent).

Material:

- Pure resin Regalrez 1126<sup>®</sup> in pellets
- Pure Cosmoloid 80H<sup>®</sup> wax in pellets
- Petroleum benzene (White spirit with low aromatic content)
- Stainless steel spatula
- Analytical balance
- Aluminum receptacles
- Glass beakers
- Funnel
- 500 mL glass receptacle with lid/stopper, resistant to solvent
- Magnetic stir bar
- Hot plate
- Mask
- Gloves
- Sterile gauze compresses

Procedure:

1. Weigh the required amounts of resin and wax pellets separately. Weigh the required quantity of solvent in a glass beaker.
2. Add the wax pellets to the solvent and let sit for a few hours, then stir the solution to obtain a homogeneous solution.
3. In the fumehood, cover the solution and heat to 70°C to dissolve the wax prior to adding the resin. Add the solution to a bottle that can be closed/stoppered.
4. Place the resin pellets in gauze compress and suspend in the bottle filled with the dissolved wax solution by hooking the gauze over the neck of the bottle and closing the lid.
5. Leave the resin to swell for two days, and then remove the gauze.

Notes for application:

Application of the solution is done at room temperature; however, it must be mixed well prior to using to ensure a homogeneous distribution of the two components.



## Appendix E. Assessment of sampling possibility on historic objects in CNAM collections

Table Appendix E-1 Assessment of sampling possibility on historic objects in CNAM collections based on state of conservation.

Tri Titre	Possibilités d'écailles/de prélèvement
SÉRIE DE 7 MESURES DE CAPACITÉ EN MÉTAL PEINT POUR LES GRAINS	Quelques écailles et soulèvements
BALANCE DE VÉRIFICATEUR POUR 50 KILOGRAMMES	Nombreuses écailles de peinture OUI
SÉRIE DE SIX MESURES	Quelques écailles, soulèvements et lacunes
OBJET À IDENTIFIER, MACHINE À ÉGRENER ?	Nombreuses écailles et soulèvements OUI
MODÈLE : INDICATEUR MAGNÉTIQUE DE NIVEAU	Quelques soulèvements ; Corrosion efflorescente
LANTERNE À TROIS FEUX À ACÉTYLÈNE AVEC VOLETS POUR CHEMIN DE FER	Écailles de peinture et soulèvements OUI
MODÈLE : FREIN DE CHEMIN DE FER À EMBRAYAGE ET À TRANSMISSION DE VÉHICULE À VÉHICULE	Quelques lacunes mais pas d'écailles ni de soulèvements
LOCOMOTIVE À VAPEUR DE TYPE 110 PLANET ENGINE "MATHIEU MURRAY"	Quelques lacunes mais pas d'écailles ni de soulèvements
VOITURE AUTOMOBILE B14	Quelques écailles et lacunes
CHÂSSIS AUTOMOBILE SYSTÈME ANGELI	Lacunes importantes mais pas d'écailles et quelques soulèvements
VOITURE AUTOMOBILE VESPA 400	Pas d'écailles mais des soulèvements sous forme de boursouffures
GÉNÉRATEUR HAUTE TENSION POUR RADIOTHÉRAPIE : CAISSON PRINCIPAL ET PIED MOBILE	Quelques écailles et soulèvements
TANDEM 4 PLACES À MOTEUR AUXILIAIRE	Quelques écailles (de taille conséquente) et soulèvements (surtout au niveau du réservoir) OUI
VÉLOMOTEUR ÉLECTRIQUE	Nombreuses lacunes mais pas d'écailles ni de soulèvements
CHARRUE BRABANT DOUBLE	Quelques écailles, soulèvements et lacunes (plusieurs couches, stratigraphie à prévoir) OUI
MODÈLE : VOITURE DE PREMIÈRE CLASSE	Quelques écailles
MOTEUR	Quelques lacunes mais pas d'écailles ni de soulèvements
DYNAMO DE GRAMME	Quelques écailles et lacunes (stratigraphie à prévoir ?)

## Appendix F. Object sampling locations

### Appendix F.i Tandem (inv. 21811): sampling locations

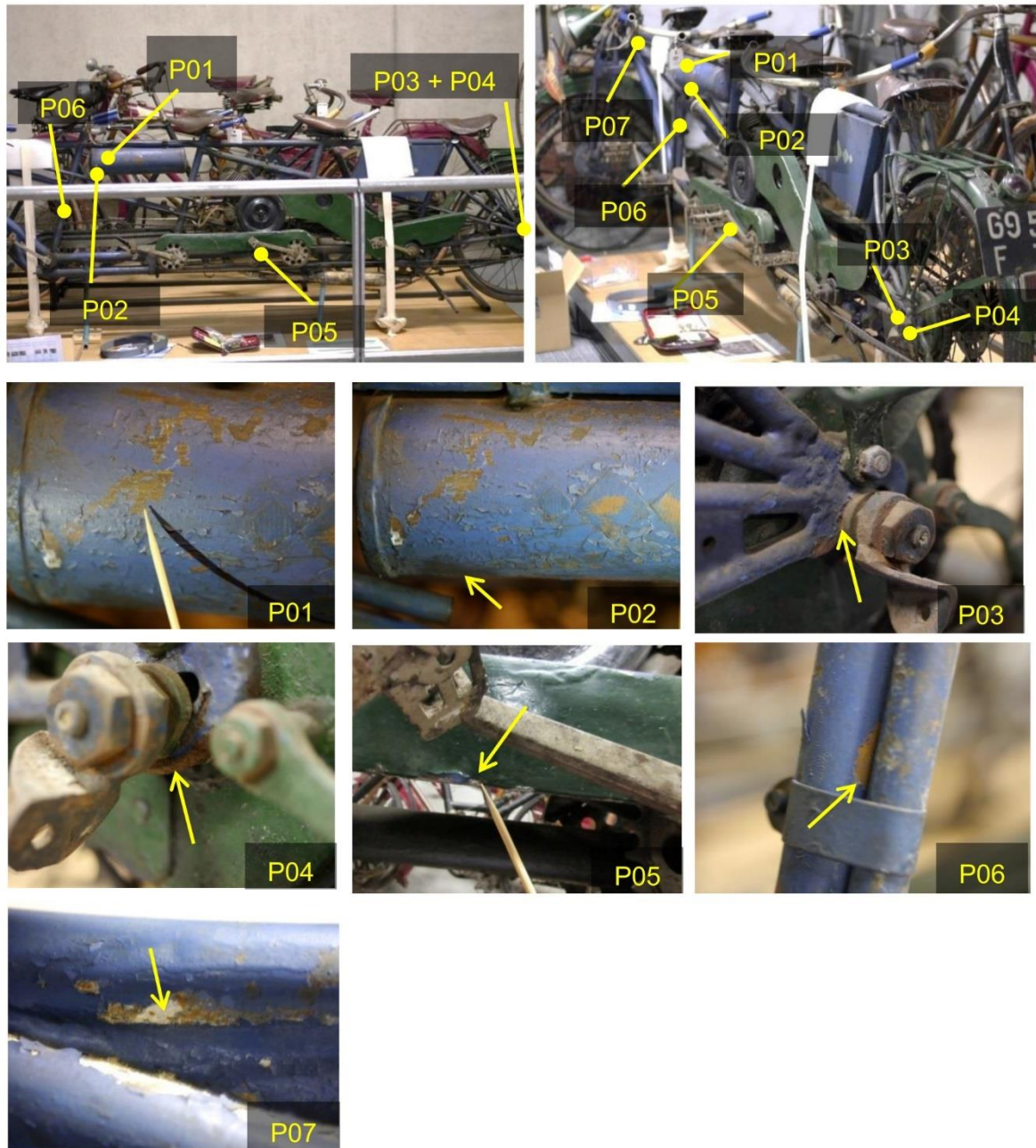


Figure Appendix F-1 Sampling locations on the *Tandem*.

**Table Appendix F-1: Details of samples acquired on the Tandem.**

Sample name	Description of sampling zone	Type of sample acquired
P01	Sample acquired on the left side of the reservoir. Blue paint (at least 2 layers). Nature of metal support is unclear (Cu?).	Paint sample
P02	Sample acquired on the bottom of the reservoir. Blue paint (at least 2 layers). Nature of metal support is unclear (Cu?). Same as P01 but more dust/grime is present.	Paint sample
P03	Sample acquired close to the screw of the back wheel. Thick blue paint. The underlying iron-based support is corroded.	Paint sample
P04	Corrosion products sampled from under the screw of the back wheel. Iron-based metal support.	Corrosion products
P05	Sample acquired on the chain guard. 2 layer paint system: green paint on top of blue paint. The metal support is a white metal (Al?).	Paint sample
P06	Sample acquired on vertical frame under the first seat. Blue paint. Iron-based metal support.	Paint sample
P07	Sample acquired on the horizontal frame close to the handlebars. Blue paint on top of an underlying white paint layer. Iron-based metal support.	Paint sample

Appendix F.ii Charrue (inv. 17001): sampling locations

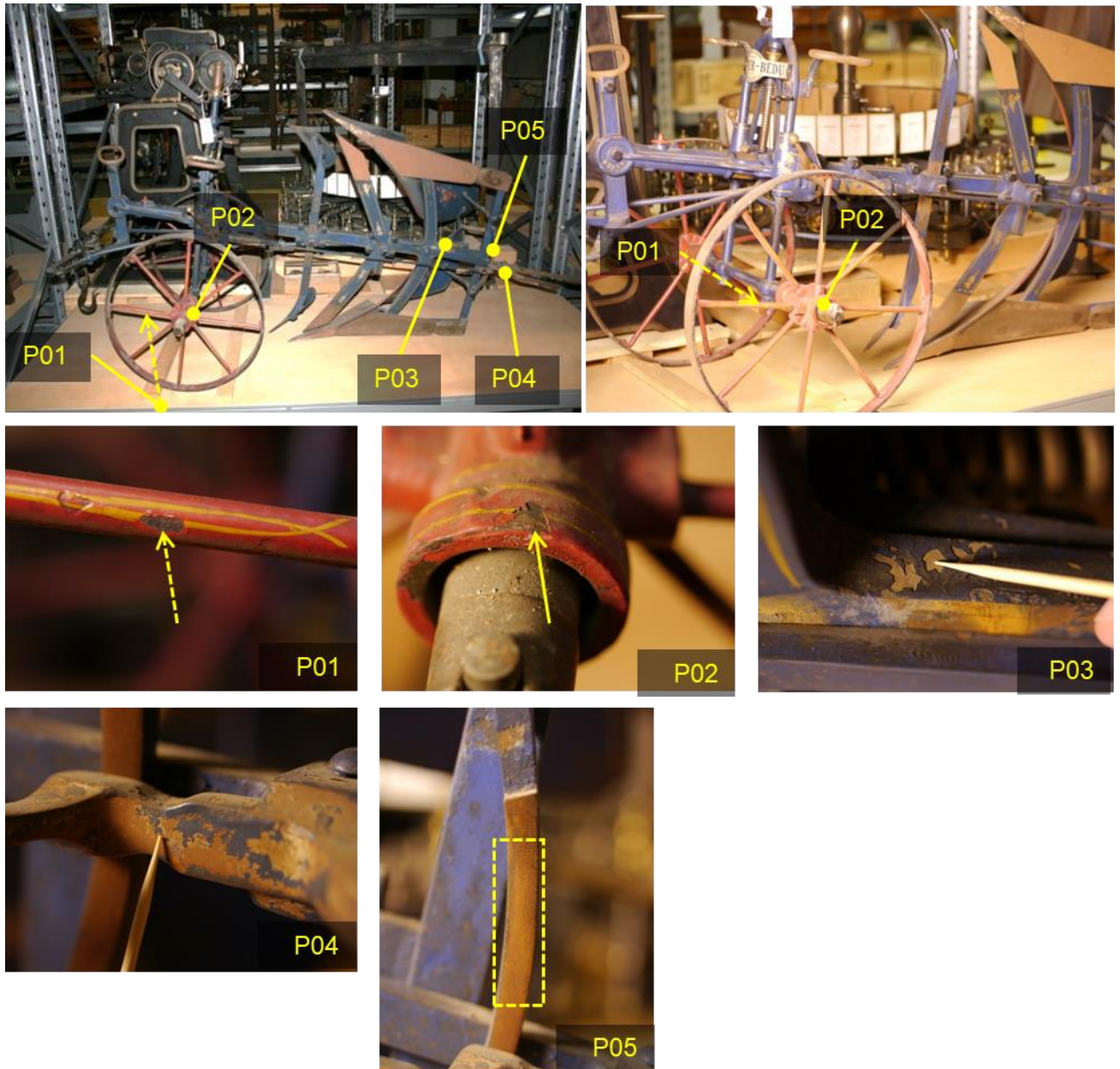


Figure Appendix F-2 Sampling locations on the *Charrue*.

Table Appendix F-2 Details of samples acquired on the *Charrue*.

Sample name	Description of sampling zone	Type of sample acquired
P01	Sample acquired from under object, originating from a spoke of the wheel. Red paint with yellow painted details on iron-based support. The coating has a superficial layer of dust. Some paint loss is noted and the exposed metal is corroded.	Paint sample
P02	Sample acquired from the centre of the wheel. Red paint with yellow painted details on iron-based support. The coating has a superficial layer of dust. Some paint loss is noted and the exposed metal is corroded.	Paint sample
P03	Sample acquired along the central beam, after the third perpendicular intersection (front right). Blue paint and corrosion on iron-based support. The paint coating is thick, presents superficial dust and has flaked off in some areas. The underlying metal support presents is yellowed and corroded.	Paint sample
P04	Sample acquired close to the fourth perpendicular intersection. Blue paint and corrosion on iron-based support. Zone is more dusty and corroded than P03.	Paint sample
P05	Corrosion powder acquired on an unpainted vertical section close to P04. Iron-based metal support.	Corrosion products

Appendix F.iii Chaudière (inv. 36181): sampling locations



Figure Appendix F-3 Sampling locations on the *Chaudière*.

Table Appendix F-3 Details of samples acquired on the *Chaudière*.

Sample name	Description of sampling zone	Type of sample acquired
P01	Sample acquired on the left section of the white-painted piece. White paint on white metal (possibly tinfoil). The zone shows paint loss and corrosion of underlying metal support.	Paint sample
P02	Sample acquired on the right section of the white-painted piece. White paint on white metal (possibly tinfoil). The zone shows paint loss and corrosion of underlying metal support.	Paint sample
P03	Sample acquired on the upper corner of the right section of the white-painted piece. The zone shows paint loss and corrosion of underlying metal support.	Corrosion products
P04	Sample was collected from the base of the object after falling from an area painted with fake rivets on the left cylinder. Red paint on iron-based metal support. The zone shows discolouration (darkening) of the paint.	Paint sample
P05	Sample acquired from the left cylinder. Red paint on iron-based metal support. The zone shows discolouration (darkening) of the paint.	Paint sample
P06	Sample acquired from the interior face of the left cylinder. Black paint on white metal (possibly tinfoil). The zone shows cracking and paint loss.	Paint sample
P07	Sample acquired from a hinge piece on the interior face of the left cylinder. Black paint on iron-based support. The zone shows paint flaking and corrosion.	Paint sample
P08	Sample collected from paint flakes that fell from the right wood-based cylinder onto the base below. Red paint on <u>wood</u> .	Paint sample
P09	Sample collected from paint flakes that fell from the white-painted pieces onto the base below. White paint on white metal (possibly tinfoil).	Paint sample
P10	Grey dust under object.	Dust particles
P11	Sample acquired on upper corner of the right section of the white-painted piece. The zone shows paint flaking, corrosion and discolouration (browning) of the paint. White paint and corrosion on iron-based (tinfoil?) metal support.	Paint sample
P12	Sample acquired on upper corner of the right section of the white-painted piece. The zone shows paint flaking, corrosion and discolouration (browning) of the paint. White paint and corrosion on iron-based (tinfoil?) metal support.	Paint sample

Appendix F.iv Série de Mesures (inv. 60005): sampling locations



Figure Appendix F-4 Sampling locations on the *Série de Mesures*



Table Appendix F-4 Details of samples acquired on the *Série de Mesures*.

Sample name	Description of sampling zone	Type of sample acquired
P01	Sample acquired on the ledge of the bottom border (under the painted letter R of "hectolitre"). Black and orange paint and corrosion products from iron-based support. The surface presents superficial dust and gaps in the paint coating.	Paint sample
P02	Sample acquired below the top border (above the painted letter R of "hectolitre"). Black and orange paint and corrosion products from iron-based support. The surface presents superficial dust and gaps in the paint coating.	Paint sample
P03	Sample acquired on the ledge of the bottom border (under the painted letter R of "hectolitre"). Black and orange paint and corrosion products from iron-based support. The surface presents superficial dust and gaps in the paint coating.	Paint sample
P04	Sample acquired just above the bottom border (under the painted letter R of "hectolitre"). Black and orange paint and corrosion products from iron-based support. The surface presents superficial dust and gaps in the paint coating.	Paint sample
P05	Sample acquired just above the bottom border (under the painted letter R of "hectolitre"). Black and orange paint and corrosion products from iron-based support. The surface presents superficial dust and gaps in the paint coating.	Paint sample

Appendix F.v Balance (inv. 05005): sampling locations

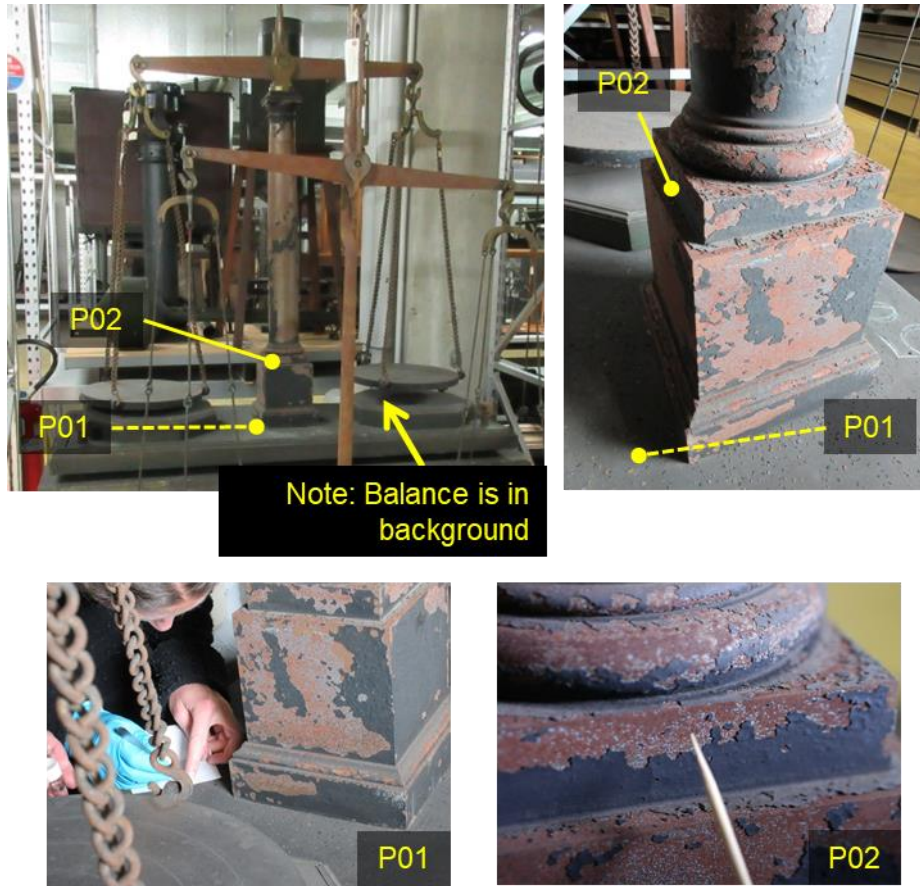


Figure Figure F-5 Sampling locations on the *Balance*.

Table Appendix F-5 Details of samples acquired on the *Balance*.

Sample name	Description of sampling zone	Type of sample acquired
P01	Sample acquired from flakes that fell onto base from the corroded central column. Black paint on blue paint on iron-based support.	Paint sample
P02	Sample acquired from the back on the first rectangular plate under the column. Black paint on blue paint on iron based support.	Paint sample

Appendix F.vi Lanterne (inv. 16726): sampling locations

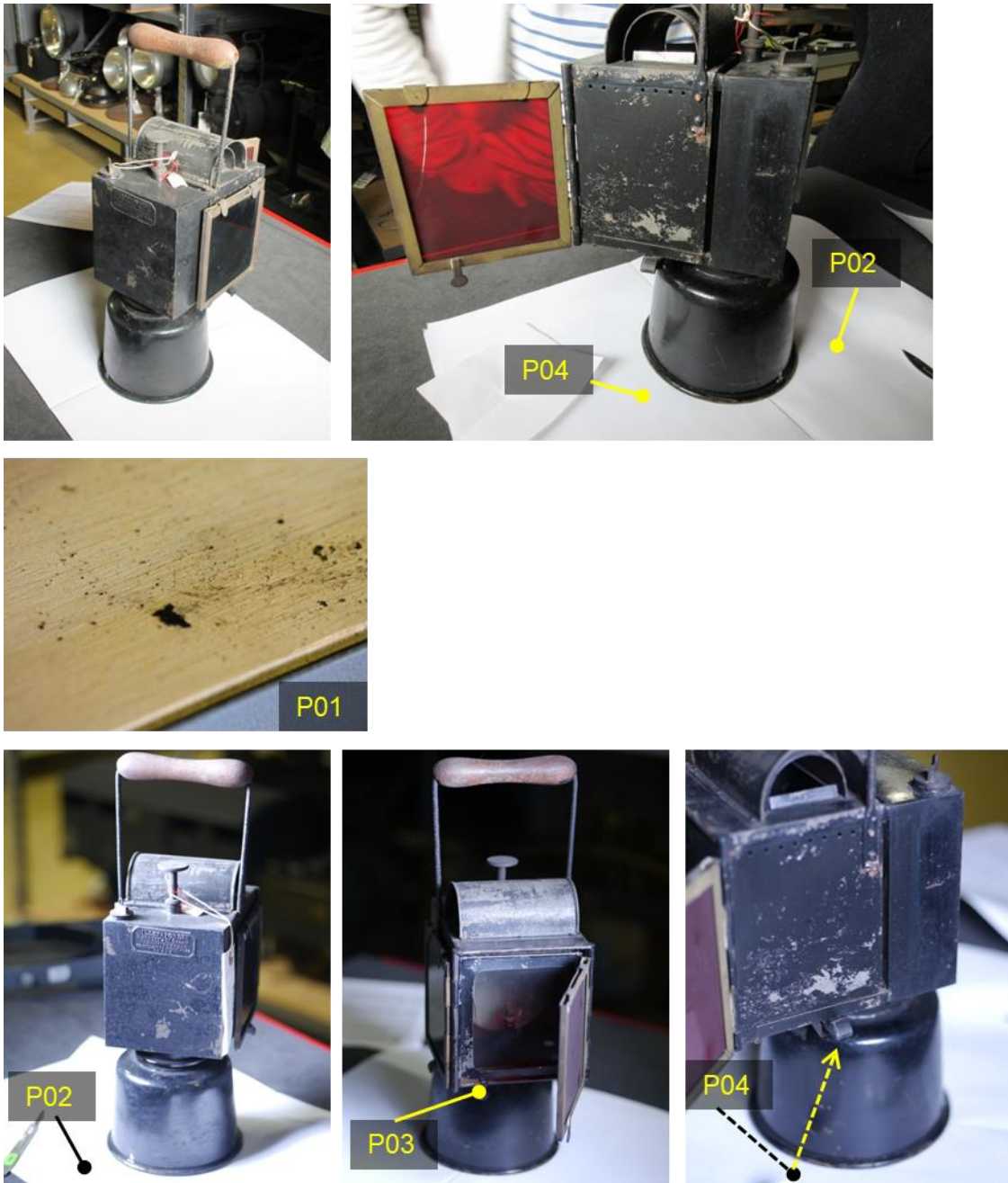


Figure Appendix F-6 Sampling locations on the *Lanterne*.

Appendix

Table Appendix F-6 Details of samples acquired on the *Lanterne*.

Sample name	Description of sampling zone	Type of sample acquired
P01	Samples acquired from detached paint flakes that had fallen onto wooden shelf. Black paint.	Paint sample
P02	Sample that fell from back of lantern during displacement of the object. Black paint on iron-based support.	Paint sample
P03	Powder of corrosion products acquired from the bottom left corner of the pane. Iron-based support.	Corrosion products
P04	Sample that fell off object, most likely acquired from the area close to the hinge. Black paint on iron-based support.	Paint sample

Appendix F.vii Locomotive (inv. 16732): sampling locations

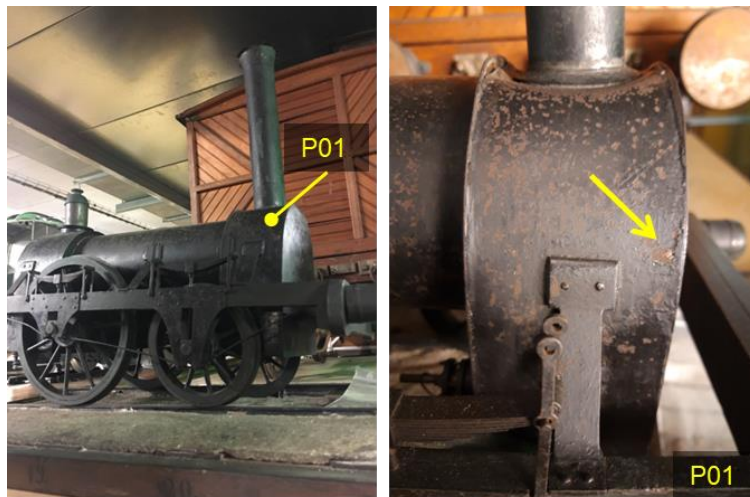
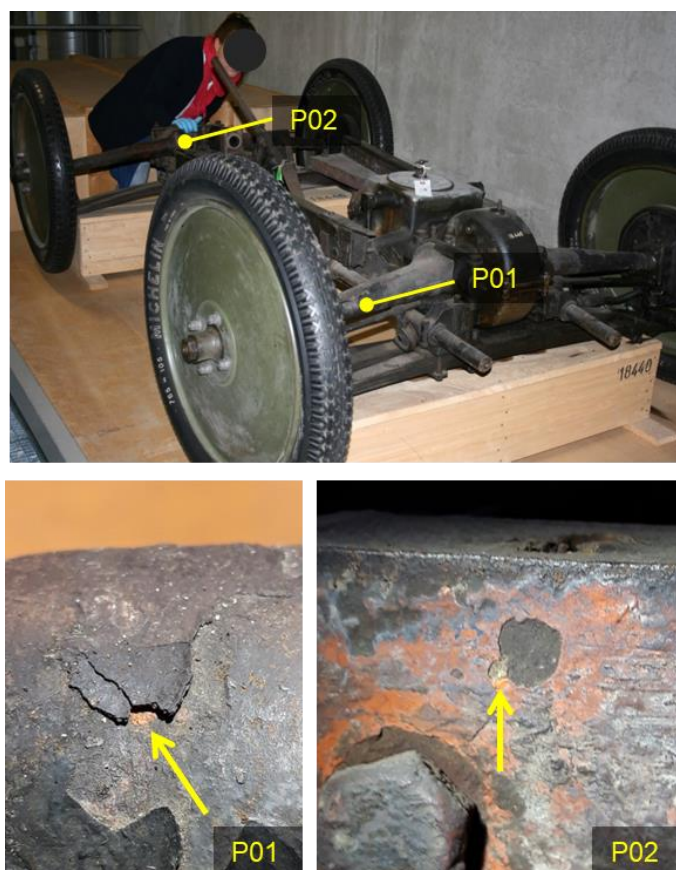


Figure Appendix F-7 Sampling locations on the *Locomotive*.

Table Appendix F-7 Details of samples acquired on the *Locomotive*.

Sample name	Description of sampling zone	Type of sample acquired
P01	Sample acquired from the front right side of the locomotive. Black paint on grey paint, underlying metal is corroded. Iron support.	Paint sample

## Appendix F.viii Châssis (inv. 18440): sampling locations

Figure Appendix F-8 Sampling locations on the *Châssis*.Table Appendix F-8 Details of samples acquired on the *Châssis*.

Sample name	Description of sampling zone	Type of sample acquired
P01	Sample acquired from an area on the front right axle (next to the wheel) presenting paint lifting. Black paint on red paint on iron-based support.	Paint sample
P02	Sample acquired from the frame at the back left of the chassis. Red paint on grey-black paint on iron-based support.	Paint sample

## Appendix F.ix VéloMOTEUR (inv. 20564): sampling locations



Figure Appendix F-9 Sampling locations on the *VéloMOTEUR*.

Table Appendix F-9 Details of samples acquired on the *VéloMOTEUR*.

Sample name	Description of sampling zone	Type of sample acquired
P01	Sample acquired at the top of the head tube (under the handlebars). Black paint on red paint on iron-based support.	Paint sample
P02	Sample acquired from the bottom left outside corner of the front fender. Black paint on iron-based support, no corrosion observed under sample.	Paint sample
P03	Sample acquired from front right corner of the front fender. Black paint, corrosion, underlying iron-based support included (full painted metal system).	Paint coating and metal support

## Appendix G. Measurement of coating thickness before aging

The thickness of each type of coating (unpigmented linseed oil, lead white-based paint, chrome green oxide-based paint) was measured on three replicate coupons for each type and the results displayed in Figure Appendix G-1. The measurements were acquired on the coatings in their initial fresh state before any treatment or aging.

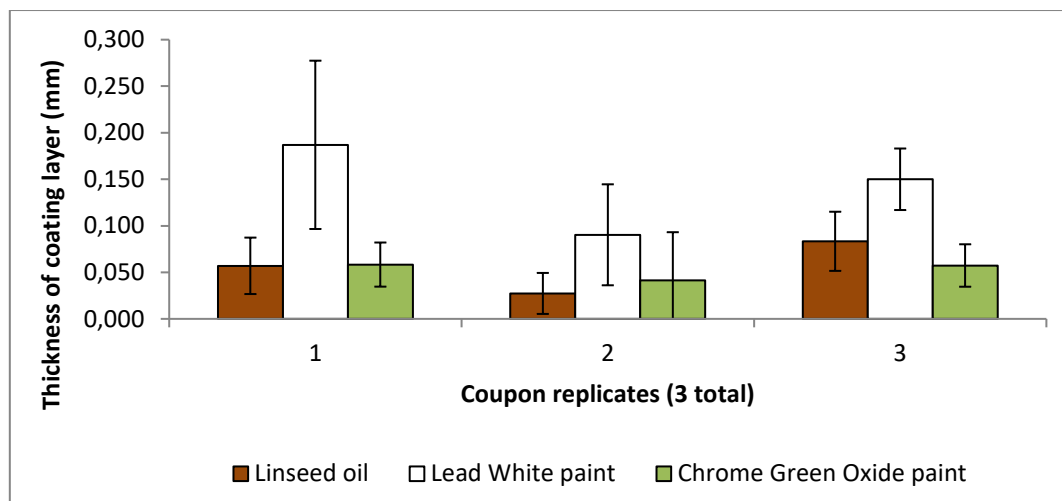


Figure Appendix G-1 Thickness of coatings on metal coupons before aging (three replicates per coating type, three measurements collected/replicate): linseed oil binder (brown); lead white-based paint (white); chrome green oxide-based paint (green). Error bars represent the standard deviation of the three measurements.

The data shows a high level of variability which is expected since the method of measurement chosen was intended to give a rough estimate of the coating thickness. Despite the large error in the measurements, the graph demonstrates that the lead white paint coating has a greater thickness than the other two coatings. This could be related to the large grain size of the lead white pigment dispersed in the coating. The thickness of the chrome green oxide-based paint and the linseed oil binder are approximately equal. The average thickness for each coating is listed in Table Appendix G-1.

Table Appendix G-1 Average thickness of each type of model coating.

Paint coating	Average thickness (mm)
Linseed oil (binder)	0.056 +/- 0.049
Lead white paint	0.142 +/- 0.110
Chrome green oxide paint	0.052 +/- 0.061



## Appendix H. Colorimetry data

### Appendix H.i Colorimetry data: Linseed oil-coated coupons

Table Appendix H-1 Colour measurements of linseed oil-coated coupons throughout artificial aging.

n° coupon	Code	Before aging			RH-I			RH-II		
		L*	a*	b*	L*	a*	b*	L*	a*	b*
26a	LO.f.	53.27	0.71	29.42	38.34	10.25	31.87	28.82	14.67	26.53
26b	LO.f.Cl	56.95	-0.29	23.7	41.88	7.62	31.59	46.03	5.48	25.04
31a	LO.f.	57.49	-0.2	20.12	44.01	6.77	26.35	27.81	14.94	26.03
31b	LO.f.RW	55.16	-0.13	29.08	55.89	1.35	16.23	36.93	10.38	27.83
28a	LO.pa.	47.48	3.51	26.71	46.34	4.36	28.41	46.62	4.83	27.81
28b	LO.pa.Cl	51	2.1	22.39	46.67	4.26	26.9	50.34	3.11	24.6
34a	LO.pa.	38.85	9	23.67	35.53	9.09	16.35	23.85	15.43	18.25
34b	LO.pa.RW	42.29	6.78	19.85	35.58	9.92	17.74	27.71	14.42	22.49
		After LT								
n° coupon	Code	L*	a*	b*						
39A	LO.f.	58.56	0.98	10.18						
39B	LO.f.Cl.LT	59.89	-0.31	7.73						
43A	LO.f.	59.16	1.42	12.53						
43B	LO.f.RW.LT	57.22	1.72	13.35						
40A	LO.pa.	40.32	9.26	18.61						
40B	LO.pa.Cl.LT	43.3	7.08	20.89						
46A	LO.pa.	45.52	5.3	13.55						
46B	LO.pa.RW.LT	40.55	9.46	19.23						

Table Appendix H-2 Difference in colour ( $\Delta E^*$ ) calculated from the colorimetric measurements acquired on the untreated and treated zones of linseed oil binder during each stage of artificial aging.

Coating	Initial state	Treatment	Aging method	$\Delta E^*$ (treated – untreated)		
				Before aging	Phase I aging	Phase II aging (RH only)
LO (binder)	f	Cl	RH	6.87	4.42	19.57
LO (binder)	pa	Cl	RH	5.75	1.55	5.21
LO (binder)	f	RW	RH	9.26	16.52	10.35
LO (binder)	pa	RW	RH	5.60	1.62	5.82
LO (binder)	f	Cl	LT	6.87	3.07	/
LO (binder)	pa	Cl	LT	5.75	4.34	/
LO (binder)	f	RW	LT	9.26	2.13	/
LO (binder)	pa	RW	LT	5.60	8.62	/

## Appendix H.ii Colorimetry data: Lead white-painted coupons

Table Appendix H-3 Colour measurements of lead white-painted coupons throughout artificial aging.

n° coupon	Code	Before aging			After phase I aging (RH)			After phase II aging (RH only)		
		L*	a*	b*	L*	a*	b*	L*	a*	b*
1a	LW.f.	89.64	-5.57	22.08	85.41	-3.04	22	85.09	-2.1	22.03
1b	LW.f.CI	89.67	-5.62	22.97	85.14	-1.81	29.81	84.42	-1.27	25.73
7a	LW.f.	89.27	-5.55	19.48	83.56	-2.06	29.88	81.76	-0.76	29.28
7b	LW.f.RW	89.3	-5.51	19.93	82.28	-0.94	31.98	80.77	-0.12	30.88
4a	LW.pa.	85.88	-3.34	21.24	82.89	-2.2	23.26	82.17	-2.32	20.56
4b	LW.pa.CI	86.28	-2.86	22.82	83.03	-0.81	28.58	81.95	-0.69	26.11
10a	LW.pa.	83.92	-2.06	28.31	82.24	-0.63	29.43	80.99	0.54	31.82
10b	LW.pa.RW	84.9	-2.27	29.14	82.08	-0.34	30.08	80.81	0.56	30.95
		After phase I aging (LT)								
n° coupon	Code	L*	a*	b*						
13a	LW.f.	89.04	-1.81	6.48						
13b	LW.f.CI.LT	89.70	-2.10	10.07						
19a	LW.f.	88.97	-1.76	6.26						
19b	LW.f.RW.LT	88.53	-2.56	12.40						
16a	LW.pa.	89.01	-1.46	7.12						
16b	LW.pa.CI.LT	88.53	-1.47	6.63						
22a	LW.pa.	86.39	-1.08	7.91						
22b	LW.pa.RW.LT	88.16	-2.00	12.49						

## Appendix H.iii Colorimetry data: Chrome green oxide-painted coupons

Table Appendix H-4 Colour measurements of chrome green oxide-painted coupons throughout artificial aging.

n° coupon	Code	Before aging			After phase I aging (RH)			After phase II aging (RH only)		
		L*	a*	b*	L*	a*	b*	L*	a*	b*
49a	CrGO.pa.	36.49	-17.74	13.88	36.12	-16.56	12.77	31.73	-18.49	14.96
49b	CrGO.pa.Cl	35.48	-18.95	14.68	35.32	-16.59	12.66	33.6	-15.36	12.01
52a	CrGO.pa.	35.84	-19.93	15.41	35.12	-18.4	14.09	32.7	-17.76	13.43
52b	CrGO.pa.RW	35	-19.76	14.88	33.73	-18.89	14.14	32.8	-17.86	13.72
62a	CrGO.f	37.18	-22.25	17.65	34.83	-21.63	17.02	33.31	-19.04	15.15
62b	CrGO.f.Cl	37.39	-22.33	17.8	35.15	-21.44	17.01	33.08	-18.8	15.19
63a	CrGO.f	36.95	-22.49	17.62	34.24	-21.58	17.21	32.79	-18.74	14.8
63b	CrGO.f.RW	38.22	-21.47	17	35.54	-20.03	15.88	33.12	-18.53	14.33
		After phase I aging (LT)								
n° coupon	Code	L*	a*	b*						
56a	CrGO.pa.	38.15	-20.61	16.6						
56b	CrGO.pa.Cl	39	-21.92	18.25						
59a	CrGO.pa.	39.71	-19.24	16.93						
59b	CrGO.pa.RW	36.76	-19.41	16.98						

## Appendix I. Object Data Sheets

See separate document for the supplementary information and analyses acquired on the historical samples.



## Résumé

Ce travail aborde les questions relatives à la conservation des objets métalliques peints du patrimoine technique actuellement présents dans les collections muséales. Ces objets présentent un défi pour la conservation en raison de leur nature composite, ainsi que leur état d'altération en fonction des conditions environnementales subies notamment avant d'entrer dans l'environnement contrôlé d'un musée. La stabilisation des métaux peints doit être réalisée en utilisant des stratégies de conservation qui prennent en compte les réactivités de tous les composants du système. Cette thèse est composée de deux axes de recherche qui abordent des considérations clés pour améliorer la conservation des objets historiques en métal peint : le besoin d'études détaillées d'objets historiques, y compris l'identification de leur composition originale et de leur état d'altération ; et la nécessité d'une validation expérimentale de traitements de conservation adaptés aux objets en métal peint. Le premier axe de recherche consiste en l'étude d'un corpus d'objets historiques en métal peint datant du 19<sup>e</sup> au début du 20<sup>e</sup> siècle. Des micro-échantillons ont été prélevés puis caractérisés à l'aide de techniques analytiques complémentaires et multi-échelles. Ces analyses ont permis de déterminer les matériaux en présence et d'observer les processus à l'origine des phénomènes de dégradation visuelle observés. Les récurrences suivantes ont été soulignées : identification d'un liant à base d'huile, présence de pigments aux propriétés anticorrosives et d'une sous-couche de préparation contenant le pigment lithopone. Le deuxième axe de recherche étudie l'effet de deux traitements de conservation prometteurs appliqués sur des coupons de métal peints modèles : une solution d'inhibiteur de corrosion ( $\text{NaC}_{14}$ ), et un revêtement composé d'un mélange résine et cire (Regalrez 1126®-Cosmoloid H80®). Deux conditions de vieillissement artificiel différentes (humidité relative et lumière) ont été utilisées pour altérer les coupons modèles traités, et leur évolution a été suivie par documentation photographique, colorimétrie, FTIR et XAS afin de recueillir des informations complémentaires sur les caractéristiques visuelles, moléculaires et structurales du système. Ceci a permis une évaluation détaillée de l'effet des traitements de conservation sur le système modèle de métal peint dans différentes conditions de vieillissement. Il a été observé que les traitements n'interagissent pas de manière nuisible avec les composants du système métal peint ; cependant, un effet protecteur/inhibiteur n'a pas toujours été révélé dans les conditions de vieillissement appliquées. Le mélange résine-cire s'est avéré avoir des propriétés protectrices significatives contre les effets du vieillissement causés par l'exposition à la lumière. Les résultats obtenus au cours de cette thèse ont permis de rassembler des informations originales sur techniques historiques de préparation des objets en métal peint, de documenter les processus à l'origine des altérations, et de réaliser une première évaluation expérimentale de l'efficacité de deux traitements de conservation répondant aux exigences d'utilisation sur des objets historiques en métal peint.

**Mots-clés :** Matériaux du patrimoine culturel, Peinture, Revêtement, Métal, Conservation, Caractérisation, Analyses physico-chimiques

## Summary

This work addresses the questions surrounding the conservation of painted metal objects of technical heritage currently stored in indoor museum collections. These artefacts present a challenge for conservation because of their composite nature, as well as their various possible states of alteration depending on the environmental conditions experienced before entering the controlled environment of a museum facility. The stabilization of painted metals should be achieved using conservation strategies that consider the vulnerabilities of all the components of the composite system. This thesis is composed of two research axes that address key considerations for improving the conservation of historic painted metal objects: the need for a comprehensive study of historic artefacts, including the identification of their original composition and their current states of alteration; and the need for experimental validation of suitable conservation treatments for painted metal artefacts. The first research axis consists of a study of a corpus of historic painted metal objects from the 19<sup>th</sup> to early 20<sup>th</sup> centuries. Micro-samples were acquired and characterised using complementary, multi-scale analytical techniques. These analyses allowed for the documentation of the types of materials that can be encountered on these artefacts and provided insight into the processes behind the observed visual degradation phenomena. Common trends included the identification of an oil-based binder, pigments with anticorrosive properties, and a recurring base layer containing the pigment lithopone. The second research axis investigates the effect of two promising conservation treatments applied on model painted metal coupons: a corrosion inhibitor solution of NaC<sub>14</sub>, and a transparent coating composed of a resin-wax mixture of Regalrez 1126<sup>®</sup>-Cosmoloid H80<sup>®</sup>. Two different artificial aging conditions (relative humidity and light) were used to age the treated model coupons, and their evolution was monitored using photodocumentation, colorimetry, FTIR, and XAS to gather complementary information about the visual, molecular, and structural nature of the system. This allowed a comprehensive evaluation of the effect of the conservation treatments on the model painted metal system under different aging conditions. The treatments were not observed to interact in a harmful way with the components of the painted metal system; however, a protective/inhibitory effect was not always revealed under the applied aging conditions. The resin-wax mixture proved to have significant protective properties against the aging effects caused by light exposure. The results obtained during this thesis have provided a new understanding of the historical preparation techniques used for painted metal objects, the processes behind their characteristic alteration phenomena, and an initial experimental assessment of the effectiveness of two conservation treatments that fit the requirements for use on historic painted metal objects.

**Keywords:** Cultural heritage materials, Paint, Coatings, Metal, Conservation, Characterisation, Physico-chemical analyses